Whole Genome Doubling Propagates Chromosomal Instability and Accelerates Cancer Genome Evolution

Sally Marianne Dewhurst

University College London

and

Cancer Research UK London Research Institute

PhD Supervisor: Professor Charles Swanton

A thesis submitted for the degree of

Doctor of Philosophy

University College London

September 2015

Declaration

I, Sally Marianne Dewhurst, confirm that the work presented in this thesis is my own. Where information has been derived from other sources, I confirm that this has been indicated in the thesis.

Abstract

Tetraploidy has long been proposed as an intermediate cellular stage en route to the aneuploidy and chromosomal instability that is observed in many cancer types. Although tetraploidy has been shown to be an unstable cellular state, an in depth analysis of the effect of a spontaneous tetraploidisation event on the cancer genome has not been carried out.

Using an isogenic system of naturally occurring tetraploid cells derived from a chromosomally stable colorectal cancer cell line, the effect of tetraploidisation on genome stability over time was assessed. Tetraploid cells were shown to have increased structural and numerical instability on a per cell but not per chromosome basis. Over time the tetraploid genome became increasingly genomically unstable, which is likely due to the increased ability of tetraploid clones to propagate segregation errors. The genomic landscape of tetraploid clones began to recapitulate the genomic architecture of chromosomally unstable colorectal cancer, and allowed for the selection of clinically high risk chromosomal losses over time. Genome doubling was further shown to be a predictive marker of poor prognosis in colorectal cancer. Exhaustive analysis of DNA and mRNA failed to reveal any common changes in tetraploid clones that are likely to explain their aneuploidy tolerance phenotype. Instead a focussed siRNA screen of genes commonly mutated in genome-doubled tumours of multiple cancer types was carried out.

Given the high-risk clinical phenotypes associated with tetraploidy and chromosomal instability, it remains a priority to identify the mechanisms allowing tumour cells to undergo tetraploidisation and to sustain chromosome segregation errors.

Acknowledgement

I would firstly like to thank my PhD supervisor Charlie for the opportunity to carry out research in his laboratory, as well as for his constant enthusiasm and invaluable advice during the completion of this project.

Secondly I would like to thank all the members of the Translational Cancer Therapeutics Laboratory, past and present, for their encouragement and guidance, as well as for making my time at the LRI thoroughly enjoyable. In particular I would like to thank Andrew Rowan for helping me master new techniques when I first joined the laboratory (and for being invaluable for technical advice throughout), and Rebecca Burrell for her supervision of my project in the early stages. I would also like to thank Laurent Sansregret for his guidance whilst entering the formidable world of siRNA screening, and for his and Eva Gronroos' critical reading of this thesis. Special thanks and acknowledgment must go to Nicholas McGranahan, who has carried out the majority of the bioinformatics analyses presented in this work, and without whom it would not have been possible to publish our jointly first authored paper.

I am grateful to our external collaborators for their provision of data that has contributed to this project, in particular Oliver Sieber and his team in Australia and Marcell Szasz in Hungary.

The excellent core facilities at the LRI have been indispensible in the completion of this thesis. I would like to particularly thank Harshil Patel and Stuart Horswell from Bioinformatics and Biostatistics, Mike Howell and the High-Throughput Screening facility, May Zaw-Thin and the late Francois Lassailly from the In-Vivo Imaging facility, everyone in the Flow Cytometry laboratory and Clare Millum from the Biological Resources Unit. I would also like to acknowledge my thesis committee, Professor Julian Downward and Dr Mark Petronczki for their guidance.

I would finally like to thank my friends and family for their unwavering support.

Table of Contents

List of figures

Chapter 1: Introduction

Chapter 2: Materials and Methods

Chapter 3: Results 1

Chapter 4: Results 2

Chapter 5: Results 3

Chapter 6: Results 4

List of tables

Abbreviations

ANA - Anaphase

BRDu – 5-bromo-2'-deoxyuridine

CDK – Cyclin dependent kinase

CGH – Comparative genome hybridisation

CIN – Chromosomal instability

CKI – Cyclin dependent kinase inhibitor

CPC – Chromosomal passenger complex

CRC – Colorectal cancer

DAPI – 4',6-diamidino-2-phenylindole

DCB – Dihydrocytochalasin-B

DMSO – Dimethyl sulfoxide

DSB – DNA double strand break

ER – Endoplasmic reticulum

FACS – Fluorescence-activated cell sorting

FISH – Fluorescence in-situ hybridisation

FUCCI – Fluorescent ubiquitin- based cell cycle indicator

GD – Genome doubling

H&E – Haematoxylin and eosin

H2B – Histone 2B

HPV – Human papillomavirus

LCC – Last chromosome congressed

LOH – Loss of heterozygosity

MCC – Mitotic checkpoint complex

MIN – Microsatellite instability

MMECs – Mouse mammary epithelial cells

MMR –Mismatch repair

MOSEC – Mouse ovarian surface epithelial cells

MSI – Microsatellite instability

MSS –Microsatellite stable

NBF – Neutral buffered formalin

NEBD – Nuclear envelope breakdown

PI – Propidium Iodide

RFP – Red fluorescent protein

ROS – Reactive oxygen species

RT – Room temperature

SAC – Spindle assembly checkpoint

SCNAs – Somatic copy number aberrations

siRNA – Small interfering ribonucleic acid

SKY – Spectral karyotype

SPB – Spindle pole body

ssDNA – single stranded DNA

TCGA – The Cancer Genome Atlas

TGCs - Trophoblast giant cells

UV light – Ultra-violet light

WES- Whole exome sequencing

wGII – Weighted genome instability index

γH2AX – phosphorylated (gamma) histone variant 2.AX

Chapter 1. Introduction

Intra-tumour heterogeneity has been observed in many different cancer types, and is likely to represent a significant barrier to the effective treatment of advanced disease (Gerlinger et al., 2014, McGranahan and Swanton, 2015). This observed heterogeneity within different regions or cells of the same tumour is likely caused by a multitude of genetic instability processes, coupled with differing selection pressures within the tumour microenvironment. A driver of inter-cellular heterogeneity is chromosomal instability (CIN), the continual alteration of chromosome number and structure across multiple generations (Lengauer et al., 1997). CIN is associated with worse patient prognosis across many different cancer types (McGranahan et al., 2012), as well as with intrinsic drug resistance (Lee et al., 2011). Typically CIN is characterised in tumour cells by high levels of aneuploidy, an unbalanced chromosome number.

Tetraploid cells, with a complete doubling of the diploid chromosome number, have been observed in the early stages of carcinogenesis in several different cancer types, including oesophageal adenocarcinoma and cervical cancer (Galipeau et al., 1996, Olaharski, 2006). Recent genomics analyses have used copy number data to infer that a tetraploidisation, or genome-doubling event is common in the evolution of many different cancer types (Carter et al., 2012, Zack et al., 2013). Tetraploidy has long been suggested to be an unstable cellular state, leading to the production of aneuploid cells (Shackney et al., 1989, Lv et al., 2012). However the relationship between tetraploidy and the dynamic state of CIN has not been fully explored.

Understanding the interplay between different drivers of genetic instability, including tetraploidy, aneuploidy and chromosomal instability is of clear importance to better define their contribution to intra-tumour heterogeneity. In this thesis, a study of the contribution of tetraploidy to the genetic instability observed in colorectal cancer, through in vitro studies combined with bioinformatics analyses has been carried out.

Parts of this thesis have been published as primary research papers and reviews, a full list of which can be found in the Appendix, Section 8.1.

1.1 The mammalian cell cycle

Cell growth and division is tightly controlled in mammalian cells to ensure that cells divide in a timely fashion with a correctly and completely duplicated genome. Furthermore, external signals are integrated into this decision to grow or divide to ensure the correct response to external stimuli such as growth factors. Together this complex signalling network is sometimes called the cell cycle clock, and is governed by the different activities of master cell cycle regulators called cyclins, and their activators and inhibitors (Lim and Kaldis, 2013).

1.1.1 Phases of the cell cycle

The different stages of cell growth and division are commonly divided into phases. There are two 'gap' phases, known as gap 1 (G1) and gap 2 (G2). These phases are separated by the synthesis phase (S phase), where the entire genome is replicated. In G1, cells make critical decisions about whether to continue growing or not, and are responsive to external stimuli. However, once the cell cycle has proceeded past a certain point in G1, originally called the restriction point, or R point, cells are no longer responsive to external stimuli and will proceed through the rest of the cell cycle phases in a manner that is independent of external signalling. After synthesis of DNA during S phase, cells enter the second gap phase G2. During G2 cells prepare for entrance into the next phase, which is mitosis (or M phase). During M phase duplicated DNA is condensed into chromosomes during prophase, aligned at the metaphase plate in metaphase, and each sister chromatid is separated to a daughter cell pole during anaphase. The final stage of M phase is telophase, where the nuclear envelope starts to re-form around each of the daughter nuclei, followed by cytokinesis, the physical separation of the two new daughter cells. A representation of the main cell cycle phases and the stages of mitosis are shown in Figure 1.1.

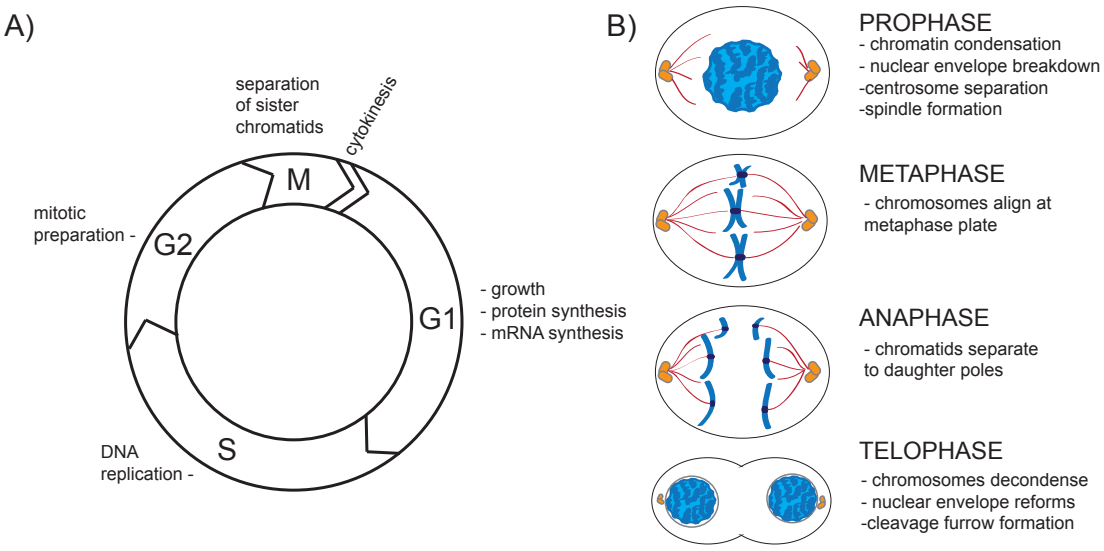

Figure 1.1: The cell cycle and phases of mitosis

A) The phases of the mammalian cell cycle and their functions.
B) The main stages of mitosis.

1.1.2 Cyclins and cyclin dependent kinases

The main drivers of the cell cycle are the cyclin-dependent kinases (CDKs), and their regulatory binding partners, the cyclins. The binding of CDKs, which are serine/threonine kinases, to specific regulatory cyclins activates their catalytic activity. Each CDK has many downstream targets that carry out the activities necessary for each cell cycle phase. Different cyclins are differentially regulated throughout the cell cycle, leading to differential activity of their partner CDKs (Morgan, 1997). In G1 two main CDKs, CDK4 and CDK6 are responsible for driving cell cycle progression in partnership with a family of D type cyclins (cyclin D1, D2 and D3) that are regulated in response to external stimuli. After the restriction point, when cells can no longer respond to external growth cues, CDK2 becomes active when binding to E type cyclins and initiates the entry into S phase. The main regulator of the transition from G1 to S phase is the protein Rb (retinoblastoma), which is hyper-phosphorylated by cyclin E-CDK2 complexes, and leads to dissociation with E2F transcription factors that govern the entry of the cell into S phase. During S phase CDK2 binds to A-type cyclins, allowing S phase progression. At the culmination of S phase the A-type cyclins dissociate from CDK2 and bind to CDC2 (also called CDK1). As G2 phase commences A-type cyclins are

replaced by B-type cyclins. The complexes of CDC2 and B-type cyclins drive many of the processes necessary for entry into M phase.

Control of cell cycle progression is maintained by differential activity of these different cyclin-CDK complexes. The main regulation of these complexes is through the rapid degradation and gene transcription of different cyclins in different phases of the cell cycle (Morgan, 1997). This concerted regulation of cyclin-CDK activity ensures that the cell cycle can only proceed in one direction.

1.2 Polyploidy in normal development

Polyploidy describes cells with multiple complete sets of the normal diploid complement of homologous chromosomes. Tetraploidy is a specific type of polyploidy in which a cell has twice the normal chromosome number. Whole organism polyploidy is common among some genera, in particular plant species (Otto and Whitton, 2000). However, among mammals there are no known cases of polyploid organisms (Svartman et al., 2005). The fact that whole-organism polyploidy is likely to be incompatible with survival in mammals is illustrated by the fact that 20% of human miscarriages caused by chromosomal abnormalities are due to polyploidy (Stephenson and Kutteh, 2007).

Although polyploidy is not observed in mammals at the whole-organism level, there are several examples of specialised cell types that display polyploidy.

1.2.1 Placental giant trophoblast cells

Trophoblast giant cells (TGCs) are extra-embryonic cells that are important for the correct implantation of the fertilised egg into the placenta during embryogenesis (Zybina and Zybina, 1996, Hu and Cross, 2010). TGCs arise from the trophoectoderm of the blastocyst, and undergo repeated rounds of endocycling, in which cells cycle from G1 to S phase of the cell cycle with no cell division (Lee et al., 2009). This results in highly polyploid cells containing polytene chromosomes, where the replicated sister chromatids remain synapsed together (Lee et al., 2009).

The specialised endocyling in TGCs involves reduced association of cyclin B and CDK1 during G2 phase, which is likely to be caused by inhibition of CDK1 by p57 (Ullah et al., 2008). Subsequent oscillations of p57 protein levels are thought to define the two phases of the endocycle: a G2 phase in which p57 levels are high, and a G1 phase where p57 levels decline before entry into S phase (Hattori et al., 2000).

In general it is thought that cell volume increases alongside genome size (Gregory, 2001), and therefore polyploidisation could be an efficient way to grow specialised tissues without expending excess energy, for example on new membrane synthesis during cell division (Lee et al., 2009). The exact function of the polyploidy observed in TGCs is not known, however it has been speculated that the synthesis of DNA without cell division conserves energy that can be used for protein synthesis (Hu and Cross, 2010). The continual replication without mitosis could also be a method to protect against tumour formation in a cell type that is specialised to invade the local placenta (Hemberger, 2008).

1.2.2 Megakaryocytes

Megakaryocytes are blood cells that are responsible for the formation of thrombocytes (platelets). These cells go though a normal mitosis forming daughter nuclei, but cytokinesis fails, leading to a polyploid cell with two nuclei. The cytokinesis failure is thought to occur due to low levels of cyclin B/Cdk1 complexes (Ravid et al., 2002). The newly formed nuclear envelopes break down and the DNA is encompassed into one nucleus (see Figure 1.2B). The cell can re-enter S phase from this G1 like state may times, resulting in cells with up to 128N (diploid =2N) DNA content (Ravid et al., 2002).

The polyploidisation of megakaryocytes is associated with an increase in cell size, mRNA and protein synthesis (Ravid et al., 2002). Since the function of these cells is to produce large amounts of thrombocytes, it may be more energy efficient to increase cell size and production capacity by increasing DNA content rather than by cell number (Davoli and de Lange, 2011).

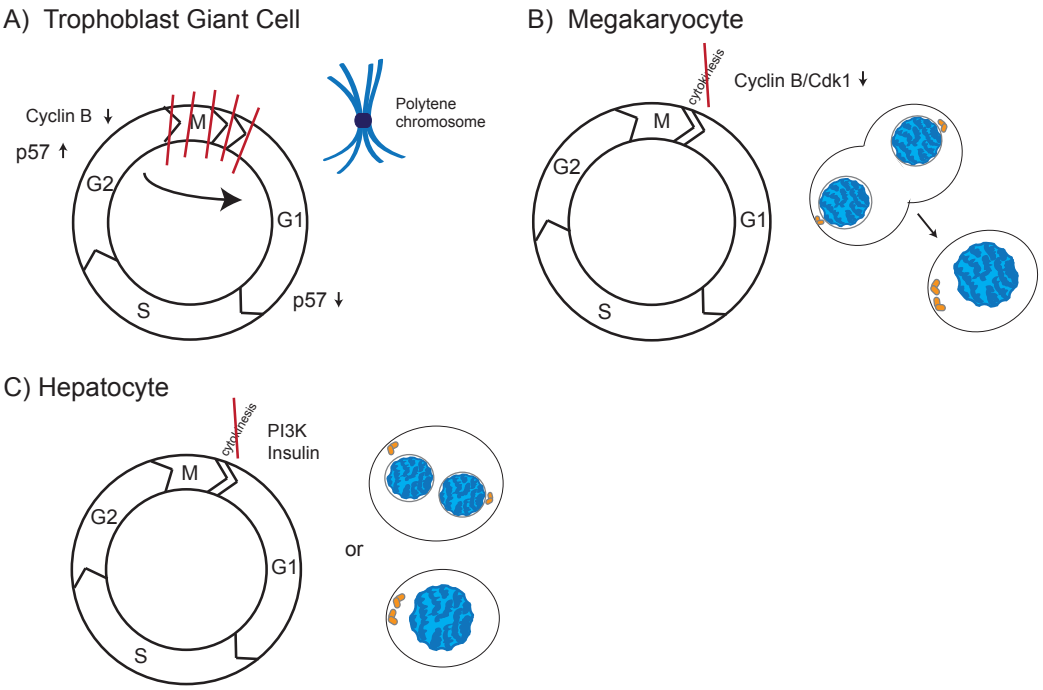

Figure 1.2: The cell cycles of specialised polyploid somatic cells

A) The specialised endocycle of a TGC. The cell cycles continuously between G1, S and G2, skipping mitosis (M) completely. Chromosomes are not separated after G2, and hence form polytene chromosomes.
B) After cytokinesis failure, binucleated megakaryocytes will become mononucleated.
C) Hepatocytes can either be multinucleated or mononucleated after cytokinesis failure. For references see text.

1.2.3 Hepatocytes

In mammalian liver the incidence of polyploid cells increases as the organ develops (Gupta, 2000). In fact, in adult humans 40% of all liver cells are tetraploid (Toyoda et al., 2005). The formation of polyploid cells in rodent liver occurs due to failure to establish a cleavage plane during cytokinesis, likely due to defects in the recruitment of Rho GTPase because of altered cytoskeletal dynamics (Margall-Ducos et al., 2007). It was shown that signalling from insulin through the Phosphoinositide-3 kinase (PI3K)/Akt (Protein kinase B) pathway leads to increased cytokinesis failure, and as such, inhibition of Akt prevented formation of tetraploid hepatocytes (Celton-Morizur et al., 2009).

In normal development it is not clear what function the polyploidisation of hepatocytes plays. It has been suggested that as liver tissue is exposed to high levels of environmental stress, including the metabolism of toxic compounds, that increased polyploidy can protect cells from genotoxic stress (Gentric et al., 2012). In support of this hypothesis, the levels of endoreduplication in the liver increase in response to DNA damage induced by telomere dysfunction (Lazzerini Denchi et al., 2006). In this way the liver can regenerate using growth of endoreduplicating cells instead of through cell division, which is inhibited when the genome has been subjected to extensive DNA damage (Lazzerini Denchi et al., 2006). Polyploidy in the normal liver could also be a mechanism for triggering particular patterns of gene expression that may be associated with promoting cell survival in stressful conditions (Anatskaya and Vinogradov, 2007).

It has been shown that as well as increasing their ploidy, hepatocytes can undergo reductive rounds of cell division to create a genetically diverse pool of cells (Duncan et al., 2010). These reductive cell divisions often involved multipolar mitosis, where chromosomes are randomly segregated into multiple daughter cells, resulting in aneuploidy. Specific chromosome aneuploidies in liver cells have been shown to lead to resistance to chronic liver injury (Duncan et al., 2012), suggesting that formation of diverse aneuploid daughter cells in the liver could be advantageous in response to exogenous stresses.

1.2.4 Polyploidy incidence under stress

As described above, the incidence of polyploidy (via endoreduplication) in liver hepatocytes increases in response to genotoxic stress caused by telomere dysfunction (Lazzerini Denchi et al., 2006). An increase in the ploidy of liver cells is also observed after oxidative stress (Gorla et al., 2001). A similar increase in polyploidy under varied exogenous stresses has been observed in other tissue types, including cardiac tissue after myocardial infarction (Meckert et al., 2005), and in inflamed bronchial lesions (Lothschutz et al., 2002). It has been suggested that this increase in polyploidy under stressful conditions could help tissue recovery and growth in scenarios where the genome may be compromised (Lee et al., 2009),

although the specific function of polyploidisation in most of these scenarios remains unknown. It is possible that polyploidisation in these instances reflects general cellular dysfunction after stress resulting in failure to complete normal cell cycles, rather than a specialised function. However, the activation of specific gene expression profiles after polyploidisation in both liver and heart tissue suggest that polyploidisation can act as a tool for adaptation to stress (Anatskaya and Vinogradov, 2010). For example in the heart, polyploidisation results in up-regulation of more energy efficient contractile proteins such as beta myosin heavy chain, and coincident down-regulation of energy intensive proteins such as alpha myosin heavy chain which utilises three times as much ATP (Anatskaya and Vinogradov, 2010).

1.3 Evidence for polyploidisation in cancer

Many in vitro studies and in vivo observations indicate that tetraploidy could occur as an early event during tumour formation and progression. It has been shown that tetraploidy occurs alongside spontaneous neoplastic transformation in different rodent cell lines when cultured in vitro (Hsu et al., 1961, Barski and Cassingena, 1963, Jackson et al., 1970), and that transformation of normal fibroblasts with SV40 can also lead to tetraploidisation (Cooper and Black, 1963, Moorhead and Saksela, 1965). Polyploid cells are observed in different cancer types with varying frequency. Many tumour types exhibit a distinct bimodal pattern of chromosome numbers, with a peak near diploid chromosome numbers (46 chromosomes) and a second peak with triploid or near-tetraploid chromosome numbers (Mitelman F, 2015, Storchova and Kuffer, 2008, Davoli and de Lange, 2011). This suggests that many tumours may have undergone polyploidisation at some point in their evolutionary histories, as tumours with high numbers of chromosome are more likely to have arisen in a single tetraploidisation event generating twice as many chromosomes, compared to continued chromosome non-disjunction resulting in chromosome increases (Storchova and Kuffer, 2008, Davoli and de Lange, 2011).

1.3.1 Tetraploidy and aneuploidy in cancer

A model to describe the origin of tumours with high chromosome numbers was first proposed by Shackney and colleagues in 1989 (Shackney et al., 1989). They

proposed that a tetraploidisation event followed by chromosome loss is the most likely route to aneuploid tumour cells with high numbers of chromosomes, based on computer simulations, but also on cytogenetic evidence suggesting that tetraploidy and subsequent chromosome losses are common events in multiple different cancer types (Shackney et al., 1989). In the pre-malignant condition of Barrett's oesophagus that predisposes patients to the onset of oesophageal adenocarcinoma, tetraploid cells are observed before the onset of aneuploidy and progression to malignant disease (Galipeau et al., 1996). Of 75 patients whose disease did not initially show an increase in the 4N cell fraction, only 11% progressed to aneuploidy in subsequent biopsies. However, in the 15 patients who initially had elevated levels of 4N cells, 73% progressed to aneuploidy. The presence of 4N cells was significantly correlated with loss of the chromosome region 17p, which harbours the tumour suppressor gene *TP53* (Galipeau et al., 1996). In cervical cancer tetraploidy has also been implicated as a precursor to aneuploidy. In a study of 143 patient samples of cervical malignancy, tetraploidy (as assessed by dual chromosome probes for chromosome 3 and 17) was frequently observed without aneuploidy (23.8% of cases) (Olaharski, 2006). However, it was rare to observe aneuploidy without tetraploidy (only 4.2% of cases). Indeed, when aneuploid cells were observed, they were commonly near-tetraploid aneuploid (74.3% of cases). This suggests that tetraploidy is an early event in cervical carcinogenesis and is likely to precede aneuploidy development (Olaharski, 2006).

A careful in vitro analysis of the transformation of mouse surface ovarian cells has also shown that tetraploidy can lead to aneuploidy (Lv et al., 2012). Mouse ovarian surface epithelial cells (MOSECs) can be cultured in vitro as a model to characterise ovarian carcinogenesis (Roberts et al., 2005). Lv and colleagues utilised this model to observe changes in ploidy and chromosome number during carcinogenic progression (Lv et al., 2012). The proportion of diploid cells in a MOSEC culture decreased steadily until passage 36, when they were no longer present. In contrast, the percentage of tetraploid cells increased through culture. Using chromosome counting from metaphase spreads, fluorescence in situ hybridisation (FISH) and live cell imaging, the authors showed that the first

aneuploid cells to emerge were near-tetraploid aneuploid, and concluded that aneuploid MOSECs are derived from tetraploid cells (Lv et al., 2012).

Taken together these studies indicate that tetraploidy is likely to be a frequent event in cancer that can predispose to the onset of aneuploidy. How tetraploid cells can lead to aneuploidy is discussed in Section 1.10.

1.3.2 Inference of polyploidisation from genomics studies

In recent years there has been a dramatic rise in the number of tumours being subjected to genomics analysis, predominantly through next-generation sequencing (Koboldt et al., 2013). Using advanced bioinformatics tools has allowed researchers to reconstruct the evolutionary histories of tumours in unprecedented detail (Nik-Zainal et al., 2012). Analysing the sub-clonal architecture of one particular breast cancer sequenced to a high depth revealed a sub-clone that was likely to have undergone tetraploidisation, with subsequent chromosome losses affecting 11 chromosomes (Nik-Zainal et al., 2012). This indicates that tetraploidy can occur as a late event in tumours.

The frequency of tetraploidisation has also been inferred from tumour copy number data (Carter et al., 2012). Carter and colleagues devised a bioinformatics method for assigning copy number information across the whole genome of cancer samples using either massively parallel sequencing or DNA microarrays. Many tumours that were analysed exhibited a bimodal distribution of copy numbers, similar to previous observations (Storchova and Kuffer, 2008, Mitelman F, 2015). In order to ascertain whether the high ploidy copy numbers were more likely to have arisen from a single whole genome duplication followed by copy number loss, or through sequential gains of individual chromosomes, the authors developed a bioinformatics algorithm to infer the most likely route by which the copy number state of individual tumours occurred (Carter et al., 2012). If a tumour undergoes whole genome duplication, then both homologous chromosomes will be present at two copies across the whole genome. If there is subsequent loss of genetic material from one chromosome, then that chromosome will be reduced to an odd

copy number (i.e. a copy number of one). However the other allele will still be present at an even number of copies (i.e. two copies) throughout the genome (see Figure 1.3). When the authors assessed the allele-specific copy number of higher ploidy samples, they found that the higher of the two alleles (also called the major allele) tended to have an even copy number across the majority of the genome (Carter et al., 2012). Using simulations of multiple chromosome gains compared to a single whole genome duplication event, they found that higher copy number states were significantly more likely to have occurred through genome doubling ($P<10^{-3}$) (Carter et al., 2012).

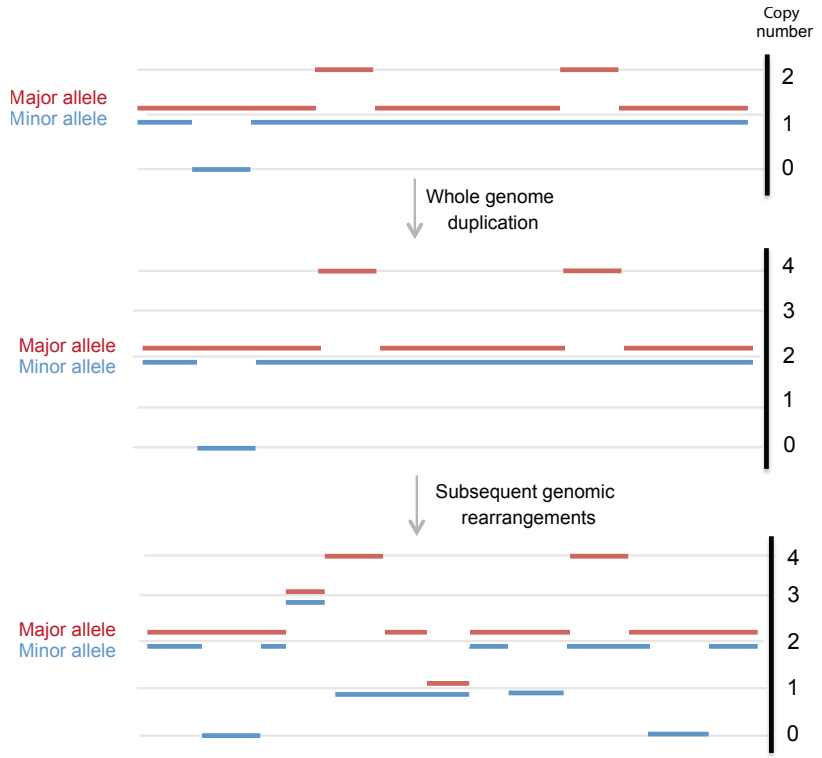

Figure 1.3: Assessing copy number state after whole genome duplication

A representation of the possible copy number changes after whole genome duplication. Even after complete duplication and subsequent copy number loss, the major allele will have a copy number of two across the majority of the genome. Carter and colleagues devised an algorithm to assess whether the copy number state of tumours was likely to have occurred through genome duplication or sequential gains of individual chromosomes (Carter et al., 2012).

The frequency of genome doublings was varied across the different cancer types analysed, which included acute lymphoblastic leukemia, myeloproliferative disease, glioblastoma multiforme, renal cell carcinoma, prostate cancer, sarcomas,

hepatocellular carcinoma, medulloblastoma, liposarcoma, colorectal cancer, breast cancer, high-grade serous ovarian carcinoma, lung adenocarcinoma and oesophageal adenocarcinoma. Genome doubling was almost completely absent from the hematopoietic malignancies, and most common in epithelial cancers. Oesophageal adenocarcinoma had the highest incidence of genome doubling, which is consistent with the known involvement of tetraploidy at early disease stages (Galipeau et al., 1996, Maley, 2007).

An extension of this work by the same group also showed genome doubling to be a common event across different cancer types, ranging from 11% of samples in glioblastoma multiforme to 64% of squamous cell lung cancer samples (Zack et al., 2013). Tumours that showed evidence of whole genome doubling had higher rates of every type of copy number aberration analysed, including focal aberrations and arm-level aberrations, but especially deletions (Zack et al., 2013). The authors speculate that genome duplication is an early event in the majority of cancers they analysed, as most aberrations appear to occur after genome doubling.

Taken together, these studies show that polyploidisation is likely to be an important driver of cancer evolution. It appears as though tetraploidy is frequently a precursor to aneuploidy in tumours and in in vitro studies (Galipeau et al., 1996, Olaharski et al., 2006 2012). Sophisticated analysis of copy number data from multiple cancer types has also shown that genome duplications are common events, which in many cases precede further genomic alterations (Carter et al., 2012, Zack et al., 2013).

As discussed above, polyploidy is not well tolerated in mammals at the whole organism level. However unscheduled polyploidisation clearly occurs relatively frequently in cancer. The cell cycle checkpoints normally maintaining a diploid chromosome complement throughout the cell cycle, and the mechanisms that can generate tetraploid cells and result in whole genome duplication in tumours will now be considered.

1.4 Cell cycle checkpoints

Although the phases of the cell cycle are carefully coordinated, as discussed in Section 1.1, the capacity to halt progression must still exist in order to ensure the integrity of the genome. This function is mainly carried out by cyclin-dependent kinase inhibitors (CKIs), which inhibit the function of cyclin-CDK complexes. CKIs can be broadly categorised into two classes: the INK4 proteins ($p16^{INK4a}$, $p15^{INK4b}$ $p18^{INK4c}$ and $p19^{INK4d}$), which inhibit CDK4 and CDK6 in G1, and the Cip/Kip proteins ($p21^{Cip1}$, $p27^{Kip1}$ and $p57^{Kip2}$), which inhibit all of the other cyclin-CDK complexes (Sherr and Roberts, 1999). Various signalling checkpoints activate these CKIs to halt progression of the cell cycle and ensure the integrity of the DNA. These cell cycle checkpoints are discussed below.

1.4.1 DNA damage checkpoints

The DNA in cells is constantly susceptible to damage, from both exogenous and endogenous sources. Endogenous biochemical processes such as deamination, where the amine groups of bases are lost, can damage DNA. This can lead to transition mutations as deaminated bases get mis-read by replication machinery (Lindahl and Barnes, 2000). Spontaneous deamination is particularly common at 5-methlycytosine bases, and particularly dangerous, as it forms a natural thymine product that is not recognised as an incorrect base. DNA damage can also arise spontaneously from errors in DNA replication and repair. These spontaneous DNA damage processes have been estimated to result in up to 10^5 lesions per cell per day (Hoeijmakers, 2009). DNA can also be affected by multiple exogenous sources. Ionising radiation can cause both single and double strand breaks through the generation of reactive oxygen species (ROS). Ultra-violet (UV) light also affects DNA, resulting in the formation of covalent bonds between adjacent pyrimidine bases (called pyrimidine dimers). Furthermore, a variety of chemical compounds that enter cells from exogenous sources can cause DNA damage, such as the alkylation of DNA bases by alkylating chemotherapeutic agents.

Multiple pathways exist to repair different types of DNA damage, and DNA repair is normally coordinated by cell cycle phase. There are three main checkpoints that

operate in cells in response to DNA damage. These are the G1/S phase checkpoint, the intra-S phase checkpoint and the G2/M checkpoint. The DNA damage response is primarily activated by two different kinases ATM (ataxia telangiectasia mutated) and ATR (ATM and Rad-3 related) that mediate the DNA damage response through activation of their downstream targets the checkpoint kinases CHK1 and CHK2 (Stracker et al., 2009). ATM is predominately activated in response to double strand breaks (DSBs) and ATR in response to single-stranded DNA (ssDNA) which can be formed during DNA repair processes and also at stalled or collapsed replication forks (Ciccia and Elledge, 2010). Recruitment of ATM to DSBs results in the phosphorylation of the histone variant H2AX by ATM, resulting in phospho-H2AX (known as γ-H2AX), which is commonly used as a marker for DNA damage (Bonner et al., 2008).

1.4.1.1 The G1/S checkpoint

It is important for a cell not to enter S phase with damaged DNA to avoid copying errors into the newly synthesised DNA strand. Therefore at the boundary between G1 and S phase, DNA damage signalling through ATM and CHK2 results in the phosphorylation and destruction of CDC25 phosphatase, which controls CDK activity at the G1-S boundary, thereby blocking S phase entry by inhibition of cyclin E-CDK2 activity (Mailand et al., 2000, Falck et al., 2001). CHK2 further inhibits cell cycle progression indirectly through the degradation of MDM2, which normally ubiquitinates p53, thereby resulting in up-regulation of p53 and its downstream target, the CKI $p21^{Cip1}$ (Chen et al., 2005, Jin et al., 2006). DNA damage also results in the up-regulation of one of the INK4 proteins, $p16^{INK4a}$, which prevents the hyper-phosphorylation of Rb and results in G1 arrest (Gil and Peters, 2006). Cells with defective p53 or Rb signalling responses cannot sustain a G1 arrest (Kuerbitz et al., 1992, Bunz et al., 1998).

1.4.1.2 The intra-S phase checkpoint

During replication DNA is subject to damage, usually occurring near the replication fork. Stalled or collapsed replication forks results in single stranded DNA tracts

which become coated in the ssDNA binding protein RPA (heterotrimeric replication protein A) which recruits ATRIP, the targeting subunit of ATR (Zou and Elledge, 2003). Subsequent stimulation of ATR by TOPBP1 results in the activation of the ATR signalling cascade (Mordes et al., 2008). Downstream checkpoint signalling at replication forks is additionally controlled by Claspin, which mediates CHK1 phosphorylation by ATR (Kumagai and Dunphy, 2000). Unlike the G1-S phase checkpoint, the intra-S checkpoint is a transient arrest that functions to allow the re-start of stalled replication forks. Inhibition of CDK2 by the intra-S phase checkpoint results in a delay of several hours to S phase completion (Falck et al., 2001).

1.4.1.3 The G2/M checkpoint

DNA damage that is sensed in G2 results in cell cycle arrest in order to prevent a cell entering mitosis and segregating damaged DNA to the new daughter cells. Both the ATM and ATR signalling pathways tend to be activated together in G2. ATM is activated by DSBs as in G1, but the resection of DSBs for repair by homologous recombination also results in ATR activation (Jazayeri et al., 2006). The activation of CHK1/2 leads to cell cycle arrest through the inhibition of CDC25, which subsequently cannot activate CDC2-cyclin B complexes, and therefore entry into M phase is inhibited. Unlike the G1-S checkpoint, the G2-M checkpoint is not dependent on p53, so p53 mutant cells can still display a G2 arrest in response to DNA damage (Kastan and Bartek, 2004).

1.4.2 The spindle assembly checkpoint and error correction machinery

As well as responding to DNA damage to ensure genome integrity, the events during M phase must be coordinated to ensure that one copy of each sister chromatid is segregated to each new daughter cell. The timely segregation of chromosomes is controlled by the spindle assembly checkpoint (SAC), whilst the error correction machinery monitors incorrect kinetochore-microtubule attachments.

After prophase, when chromosomes have condensed, the spindle apparatus must correctly attach to all kinetochores so that when anaphase begins, sister

chromatids are pulled to opposite poles (Figure 1.1B). The entry into anaphase is initiated by the anaphase promoting complex (APC/C), a E3 ubiquitin ligase that degrades cyclin B and securin, allowing mitotic exit and chromosome separation (Pines, 2011). Unattached kinetochores assemble complexes that signal to and inhibit the APC/C, delaying anaphase until all chromosomes are attached to the spindle (Rieder et al., 1995). The signal at kinetochores that inhibits the APC/C is called the mitotic checkpoint complex (MCC). It is generated by a network of proteins that assemble at unattached kinetochores known as the KMN network (Sacristan and Kops, 2015). The KMN network is composed of KNL1-C, MIS12-C and NDC80-C protein complexes (DeLuca and Musacchio, 2012, Lara-Gonzalez et al., 2012). The formation of the MCC at kinetochores is regulated by the kinase MPS1, which is associated with the NDC80-C part of the KMN network (Nijenhuis et al., 2013). MPS1 then recruits other SAC proteins to the kinetochores, including BUB1, BUB3, MAD1, MAD2 and BUBR1/Mad3 (Sacristan and Kops, 2015). The assembly of the MCC complex at kinetochores inhibits the APC/C through inhibition of CDC20. The precise role for all the proteins present at the kinetochore in the MCC has not yet been established, but it is clear that MAD2 and BUBR1 are critical for the correct binding and inhibition of the APC/C (Sudakin et al., 2001, Herzog et al., 2009, Sacristan and Kops, 2015). Once a kinetochore is correctly attached to the spindle, MAD20 is removed from kinetochores by transport along microtubules (Howell et al., 2001). Once all kinetochores are attached, there is no longer inhibition of the APC/C, leading to ubiquitination of its substrates cyclin B and securin. The degradation of securin leads to separase activation. Separase cleaves the cohesion complexes which hold sister chromatids together during metaphase, resulting in their separation (Reddy et al., 2007, Pines, 2011).

A second important point of regulation during M phase involves the ‘error correction machinery’ that corrects kinetochore-microtubule attachment errors. Incorrect attachments include syntelic attachments, where both sister chromatids are attached to the same pole, or merotelic attachments, where one kinetochore is attached to both poles (see Figure 1.4A and Cimini et al., 2001). These types of attachment can satisfy the SAC, as kinetochores are attached to microtubules, but may result in lagging chromosomes and chromosome non-disjunction (Cimini et al., 2001, Cimini et al., 2002). Hence, it is important that error correction machinery

exists during M phase to correct these errors. Improper-kinetochore microtubule attachments are monitored by the activity of Aurora kinase B (Aurora B) and the chromosomal passenger complex (CPC) (see Figure 1.4B and Hauf et al., 2003).

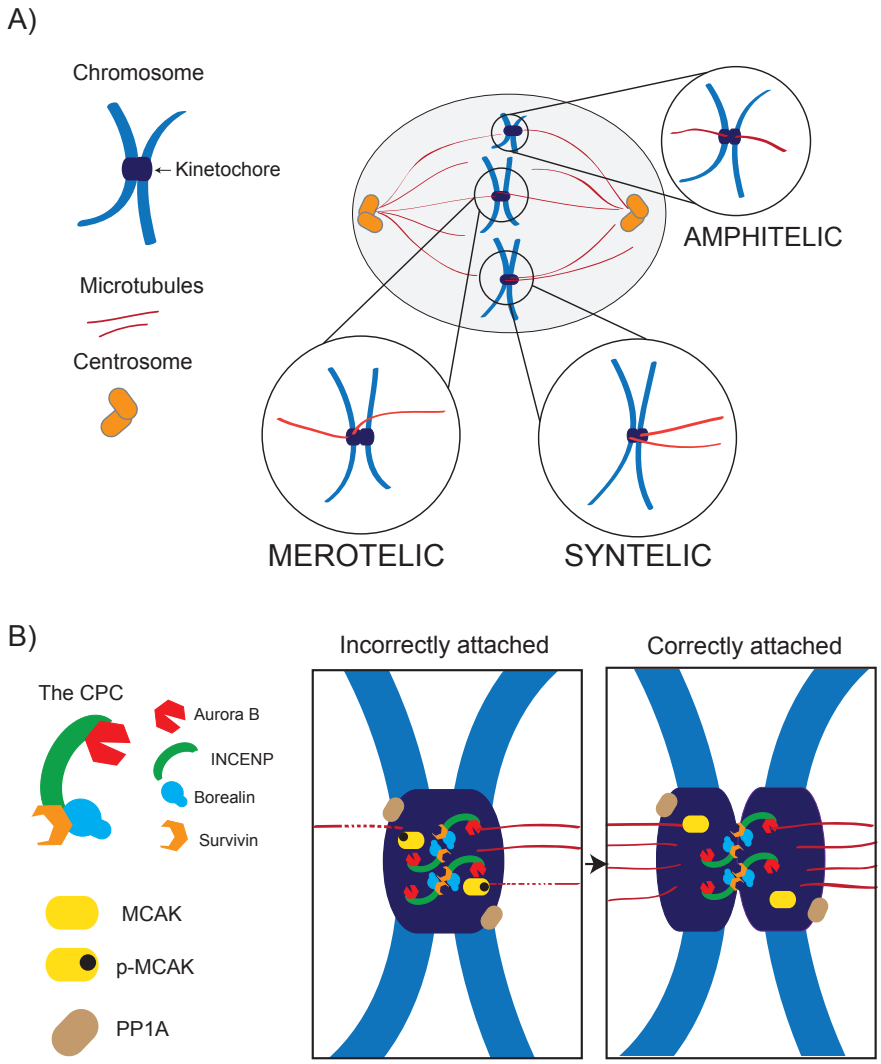

Figure 1.4: Kinetochore-microtubule attachment and error correction

A) Different types of kinetochore-microtubule attachments. Amphitlelic attachments occur when each kinetochore is correctly attached to both spindle poles. Merotelic attachments mean one kinetochore is attached to both spindle poles, and syntelic attachments are where both kinetochores are attached to one pole.
B) The mechanism of error correction at incorrectly attached kinetochores. The Chromosomal Passenger Complex (CPC) is located at the inner kinetochore. When there is no tension between sister chromatids the CPC is able to phosphorylate targets such as MCAK, which destabilises microtubules. Upon correct amphitelic attachment, the CPC is no longer able to phosphorylate its targets, and substrates such as MCAK as dephosphorylated by phosphatases such as PP1A, which is located at the outer kinetochore.

Aurora B is the catalytic component of the CPC, which is also comprised of Survivin, Borealin and INCENP (Ruchaud et al., 2007). The CPC is localised to the centromere, and in the absence of the correct microtubule tension emanating from opposite poles, it can access its substrates in the outer kinetochore and phosphorylate them (Liu et al., 2009). All components of the CPC are essential for its localisation to centromeres during mitosis (Honda et al., 2003, Klein et al., 2006). One of the most important substrates of the CPC is the microtubule depolymerase MCAK (mitotic centromere-associated kinesin, also called Kif2c) (Andrews et al., 2004). When activated by the CPC, MCAK destabilises microtubules and therefore removes the incorrect attachment (Liu et al., 2009). Aurora B also destabilises microtubule attachments through phosphorylation of the N-terminal tail of NDC-80, one of the KMN network components, as well as other proteins present at the kinetochore such as KNL1 and Mis12 (DeLuca et al., 2006, Welburn et al., 2010). When a kinetochore is correctly attached to spindles emanating from both poles, it is hypothesised that tension pulls sister kinetochores apart, meaning the CPC can no longer access important substrates such as MCAK (Tanaka et al., 2002, Lampson et al., 2004). Furthermore, when balanced (amphitelic) attachments are created, a counteracting phosphatase to Aurora B called protein phosphatase 1 (PP1) dephosphorylates Aurora B targets at the outer kinetochore, resulting in the stabilisation of attachments (Liu et al., 2010a). However, if merotelic attachments create sufficient tension across the kinetochore to prevent Aurora B kinase activity, then these mis-attachments can go undetected, and result in lagging chromosomes (Cimini et al., 2001, Cimini et al., 2002).

1.4.3 Regulation of cytokinesis – the abscission checkpoint

As well as controlling the separation of chromosomes during M phase, cells must also coordinate cytokinesis to complete the correct segregation of DNA into two daughter cells. At the onset of cytokinesis the mitotic spindle undergoes reorganisation to form a dense array of anti-parallel filaments at the equator of the cell, which is known as the spindle mid-zone (Fededa and Gerlich, 2012). There is subsequent formation of a contractile ring around the spindle mid-zone, which is composed of actin and myosin filaments. Myosin II activity at the contractile ring provides the main force that results in the constriction of the cell membrane,

forming a cleavage furrow (Robinson and Spudich, 2004, Nagasaki et al., 2002). As the cleavage furrow ingresses, the cytoplasm becomes separated, eventually only being joined by a narrow bridge formed by a dense array of microtubules that are joined at the centre by a structure known as the mid-body (or Flemming body) that anchors the cleavage furrow (Mullins and Biesele, 1977, Fededa and Gerlich, 2012). The final stage in cytokinesis is abscission, where the plasma membrane is split between the two daughter cells. Abscission is mediated by a group of proteins called the ESCRT complex (Endosomal Sorting Complex Required for Transport) (Carlton and Martin-Serrano, 2007, Morita et al., 2007, Hurley and Hanson, 2010).

The events of cytokinesis need to be regulated to ensure all chromosomes have properly segregated into two daughter cells to avoid aneuploidy. Furthermore, it has been shown that chromosomes trapped in the mid-zone during cleavage furrow formation can sustain significant DNA damage (Janssen et al., 2011). Hence it is crucial that the events of cytokinesis are coupled to the segregation of DNA during mitosis to ensure genomic integrity. In yeast, the presence of DNA in the cleavage furrow results in regression of the furrow and cessation of cytokinesis. The pathway controlling this regression is termed the NoCut pathway (Norden et al., 2006, Mendoza et al., 2009). It is thought that a similar checkpoint exists in mammalian cells that is regulated by Aurora B kinase signalling (Steigemann et al., 2009). A subunit of the ESCRT complex, CHMP4C, was shown to be involved in the regulation of abscission delay in response to trapped chromatin (Carlton et al., 2012). CHMP4C was shown to bind the CPC through interaction with Borealin, and inhibited abscission upon phosphorylation by the active kinase of the CPC, Aurora B (Carlton et al., 2012). It was recently shown that a novel protein ANCHR (Abscission/NoCut Checkpoint Regulator; ZFYVE19) can regulate this checkpoint though spatial regulation of another member of the ESCRT complex, VSP4 (Thoresen et al., 2014). VSP4 normally catalyses the final step in membrane abscission through its ATPase activity (Carlton and Martin-Serrano, 2007, Morita et al., 2007, Hurley and Hanson, 2010). The association of ANCHR and CHMP4C are proposed to act by tethering VSP4 to the mid-zone and preventing its re-localisation to the abscission zone (Thoresen et al., 2014). A key future direction will be to identify how Aurora B is activated in response to trapped chromatin to control this abscission checkpoint.

1.5 The generation of tetraploid cells in cancer

Despite the multitude of cell cycle checkpoints that exist in mammalian cells, polyploidy is observed frequently in cancer (as discussed in Section 1.3). The different ways in which these tetraploid cells could arise are described below, and also depicted in Figure 1.5.

1.5.1 Cytokinesis failure

Gross abnormalities in mitosis that result in chromatin lagging within the cleavage furrow result in the failure of cytokinesis (Mullins and Biesele, 1973, Mullins and Biesele, 1977). If cytokinesis fails to complete a binucleated tetraploid cell will be formed. If this cell can continue to subsequent rounds of cell division it will likely form a mononucleated tetraploid cell. The signalling pathways responsible for cleavage furrow regression in response to trapped DNA are just beginning to be elucidated (see Section 1.4.3). Many different defects can lead to chromatin lagging at the cleavage furrow, and so this mechanism could potentially account for a proportion of the tetraploid cells observed in cancer (Davoli and de Lange, 2011).

Chromosome non-disjunction has also been shown to lead to cytokinesis failure and tetraploidy, rather than aneuploidy (Shi and King, 2005). Increasing the rate of chromosome missegregation by genetic and chemical means resulted in a higher frequency of binucleated daughter cells in HeLa cells and immortalised keratinocytes. However the majority of binucleated tetraploid cells appeared to arise from a normal bipolar mitosis, but that underwent delayed regression of the cleavage furrow (an average of 13.6 hours after mitosis) (Shi and King, 2005). Upon analysis of the chromosome copy number status of these cells by FISH, the authors estimated that 94% of binucleated cells were likely to have undergone chromosome non-disjunction. However, binucleation did not appear to be tightly coupled with lagging chromosomes or bridges, but rather the presence of a missegregated chromosome in the daughter nuclei. Although there is no mechanistic basis proposed for how a missegregated chromosome could lead to cleavage furrow regression, this intriguing finding could explain why tetraploid cells

are frequently seen in cancer, since many tumour cells exhibit high levels of chromosome missegregation (Lengauer et al., 1997, Shi and King, 2005, King, 2008). However, the generality of this mechanism has yet to be proven, as defects in SAC activation can directly lead to aneuploid cells, and so chromosome non-disjunction cannot always be coupled with cytokinesis failure (King, 2008).

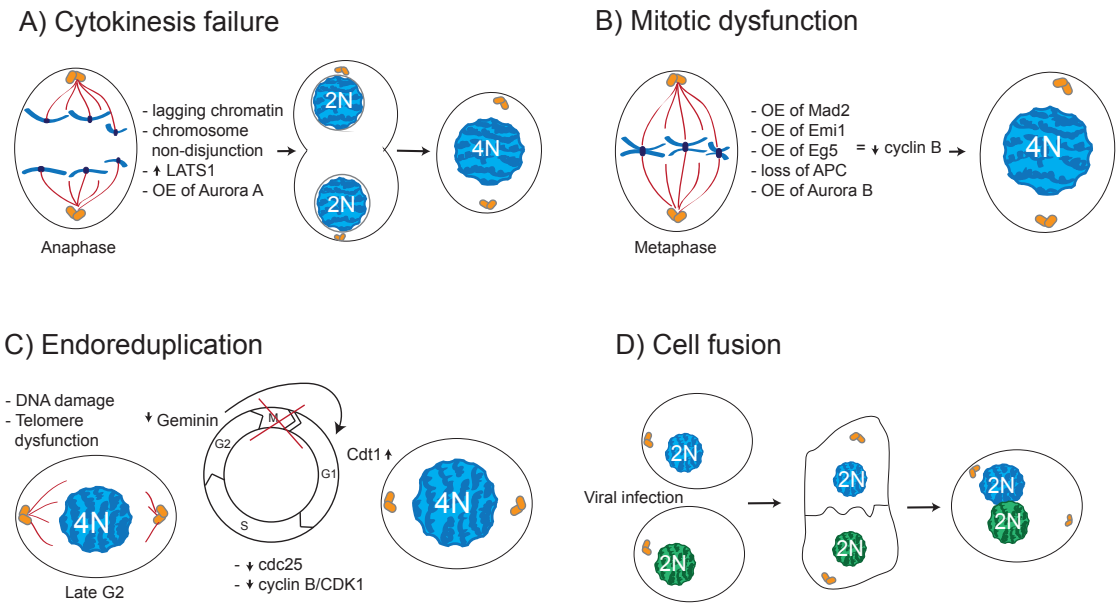

Figure 1.5: Proposed mechanisms of tetraploidisation in cancer

A) Cytokinesis failure generates tetraploid cells. OE = over expression.
B) Mitotic dysfunction can lead to cells exiting mitosis with duplicated DNA
C) Endoreduplication is a specialised cell cycle that skips mitosis.
D) The fusion of two diploid cells will create a tetraploid cell. For references see text.

Defects in several different signalling pathways have also been shown to lead to cytokinesis failure and the production of tetraploid daughter cells. Inhibition of the kinase large tumour suppressor 1 (LATS1) results in cytokinesis failure (Yang et al., 2004). LATS1 regulates cytokinesis through its regulation of the kinase LIMK1, which controls actin polymerisation at the contractile ring (Yang et al., 2004). Overexpression of the mitotic kinase Aurora A has also been shown to lead to an abortive cytokinesis and subsequent increase in binucleated daughter cells (Meraldi et al., 2002). Aurora A is also amplified or overexpressed in many solid tumour types (Nikonova et al., 2013).

1.5.2 Mitotic dysfunction

Prolonged arrest in mitosis by the SAC can lead to cells escaping mitosis, and returning to a G1 phase, but with a duplicated DNA content (Elhajouji et al., 1998). This is known as mitotic slippage. The escape from mitosis is brought about by gradual degradation of cyclin B, which eventually falls below a critical threshold to maintain mitosis, and the cell escapes into G1 phase (Brito and Rieder, 2006). Unlike cytokinesis failure, mitotic slippage will result in a mononucleated tetraploid daughter cell (Figure 1.5B). A variety of cell cycle defects can lead to tetraploid cells after mitotic slippage. Overexpression of the SAC protein Mad2 leads to the accumulation of 4N cells after stalling of the cell cycle in G2/M (Sotillo et al., 2007). Overexpression of another regulator of the APC/C, Emi1, also leads to tetraploidisation in p53 deficient cells (Lehman et al., 2006). Both Mad2 and Emi1 can be overexpressed in several different cancer types (Lehman et al., 2007, Kim et al., 2014, Teixeira et al., 2015). Overexpression of the mitotic kinesin Eg5 in mice, which functions to ensure bipolar division by regulating centrosome separation, also leads to an accumulation of 4N mouse embryonic fibroblasts (MEFs) due to prolonged G2/M arrest (Castillo et al., 2007). Overexpression of Eg5 has also been linked to cancer progression and poor patient prognosis (Liu et al., 2010b, Ding et al., 2011). Problems with the spindle assembly checkpoint can be caused by loss of the APC (Adenomatous polyposis coli) gene, which plays a crucial role in the development of most colon cancers (Fodde et al., 2001, Dikovskaya et al., 2007). APC loss can cause mitotic slippage, a reduction in apoptosis and the production of a viable pool of tetraploid cells (Dikovskaya et al., 2007). Other problems in mitosis can also lead to the production of tetraploid cells. Overexpression of the mitotic kinase Aurora B has been shown to lead to the generation of tetraploid cells through a mechanism of premature chromatid separation in anaphase (Nguyen et al., 2009). It is thought that this may occur due to rapid exit from mitosis caused by excessive dissociation of the cohesin complex (Nguyen et al., 2009).

1.5.3 Endoreduplication

Endoreduplication describes variation in the normal cell cycle progression from G1 through to M phase, which results in cells with more than 2N DNA content (Lee et

al., 2009). As discussed above (see Section 1.2.1) some cells are programmed to undergo specialised programmes of repeated DNA synthesis without cell division to achieve high levels of ploidy. Endoreduplication is normally characterised by a complete skipping of the mitotic phase of the cell cycle, with cells entering G1 immediately after G2 (Lee et al., 2009).

It has been shown that persistent DNA damage signalling can lead to endoreduplication and the formation of tetraploid cells in the absence of p53 function (Davoli et al., 2010). Davoli and colleagues induced telomere dysfunction by the deletion of the mouse shelterin proteins POT1a and POT1b in immortalised MEFs (Hockemeyer et al., 2006, Davoli et al., 2010). This results in a persistent ATR kinase response, resulting in activation of CHK1 and CHK2, and the formation of polyploid cells (Denchi and de Lange, 2007, Hockemeyer et al., 2006). The authors show that polyploidisation can also be induced by a persistent DNA damage signal induced by zeocin, doxorubicin, bleomycin or repeated UV irradiation. Analysis of chromosome structure following persistent DNA damage revealed diplo-chromosomes, which are a hallmark of cells that have undergone repeated rounds of DNA replication without cohesin destruction and sister chromatid separation (Davoli et al., 2010). The continuous signalling though CHK1 and CHK2 seemed to result in CDC25 degradation and lower cyclin B- CDC2 (CDK1) activity, delaying M phase entry. The authors observed subsequent degradation of Geminin, which normally functions to inhibit DNA replication, and the re-expression of Cdt1 which can re-license replication origins (Davoli et al., 2010). One of the most likely causes of a persistent DNA damage response in cancer is telomere damage, which is thought to occur as a relatively early event in most cancer types (Davoli and de Lange, 2011). The authors therefore suggest that loss of p53 followed by persistent DNA damage induced by telomere dysfunction, and subsequent tetraploidisation could be an important driver of genetic instability in some cancer types (Davoli et al., 2010). In a follow up study the same group showed that telomere crisis and subsequent tetraploidisation also occur in human fibroblasts and mammary epithelial cells that underwent a natural telomere crisis after continual passaging (Davoli and de Lange, 2012). This study shows that in cancer-relevant cell types, telomere crisis leads to tetraploidisation. However, since a specific sequence of events needs to occur in order for tetraploid cells to

proliferate in this setting, it remains to be elucidated how common this mechanism of tetraploidisation is in human tumours.

Other scenarios in which the DNA damage response has been activated have been shown to cause endoreduplication. For example, in XRCC3 deficient cells, which are defective in homologous recombination, a low level of endoreduplication was observed (Yoshihara et al., 2004). Further, deletion of Nbs1 or Rad17, proteins involved in the DSB repair response also result in endoreduplication (Reina-San-Martin et al., 2005, Wang et al., 2003). Oncogene-induced replication stress could also result in a persistent DNA damage response, which could lead to tetraploidisation through endoreduplication (Bartkova et al., 2005, Davoli and de Lange, 2011).

1.5.4 Cell fusion

The fusion of two diploid cells will create a cell with a tetraploid DNA content. Cell fusion has been observed during both normal development and disease (Zhou and Platt, 2011). Cell-to-cell fusion can also occur when cells are infected with viruses. This was first observed for cells infected with the respiratory rodent virus Sendai virus (Wainberg and Howe, 1973). Some human cancers have an etiological link with viral infection, for example human papillomavirus (HPV) infection and cervical cancer (Reid, 1983). It has been shown that HPV infection can cause cell fusion resulting in binucleated cells, which are a hallmark of pre-cancerous cervical lesions (Hu et al., 2009, Mittal et al., 1990). A significant proportion of diagnosed cancers worldwide are thought to be related to viral infection (Parkin, 2006). It will be interesting to investigate whether these viruses act oncogenically though cell-fusion and production of 4N cells.

1.6 Limiting the proliferation of tetraploid cells

As discussed in Section 1.2, there are only a few specialised cell types in mammals that are polyploid. Although tetraploidy is commonly found in tumours, many cancers have deregulated cell cycles, and dysfunctional checkpoints (Williams and

Stoeber, 2012). This leads to the question of which checkpoints are normally activated by tetraploidy, and act to prevent tetraploidisation in somatic tissue. Studies using spindle poisons which disrupt the mitotic spindle have shown that cells undergo mitotic slippage but without segregation of chromosomes, resulting in a prolonged arrest in a tetraploid G1 state (Yvon et al., 1999, Rieder and Maiato, 2004). It was not known whether this arrest was caused by a specific cell cycle checkpoint that could sense a tetraploid state, or whether the arrest was due to errors in mitosis caused by the use of spindle poisons.

Data demonstrating the existence of a “tetraploidy checkpoint” was first shown by Andreassen and colleagues (Andreassen et al., 2001). Using cytochalasin D, an inhibitor of actin assembly, to block cytokinesis, the authors showed that primary rat embryo fibroblast cells (REF52 cells), but not transformed versions of the same cells, arrested in G1 following cytokinesis failure (Andreassen et al., 2001). They noted that cells arrested even when they had undergone a normal bipolar mitosis without errors, suggesting that subsequent G1 arrest was not dependent on mitotic errors brought about by spindle poison treatment. This arrest was dependent on p53, as when cells were infected with a dominant negative p53 mutant, they did not arrest. The authors proposed that this p53 dependent mechanism exists in non-transformed cells to protect against genomic instability. However, later work showed that the cell cycle arrest initiated by cytochalasin D could be dependent on drug concentration, as lower concentrations did not elicit G1 arrest, even in the same REF52 cells (Uetake and Sluder, 2004). These authors speculate that actin cytoskeleton disorganisation that persists even after drug washout could be responsible for the arrest, however they do not speculate as to why this affects binucleated (tetraploid) cells to a greater extent than diploid cells, which did not arrest at higher concentrations (Uetake and Sluder, 2004). It is possible that DNA damage resulting from the cytokinesis inhibitors and cell synchronisation treatments could be responsible for causing a G1 arrest (Wong and Stearns, 2005). Furthermore it seems as though cells do not arrest in response to a direct sensing of chromosome number, as when diploid cells were fused together they could re-enter a subsequent cell cycle (Wong and Stearns, 2005). It was also shown that the presence of extra centrioles could not cause an arrest, as when diploid cells

were fused to enucleated cells containing centrioles they also continued to cycle (Wong and Stearns, 2005).

Despite the possibility that drug concentrations and DNA damage could be responsible for some of the results discussed above, it is interesting that higher concentrations of cytochalasin specifically affected binucleated cells (Uetake and Sluder, 2004). Furthermore, spontaneously arising binucleated cells caused by chromosome non-disjunction also often undergo cell cycle arrest (Shi and King, 2005). It appears that although there is no defined checkpoint in all cell types that can sense chromosome numbers, many cells are not able to continue to proliferate with a tetraploid DNA content. This arrest seems closely linked to p53 function. In support of this, tetraploid cells were observed to increase in frequency in Barrett's oesophagus with the loss of chromosome 17p, where p53 is located (Galipeau et al., 1996).

Additionally, mitotic slippage and a 4N DNA content can result in apoptosis (Castedo et al., 2006). In a study by Kroemer and colleagues, HCT-116 cells were acutely treated with the spindle poison nocodazole, which results in an accumulation of >4N cells. These cells tended to undergo apoptosis, which was measured by the loss of mitochondrial transmembrane potential (Castedo et al., 2006). This apoptotic phenotype was linked to p53 activation, as p53 knockout cells had reduced levels of apoptosis. Apoptotic levels could also be rescued by knockout of the pro-apoptotic factor Bax (Castedo et al., 2006). These results indicate that tetraploidy can result in apoptosis as well as cell cycle arrest.

It has also been shown that tetraploid cells formed through DNA damage induced endoreduplication require inactivation of the tumour suppressor Rb, as well as p53 inactivation, in order to proliferate (Davoli and de Lange, 2012). Rb blocked entry into S phase in cells that experienced DNA damage in G1, but was not sufficient to block endoreduplication if cells experienced DNA damage in G2 (Davoli and de Lange, 2012). The presence of near-tetraploid karyotypes across different tumour types correlates well with inactivation of the Rb pathway (Davoli and de Lange, 2011).

1.6.1 What triggers p53 in tetraploid cells?

It seems clear that p53 has a role to play in limiting the long-term proliferation of tetraploid cells. Many studies have been carried out to try and identify the nature of the signal in tetraploid cells that can activate p53.

Using tetraploid clones derived from HCT-116, Kroemer and colleagues showed that tetraploidy frequently resulted in aberrant mitoses (Vitale et al., 2007). Tetraploid cells that underwent aberrant mitoses tended to display phosphorylation of p53 at serine-15, suggesting that catastrophic mitoses trigger p53 in tetraploid cells (Vitale et al., 2007). In support of this finding Kuffer and colleagues demonstrated through live cell imaging that HCT-116 and RPE-1 cells treated with dihydrocytochalasin D (DCD) to prevent cytokinesis mainly arrested or died after the first mitosis with a tetraploid DNA content (Kuffer et al., 2013). In accordance with this response being due to p53 activation, HCT-116 p53-/- cells did not exhibit the same arrest. Similar to the results of Kroemer and colleagues, the arrest in 4N HCT-116 cells seemed to be coupled to abnormal mitoses, as either multipolar divisions or chromosome segregation errors after bipolar divisions most frequently resulted in arrest (Vitale et al., 2007, Kuffer et al., 2013). The increased levels of p53 that were observed in tetraploid cells did not seem to be caused by DNA damage, as the kinetics of γH2AX foci formation did not correlate with the nuclear accumulation of p53 (Kuffer et al., 2013). Instead, the authors found a link with increased oxidative stress (as measured by 8-hydroxy-2-deoxyguanosine detection) in tetraploid cells, which correlated well with the increase in p53. Using siRNA to test a range of mitotic kinases for their ability to activate p53, the authors found that ATM depletion could increase the percentage of cycling cells, and conclude that ATM is likely to be responsible for the p53 activation in tetraploid cells (Kuffer et al., 2013). It will be of interest to determine how abnormal mitoses cause an increase in levels of oxidative stress in tetraploid cells.

It has been shown that actin damage caused by cytokinesis inhibitors such as cytochalasins induces phosphorylation of p53 at serine-15 and serine-37 immediately after cytokinesis failure (Chae et al., 2012). In contrast to the results of Kuffer and colleagues, p53 did not seem to be up-regulated by ATM in these

conditions (Kuffer et al., 2013, Chae et al., 2012) The up-regulation of p53 was not observed when cells were treated with actin damaging agents in S phase (Chae et al., 2012). These results suggest that there is a specific trigger of p53 in polyploid arrested cells. This signal could emanate from the extra centrioles present in tetraploid cells formed through cytokinesis failure. Centriole damage can up-regulate p53 through the stress response kinase p38 (Mikule et al., 2007). Depletion of different centrosomal proteins led to p38 activation, subsequent p53 phosphorylation and cell cycle arrest though p21 activation. Inhibition of p38 abrogated this G1 arrest (Mikule et al., 2007). It is possible that extra centrioles present after cytokinesis failure could also activate this stress response, resulting in G1 arrest.

Aylon and colleagues demonstrated a mechanism linking both cytoskeletal damage and centrosome dysfunction to p53 up-regulation in G1 arrested tetraploid cells (Aylon et al., 2006). The authors report that LATS2 (large tumour suppressor 2) is a key mediator of p53 up-regulation after spindle disruption. LATS2 is a centrosomal protein that is also thought to play in a role in proper spindle formation (Toji et al., Abe et al., 2006). LATS2 knockout cells display defects in cytokinesis, centrosome amplification, multipolar mitoses and genetic instability (McPherson et al., 2004). LATS2 was shown to interact with the negative regulator of p53, the E3 ubiquitin ligase MDM2 (Aylon et al., 2006). This interaction was enhanced upon treatment with the microtubule depolymeriser nocodazole, which arrests cells at G2/M, and also disrupts centrosome homeostasis (Uzbekov et al., 2002, Burakov et al., 2003). Binding of LATS2 to MDM2 decreased p53 ubiquitination, resulting in p53 stabilisation (Aylon et al., 2006). After nocodazole treatment, LATS2 translocated from its centrosomal location to the nucleus, where it could bind MDM2 and stabilise p53 levels. This effect was not observed upon DNA damage, suggesting that LATS2 relocates to the nucleus specifically in response to spindle disruption. The authors describe a positive feedback loop between LATS2 and p53, since LATS2 transcription was enhanced by p53 activation (Aylon et al., 2006). Increased LATS2 transcription in response to spindle damage was specific to cells in G2/M phase. Increased expression of LATS2 in U2OS cells that do not normally arrest in response to nocodazole resulted in the restoration of cell cycle arrest. This arrest was dependent on the kinase function of LATS2, as a kinase dead version could

not initiate an arrest (Aylon et al., 2006). Furthermore, knockdown of LATS2 phenocopied p53 knockdown with respect to abrogating cell cycle arrest after cytokinesis failure. This important finding demonstrates that LATS2 is a key regulator of cell cycle arrest that is activated in response to microtubule or centrosome disruption.

Pellman and colleagues, who identified LATS2 in a screen for regulators of cell cycle arrest after cytokinesis failure, further described the mechanism that activates LATS2 in tetraploid cells (Ganem et al., 2014). They noted that as well as the p53 induction due to MDM2 binding described by Aylon and colleagues, LATS2 also caused cell cycle arrest through its canonical downstream pathway members YAP and TAZ (Aylon et al., 2006, Ganem et al., 2014). Depletion of LATS2 by siRNA resulted in an increase in YAP expression and accumulation of YAP in the nucleus. YAP and TAZ activation normally initiate oncogenic proliferation; therefore activation of LATS2 after cytokinesis failure normally inhibits YAP and stops cell cycle progression (Ganem et al., 2014). To understand how LATS2 was activated in tetraploid cells Ganem and colleagues looked for upstream regulators of LATS2 signalling. Reduced RhoA activity and cytoskeletal reorganisation have previously been shown to activate LATS2 (Zhao et al., 2012, Yu et al., 2012) Ganem and colleagues found that RhoA activity was reduced in tetraploids, and could partially attribute this to the increase in Rac1 activity in tetraploid cells that is due to the presence of extra centrioles (Godinho and Pellman, 2014, Ganem et al., 2014). Although they do not show a functional link between Rac1 and RhoA, they demonstrate that the Hippo pathway is activated in response to the presence of extra centrosomes induced by PLK4 overexpression, and in mouse hepatocytes that become tetraploid as the adult liver develops. Although the authors establish that RhoA and reduced cytoskeletal contractility are important for LATS2 activation in tetraploid cells, it is still unknown how RhoA inhibits the Hippo pathway. Intriguingly however, the authors show that in high ploidy tumours, there is a significant correlation with YAP amplification and deletion of LATS2 suggesting that inactivation of the Hippo pathway may be a key event necessary for the sustained proliferation of polyploid tumours (Ganem et al., 2014).

The above work has contributed greatly to an understanding of the fundamental pathways that limit the proliferation of tetraploid cells, which are summarised in Figure 1.6.

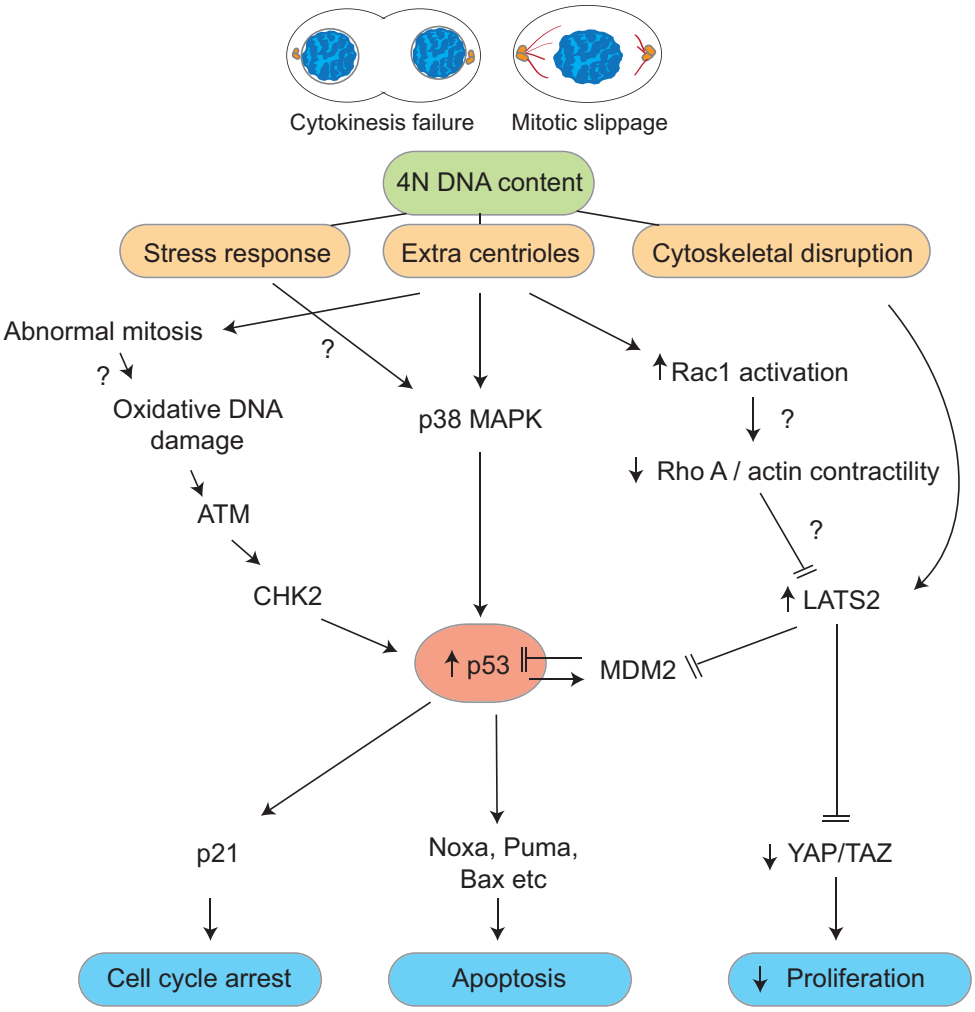

Figure 1.6: Mechanisms to limit tetraploid cell proliferation

Schematic representing the main pathways in tetraploid cells (formed through cytokinesis failure or mitotic slippage) that either result in cell cycle arrest or apoptosis. For references see text.

Clearly p53 is the master regulator of signals occurring in tetraploid cells that generally lead to cell cycle arrest or apoptosis. However, there are still unanswered questions, such as elucidating exactly how oxidative damage is caused by abnormal mitosis and chromosome missegregation (Kuffer et al., 2013). There may well also be additional stresses occurring in tetraploid cells that have not yet been

uncovered. The role of LATS2 in regulating not only the p53 response to mitotic slippage and cytokinesis failure, but also the inhibition of YAP and TAZ mediated transcription is becoming clear (Aylon et al., 2006, Ganem et al., 2014). However, the exact mechanism linking Rac1 activation, decreased RhoA contractility and increased LATS2 still requires refinement. In addition the applicability of this pathway to different cell types could be investigated.

1.6.2 An indirect mechanism to eliminate tetraploid cells

A novel mechanism to eliminate tetraploid cells within the tumour environment has also been demonstrated. Senovilla and colleagues showed that tetraploid cancer cells formed through cytokinesis failure exhibit an endoplasmic-reticulum (ER) stress response, characterised by the translocation of calreticulin to the cell surface (Senovilla et al., 2012). The expression of calreticulin on the cell surface is thought to be one of the factors determining whether immunogenic cell death occurs after cytotoxic treatments (Obeid et al., 2007). Hence, the authors tested whether polyploid cancer cells were more easily recognised and culled by the immune system of mice (Senovilla et al., 2012). Indeed, they found that polyploid cancer cells grew more slowly in immune-competent mice than diploid cancer cells. Furthermore tumours that had arisen from polyploid cancer cells appeared to have undergone ‘immuno-selection’ for cells with a lower DNA content (Senovilla et al., 2012). This intriguing mechanism of ploidy ‘immuno surveillance’ could be an interesting anti-cancer immune mechanism to limit the proliferation of genetically unstable polyploid cells (Senovilla et al., 2012). The exact cause of the ER-stress and calreticulin membrane localisation in tetraploid cancer cells has yet to be elucidated.

1.7 The consequences of tetraploidisation

Since tetraploidy appears to be a common occurrence in cancer, many studies have been undertaken using tetraploid cells generated in different ways to assess how tetraploidy could be linked to tumour formation. The consequences of experimentally induced tetraploidisation are discussed below.

1.7.1 Increased tumorigenicity of tetraploid cells

A landmark study by the Pellman laboratory was the first to show that tetraploid cells generated from cytokinesis failure were more tumorigenic than diploid cells (Fujiwara et al., 2005). Using the cytokinesis inhibitor dihydrocytochalasin B (DCB), the authors generated a proliferating population of p53-/- mouse mammary epithelial cells (MMECs). Consistent with the notion that p53 plays an important role in limiting the proliferation of tetraploid cells, p53 proficient tetraploid MMECs could not be propagated in culture. Using an initiation/promotion transformation assay, the authors showed that only tetraploid p53-/- MMECs exhibited anchorage independent growth in soft agar. Even more strikingly, only tetraploid p53-/- MMECs developed tumours when injected subcutaneously into nude mice, whilst diploid p53-/- MMECs did not form any tumours (Fujiwara et al., 2005).

Tetraploid cells formed through defects in mitosis have also been indirectly shown to be tumorigenic. The overexpression of Aurora A causes premature chromatid separation and the formation of tetraploid cells (Meraldi et al., 2002). In a study of transgenic mice overexpressing Aurora A, tetraploid cells were seen in premalignant stages of mammary gland tumourigenesis, suggesting they may be a cause of tumour formation (Nguyen et al., 2009).

Direct evidence that tetraploidy can cause tumourigenesis was also shown for tetraploid cells formed through cell fusion. Normal human diploid fibroblasts were altered by the expression of adenoviral E1A, which inactivates Rb, and the oncogene HRAS, which prevents apoptosis (Duelli et al., 2007). A population of fibroblasts was then fused by infection with an otherwise harmless retrovirus $MPMV^{E}$. One out of three cell populations that had deregulated oncogenes and had been fused with the virus formed tumours when injected into nude mice, but none of the other cell populations formed tumours (Duelli et al., 2007).

Endoreduplication caused by telomere crisis has also been shown to result in increased tumourigenesis (Davoli and de Lange, 2012). MEFs lacking the shelterin proteins POT1a and POT1b have been shown previously to form tetraploid cells through endoreduplication (Davoli et al., 2010). These tetraploid MEFs showed

enhanced growth in soft agar compared to diploid MEFs, and also formed a greater frequency of tumours when injected into nude mice (Davoli and de Lange, 2012).

Taken together these studies show that tetraploidisation, which can be experimentally achieved through multiple routes, frequently leads to an enhanced ability to form tumours. This work sheds light on the observation of tetraploid cells at early stages of premalignant conditions such as Barrett's oesophagus (Galipeau et al., 1996).

1.7.2 Genetic instability in tetraploid cells

In the above studies experimentally induced tetraploidisation frequently led to numerical and structural chromosomal instability as well as increased tumourigenesis. In the study by Fujiwara and colleagues, tetraploid cells induced via cytokinesis failure exhibited increased levels of gross chromosomal rearrangements and whole chromosome aneuploidy compared to diploid cells (Fujiwara et al., 2005). However diploid MMECs do exhibit both whole chromosome aneuploidy and gross chromosomal rearrangements, suggesting that the mechanisms generating these types of genetic instability are already present in diploid cells. As the tetraploid cells formed tumours whereas the diploid MMECs did not, the karyotype of tetraploid-derived tumours was assessed by array CGH. Tetraploid derived MMEC tumours displayed both numerical and structural chromosome aberrations. Furthermore all tumours analysed showed a recurrent gain of a segment of chromosome 9, containing a cluster of matrix metalloproteinase (MMP) genes that are also overexpressed in human breast cancers (Fujiwara et al., 2005).

Tetraploid cells generated through cell fusion also showed gross chromosomal abnormalities (Duelli et al., 2007). These included both numerical and structural chromosome aberrations that were diverse between different cells of the same population: in a spectral karyotyping (SKY) analysis, all of the ninety cells that were analysed had a different karyotype (Duelli et al., 2007). The degree of chromosomal instability observed in these virally fused cells was much greater than

that from the Fujiwara study of tetraploid cells derived from cytokinesis failure, suggesting that the mechanism of tetraploidisation, as well as the genetic background of the cell type used, can affect the degree of chromosomal instability (Fujiwara et al., 2005, Duelli et al., 2007).

Telomere-driven tetraploidisation also results in tumours that are genetically diverse (Davoli and de Lange, 2012). Cell lines were established from tumours derived from MEFs that had undergone telomere crisis and become tetraploid. Upon passaging of these tetraploid-tumour derived cell lines there was an increase in numerical chromosome instability, as assessed by metaphase chromosome counting (Davoli and de Lange, 2012). The tetraploid cell lines showed high rates of chromosome loss compared to diploid-derived tumours (Davoli and de Lange, 2012).

Table 1.1: Summary of studies investigating genome stability after tetraploidisation (TP)

Study	Cell line	Mechanism of TP	Method of TP	p53 status	Rb status	Structural instability	Numerical instability
Fujiwara et al., 2005	MMECs - mouse epithelial cells	Cytokinesis failure	DCB 2μM	p53-/-		SKY number of translocations	Chromosome counts - metaphase spreads
Duelli et al., 2007	D551 - human diploid fibroblasts	Virally induced cell fusion	Adenoviral E1A + HRAS + $MPMV^{E}$ infection		Rb inactivated	SKY	SKY
Davoli et al., 2012	MEFs	Telomere dysfunction	POT1a-tetOFF	p53 inactivated	Rb inactivated	NA	Chromosome counts - metaphase spreads *(from TP derived tumours)*

These studies all indicate that tetraploidy results in karyotypic diversification. That tetraploid cells formed though different mechanisms all show genetic instability suggests that this phenotype is related to tetraploidy itself, rather than the experimental procedures used to generate it, although different mechanisms of tetraploidisation can affect the levels of genetic instability (Duelli et al., 2007, Fujiwara et al., 2005). Interestingly all the above studies have used cell lines in

which p53 and/or Rb function was disrupted (Table 1.1). This could have affected the prevalence of genetic instability observed in these studies.

1.7.3 Altered response to drug treatment in tetraploid cells

Several studies have shown an altered response to drug treatment in tetraploid cells. An acute tetraploid cell cycle arrest has been shown to lead to resistance to the DNA damaging drug cisplatin (Shen et al., 2013). Naturally occurring cisplatin sensitive and cisplatin resistant clones were isolated from HCT-116. The resistant clones had both a prolonged G2 arrest, and a G1 tetraploid arrest in response to cisplatin treatment. Abrogation of either of these arrests with inhibition of cell cycle regulators led to cisplatin sensitisation (Shen et al., 2013). This result indicates that in the initial response to cisplatin treatment, a 4N arrest is necessary for cell survival, otherwise cells continue to catastrophic mitosis and die. Tetraploidy has also been shown to be important in the long-term treatment of cells with DNA damaging agents. In a study by Kroemer and colleagues investigating the regulation of apoptosis in tetraploid cells, it was found that tetraploids from both HCT-116 and RKO colorectal cancer cell lines were more resistant to cisplatin, oxaliplatin and camptothecin, as well as physical DNA damage induced by UV or γ-irradiation (Castedo et al., 2006). The authors found that this resistance was due to a small number of p53 target genes found to be transcriptionally altered between diploid and tetraploids. In particular the knockdown of p53R2 (p53-inducible ribonucleotide reductase-2, RRM2B) could re-sensitize tetraploid RKO clones to cisplatin (Castedo et al., 2006). This interesting study demonstrates that small differences in transcriptional regulation between diploid and tetraploid clones can result in marked differences in response to drugs. Another study has shown that tetraploid cells that have arisen through endoreduplication are also more resistant to both cisplatin and ionising radiation (Shen et al., 2008). The continued treatment of HCT-116 and U2OS cells with the MDM2 antagonist Nutlin-3a, which results in p53 stabilisation, caused prolonged arrest in G2 from which cells eventually re-replicated their DNA to become tetraploid (Shen et al., 2013). These endoreduplicated cells were shown to be more resistant to cisplatin and ionising radiation, evidenced by reduced apoptosis. However, prolonged treatment with

ionising radiation revealed that long-term clonogenic survival of tetraploid HCT-116 cells in response to ionising radiation was not increased (Shen et al., 2013).

In contrast to the above studies, tetraploid hepatocellular carcinoma cancer cells derived from mitotic failure caused by nocodazole treatment exhibited increased sensitivity to DNA damage (Hau et al., 2006). Tetraploid Hep3B cells were more sensitive than parental diploid Hep3B cells to ionizing radiation, and also to the topoisomerase II inhibitor Adriamycin. The authors concluded that the increased sensitivity of tetraploid cells to these DNA damaging treatments was likely due to the increased DNA content, since tetraploid Hep3B cells contained more γ-H2AX foci than diploid cells in response to the same dose of irradiation (Hau et al., 2006). In a further study using the same hepatocellular carcinoma cells, the authors found that tetraploid Hep3B were also more sensitive to Aurora B inhibition (Marxer et al., 2012). In addition, tetraploid cells formed through fusion of Swiss 3T3 fibroblasts were also more sensitive to Aurora B inhibitors. The apoptosis induced by Aurora B inhibition appeared to be dependent on cells undergoing repeated rounds of failed cytokinesis and genome reduplication. In support of this, the same sensitivity was observed in tetraploid cells in response to cytochalasin B, which inhibits cytokinesis. In diploid cells this apoptosis seemed to occur in very high ploidy cells (of up to 16N) (Marxer et al., 2012). The authors therefore hypothesise that the increased sensitivity of tetraploid cells is due to them reaching this critical ‘ploidy limit’ quicker than diploid cells, as they start with a higher DNA content (Marxer et al., 2012).

Studies have also been undertaken to try and find specific vulnerabilities in tetraploid cancer cells that could be exploited therapeutically. Using the same tetraploid cells derived from HCT-116 and RKO in which they had demonstrated increased resistance to cisplatin and other DNA damaging agents, Kroemer and colleagues searched for specific kinases that may be able to target tetraploid cells (Vitale et al., 2007). They found that tetraploidy was linked to abnormal mitosis, even in the presence of a functional SAC, and speculated that tetraploid cells may therefore be more vulnerable to inhibition of the checkpoint kinase CHK1 (Vitale et al., 2007). Indeed tetraploid cells were more sensitive to CHK1 knockdown and chemical inhibition, which resulted in increased apoptosis compared to diploid cells. The authors found that CHK1 inhibition resulted in the up-regulation of many

apoptotic p53 target genes specifically in tetraploid cells. The mechanism by which CHK1 kills tetraploid cells was not elucidated, but the authors speculate it could be due to CHK1 depletion resulting in premature mitotic exit due to CDK1-cyclin B activation (Vitale et al., 2007). The same group later showed that CHK1 inhibition up-regulated p53 through p38 MAPK (Vitale et al., 2010a).

Other vulnerabilities that also target mitosis have been found in tetraploid cells. Since many tetraploid cells contain extra centrosomes, Kwon and colleagues inhibited centrosome clustering by knocking down the kinesin HSET (Kwon et al., 2008). HSET knockdown increased the frequency of multipolar anaphases in tetraploid BJ fibroblasts and NIH3T3 cells, which they showed can lead to increased cell death in other cell lines with extra centrosomes (Kwon et al., 2008). Inhibition of another mitotic kinesin, Eg5 (or KIF11), which normally separates centrosomes for proper bipolar spindle formation, was also more effective at killing tetraploid cells (Rello-Varona et al., 2009). In an unbiased screen for agents that could selectively kill tetraploid cells, resveratrol and other AMPK (AMP-activated protein kinases) inhibitors were found to specifically target tetraploid cancer cells (Lissa et al., 2014). Although the cause of the vulnerability to these agents in tetraploid cells was not uncovered, it was shown that treatment of a mouse model of colon cancer with resveratrol reduced the frequency of tetraploid cells (Lissa et al., 2014). Whether this reduction in tetraploid cell formation is directly responsible for the previously reported chemo-preventive effect of this compound is not yet known (Schneider et al., 2001, Sale et al., 2005).

Taken together these studies demonstrate that there is likely to be cell-type specific effects of tetraploidy on the response to drugs. Although some studies have shown increased resistance to DNA damaging agents, others have shown increased sensitivity in tetraploid cells. In several of these studies the HCT-116 colorectal cancer has been used to test the response of diploid and tetraploid clones to cisplatin. However, since HCT-116 has been shown to contain cells that have a varied response to cisplatin (Shen et al., 2013), the differences noted between diploids and tetraploids could be due to inherent clonal variation within the HCT-116 population. Larger studies still need to be conducted on tetraploid cells formed

through different mechanisms to conclude whether tetraploidy inherently leads to drug resistance or drug sensitivity.

1.7.4 An altered response to DNA damage in polyploid cells

An increased level of replication stress normally activates cell cycle checkpoints that act as a barrier to tumourigenesis. This replication stress can be modelled by introducing mutations in key DNA replication genes such as FEN1 (flap-endonuclease-1) (Zheng et al., 2011). Interestingly, when cells are subjected to this replication stress they frequently become tetraploid and aneuploid (Zheng et al., 2011). Using a mouse model with mutations in the FEN1 gene, the same authors showed that near-polyploid aneuploid cells have a unique response to DNA replication stress (Zheng et al., 2012). Upon serial expansion of MEFs from these FEN1 mutant mice, populations of cells with unlimited proliferative potential were isolated. These cells were near-polyploid aneuploid and appeared to have altered their response to DNA damage in order to overcome replication stress induced senescence (Zheng et al., 2012). The polyploid cells exhibited reduced CXCL2 expression, which normally activates ATR/ATM mediated DNA damage response signalling, as well as a reduction in the expression of p53 and p21 target genes. Further, the polyploid cells heterogeneously overexpressed BRCA1 and the $p19^{INK4D}$ ARF protein, which appeared to enhance their capacity for single stranded DNA repair. Polyploid cells also showed an increased capacity for NHEJ (non-homologous end joining) repair. These results suggest there is flexibility within a polyploid genome that can allow cells to overcome barriers to tumour progression (Zheng et al., 2012). Interestingly these cells did not have a p53 mutation, but appeared to have methylated several downstream targets of p53, such as p21, resulting in loss of expression, and allowing the polyploid cells to continue proliferating (Zheng et al., 2012). It will be of interest to discover whether polyploidisation and subsequent adaptation to escape replication stress induced senescence occur in different tumour types. Furthermore it would be interesting to investigate whether similar changes in the response to DNA damage had occurred in other tetraploid cell models, especially those which have been shown to be either

sensitive or resistant to DNA damaging agents (Castedo et al., 2006, Hau et al., 2006).

1.8 Mechanisms of chromosomal instability

Chromosomal instability (CIN) is a dynamic process that describes a continual change in karyotype between cell generations. It is characterised by changes both in chromosome number and structure (Lengauer et al., 1997). CIN is a common feature of most solid tumour types (Thompson and Compton, 2011b, Beroukhim et al., 2010). Although CIN is normally described separately in terms of W-CIN (whole chromosome CIN, or numerical CIN) and S-CIN (structural CIN), both forms of CIN are usually observed together in tumours (Venkitaraman, 2007, Gaasenbeek et al., 2006). This observation suggests that there may be mechanisms simultaneously responsible for causing both W-CIN and S-CIN (Venkitaraman, 2007). Studies of CIN in cell lines have shown that this phenotype is normally characterised by an elevated rate of chromosome missegregation (Lengauer et al., 1997, Roschke et al., 2003, Thompson and Compton, 2008). Therefore investigations into mechanisms of chromosomal instability (and in particular W-CIN) have largely focussed on the cause of the increase in anaphase chromosome segregation errors.

1.8.1 Mitotic checkpoint defects in CIN cells

As the SAC and error correction machinery are normally responsible for ensuring faithful chromosome partitioning into two daughter cells at anaphase (see Section 1.4.2), defects in these pathways have been suggested to lead to CIN (Kops et al., 2004). Some rare somatic mutations have been found in mitotic checkpoint genes such as *BUB1B* (BUBR1) (Cahill et al., 1998) and members of the KMN network such as ROD and ZWILCH (Wang et al., 2004b). However, in vivo studies have shown that complete loss of the mitotic checkpoint is embryonic lethal in mice (Kalitsis et al., 2000), and ablation of the checkpoint is also lethal to cancer cells in vitro (Kops et al., 2004). These data have led to speculation that the mitotic checkpoint is more likely to be weakened in CIN tumours than completely

abolished (Michel et al., 2004, Iwanaga et al., 2007, Janssen and Medema, 2012). Indeed, altered expression of many mitotic checkpoint genes have been shown in human cancers to affect the functioning of the mitotic checkpoint (Janssen and Medema, 2012). A common alteration in a mitotic checkpoint gene is the overexpression of MAD2, which can be caused by dysfunction of the Rb pathway, a common occurrence in cancer (Hernando et al., 2004). MAD2 overexpression leads to aneuploidy and spontaneous tumour formation in mice (Sotillo et al., 2007). Taken together, mutations in checkpoint genes and decreased expression of checkpoint proteins do occur in some cancers, albeit rarely. A more common mechanism of checkpoint weakening appears to be altered expression of a variety of checkpoint genes, but in particular MAD2 (Janssen and Medema, 2012).

1.8.2 Chromosome attachment errors and CIN

CIN cell lines are characterised by an increase in chromosome segregation errors. Although checkpoint defects are relatively rare in CIN cancers, some types of chromosome mis-attachments to the mitotic spindle are not recognised by the error correction machinery (see Section 1.4.2). Merotelic attachments, where one kinetochore is attached to microtubules from both poles (see Figure 1.4), lead to lagging chromosomes and missegregation (Cimini et al., 2001, Thompson and Compton, 2011a). The different causes of merotelic attachments, and their relevance to cancer are discussed below.

1.8.2.1 Spindle morphology and merotelic attachments

The formation of a bipolar spindle is essential for the correct progression through mitosis. Correct spindle formation largely relies on the separation and positioning of centrosomes at opposite poles of the cell (Bettencourt-Dias and Glover, 2007). The centrosome is the microtubule organising centre of mammalian cells, and in mitosis controls microtubule mediated separation of genomic material (Nigg, 2006, Bettencourt-Dias and Glover, 2007). Centrosomes either separate before nuclear envelope breakdown (NEBD) in prophase, or after NEBD, in pro-metaphase (Toso et al., 2009).

It has been shown that cells in which centrosome separation occurs after NEBD are more likely to contain increased frequencies of chromosomes that are mis-attached to the mitotic spindle (Silkworth et al., 2012). This is thought to be due to cells proceeding through an intermediate monopolar spindle stage, where both centrosomes are in close proximity to each other (Silkworth et al., 2012). In support of this, treating cells with monastrol, a drug that induces monopolar spindle formation through inhibition of the kinesin Eg5 (KIF11) can increase segregation error frequency (Choi and McCollum, 2012). The deubiquitinase USP44 has been shown to play a role in correct centrosome separation by direct binding to the centriolar protein centrin (Zhang et al., 2012). Loss of USP44 delays centrosome separation and increases the frequency of segregation errors. Furthermore, USP44 knockout mice developed an increased frequency of spontaneous tumours (Zhang et al., 2012).

As well as delayed centrosome separation, accelerated centrosome separation has also been shown to increase the frequency of chromosome segregation errors (Nam and van Deursen, 2014). The overexpression of cyclin-B2, which is a common occurrence in cancer, was shown to accelerate centrosome separation and result in lagging chromosomes (Nam and van Deursen, 2014). The mechanism by which accelerated centrosome separation increases the frequency of mis-attached chromosomes has yet to be revealed, but it has been suggested that mature kinetochore structures that usually correct these errors may not have formed properly in early pro-metaphase (Nam et al., 2015).

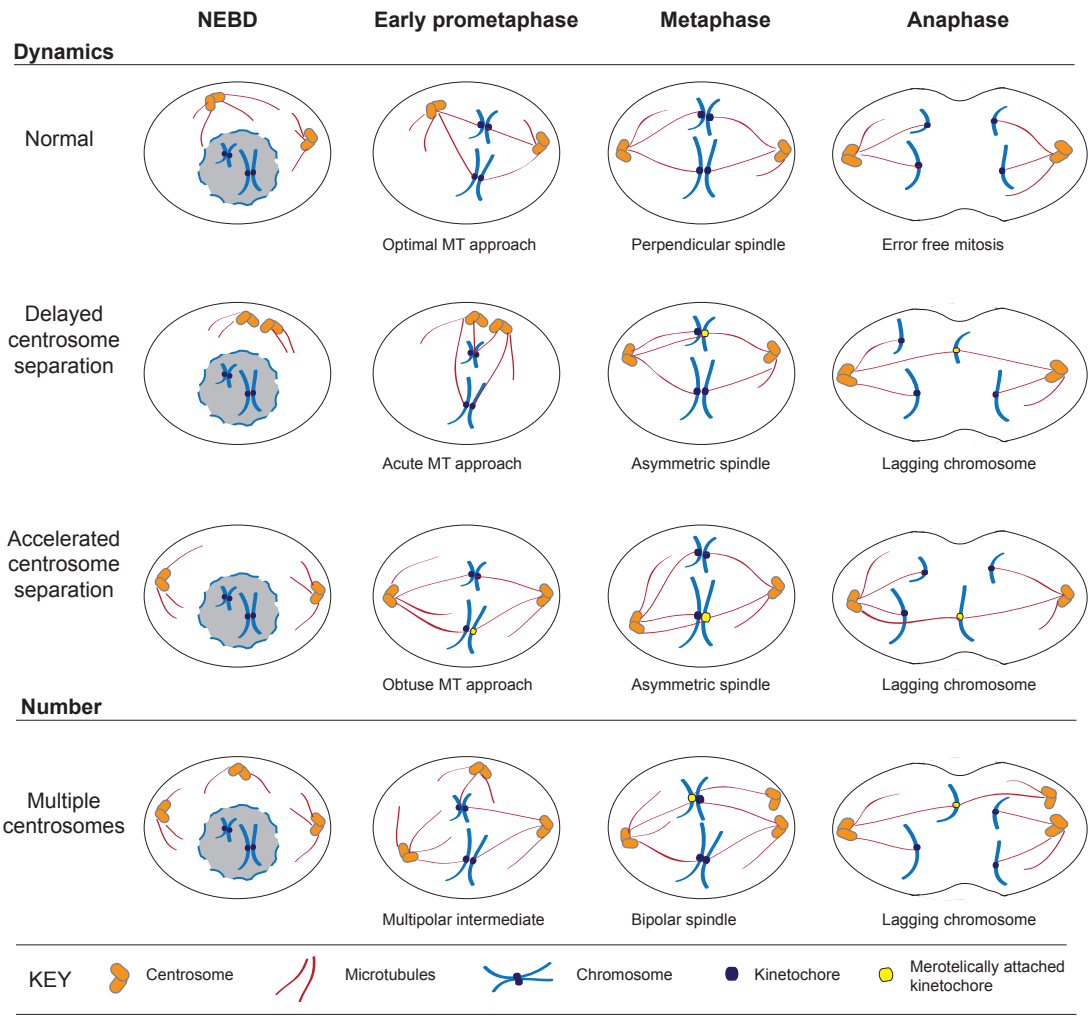

Figure 1.7: Centrosome dynamics influence chromosome segregation fidelity

Figure adapted from (Nam et al., 2015). Aberrant centrosome dynamics and centrosome numbers can influence chromosome attachment to the mitotic spindle. Merotelically attached chromosomes will result in lagging chromosome at anaphase. For references see text in Section 1.8.2.1. MT= microtubule.

As well as correct centrosome separation, centrosome number also impacts upon spindle morphology and kinetochore-microtubule attachments. Centrosome amplification is common in tumours (Pihan et al., 1998, Nigg, 2006). An early theory, proposed by Theodor Boveri, suggested that extra centrosomes would result in aneuploidy by causing multipolar cell divisions (Boveri, 2008). However, work from the Pellman laboratory showed that cancer cells with extra centrosomes rarely undergo multipolar divisions (Ganem et al., 2009). Instead, the authors showed that these cells undergo a transient multipolar stage, but eventually cluster

their centrosomes and divide in a bipolar fashion. This multipolar spindle intermediate causes an increase in the frequency of merotelic chromosome attachments (Ganem et al., 2009, Silkworth et al., 2009). The kinesin, HSET, is specifically required for cells with supernumerary centrosomes, including tetraploid cells, to form a bipolar spindle (Kwon et al., 2008).

Increased microtubule assembly rates have also been shown to contribute to CIN through abnormal spindle geometry (Ertych et al., 2014). Using a fluorescently tagged microtubule plus end binding protein, EB3, the authors tracked microtubule assembly rates in a panel of CIN- and CIN+ colorectal cancer cell lines, and showed CIN+ cell lines had consistently higher microtubule plus end assembly rates (Stepanova et al., 2003, Ertych et al., 2014). Crucially, restoration of normal microtubule assembly rates could stabilise the karyotypes of CIN cells. Increased microtubule assembly rates altered normal spindle morphology, promoting transient abnormalities in spindle axis positioning that resulted in lagging chromosomes. The increase in microtubule assembly rates was shown to be linked to two genetic alterations that are common in colorectal cancer, Aurora kinase A overexpression, and loss of CHK2 (Ertych et al., 2014).

1.8.2.2 Microtubule dynamics and merotelic attachments

The correction of merotelic attachments depends upon the ability of the error correction machinery to depolymerise microtubules. It has been shown that an increased stability of kinetochore-microtubule attachments in CIN cells underlies the increase in merotelic attachments and chromosome segregation errors (Bakhoum et al., 2009a). Inhibiting the ability of the error correction machinery to destabilise attachments in normal diploid RPE-1 cells, for example by inhibiting MCAK activity, resulted in an increase in segregation errors comparable to the levels observed in CIN cells (Bakhoum et al., 2009b). Intriguingly, the overexpression of the checkpoint protein MAD2 can increase the stability of kinetochore-microtubule attachments through a reduction in Aurora B activity at centromeres (Kabeche and Compton, 2012). This reduction in Aurora B activity is independent of the normal checkpoint function of MAD2, but the exact mechanism

by which it impedes Aurora B has yet to be established (Kabeche and Compton, 2012, Janssen and Medema, 2012).

1.8.3 Defective sister chromatid cohesion

During cell division sister chromatids are held together by the cohesin complex before separation during anaphase. Maintaining proper cohesion between sister chromatids until anaphase onset is critical for ensuring accurate chromosome segregation (Jallepalli et al., 2001, Iwaizumi et al., 2009). Many different cancer types show evidence of mutations in various subunits of the cohesin complex (Barber et al., 2008, Wang et al., 2004a, Thota et al., 2014). Mutations in the cohesin complex have been suggested to underlie chromosomal instability in colorectal cancer, as their down-regulation caused cohesion defects and segregation errors in cultured cells (Barber et al., 2008). The cohesin complex subunit STAG2 is mutated in multiple cancer types, and deletion of STAG2 in diploid cell lines resulted in segregation errors (Solomon et al., 2011). Furthermore, reconstitution of STAG2 in aneuploid cell lines lacking the endogenous locus restored chromosomal stability (Solomon et al., 2011). STAG2 has recently been shown to have a role in error correction during mitosis (Kleyman et al., 2014). STAG2 depleted cells showed an increase in the stability of kinetochore-microtubule attachments, and improper localisation of the CPC components Aurora B and Bub1 (Kleyman et al., 2014). How STAG2 normally corrects improper-kinetochore attachments and affects localisation of the CPC during mitosis has not been determined. However, recent genomics studies have shown that STAG2 mutations are not associated with aneuploidy in tumours (Balbas-Martinez et al., 2013, Djos et al., 2013, Taylor et al., 2014). Given that cohesin has multiple roles in the cell besides cohesion of sister chromatids, including transcriptional regulation, DNA repair and telomere protection, the precise contribution of STAG2 mutations to cancer development requires further investigation.

Depletion of the retinoblastoma protein (Rb) has been shown to cause cohesion defects and increased chromosome segregation in diploid cells (Manning et al., 2010, van Harn et al., 2010). Rb depletion was shown to lead to an altered

distribution of cohesin on chromatin, likely because of altered histone 4 methylation (H4K20 marks) (Manning et al., 2014). The cohesion defects in these cells produced altered replication dynamics, DNA damage and impaired mitotic fidelity, which could all be rescued by establishment of proper cohesion (Manning et al., 2014). Increasing cohesion by inactivation of WapI, a cohesin antagonist, could also rescue CIN in Rb deficient cancer cells (Manning et al., 2014). The mechanism by which cohesion loss leads to replication defects will be an interesting area of future research.

1.8.4 DNA damage in CIN cancers

Many different sources of DNA damage, both endogenous and exogenous, pose a risk to genomic integrity (see Section 1.4.1), and most structural chromosome aberrations are caused by either mis- or un-repaired double-strand breaks (DSBs) (Thompson and Compton, 2011b, Gisselsson, 2008, Janssen and Medema, 2012). Many cancers are caused by germline mutations in DNA repair factors, emphasising the importance of correct DNA repair in genetic stability (Duker, 2002, Hartlerode and Scully, 2009). Structurally abnormal chromosomes can lead to an increase in chromosome segregation errors in mitosis such as anaphase bridges, and acentric chromosome fragments (Gisselsson, 2008). Anaphase bridges (a continual bridge of DNA between the two daughter chromosome masses) occur as the normal mitotic machinery tries to segregate chromosomes that have two centromeres (dicentric chromosomes). Dicentric chromosomes are either formed from sister chromatid fusion, or fusion between different chromosomes following DNA damage and erroneous repair. Dicentric chromosomes and anaphase bridges can also be caused by DNA damage specifically at the telomeres (Artandi et al., 2000, Gisselsson et al., 2001). Acentric lagging chromosomes occur because the acentric fragment is unable to attach to the mitotic spindle, and is therefore segregated randomly between the daughter cells.

1.8.5 DNA replication stress

Replication stress is a broad term that encompasses the many processes that can result in hindrance of the replication fork during S phase (Gaillard et al., 2015). These processes include DNA damage, oncogene activation, tumour suppressor loss, replication machinery defects, nucleotide deficiency, DNA secondary structures and hard to replicate sequences (Gaillard et al., 2015, Bartkova et al., 2006, Bester et al., 2011, Schwartz et al., 2006, Branzei and Foiani, 2010). Replication defects can result in DNA damage, chromosome rearrangement and chromosome missegregation (Gaillard et al., 2015). It has been shown in this laboratory that CIN+ colorectal cancer cell lines exhibit signs of replication stress, including delayed replication fork speed (Burrell et al., 2013). Furthermore, a frequent region of chromosome loss in CIN+ colorectal cancers, chromosome 18q, was found to encode three novel CIN suppressor genes that when silenced could increase replication stress and chromosome missegregation in diploid cell lines (Burrell et al., 2013). It has also recently been shown that Rb deficiency leads to replication stress and aneuploidy (Coschi et al., 2014). As discussed above (Section 1.8.3), Rb deficiency has been shown to result in defective chromatid cohesion and mitotic defects (Manning et al., 2010, Manning et al., 2014). In a new study Rb haploinsufficiency is shown to disrupt the formation of Rb-E2F1-Condensin II at pericentromeric loci, which results in replication stress (Coschi et al., 2014). It is suggested that reduced localisation of this complex to pericentromeric regions could lead to unresolved replication intermediates and centromere and kinetochore disruption (Coschi et al., 2014). Clearly, since many defects can lead to replication stress, shown to link chromosome structure and proper chromosome segregation, this phenomenon is likely to be a significant driver of chromosomal instability in human cancers.

1.8.6 Mechanisms that link numerical and structural CIN

Since W-CIN and S-CIN are frequently observed together in cancer, efforts have been made to establish whether singular mechanisms can explain both phenotypes (Venkitaraman, 2007). Since some genes have roles both in regulating DNA replication and/or repair processes and in mitotic progression, defects in these

genes could simultaneously lead to changes in chromosome number and structure. Examples of these categories of genes would include BRCA1 and CHK2, which are reported to function in mitotic fidelity as well as in the DNA damage response (Stolz et al., 2010). Structural chromosome aberrations, such as telomere dysfunction that can generate dicentric chromosomes, also increase the frequency of numerical chromosomal aberrations (Pampalona et al., 2010). Replication stress mediated by loss of three novel CIN suppressor genes was also shown to lead to numerical chromosomal instability (Burrell et al., 2013). Recent work has also shown that lagging chromosomes can become trapped in the cleavage furrow during cytokinesis and sustain DNA damage, resulting infrequently in chromosome translocations (Janssen et al., 2011). Furthermore lagging chromosomes can become entrapped in micronuclei, which may then fail to completely replicate before a subsequent mitosis, resulting in catastrophic chromosome breakages, or chromothripsis (Crasta et al., 2012, Zhang et al., 2015). Activation of the DNA damage response after chromosome missegregation has also been shown to induce further numerical instability (Bakhoum et al., 2014). The authors showed that after chromosomes were damaged during mitosis, there was an increase in the stability of kinetochore-microtubule attachments, resulting in an increase in lagging chromosomes at the next mitosis (Bakhoum et al., 2014).

Since CIN is so frequently observed in cancer, occurring in many different tissues of origin and genetic contexts, it has been hard to ascribe a single mechanism to explain the origin of CIN in all cancer types. It is likely that a combination of all the above mechanisms can be responsible for CIN, but these mechanisms may occur together or separately, and at different times in tumour development. More work is needed to understand how CIN shapes the genomic evolution of different cancer types.

1.9 Consequences of chromosomal instability

As CIN manifests itself as an increase in chromosome missegregation rates, many studies have investigated the cellular consequences of missegregated chromosomes.

It has been shown that chromosome missegregation induces p53 and p21 in diploid cells, and that this acts to supress the generation of aneuploid and CIN cells (Thompson and Compton, 2010). It has further been demonstrated that this activation of p53 can be linked to ATM (Li et al., 2010). The activation of ATM could be due to increasing levels of ROS that have been noted in aneuploid cells (Kumari et al., 2014, Li et al., 2010). This data correlates well with the fact that many CIN and aneuploid tumours exhibit defects in the p53 pathway (Tomasini et al., 2008). However, there are still many open questions in the field about the exact mechanism by which p53 is activated after chromosome missegregation.

A single missegregated chromosome will result in aneuploidy in both daughter cells. The cellular consequences of single chromosome aneuploidies have been extensively investigated in yeast (Torres et al., 2007, Pavelka et al., 2010, Zhu et al., 2012, Sheltzer et al., 2011, Sheltzer et al., 2012). Simple chromosome aneuploidies have also been studied in human cells, showing that aneuploidy can lead to defects in cell proliferation (Williams et al., 2008) and conserved transcriptional and proteomic changes, including activation of autophagy (Stingele et al., 2012, Durrbaum et al., 2014). Aneuploid cells have also been reported to be deficient in HSP90-mediated protein folding response (Donnelly et al., 2014). This defect in protein folding was shown to be due to decreased expression of the heat shock factor HSF-1 in aneuploid cells, and re-expression of HSF-1 could rescue the defect in protein folding (Donnelly et al., 2014). These studies are supported by the fact that trisomic MEFS have been found to be more sensitive to autophagy inhibitors and inhibition of the chaperone protein HSP90 (Tang et al., 2011). How these studies of stable simple chromosome aneuploidies in human cells relate to the more complex chromosomal instability found in cancer cells remains an open question.

1.9.1 CIN and patient prognosis

CIN has been shown to correlate with poor patient prognosis across a range of different cancer types (McGranahan et al., 2012). These include lung cancer, breast cancer, colon cancer, ovarian cancer, endometrial cancer and diffuse large

B-cell lymphoma (Choi et al., 2009, Carter et al., 2006, Kronenwett et al., 2004, Walther et al., 2008, Mettu et al., 2010, Murayama-Hosokawa et al., 2010, Bakhoum et al., 2011). The connection between CIN and poor patient prognosis could stem from the fact that CIN is likely to create a highly genetically diverse pool of cells within a tumour due to its dynamic nature. This genetic diversity could mean that tumours are harder to treat with drugs, as there is a greater chance of developing resistance (Lee et al., 2011 2009, Duesberg, 2000). Indeed, CIN+ cell lines have been shown to acquire multidrug resistance faster than diploid cells (Duesberg et al., 2000). This laboratory has also shown that a panel of CIN+ colorectal cancer cell lines are more resistant to a large panel of kinase inhibitors than diploid CIN- colorectal cancer cell lines (Lee et al., 2011).

Conversely it has also been shown that extremely high levels of CIN can be beneficial for patient survival (Roylance et al., 2011, Jamal-Hanjani et al., 2015). This data suggest that there may be an optimal level of CIN that can be tolerated by cancer cells, and above this threshold there may be too much instability for a cell to survive, especially when tumours are challenged with chemotherapeutics.

1.10 Linking tetraploidy and chromosomal instability

Although there is a correlation between tetraploidy and aneuploidy in cancer (see Section 1.3.1), and experimental studies have shown that tetraploidisation can result in increased numerical and structural chromosome changes (see Section 1.7.3), the mechanisms specific to tetraploid cells that could lead to chromosomal instability are not fully understood.

A comprehensive genetic analysis of polyploidy in yeast revealed several potential pathways that are specifically required for survival in polyploids that could shed light on this question (Storchova et al., 2006). Storchova and colleagues analysed gene deletions for a total of 3540 genes in polyploid yeast strains, and identified three key categories of genes that were specifically required for polyploid yeast cell survival. These gene groups were DNA repair through homologous recombination, sister chromatid cohesion and mitotic spindle function (Storchova et al., 2006).

These results suggest that there is a genetic instability defect inherent to polyploid yeast. The authors observed a 200-fold increase in the rates of chromosome loss and an increase in spontaneous DNA damage that correlated with DNA content. Most striking was the mitotic defect present in tetraploid yeast, which manifested in a 3.6 fold increase in the frequency of syntelic kinetochore-microtubule attachments (Storchova et al., 2006). The authors suggest that this increase could be due to unequal scaling effects observed in tetraploid cells. The spindle length was the same in tetraploid yeast as both haploid and diploid yeast, although the cell volume was increased. Further, the spindle pole body (SPB) had a greater surface area in tetraploids. The authors suggest that these mismatches in scaling of core mitotic components could result in the increase in syntelic attachments (Storchova et al., 2006).

Studies have shown that tetraploid cells are subject to a higher rate of chromosomes loss (Mayer and Aguilera, 1990, Andalis et al., 2004, Fujiwara et al., 2005, Storchova et al., 2006, Davoli and de Lange, 2012). Since tetraploids formed through mitotic dysfunction or cytokinesis failure will contain extra centrosomes, this could provide a link between tetraploidy and numerical chromosomal instability. Extra centrosomes can lead to multipolar division, which would randomly segregate chromosomes into daughter cells, and could lead to high levels of aneuploidy (Gisselsson et al., 2008). However, most multipolar mitoses do not result in viable daughter cells, and so whether this mechanism contributes to tetraploidy-mediated chromosomal instability remains unclear (Ganem et al., 2009, Kuffer et al., 2013). As discussed in section 1.8.2.1, extra centrosomes can also lead to chromosome missegregation though transient multipolar spindles and an increased frequency of merotelic attachments (Ganem et al., 2009). This mechanism could be responsible for numerical chromosomal instability in tetraploid cells. However, as the yeast analysed by Storchova and colleagues did not have additional SPBs and still showed evidence of chromosomal instability, tetraploid mammalian cells may be subject to other mechanisms driving numerical instability aside from an increase in centrosome number (Storchova et al., 2006, Storchova and Kuffer, 2008, Ganem et al., 2007).

Tetraploid cells have also been shown to have an increase in structural chromosome aberrations (Fujiwara et al., 2005). How tetraploidy *per se* leads to this increase in structural chromosome aberrations remains unclear. One possibility is an increase in the level of spontaneous DNA damage in tetraploids, since tetraploid cells have more DNA. This is seen in tetraploid yeast strains (Storchova et al., 2006). However, no increase in DNA damage foci was reported for cells that had undergone cytokinesis failure, suggesting that tetraploidy may not always lead to an increase in DNA damage (Fujiwara et al., 2005). However, some studies have demonstrated increased sensitivity to DNA damaging agents in tetraploid cells, suggesting that tetraploid cells may have deficient DNA repair, or exceed a threshold of tolerable DNA damage faster than diploid cells (Hau et al., 2006). DNA damage and structural instability could also occur in tetraploid cells due to catastrophic missegregation of chromosomes in a multipolar division (Gisselsson et al., 2008). The frequency of these multipolar divisions in the long-term propagation of tetraploid cells has yet to be established, but it may be relatively infrequent (Ganem et al., 2009). Alternatively DNA could be damaged during missegregation of chromosomes in normal bipolar divisions (Janssen and Medema, 2012, Crasta et al., 2012).

1.11 Genomic instability in colorectal cancer

Colorectal cancer (CRC) is the second most prevalent cancer worldwide (Bray et al., 2013). The genetics of colorectal cancer are fairly well understood, with 15-20% of CRCs displaying microsatellite instability (MSI/MIN), and the majority displaying chromosomal instability (CIN). MIN and CIN do not generally co-occur in CRC, possibly suggesting that excessive genetic instability is detrimental to a cancer (Sieber et al., 2002, Abdel-Rahman et al., 2001, Lengauer et al., 1997). In general, MSI is a marker for better patient prognosis, and CIN has been shown to lead to poor patient prognosis (Guastadisegni et al., 2010, Lengauer et al., 1998, Mouradov et al., 2013).

Microsatellite instability is caused by mutations or defects in the mismatch repair (MMR) machinery (MSH2, MSH6, MLH1 and PMS2). The MMR pathway usually

corrects DNA replication errors that frequently occur when copying microsatellite repeats; repeated sequences of DNA found throughout the genome. MSI tumours therefore have a high frequency of mutations, particularly in genes that contain microsatellite sequences, for example *TGFBR2* (TGF-β type II receptor). Germ-line mutations in MMR genes cause a hereditary form of colon cancer, called Lynch syndrome (also formerly known as hereditary non-polyposis colon cancer, HNPCC). The most commonly mutated Lynch syndrome genes are *MLH1* and *MSH2* (90% of cases), whilst mutations in *MSH6* and *PMS2* are relatively uncommon (Grady and Carethers, 2008). Germline mutations in Lynch syndrome patients are followed by inactivation of the remaining wild type allele. Lynch syndrome patients account for 2-5% of all CRC cases (Umar et al., 2004). In sporadic CRC, MSI is most frequently caused by hyper-methylation of the *MLH1* gene promoter, resulting in loss of MLH1 expression (Herman et al., 1998, Veigl et al., 1998). MSI tumours tend to be diploid, with a high mutation rate. They also tend to occur on the right-side colon, and display mucinous histology and high lymphocytic infiltrate (Kim et al., 1994).

In a large cohort of tumours subject to exome-sequence analysis, the eight most frequently mutated genes in non-hypermutated CIN+ tumours were *APC, TP53, KRAS, PIK3CA, FBXW7, SMAD4, TCF7L2* and *NRAS* (Cancer Genome Atlas, 2012). Hypermutated tumours in this cohort tended to have mutations in different genes than the non-mutated cohort, supporting a separate genetic basis for these two kinds of instability in CRC (Cancer Genome Atlas, 2012). As expected, the number of somatic copy number aberrations (SCNAs) was greater in non-hypermutated tumours (Cancer Genome Atlas, 2012). Over 94% of these tumours had mutations in one or more genes in the WNT signalling pathway, and other deregulated signalling pathways included the MAPK, Pi3K, TGF-β and p53 pathways (Cancer Genome Atlas, 2012). The contribution of these different mutations to the CIN phenotype currently remains unclear.

1.12 Conclusion

Tetraploidy is a common occurrence in many different cancer types, where it seems to be associated with the onset of aneuploidy. In vitro studies of experimentally induced tetraploidisation have shown that tetraploidy is associated with increased tumorigenicity and genomic instability in short-term assays. The cellular consequences of tetraploidisation, and how these might impact upon its association with carcinogenesis have been less well explored. Furthermore, the long-term impact of tetraploidisation on a stable diploid genome have not been investigated, and nor have the mechanisms by which tetraploidy might contribute to the dynamic phenotype of CIN in vivo. Understanding the contribution of tetraploidy to CIN will help define the processes that drive cancer evolution and the emergence of intra-tumour heterogeneity.

In this thesis, the impact of tetraploidisation on the long-term genomic stability of a diploid genome was explored. Using a diploid cell line with a naturally occurring tetraploid fraction, isogenic diploid and tetraploid clones could be compared over longer than 18 months of continuous culture. This revealed that tetraploid cells were able to specifically propagate both numerical and structural chromosome aberrations, resulting in a markedly altered genomic profile. A mutational mechanism for this CIN tolerance phenotype was not uncovered, leading to the conclusion that tetraploidy could be a permissive state for chromosomal instability. The genetic changes that initially allow tetraploid cells to overcome cell-cycle checkpoint barriers were then considered. A targeted screen was carried out to identify regulators of cell cycle re-entry after cytokinesis failure, which is thought to be one of the most common routes to tetraploidisation in cancer.

Chapter 2. Materials & Methods

2.1 Cell culture

HCT-116 and RKO cells were obtained from the European Collection of Animal Cell Cultures (ECACC) by Cancer Research UK, HCT-116_MLH1.3 was kindly gifted by Françoise Praz (Saint-Antoine Research Centre Paris) and RPE-FUCCI cells were a kind gift from Dr Laurent Sansregret (Cancer Research UK). All cell lines were grown in Dulbecco's Modified Eagle Medium (DMEM) with 4.5/L D-glucose, L-glutamine and pyruvate (Gibco, Life Technologies), containing 10% FBS (LabTech) and 1X Penicillin Streptomycin (Sigma) at 37°C in a 5% CO_2 atmosphere.

2.2 Isolating diploid and tetraploid clones from cell lines

To isolate diploid and tetraploid clones from cell lines, cells were trypsinised and stained in 10µg/mL Hoescht 33342 (Sigma) for 1 hour at 37°C with occasional shaking. Cells were then washed twice in PBS, before straining using a 70µm cell strainer. Fluorescent-activated-cell sorting (FACS) was carried out using a MoFLo Cell Sorter (Beckman Coulter) equipped with a UV laser. Single cells were sorted into 96-well plates containing 20% FBS media. Diploid clones were selected from the 2N peak, and tetraploid cells were selected from the >4N peak. Andrew Rowan carried out the original isolation of diploid and tetraploid clones. The ploidy of all clones was checked using flow cytometry for DNA content (see below). Diploid and tetraploid clones were passaged once a week by seeding 150,000 cells into a 10cm dish containing fresh media. All passage numbers represented in figures are correct to within <4 passages.

The cloning efficiency of HCT-116 diploid cells was assessed using CellTiter-Blue (Promega) according to the manufacturer's instructions, colonies were counted as wells that had CellTiter-Blue values >1.5 the mean value of blank wells. Data was corrected using the Poisson distribution; efficiency = (-100) x ln(# of wells with no colony/total #of wells) % (Leight and Sugden, 2001). The cloning efficiency of HCT-

116 tetraploid cells was calculated after verification of the ploidy of all surviving clones. The cloning efficiency was calculated from the number of tetraploid clones arising from a given number of wells. Cloning efficiency was estimated across three independent experiments.

2.3 Transfections

2.3.1 Plasmid preparation

The H2B-mRFP plasmid was a gift from Anne Straube (University of Warwick, Coventry, UK).

Plasmids were prepared using heat-shock of XL-10^{TM} Gold Ultracompetent Cells (Agilent) following the manufacturer's instructions. Bacteria were then spread on agar plates containing appropriate antibiotics (Ampicillin, Sigma) and grown overnight at 37°C, before colony selection and expansion in L-broth also containing the relevant antibiotic. DNA was extracted using Quiagen Cartridge Midi/Maxi kits according to the manufacturer's instructions, and the concentration and quality of the DNA was quantified on a spectrophotometer (NanoDrop, Thermo Scientific).

2.3.2 Plasmid transfection

The H2BmRFP plasmid was transfected using Fugene 6.0 (Promega). Per 10 cm^2 dish, 9µL of Fugene was incubated with 300µL of Opti-MEM® reduced serum media (Gibco, Life Technologies) for 5 minutes, before adding 3µg of plasmid. This was further incubated for 15 minutes before adding to cells with 6mL of media. Cells were selected after 48 hours using 1µg/mL G418 (Life Technologies), and cell-sorted using fluorescence for RFP expression. After sorting, cells were maintained in 0.5µg/mL of G418 containing media.

2.3.3 siRNA preparation

siRNAs were ordered from Dharmacon, and were On-Target-Plus siRNAs unless otherwise stated. siRNAs were re-suspended using 5X siRNA buffer (Thermo

Scientific) diluted with nuclease free water (Ambion) to the desired concentration and mixed at RT (room temperature) for 30 minutes before storage at -20°C.
A list of common siRNA sequences used is shown in Table 2.4, and the full list of sequences ordered for the screen described in Chapter 6 is shown in the Appendix (Section 8.2).

2.3.4 siRNA transfection

The final concentration of siRNA used in all experiments was 40nM. The different transfection agents used were Lipofectamine™ RNAiMax (Invitrogen), Lullaby (OZ Biosciences) and INTERFERin® (Polyplus Transfections™).
For 96-well plate transfections, siRNAs were diluted in Hank's buffered salt solution (HBSS, without $CaCl_2$ or $MgCl_2$, Gibco, Life Technologies) to 400nM (10X final concentration), and 10µL was added to each well. Opti-MEM® reduced serum media (Gibco, Life Technologies) was mixed with transfection reagents and left at RT for 5 minutes, before 10µL was added to each well. The concentrations of transfection reagent per well are indicated in the figures and text of this thesis. The mixture of siRNA in HBSS and transfection reagent in Opti-MEM was left at RT in 96-well plates for 30 minutes, before 80µL of cells in suspension in normal media were added, bringing the total volume in each well to 100µL.
For 6-well plate transfections, 3µL of 20µM siRNA was mixed with 250uL of Opti-MEM in eppendorf tubes. Simultaneously, 3.5µL of transfection reagent was added to 250µL of Opti-MEM and left at RT for 5 minutes. This was then mixed with the siRNA containing Opti-MEM and left at RT for 30 minutes. 1mL of cells in suspension in normal media were then added to wells, and 500µL total volume of transfection mix was added.

2.3.5 Virus preparation

The pBabe Hygromycin-Luciferase plasmid was a kind gift from Dr Miguel Murillo (manuscript in preparation). Viruses were prepared by Dr Carolina Navas. 293-Phoenix Packaging Cells were obtained from Cancer Research UK Cell Services facility and grown in DMEM with 4.5g/L D-glucose, L-glutamine and pyruvate (Gibco, Life Technologies), containing 10% FBS (LabTech) and 1X Penicillin

Streptomycin (Sigma) at 37°C in a 5% CO_2 atmosphere. These cells were transfected by mixing 35µL Lipofectamine™ transfection reagent (Life Technologies) and 500µL of Opti-MEM for 5 minutes at RT, before mixing with 10µg of pBabe Hygromycin-Luciferase and 500µL of Opti-MEM and adding to cells after 20 minutes. After 16 hours media was replaced. Media was then collected and replaced every 24 hours for 2 days. Collected media was filtered using 0.22µm PVDF filters.

2.3.6 Virus infection

DC-14 and TC-13 cells at passage 8 were infected with filtered virus containing media with 8µg/mL Polybrene (Sigma, H9268). Cells were maintained in virus containing media for 3 days, before splitting into selection media containing 20µg/mL Blasticidin antibiotic (Life Technologies).

2.4 Immunofluorescence

Cells were grown on 22 x 22 mm glass cover slips coated with poly-L-lysine (Sigma). Cells were washed with PBS and then fixed and permeabilised using PTMEF fixative (4% formaldehyde, 20mM PIPES, 10mM EGTA, 1mM $MgCl_2$) for 10 minutes at RT. Coverslips were rinsed in PBS, and then blocked for 1 hour at RT, or until required at 4°C, in 3% BSA-PBS. Coverslips were incubated with 150µL of primary antibody in 3% BSA-PBS for 1.5 hours at RT, washed three times with PBS, and then incubated for 1.5 hours with secondary antibodies and DAPI (1µg/mL, Roche) in 3% BSA-PBS at RT protected from light. Coverslips were washed again three times with PBS, and then mounted on glass slides with Vectashield mounting medium (Vecta H-1000), before sealing with clear nail varnish. Secondary antibodies were from Molecular probes, and used at 1:500 dilution (Goat anti-mouse conjugated to AlexaFluor [AF] 488, goat anti-rabbit AF594, goat anti-human AF647).

Primary antibodies used in this thesis are listed in Table 2.1.

Table 2.1: Primary antibodies used for immunofluorescence

Primary Antibody	Species	Company	Dilution
γ-H2AX	Mouse	Millipore 05-636	1:500
53BP1	Rabbit	Santa-Cruz sc-22760	1:500
β-tubulin	Rabbit	Abcam ab6046	1:1000
Centrin-3	Mouse	Abcam ab54531	1:1000
CREST	Human	Fitzgerald 90C-CS1058	1:2000
LaminA/C	Mouse	Santa Cruz sc-7292	1:1000
p21	Rabbit	CRUK antibody, MH9	1:2000
p53	Mouse	CalbioChem OP43	1:500

2.4.1 Image acquisition for immunofluorescence

Unless otherwise stated, all image acquisition for immunofluorescence slides was carried out using an Olympus Deltavision RT microscope (Applied Precision LLC) equipped with a CoolSnap HQ camera. Images were deconvolved using conservative settings for 8 cycles. Images were analysed using softWoRX Explorer (Applied Precision LLC).

2.4.2 Segregation error scoring

To score segregation errors, slides were stained with CREST to visualise centromeres, and β-tubulin and DAPI to identify bipolar anaphase cells. Telophase cells, where tubulin had formed a narrow bridge between the two daughter cells, were excluded from this analysis. Multipolar anaphases were also excluded. Approximately 100 z-stacks of 0.2μm were obtained for each cell to visualise the entire anaphase using an Olympus 100X 1.4 numerical aperture UPlanSApo objective.

2.4.2.1 Segregation error classification

Segregation errors were classified as follows:
Anaphase bridges – A clear DAPI signal extending from one daughter cell chromosome mass to the other.

Acentric lagging chromosome fragments – A clear DAPI signal that is between and separated from the two daughter chromosome masses that is completely devoid of centromeric CREST staining.

Lagging chromosomes – A DAPI signal that is between and separated from the two daughter chromosome masses that has a clear centromeric CREST signal.

Other – Any clear anaphase error that could not be classified into the above categories. These included lagging dicentric chromosomes joined by bridges.

Examples of segregation error types are shown in Figure 2.1.

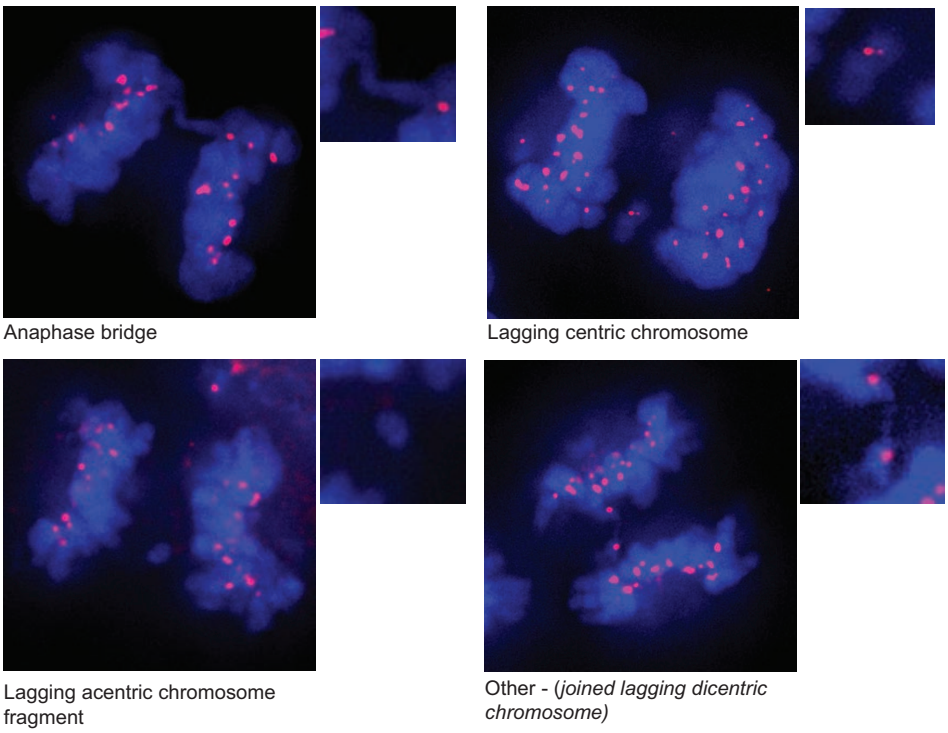

Figure 2.1: Examples of segregation error classification

Types of segregation error commonly observed in HCT-116 and derivative cell lines. DNA is stained with DAPI, and centromeres are detected using immunofluorescence with antibodies against human CREST. Inset shows a close up of error.

2.4.3 Interphase DNA damage scoring

To score interphase DNA damage foci, slides were stained with 53BP1 and γ-H2AX. Approximately 65 z-stacks of 0.2μm were obtained for each field of view, using an Olympus 40X 1.3 numerical aperture UPlanSApo objective. Interphase

cells were assessed from DAPI staining, and foci were scored when 53BP1 and γ-H2AX foci co-localised.

2.4.4 Spindle morphology

To assess spindle morphology slides were stained with β-tubulin, centrin-3 and DAPI. DAPI was used to identify pre-anaphase cells. Approximately 65 z-stacks of 0.2μm were obtained for each cell using a using an Olympus 60X 1.42 numerical aperture UPlanSApo objective.

2.4.5 Centriole number

To assess centriole number slides were stained with β-tubulin, centrin-3 and DAPI. DAPI was used to identify prophase cells. Approximately 100 z-stacks of 0.1μm were obtained for each cell using a using an Olympus 100X 1.4 numerical aperture UPlanSApo objective.

2.5 Metaphase spreads

2.5.1 Slide preparation

Cycling cells were treated for 1-2 hours with 100ng/mL Colcemid (Gibco) before trypsinisation and washing in PBS. Cells were re-suspended in a small amount of PBS, before a 7-minute incubation in a hypotonic solution (4% KCl, 4% sodium citrate) at 37°C. Cell pellets were collected by centrifugation (1000 rpm for 5 minutes) before gentle re-suspension in fixative (3:1 Methanol: Acetic Acid). Cell suspensions were left in fixative for 30 minutes at RT, centrifuged and re-suspended in fresh fixative for a further 20 minutes. After another round of centrifugation and re-suspension in fresh fixative, the solution was dropped onto glass slides using a Pasteur pipette. Slides were aged at RT for at least 48 hours before analysis.

2.5.2 Hybridisation

Slides were hybridised to an all-human centromere alpha-satellite DNA probe (FITC labelled, Posiedon) to visualise structural chromosome aberrations. Slides were incubated for 15 minutes at 37°C in 2X SSC with 0.5% Tween 20, and dehydrated through an Ethanol series (70-85-100%) before air-drying. Probe was sealed under a 22 x 22 mm coverslip sealed with rubber cement before denaturation for 10 minutes on a hot block at 75°C. Probes were hybridised overnight at 37°C in a humidified chamber. Rubber cement was removed and slides were rinsed in 2X SSC 0.5% Tween20, before a two minute wash at 72°C in 0.5X SSC with 0.4% Tween20. Slides were rinsed again at RT in in 2X SSC 0.5% Tween20 before incubation for 15 minutes in PBS containing 1µg/mL DAPI (Roche), dehydration through an Ethanol series and mounting with Vectashield (Vecta H-1000) and sealing with clear nail varnish.

2.5.3 Analysis

Slides were visualised on an Olympus Deltavision RT microscope (Applied Precision LLC) equipped with a CoolSnap HQ camera using an Olympus 60X 1.42 numerical aperture UPlanSApo objective. Approximately 15 z-sections were taken at 0.1µm intervals, and deconvolved using conservative settings for 8 cycles. Images were analysed using softWoRX Explorer (Applied Precision LLC).

2.5.4 Structural chromosome abnormalities

Structural chromosome abnormalities were classified as follows (examples are shown in Figure 2.2):

Acentric chromosome fragments – any chromosome or part of a chromosome lacking any discernible signal from the centromeric probe.
Dicentric chromosomes – chromosomes clearly harbouring two centromeric signals that were separated from each other.
Double strand breaks – Chromosome arms showing a clear break in DAPI signal, where the intact chromosome has one shorter chromosome arm as a result.

Other – Some cells showed evidence of different aberrations that could not be classified into the above three categories. These included shattered chromosomes, and abnormal chromosome shapes (see Figure 2.2 for examples).

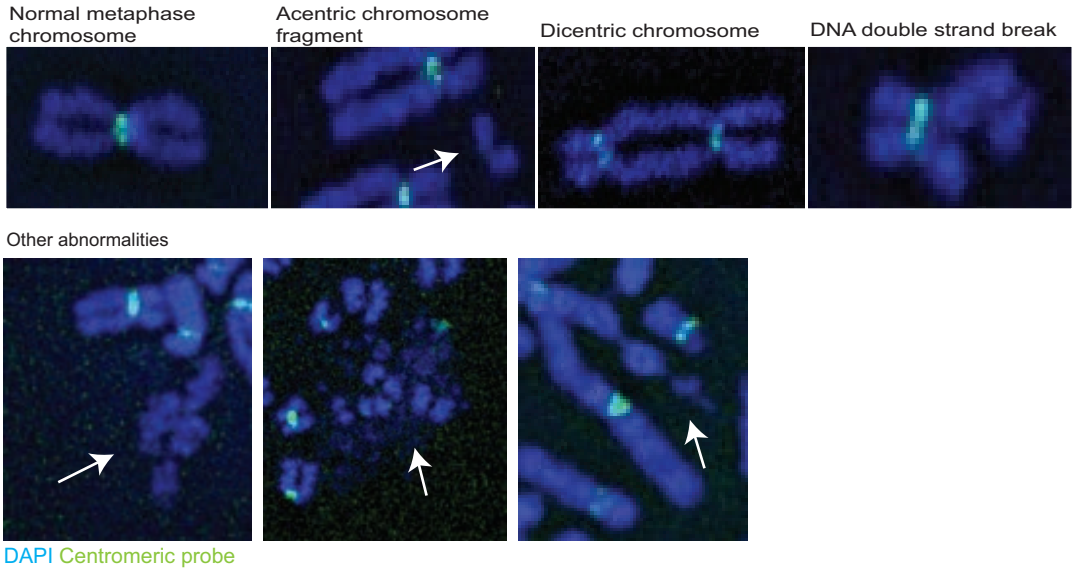

Figure 2.2: Classification of structural chromosome abnormalities

Examples of structural chromosome abnormalities scored. DNA is stained with DAPI, and centromeres are hybridised to an all-human centromeric probe. White arrows indicate chromosome of interest.

2.6 Clonal fluorescence in-situ hybridisation (FISH)

2.6.1 Slide preparation

Glass sides were coated in poly-L-lysine and placed inside a 10 cm^2 tissue-culture dish. Cells were seeded at a density of 500 cells per slide in 1mL of media. Cells were left overnight to attach to the glass slide, and the dish was filled with normal media the next day. After 10-14 days the slides were washed in PBS, cells were swelled for 7 minutes with 0.4% KCl-0.4% sodium citrate solution and fixed in 3:1 Methanol: Acetic Acid for 30 minutes before air drying and ageing at RT for at least 1 week.

2.6.2 Hybridisation

Slides were treated with SPOT-light tissue pre-treatment solution (Invitrogen) at 100°C for 10 minutes, before two 3 minute washes in PBS. Slides were then dehydrated through an Ethanol series (70-85-100%). Slides were probed with FISH

probes specific to chromosome 2 (CEP2, D271, SO) and chromosome 8 (CEP8, D872, SGn, both Abbott Molecular probes). Probes were added to slides on a 22 x 22 mm coverslip diluted with Hybridisation buffer (Abbott Molecular probes), and sealed with rubber cement. Slides were co-denatured on a hot block at 95°C for 5 minutes, before incubation in a humidified chamber overnight at 37°C. Rubber cement was removed with tweezers and slides were rinsed with 0.5 X SSC at RT to remove coverslips. Slides were washed in 0.5 X SSC for 5 minutes at 75°C, before another wash in 0.5 X SSC at RT before rinsing in ddH_20. Slides were incubated in PBS containing 1µg/mL DAPI (Roche) for 15 minutes at RT before dehydration through an Ethanol series (70-85-100%). Slides were mounted in Vectashield (Vecta H-1000) and sealed with clear nail varnish.

2.6.3 Analysis

Clonal FISH slides were scanned using an Ariol semi-automated microscope (Leica Microsystems). Slides were scanned initially at 10X magnification, and discrete colonies were selected. Colonies were then scanned at 40X magnification with z-stacks of 9 x 0.7µm. Analysis was carried out using custom-made software from Leica Microsystems that identified isolated nuclei from the DAPI signal and categorised chromosome numbers from the green and orange channels for the chromosome probes. Individual cells were categorised according to their copy number state for the two chromosomes. Data was manually curated, and cells that had been mis-categorised were re-categorised by hand. Three slides were scored using an Olympus Deltavision RT microscope (Applied Precision, LLC) equipped with a CoolSnap HQ camera with an Olympus 40X 1.3 numerical aperture oil immersion objective, and analysed with softWoRX Explorer (Applied Precision, LLC). Data was comparable between the two different scoring methods.

2.7 Flow cytometry

2.7.1 DNA profiles

Cells were trypsinised and washed in PBS before fixation and storage in 70% Ethanol until required at 4°C. Cells were washed twice in PBS, before staining with Propidium Iodide (Sigma) and treating with RNase (Life Technologies). Alternatively cells were stained with Hoechst 33342 (Sigma). DNA profiles were collected after setting laser voltages for the parental diploid cell line.

2.7.2 S phase duration

To assess the duration of S-phase, a BrdU pulse experiment was performed. Cells were treated with 10μM BrdU (Sigma, B5002) for 15 minutes, before three washes in PBS. A sample was fixed at this time point (0 hours) and then subsequent samples were fixed at 2, 4, 6, 8 and 24 hours after the BrdU pulse in 70% Ethanol until required. Samples were centrifuged (1400 rpm for 5 minutes) out of the 70% Ethanol, and rinsed in PBS containing 1% FBS, before incubation in 2M HCl for 20 minutes at RT to denature DNA. Samples were centrifuged out of HCl and rinsed in 1% FBS/PBS again, before a 5 minute wash in 0.5% TritonX-100 in 1% FBS/PBS to permeabilise cells. After two more 1% FBS/PBS washes, samples were incubated overnight at 4°C with a Mouse anti-BrdU antibody (BD Biosciences) at 1:500 dilution in 3% BSA/PBS. After primary antibody incubation, samples were washed twice with 1% FBS/PBS, before incubation protected from light at RT with a secondary antibody (Goat anti-mouse conjugated to AlexaFluor488, Molecular probes) at 1:300 dilution in 3% BSA/PBS for 30 minutes. Samples were washed twice with 1% FCS/PBS before re-suspension in PBS and staining with Propidium Iodide (Sigma) to visualise DNA. Samples were analysed on a Fortessa flow cytometer (BD Biosciences). Positive BrdU cells were identified using an untreated control sample. The cell cycle phases of BrdU positive cells at 0, 6, 8 and 24 hours were analysed using the Watson-Pragmatic cell cycle function of the FlowJo programme using standard settings (Watson et al., 1987).

2.8 Proliferation curves

To assess proliferation rates between different cell lines, all cell lines were seeded at an initial density of 2000 cells per well of a 96-well plate (6 well replicates per cell line) in 6 plate replicates. The first plate was fixed as soon as cells were attached, and then a plate was fixed every 24 hours in 70% Ethanol and stored at -20°C. Plates were washed in PBS, and stained with DAPI (Roche) at 1µg/mL for 5 minutes, before rinsing in PBS. Nuclei were counted using an Acumen cell counter (TTP LabTech). Cell number was normalised to the cell count from the first fixed plate and expressed as a fold change.

2.9 Drug sensitivity assays

To test sensitivity of different cell lines to specific drugs, cells were seeded at a density of 2000 cells per well of a 96-well plate, and treated with varying concentrations of cisplatin (Sigma, P4394), paclitaxel (LC Labs, P9600) or camptothecin (Sigma, C9911) 24 hours later. Plates were left for 72 hours in the presence of drug before treatment with CellTiter-Blue (Promega), according to the manufacturer's instructions, to assess cell viability. Viability was normalised to wells treated with a vehicle control.

2.10 Calbiochem Kinase Inhibitor Screen

Calbiochem Kinase Inhibitor libraries I and II were obtained from Merck Millipore, totalling 160 inhibitors. All cell lines were seeded in triplicate at a density of 4000 cells per well using an automated WellMate liquid handling system (Thermo Fisher Scientific). Cells were treated with all inhibitors at a concentration of 10µM 24 hours later and incubated for 72 hours in a rotating tissue culture inhibitor. To assess cell viability plates were treated with CellTiter-Blue (Promega) according to the manufacturer's instructions. 16 wells per plate were treated with DMSO as a vehicle control. All treated wells were normalised to the average value for DMSO treated wells. The average normalised value for the triplicate repeats was taken for each cell line. Dr Pierre Martinez prepared cumulative distribution frequency graphs

using the statistical programme R. A Kolmogorov-Smirnov test was performed to assess differences between cumulative distributions of diploid and tetraploid cell lines. The effect of different drugs on diploid and tetraploid clones was assessed by comparing the log fold change difference in relative cell numbers.

2.11 Exome sequencing

2.11.1 Sample preparation

DNA extraction was carried out using the Quiagen DNeasy Blood and Tissue extraction kit following the manufacturer's instructions. DNA quality was assessed using a QuBit instrument (Life Technologies). DNA preparation and sequencing was carried out by the Advanced Sequencing Facility at Cancer Research UK London Research Institute. Paired end sequencing was carried out as described (Gerlinger et al., 2012). Briefly, DNA was fragmented into 250-300 base pair (bp) fragments, before adaptors were ligated to each end. Adaptor-ligated templates were purified with Agencourt AMPure SPRI beads, and amplified by ligation mediated PCR (polymerase chain reaction). DNA was then hybridised to SureSelect Biotinylated RNA library (BAITS) and bound to streptavidin beads. Each sample was loaded onto an Illumina Genome Analyser II, and paired end sequencing was performed to at least 30X coverage. Raw image files were processed with HCS1.4.8 using default parameters to call bases.

2.11.2 Alignment and variant calling analysis

Alignment and variant calling was carried out by Harshil Patel (Bioinformatics and Biostatistics, London Research Institute). Raw reads were aligned to the human hg19 genome assembly using BWA 0.5.9 (Li and Durbin, 2009), with a maximum mismatch threshold of 4 within 101bp, all other parameters were left as default. Alignments were post-processed to remove reads that mapped to multiple genomic loci, and those that could have arisen from PCR duplication (using picard tools 1.81, Picard, 2012). The Genome Analysis ToolKit (version 2.3-9-ge5ebf34, DePristo et al., 2011) was used to perform indel realignment and indel left alignment. After filtering, a median exome coverage of 76X was observed per sample.

Base-level nucleotide counts were obtained using the deepSNV package (Gerstung et al., 2012), with a minimum base quality threshold of 20, and subsequent variant calling was performed across all samples simultaneously using scripts written in Python. Variants with a minimum nucleotide count of 5 and an allele frequency less than 0.1 were excluded from further analysis. Variant annotation was performed with ANNOVAR release 2012Oct23 (Wang et al., 2010).

2.11.3 Downstream filtering

All variant calls in all samples were filtered as follows. The number of times a variant appeared in diploid and tetraploid samples was added as a filter. Mutations occurring in any diploid sample were removed. Unique tetraploid mutations were then filtered for how many samples they occurred in. Different amino acid substitutions in the same gene occurring in the same tetraploid sample were not counted as two different samples. Only genes that were mutated in more than one tetraploid sample are shown in Table 5.4. The predicted consequence of each mutation was assessed using the tools SIFT-predictor, PolyPhen-predictor and Mutation-taster contained in the ANNOVAR variant calling package (Wang et al., 2010).

2.12 Microarray profiling

RNA was extracted using the Quiagen RNeasy extraction kit following the manufacturer's instructions. RNA quality was tested using a Qubit (Life Technologies). RNA was sent to the Cancer Research UK Manchester Institute for analysis using Affymetrix Human Gene 1.0 ST arrays.

Microarray data analysis was carried out by Probir Chakravarty, Dr Tejal Joshi, Dr Nicolai Birkbak and Nicholas McGranahan.

Data was normalised using the frozen Robust Microarray Analysis (fRMA) method (McCall et al., 2010), summarising probes sets at gene level. Genes showing significant differential expression between diploid and tetraploid cell lines were identified using a Students T-test with a significance threshold of $P<0.05$.

Significant genes were further filtered by only including genes that showed at least a two-fold difference in means. To compare against the list of genes differentially expressed between diploid and tetraploids in Castedo et al., a Spearman's rank correlation was used (Castedo et al., 2006). Statistical analysis was carried out using the R statistical environment.

2.13 Western blotting

For p53 and p21 western blots, cells were treated for 1 hour with 1μM Doxorubicin (Sigma), before recovery for 7 hours in normal media. Cells were rinsed in PBS and frozen at -80°C until required. Samples were lysed on ice using lysis buffer containing 50mM HEPES [pH 7.2], 150mM NaCl, 1mM EDTA, 20mM MaF and complete protease inhibitors (Roche). Samples were separated on NuPAGE 4-12% Bis-Tris gel (Invitrogen), with MES running buffer (Invitrogen), before semi-dry transfer to a poly-vinylidene fluoride (PVDF) membrane. Membranes were blocked with 0.1% TBS Tween20 with 5% Milk, before incubation with primary antibodies over night at 4°C (p21 Rabbit, 1:1000, Cancer Research UK Tim Hunt Laboratory; p53 Mouse, 1:500 Santa Cruz sc126; β-catenin, 1:500, 610154 BD Biosciences). After washing in 0.1% TBS Tween, secondary antibodies (actin directly conjugated HRP, 1:50000, Sigma, swine anti-goat RRP and swine anti-rabbit HRP, 1:25000, both Dako) were added for 1 hour at RT. Detection was carried out with Immobilon Chemiluminescent HRP substrate (Merck Millipore).

For LATS 2 western blotting, siRNA transfections were carried out in a 6-well plate format as described in Section 2.3.4. After 72 hours cells were rinsed in PBS and frozen at -80°C until required. Cells were lysed using RIPA buffer containing complete protease inhibitors (Roche). Samples were resolved on a NuPAGE 4-12% Bis-Tris gel (Invitrogen) with MOPS running buffer, and transferred to a PVDF membrane for 2 hours using wet-transfer with buffer containing 192mM Tris, 25mM Glycine, 10% Methanol and 0.01% SDS. Membranes were blocked for 2 hours with 0.5% TBS Tween20 with 5% Milk. Primary antibody (LATS2 Rabbit, 1:1000, Cell Signalling Technology 13646) was added overnight at 4°C. After washing,

secondary antibody (swine anti-rabbit HRP, 1:25000, Dako) was incubated at RT for 1 hour. Detection was carried out with Immobilon Chemiluminescent HRP substrate (Merck Millipore).

2.14 Live Cell Imaging

2.14.1 Mitotic timing

H2B mRFP expressing cells were seeded in 8-well glass bottomed imaging chambers (LabTek) at a density of 50,000 cells per well. Chambers were visualised on an Olympus Deltavision RT microscope (Applied Precision, LLC) equipped with a CoolSnap HQ camera in 5% CO_2 at 37°C. A total of 7 z-stacks of 2µm were taken every 3 minutes for 6 hours. The movies were analysed on softWoRX Explorer (Applied Precision LLC). The time from nuclear envelope breakdown to anaphase onset was recorded. Only cells that underwent a normal bipolar division with no errors were included for analysis.

2.14.2 Segregation error cell-fate

H2B-mRFP cells lines were seeded as for mitotic timing movies, and imaged using the same microscope equipment. A total of 7 z-stacks of 2µm were taken every 3 minutes for the first 6 hours, and then every 15 minutes for a subsequent 60 hours to record cell fate. Cells that divided during the imaging period were examined for segregation errors, and the subsequent fate of these cells was recorded. Cells were scored as arrested if they failed to divide within 48 hours of the first division. Multipolar divisions were excluded from analysis.

2.15 DNA fibre assays

Cells were sequentially labelled with 20-minute treatments of 25µM CldU (5-Chloro-2'-deoxyuridine, Sigma C6891) and then 250µM IdU (5-Iodo-2'-deoxyuridine, Sigma I7125) in fresh media, both of which were equilibrated for at least an hour in a 5% CO_2 atmosphere. Cells were washed twice with ice-cold PBS, and removed from dishes using a cell scraper, counted and diluted to 1 x 10^6 cells/mL in cold

PBS. Cells were spread on glass slides using spreading buffer (200mM Tris-HCl pH 7.4, 50mM EDTA, 0.5% SDS) and air dried before fixation in 3:1 Methanol: Acetic Acid. To stain, slides were washed twice in H_2O for 5 minutes, rinsed in 2.5M HCl, before denaturation in 2.5M HCl for 1 hour 15 minutes. Slides were rinsed twice in PBS, washed twice for 10 minutes in blocking solution (1% BSA/PBS, 0.1% Tween20), before a 1-hour incubation in blocking solution. Primary antibodies (Rat anti BrdU, Clone BU1/75 [ICR1] Santa Cruz 1:1000, Mouse anti-BrdU, BD Biosciences, 1:1000) were added and incubated for 1 hour at 37°C. Slides were rinsed 3 times in PBS before fixation for 10 minutes in 4% paraformaldehyde, followed by a further 3 PBS washes and 3 x 10-minute washes with blocking solution. Secondary antibodies (Goat anti-Rat AlexaFluor555 and Goat anti-Mouse AlexaFluor488, both 1:500, Molecular probes) were incubated for 2 hours at 37°C, before 3 rinses in PBS. Slides were mounted in Vectashield H-1000 and sealed with clear nail varnish. Slides were visualised using an Olympus Deltavision RT microscope (Applied Precision, LLC) equipped with a CoolSnap HQ camera with a 40X UPlanSApo 1.3 numerical aperture objective and the length of fibre tracks was measured using softWoRX Explorer (Applied precision LLC) and ImageJ software. Fibre track length was converted to kilobases (kb) using the conversion factor 1 μm = 2 kb.

2.16 Spheroid assays

To form spheroids, 5000 cells were seeded per well of 96-well Costar® Ultra-low attachment plates (Corning) with 2.5% growth factor reduced basement membrane Matrigel® (Corning). Plates were centrifuged for 10 minutes at -4°C at 820rpm to collect cells. Plates were imaged using an inverted Zeiss 510 light microscope with a 5X 0.13 numerical aperture objective and automatic stage. Imaging was carried out 1, 5 and 7 days after cell seeding. Dr Dominic Alibhai carried out imaging and calculation of spheroid volume. Transmitted light images were used to calculate spheroid volume, with automatic image segmentation and size determination by in-house software (Wolfram Mathematica 9.0). Briefly, background signal was removed, and small objects (i.e. unformed cell clumps) were removed. The volume of each spheroid was calculated assuming spherical symmetry and using the

appropriate scaling factor. Eight spheroids per cell line were analysed in each experiment. The growth rate of spheroids was calculated using the slope function in Excel (Microsoft).

2.17 Primary CRC and matched liver metastasis cohort

A cohort of matched primary CRC and liver metastasis blocks were obtained from Dr Marcell Szasz (Semmelweiss University, Hungary). All clinical data was provided by Dr Szasz.

2.17.1 Determination of MSI status

The MSI status of the tumours had been previously determined by Dr Szasz using standard immunohistochemistry (IHC) analysis with antibodies against MLH1, MSH2, MSH6 and PMS2. However, some samples had uncertain results from IHC analysis, or a mismatch in MSI status between the primary and metastatic lesion. Microsatellite PCR analysis was carried out on these samples.

DNA was extracted from paraffin embedded 20µm scrolls using a Quiagen DNAeasy Blood and Tissue Kit as follows. Xylene was added to eppendorf tubes containing the tissue scrolls to de-wax, tubes were spun at high speed to collect tissue, and Xylene was replaced with Ethanol in two wash steps. Sample was dried on a hot block at 37°C. 180µL of ATL buffer with 20µL of proteinase K solution was added overnight at 56°C, and after 16 hours, additional proteinase K solution was added for a further 4 hours. DNA extraction was then completed using the Quiagen DNAeasy Blood and Tissue Kit following the manufacturer's instructions. For microsatellite PCR analysis the standard CRC markers D2S 123, D17 250, D5S 346, D11 S904, BAT25 and BAT26 were used. The sequences of these primers are shown in Table 2.2.

Table 2.2: Microsatellite PCR primers

Name	Forward primer	Reverse primer
BAT25	TCGCCTCCAAGAATGTAAGT	TCTGCATTTTAACTATGGCTC
BAT26	TGACTACTTTTGACTTCAGCC	AACCATTCAACATTTTTAACCC
D11 S904	ATGACAAGCAATCCTTGAGC	CTGTGTTATATCCCTAAAGTGGTGA
D2S 123	AAACAGGATGCCTGCCTTTA	GGACTTTCCACCTATGGGAC
D17 250	GGAAGAATCAAATAGACAAT	GCTGGCCATATATATATTTAAACC
D5S346	ACTCACTCTAGTGATAAATCGGG	AGCAGATAAGACAGTATTACTAGTT

DNA was subject to PCR with these primers using Quiagen *Taq* polymerase and nucleotides. The PCR programme used was as follows: Step 1: 94°C for 5 minutes. Step 2: 94°C for 45 seconds. Step 3: 55°C for 45 seconds. Step 5: 72°C for 1 minute (repeat steps two to five 45 times). Step 6: 72°C for 10 minutes. PCR products were run on 2% agarose gels to assess concentration of PCR product, and diluted in water accordingly (standard dilution of 1:100). 3µL of diluted PCR product was subjected to microsatellite fragment analysis using an ABI 3130xl Genetic Analyser. Samples were analysed using GeneMapper software (Applied Biosystems). DNA from normal tissue and MSI+ cell lines used as controls was provided by Andrew Rowan. Samples needed to have positive results from >2 of the above PCR markers for classification as MSI+.

2.17.2 Image Cytometry

Image cytometry analysis was carried out by Damhane Oukrif (UCL Pathology).

40µm scrolls were provided for this analysis. Sections were de-waxed in Xylene, and rehydrated through an Ethanol series, before digestion with proteinase XXIV (Sigma) for 2 hours at 37°C. Samples were washed in PBS and filtered through 40µm filters. 100µL of nuclear suspension was added to a Shandon single use ez-cytofunnel (Thermo Scientific) and spun with a Shandon Cytospin 2 at 225 **g** for 5 minutes onto Superfrost Plus electrostatically positively charged blue slides (VWR). Slides were air-dried for 1 hour and fixed in 5M HCl for 1 hour. Slides were stained with Feulgen-Schiff reagent using standard methodology.
Slides were analysed using a Fairfield DNA Ploidy System (Fairfield Imaging), equipped with a Zeiss Axioplan microscope, a 546nm green filter and a high-

resolution camera (C4742-95, Hamamatsu photonics). The integrated optical density was calculated from the optical density and nuclear area of each nucleus. At least 1000 nuclei were sorted into the following categories: nuclei of interest, lymphocytes, plasma cells and fibroblasts. Lymphocytes were used as a reference for the 2C peak. Images were manually curated to remove cut or overlapping nuclei. Histograms of DNA and DNA index of nuclei of interest were provided for analysis.

2.18 Bioluminescent imaging in mice

The two cell lines expressing luciferase (as described in Section 2.3.6) were checked for luciferase activity by plating into 96-well black glass-bottomed plates (BD Falcon) at decreasing cell numbers, and treating with 150µg/mL Luciferin (D-Luciferin K salt, Caliper/Xenogen, 122796). Images were obtained using a IVIS Spectrum instrument (Xenogen) using Auto acquisition settings, and the specific luciferase activity per cell was calculated across a range of cell numbers (average flux per well/numbers of cells per well = photons/second/cell).

All mice work was carried out at Cancer Research UK London Research Institute under Home Office Project Licence Number PPL 80/2603. Nude mice (Nu/Nu) were obtained from Cancer Research UK Biological Resource Unit and kept in ultra clean conditions and individually ventilated cages. Mice were injected intravenously into the tail-vein with cells suspended in PBS. A maximum of 200µL of solution was injected per mouse. After injection mice were imaged once a week where possible to monitor tumour growth. Mice were culled when the tumour burden resulted in adverse health effects, for example significant weight loss or moribund behaviour, according to the thresholds set under the project license.

For imaging, mice were anaesthetised using 2% Isoflurane (IsoFlo, Abbott) in an induction chamber, before injection with 100µL of 30mg/mL Luciferin solution (D-Luciferin K salt Caliper/Xenogen, 122796). Mice were placed in a supine position in order to achieve maximum exposure of the lungs (the expected location of metastatic deposits) in an Animal Isolation Imaging Chamber (Caliper Life Sciences), which was imaged using an a IVIS Spectrum instrument (Xenogen) with

an XGI-8 Gas Anaesthesia System (Xenogen). Images were acquired using automated sequence acquisition settings (Binning large, FStop 1, Height 1.5, FOV D, 1.0 minute delay, 40 segments) until a plateau of luminescent signal was reached. Maximum bioluminescent signals from the whole body of the mouse were obtained using Living Image 4.3.1 software (Caliper Life Sciences) for analysis. Maximum bioluminescent signals were converted into log format for graphical representation.

The statistical analysis described below was carried out by Stuart Horswell. To compare the growth rate between the different cell lines the statistical package R was used to apply a multiple regression analysis including terms for cell line, cell dose, mouse, time, and dose: time interaction. ANOVA was used to compare the significance of these different terms. The standard R packages lm() and anova() were used in this analysis.

2.19 Histopathology

Tumour tissue was fixed in 10% Neutral Buffered Formalin for 24 hours before delivering to the London Research Institute Experimental Histopathology department for processing. Tissue was set into blocks using an automated Tissue-Tek VIP Tissue Processor. Briefly, blocks were sequentially incubated with increasing concentrations of methylated spirit (IMS) up to 100% (1 hour each), then four replacements with Xylene (1 hour each), followed by four replacements with paraffin wax for 45 minutes each (Fibrowax Pastillated, R.A.Lamp/VWR) at 45°C. Blocks were sectioned to 3μm thickness using a microtome. H&E staining was carried out using a Tissue-Tek Prisma Automated Stainer. Briefly, slides were washed in Xylene (2 x 120 seconds) then 100% IMS (2 x 30 seconds), 95% IMS (30 seconds), 70% IMS (30 seconds) and H_2O (30 seconds). Slides were then stained with Harris Haematoxylin (Thermo Scientific/Shandon 6765004) for 420 seconds, washed in H_2O for 30 seconds, then in 1% acid alcohol for 20 seconds, before washing in Lithium Carbonate Saturated Solution for 30 seconds, and H_2O again for 30 seconds. Slides were then stained with Eosin Y (VWR, 341973R) for 420 seconds, before washing with H_2O (30 seconds), and then increasing

concentrations of IMS (70, 95, 100%, 30 seconds each), a final 100% IMS wash (30 seconds), and two washes in Xylene (30 seconds).

Pathology reports from slides were produced by Professor Gordon Stamp (London Research Institute/Royal Marsden Hospital).

Images of H&E slides were acquired using a Nikon Eclipse microscope with a 4X 0.2 numerical aperture and a 20X 0.75 numerical aperture objective (Nikon Japan Plan Apo) and a Nikon Digital Sight Camera (DS-U2). The imaging software NIS Elements AR 4.00.00 64 bit (Nikon) was used to capture images.

2.20 RT-qPCR

RNA was extracted using RNeasy Quiagen Kits, with On-Column DNase I digestion (Sigma). RNA concentration was quantified on a NanoDrop instrument (Thermo Scientific). cDNA was synthesised from 1µg of RNA using an AffinityScript cDNA synthesis kit according to the manufacturer's instructions (Agilent). Real-time quantitative polymerase chain reaction (qPCR) primers were designed using Primer-BLAST (Ye et al., 2012). Multiple qPCR primers were ordered for each target gene, and after testing, the primer pairs that gave a single melt curve were retained for further use. qPCR was performed using EXPRESS SYBER® GreenER with Premixed ROX (Invitrogen) according to the comparative ΔΔCT method with normalisation to the expression of β-actin. Three replicates from each biological sample were run in each experiment in a 96-well plate on a 7500FAST machine (Applied Biosystems). qPCR primer sequences are shown in Table 2.3.

Table 2.3: RT-qPCR primers used in this thesis

Gene	Forward Primer	Reverse primer
KCNA5	ATGCAGACAGTGCCCGAAG	CCAGGCAGAGGGCATAAAGG
CNGB3	CGCTGACAAAAGTCAACAAGGT	GTTTTCTTCCTGTGCTGTGGT
LATS2	CAAACTACATCGCACCCGAG	GATCACCTTCAGCTGGGTTTC
p21	CCATGTGGACCTGTCACTGT	GGCGTTTGGAGTGGTAGAAA
β-actin	TGGATCAGCAAGCAGGAGTATG	GCATTTGCGGTGGACGAT

2.21 Screen for regulators of cell-cycle arrest after cytokinesis failure

The premise of this screen was based on the protocol described in Ganem et al., 2014.

A full list of all the siRNA sequences used in this screen is included in the Appendix (Section 8.2). A list of separately ordered siRNAs and their sequences are shown in Table 2.4.

RPE-FUCCI cells were a kind gift of Dr Laurent Sansregret (London Research Institute). On Day 0, cells were seeded at a density of 4 x 10^6 cells per 15cm tissue culture dish. After 24 hours cells were treated with dihydrocytochalasin-B (DCB, Sigma) for 16 hours. Cells were washed five times for five minutes in PBS, before trypsinisation and staining for 1 hour at 37°C with 10μM Hoechst 33342 (Sigma). Samples were prepared for sorting by filtration using 70μM filters and suspension in PBS. Samples were sorted using an Influx BD cell sorter (BD Biosciences). The FUCCI markers were excited with 561nm (emission 610/20, mCherry) and 488nm (emission 530/40, Venus) lasers, and the Hoechst with a 405nm (emission 460/50) laser. Cells in the 4N peak were selected, and mCherry(+)/Venus(-) G1 cells were sorted. Sorted cells were counted using a Countess cell counter (Life Technologies). 4000 cells per well were seeded into 96-well plates, which had been previously prepared for transfection as described above in Section 2.3.4. After incubation at 37°C for the indicated time periods, cells were treated with S-Trityl-L-cysteine (STLC) for 12 hours. STLC is an Eg5 inhibitor, which results in cells arresting in anaphase. Treatment with STLC traps cells entering M phase, and hence results in a greater difference between positive and negative cells. Plates were fixed by direct addition of 2X fixative (8% paraformaldehyde, PFA), and kept at 4°C until required. Plates were rinsed in PBS, and then simultaneously stained with DAPI (1μg/mL) and permeabilised with 0.5% Triton X-100 for 5 minutes at RT. Plates were rinsed once in PBS, and kept in PBS during imaging. Plates were imaged using a Cellomics Arrayscan Vti machine with a 10X 0.3 numerical aperture

objective. The analysis was carried out using the Target Activation Cellomics Bioapplication with standard settings.

Transfection efficiency was tested by knockdown, followed by indirect immunofluorescence for LaminA/C, p53 and p21. After the sorting procedure cells were fixed overnight at 4°C in 4% PFA, permeabilised in 0.2% Triton X-100 for 5 minutes at RT, blocked with 3% BSA/PBS for one hour at RT before treatment with primary antibodies (Lamin A/C 1:1000, Santa Cruz 636, p21 Rb 1:2000, Cancer Research UK MH9, p53 1:500 Calbiochem OP43 clone) in 3%BSA/PBS for 1.5 hours at RT. Plates were washed three times with PBS, before incubation with secondary antibody (Goat anti-mouse or Goat anti-rabbit conjugated to AlexaFluor 647 1:500) for 1.5 hours. Plates were scanned and analysed as above.

An Incucyte live cell imaging system (Essen Bioscience) was used to image plates after sorting and transfection. Plates were imaged every 30 minutes using phase-contrast and fast-fluorescence settings. Exported movies were analysed using Image J software. Fibronectin (Sigma, F0895 from human plasma, 1:250 in PBS) was used where indicated to coat plates for 30 minutes at RT before cell seeding.

Table 2.4: Additional siRNA sequences

All siRNAs were ordered from Dharmacon, and are OTP siRNAs unless otherwise stated.

TARGET	CATALOG NUMBER	SEQUENCE
Control-1	D-001810-01-05	UGGUUUACAUGUCGACUAA
Control-2	D-001810-02-05	UGGUUUACAUGUUGUGUGA
Control-3	D-001810-03-05	UGGUUUACAUGUUUUCUGA
Control-4	D-001810-04-05	UGGUUUACAUGUUUUCCUA
Control-5 (siGenome)	D-001210-05-05	UGGUUUACAUGUCGACUAA
RISC free	D-001220-01-05	NA
p53-1	J-003329-14	GAAAUUUGCGUGUGGAGUA
p53-2	J-003329-15	GUGCAGCUGUGGGUUGAUU
p53-3	J-003329-16	GCAGUCAGAUCCUAGCGUC
p53-4	J-003329-17	GGAGAAUAUUUCACCCUUC
p21	J-003471-12	AGACCAGCAUGACAGAUUU
LATS2_1	J-003865-09	GCACGCAUUUUACGAAUUC
LATS2_2	J-003865-10	ACACUCACCUCGCCCAAUA

LATS2_3	J-003865-11	AAUCAGAUAUUCCUUGUUG
LATS2_4	J-003865-12	GAAGUGAACCGGCAAAUGC
KCNA5_1	J-006215-06	CUAGAGAAGUGUAACGUCA
KCNA5_2	J-006215-07	ACAGAGGAGUCCAGCGGAA
KCNA5_3	J-006215-08	GAAAGGAGAUUCAGGCAGA
KCNA5_4	J-006215-09	GAACCCAUUUCUCUAGCAU
CNGB3_1	J-006161-06	GCAAAUAGGAUGUUAAAGU
CNGB3_2	J-006161-07	GUACUAAAGUUCUGGUUAC
CNGB3_3	J-006161-08	CUAUUUGCCUGGUGACUUU
CNGB3_4	J-006161-09	UCGAACAACUGGAUACUUG

2.22 Bioinformatics

All bioinformatics analysis was carried out by Nicholas McGranahan, except where indicated.

2.22.1 SNP array processing

Affymetrix SNP6.0 data was downloaded from The Cancer Genome Atlas (TCGA) database of Genotypes and Phenotypes (dbGaP) using accession number phs000178.v5.p5. Data from colon adenocarcinoma presented in Chapter 3 and Chapter 4 was from 422 tumours from TCGA. For data in Figure 3.1 additional SNP6.0 data from 898 breast cancers, 391 lung adenocarcinomas, 407 lung squamous cell carcinomas, 506 ovarian cancers and 503 renal cancers was obtained. For all copy number analysis any sample that failed Affymetrix Genotyping Console quality control (QC) was excluded. The aroma R package (Bengtsson et al., 2009), was used to compute LogR and B-allele frequencies (BAF). The integer copy number status was determined using OncoSNP (Yau et al., 2010).

Cell lines described in this thesis were subject to Affymetrix SNP6.0 arrays by Aros (Applied Biotechnology). Normalization and integer copy number estimation were carried out using PICNIC (Greenman et al., 2010).

Copy number for the validation cohort (used in Figure 4.8, Figure 4.9, and Table 4.1) was performed on Illumina 610 Quad arrays. GenomeStudio V2011.1 and Genotyping Module V1.9.4 were used to compute LogR and BAFs. Samples with moving standard deviations >0.28 were discarded. Copy numbers were also computed with OncoSNP (Yau et al., 2010).

Ploidy estimation for each sample was achieved by summation of the weighted median integer copy number for each chromosome, and dividing by the number of chromosomes analysed (n=22). The total number of chromosomes in each sample was calculated by summing the modal copy number from the segmented copy number profile of each chromosome analysed. Segments were weighted according to how many bases they covered. Losses and gains of segments were determined relative to the median ploidy of each sample.

The Weighted Genome Instability Index (wGII) was calculated as in Burrell et al., 2013. The GII is the proportion of base-pairs across the whole genome that are present at copy numbers that differ from 2 (Chin et al., 2007). GII was adapted to take into account the size of each chromosome, such that large chromosomes that are more likely to have more aberrations do not bias the score. The percentage of aberrant SNPs on each chromosome was calculated, and the mean percentage of aberrations across all 22 chromosomes analysed was calculated.

2.22.2 Genome doubling algorithm

A modification of the algorithm used by Carter and colleagues to assess the likelihood of genome doubling as a route to the copy number profiles observed in cancer was used (Carter et al., 2012). All samples, *s*, were represented as an aberration profile of major and minor allele copy numbers at chromosome arm resolution. The total number of aberrations, *Ns*, was then calculated, as well as the probability, *Ps*, of an aberration for each allele at each chromosome arm. Simulations were run which applied the *Ns* sequential aberrations based on the *Ps* to a diploid profile. 10,000 simulations of copy number state were run for each sample, *s*. A *P*-value for genome doubling in each sample was calculated by counting the percentage of simulations in which the proportion of chromosome

arms with a major allele copy number of >2 was higher than that which was observed in that sample. A *P*-value threshold of 0.001 was used for samples with ploidy ≤3, but for samples with a ploidy of 4, $P \leq 0.05$ was used, and all samples where ploidy exceeded 5 were classified as genome doubled.

2.22.3 Estimating the timing of genome doubling

To estimate whether genome doubling occurred before or after the majority of losses in CRC samples, the copy numbers of each sample were assessed and represented as genotype proportions reflecting copy numbers from zero to eight copies. The parental alleles were represented as either A or B. The copy number state of parental alleles where there were two copies (either AA, BB or AB) were used to assess whether loss occurred before or after genome doubling. If a loss occurred before genome doubling the alleles will be represented by either AA or BB. If the loss occurred after genome duplication the alleles will be represented by AB. The proportion of either AA/BB or AB allele copy numbers was assessed for each sample. Samples where the majority of genotype copy numbers were AB, rather than AA or BB were deemed to have undergone genome doubling before the majority of losses. Conversely, samples where the majority of losses were represented by AA or BB rather than AB where said to have incurred most of the losses before genome duplication. A representation of this logic is shown in Figure 3.2.

2.22.4 Significance of correlation between wGII and copy number loss

To determine whether the correlation of loss of chromosome 4 was significantly associated with high wGII tumours (Figure 4.5), simulations were carried out. The percentage of genomic loss in each sample was used to calculate the probability of loss in each sample, and this observed probability for loss was used to generate an aberration state for each sample. All samples were subjected to a point-biserial correlation between this aberration state and the wGII score. Different aberration states and correlations were artificially simulated 10,000 times for each sample, and a *P*-value was calculated based on how many simulations showed a greater correlation coefficient than that observed for each sample.

2.22.5 Validation cohort

Validation cohort data was kindly provided by Dr Oliver Sieber, Dr Peter Gibbs, Dr Robyn Ward, Dr Dmitri Mouradov, Dr Nicholas Hawkins and the Victorian Cancer Biobank (Australia). Patients from the validation cohort used to assess the relationship between genome doubling and survival were recruited from the Royal Melbourne Hospital (Parkville, VIC, Australia), Western Hospital Footscray (Footscray, VIC, Australia) and St Vincent's Hospital Sydney (Darlinghurst, NSW, Australia). The study was ethics approved and all patients gave informed consent. BioGrid Australia provided de-identified clinical data.

2.22.6 Survival curve analysis

Survival curves for TCGA patients and validation cohort patients were plotted using the Kaplan-Meier method in the statistical package R. Log-rank tests were used to assess the significance of univariate analyses of survival, and cox proportional hazards regression models were applied to multivariate survival analysis (R package, survival).

2.22.7 Relationship between mutational status and genome doubling

SNP6.0 and variant calls were downloaded from TCGA for bladder cancer, squamous cell lung cancer, lung adenocarcinoma, melanoma, head and neck cancer, glioblastoma, breast cancer, glioblastoma and colon adenocarcinoma. Copy number data was used to assess the likelihood of genome doubling as described above. All non-silent mutation calls were used to assess whether a difference in the prevalence of somatic aberrations was observed in specific genes in genome doubled (GD) compared to non genome-doubled (nGD) tumours. For assessment of whether a gene was significantly enriched or depleted in GD samples, a Fisher's exact test was implemented for each gene, yielding an odds ratio. The odds ratio reflects the association between mutations in a specific gene and the likelihood of genome doubling. To control for different mutation rates in

different tumour types, a permutation-based analysis was carried out that assesses the mutation rate of each sample, and produces a simulated *P*-value. MutSigCV, a statistical approach that takes into account gene size, replication timing and expression was applied separately to GD and nGD tumours to identify significantly mutated genes within each cohort (Lawrence et al., 2013).

Downstream processing of the lists of significant genes was carried out as described in Section 6.2.1, and the full list of genes included in the screen is shown in Table 6.1.

Analysis of the wGII of colon adenocarcinoma tumours was carried out as described above, and combined with the mutational data for p53. Three genes were identified that were mutated frequently in wGII high but p53 wild-type tumours. These genes were also included in the screen described in Chapter 6.

Chapter 3. Results 1: Increased numerical and structural CIN in tetraploid clones

3.1 Introduction

It has long been speculated that tetraploid cells may be a precursor to the onset of aneuploidy in tumours (see Section 1.3.1). However it is not clear whether tetraploid cells are related to the onset of the dynamic phenotype of chromosomal instability (CIN). Many studies have used artificially generated tetraploid cells to explore the effects of polyploidy on tumorigenicity, but a systematic analysis of the effects of a naturally occurring tetraploidisation event on a stable cell line have not been addressed. With a focus on colorectal cancer (CRC), it was set out to determine the relationship between tetraploidy and chromosomal instability. A novel isogenic system of diploid and tetraploid clones derived from a colorectal cancer cell line precursor was used to explore the relationship between these two phenotypes.

3.2 Results

3.2.1 An association between wGII and ploidy in multiple cancer types

The bioinformatics data presented below was performed by Nicholas McGranahan.

In order to assess the relationship between ploidy and chromosomal instability in CRC, SNP6.0 data was obtained for 404 Stage 1-4 tumours from The Cancer Genome Atlas (TCGA). To assess the level of chromosomal instability in these samples, the wGII (weighted genome instability index) was estimated. This takes into account the proportion of the genome that is either lost or gained relative to median ploidy, and is weighted on a per chromosome basis (see Methods). wGII is plotted against mean chromosome copy number for these 404 CRC samples in Figure 3.1. Polyploid tumours (ploidy ≥ 3) had significantly higher wGIIs than diploid tumours (P<0.0001, Student's T-test). Further, a modified version of a published algorithm (Carter et al., 2012) was applied to assess the likelihood of that tumour having undergone a genome-doubling event (see Methods and Section 1.3.2). This algorithm takes into account the copy number of the major allele (the allele of the

highest copy number) across the whole genome. If a tumour has undergone whole-genome duplication, then the major allele is likely to be an even number across the whole genome due to all chromosomes doubling in number at the same time. This is in comparison to tumours that may have increased their ploidy by subsequent gains of chromosomes. In this scenario the major allele will not necessarily be even across the majority of the genome. Those tumours classified as genome-doubled (GD) had significantly higher wGIIs than those classified as non genome-doubled (nGD) (*P*<0.0001, Student's T-test, Figure 1A). This indicates a possible causal role for genome doubling in the evolution of chromosomally unstable CRCs. However, there are also GD tumours with low wGII scores, and nGD tumours with high wGII scores, suggesting there are multiple routes to CIN in CRC.

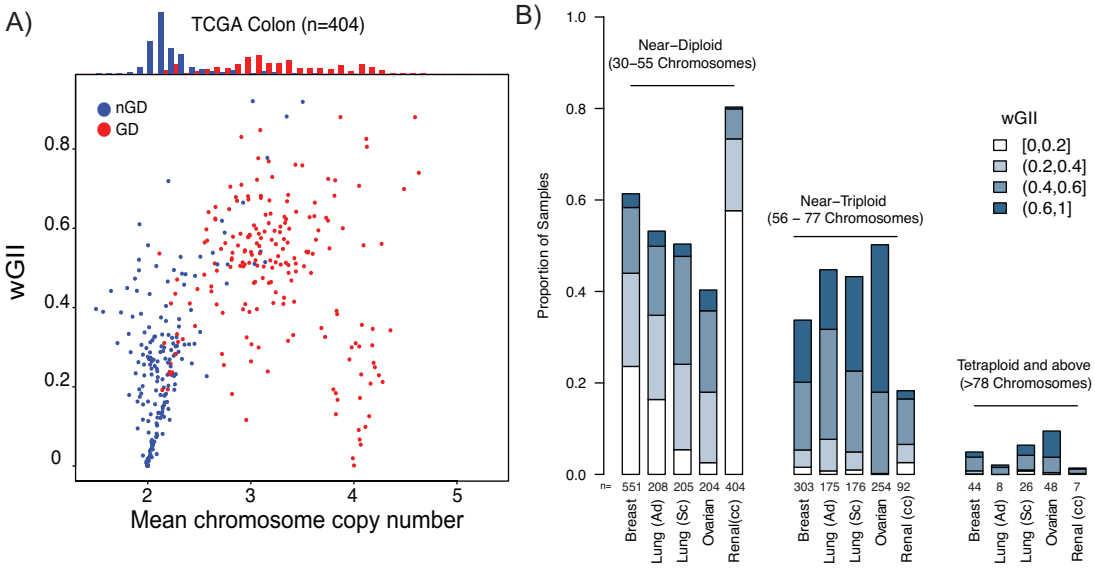

Figure 3.1: Relationship between ploidy and chromosomal instability in CRC

A) Weighted genome instability index (wGII) plotted against mean chromosome copy number for CRC tumours from TCGA. Each dot represents one tumour. Red depicts tumours likely to have undergone genome doubling (GD) (see text and Materials and Methods), and blue depicts tumours unlikely to have undergone genome doubling (non-GD, nGD). A histogram of the weighted mean chromosome copy numbers is shown above the plot.
B) Chromosome counts and wGIIs are shown for other tumours where data was available in TCGA. Lung (Ad) = lung adenocarcinoma, Lung (SC) = lung squamous cell carcinoma, Renal (cc) = renal clear cell carcinoma. Chromosome counts for each sample are a sum of the modal copy number for each chromosome. N= number of tumours analysed.

The relationship between chromosomal instability and ploidy was also investigated for other cancer types where data was available in TCGA (Figure 3.1B). For each of the cancer types analysed (breast carcinoma, lung adenoma, lung squamous cell carcinoma, ovarian carcinoma and renal cell carcinoma) increasing ploidy was significantly associated with increasing wGII score (P<0.0001, Student's T-test), suggesting there may also be a causal relationship between these two genomic aberrations in many cancer types.

In order to ascertain the relative timing of genome doubling compared to the onset of chromosomal instability, an analysis of all the genomic losses in genome-doubled CRC samples was carried out. Genomic losses occurring before a genome-doubling event on a diploid background will result in loss-of-heterozygosity (LOH) (Figure 3.2Ai), whereas losses occurring after genome doubling will not result in LOH (Figure 3.2Aii). Using this approach, it was calculated whether the majority of losses in each CRC sample in the TCGA occurred before or after the genome-doubling event (Figure 3.2B). Of 196 genome-doubled CRC samples, 130 samples showed that the majority of genomic loss events had occurred after genome doubling, whereas there were only 66 samples where the majority of losses occurred before genome doubling. This suggests that genome doubling most often occurs as an early event in the evolution of chromosomally unstable CRCs.

Across their pan-cancer analysis, Carter and colleagues found that the majority of specific large scale chromosomal arm gains and losses were more likely to have occurred before genome doubling, since the levels of chromosomal copy number alterations were similar between GD and non-GD samples in some cancers (Carter et al., 2012). In contrast to arm-level alterations, the authors found that focal somatic copy number alterations (SCNAs) were increased in samples that were inferred to have undergone GD, suggesting that genome doubling could influence genome stability. More recent work by the same group also found that GD was a common event, occurring in 37% of all cancer types analysed (range 11-64%), and also correlating with a higher overall rate of SCNAs, the majority of which were also inferred to occur after GD (Zack et al., 2013).

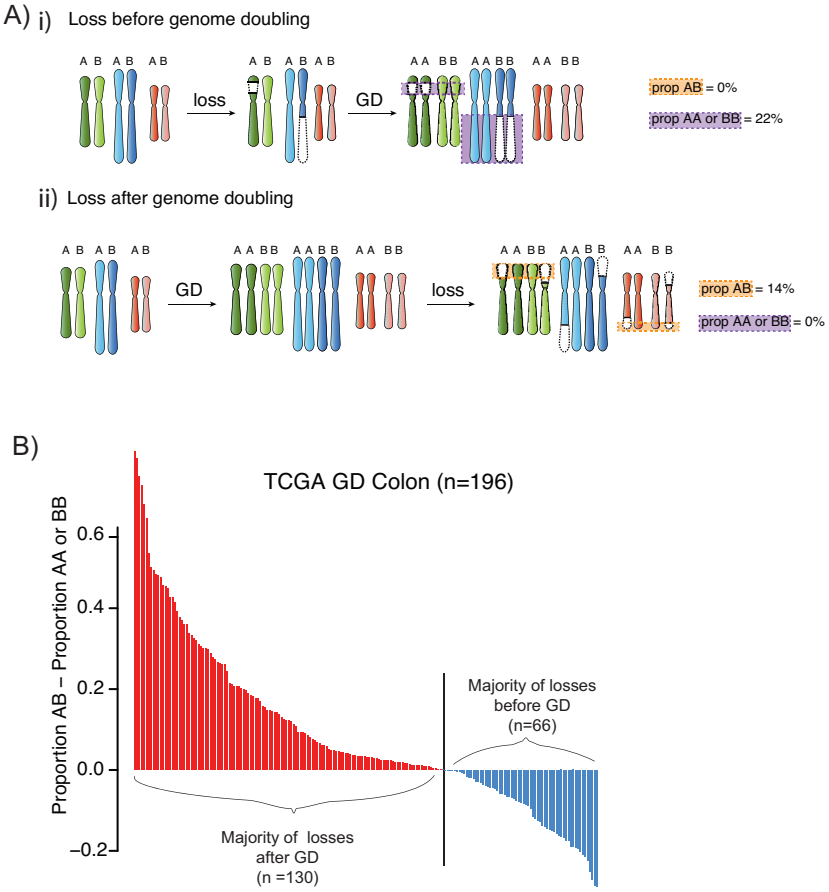

Figure 3.2: GD is an early event in the majority of CRCs

A) A representation of the expected loss-of heterozygosity (LOH) profiles of tumours that either experience loss of genetic material before (i) or after (ii) genome doubling. A and B represent the two parental alleles. Balanced losses to two copies (AB) are depicted with an orange box with orange dotted lines around them. Unbalanced losses to two copies (AA or BB) are depicted with a purple box with purple dotted lines. If the majority of losses occur after GD, then the majority of LOH events will be balanced (AB), conversely if losses occurred before GD the majority of losses will be unbalanced (AA or BB).
B) The likely timing of GD in CRC samples. The proportion of unbalanced to balanced losses for each TCGA tumour is shown. Tumours where the majority of losses are likely to have occurred after GD are shown in red (majority are balanced losses) n=130. Tumours where the majority of losses were unbalanced and likely to have occurred before GD are shown in blue (n=66).

3.2.2 An isogenic system of diploid and tetraploid cell lines

The original FACS isolation of diploid and tetraploid clones from HCT-116 discussed in this section was carried out by Andrew Rowan, all other experiments were conducted by myself.

Given the link between genome doubling and chromosomal instability demonstrated by bioinformatics analyses, the acute effects of genome doubling in an in-vitro system were explored. The microsatellite unstable (MIN) cell line HCT-116 was chosen as a model system as this cell line has a small fraction (<2%) of cells with a >4N DNA content (Figure 3.3A). Fluorescence-activated cell sorting for DNA content, using the DNA binding dye Hoechst, was employed to isolate single diploid and tetraploid cells from the parental HCT-116 population. Diploid cells were selected from the 2N peak, and tetraploid cells from the >4N fraction to avoid erroneously selecting G2 phase diploid cells in the 4N peak. The cloning efficiency of tetraploid cells was significantly lower than diploid cells (2N =63%, >4N =6%, *P*=0.032, Student's T-test), suggesting that tetraploidy is poorly tolerated in HCT-116 cells under normal culture conditions. One diploid clone (DC 8), and two of the rare surviving tetraploid clones (TC 3 and TC 4) were expanded for continued culture (Figure 3.3C). After several passages in culture, a new tetraploid sub-population was observed in the diploid clone DC 8 (Figure 3.3D). There are a variety of mechanisms that could generate tetraploid cells within a diploid population (see Section 1.5). It was not possible to categorically distinguish the mechanism that generated the tetraploid cells in the HCT116 and DC 8 cell lines at this stage.

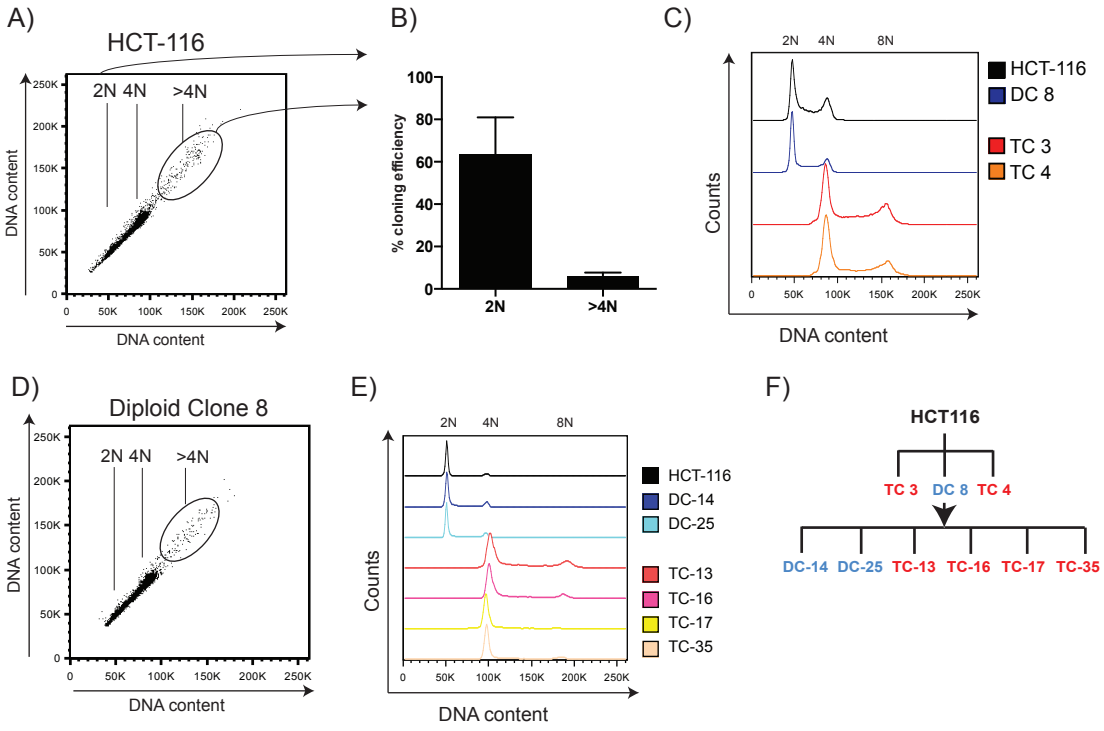

Figure 3.3: Isolation of isogenic diploid and tetraploid cell lines from HCT116

A) Flow cytometry of HCT-116 shows a small fraction of cells with >4N DNA content. 2N, 4N and >4N populations are indicated on the plot.
B) The cloning efficiency of 2N and 4N cells is shown with mean and standard error of the mean (3 experiments) with Poisson correction for 2N cells (see Methods).
C) Flow cytometry using Hoechst dye to show DNA content of one diploid clone (DC 8) and two tetraploid clones (TC 3 and TC 4) derived from HCT-116 after single cell sorting.
D) Flow cytometry for DNA content in the diploid clone DC 8 at passage 33 reveals the emergence of a population with >4N DNA content. Further single cell sorting for 2N and >4N cells was carried out on DC 8.
E) Two further diploid clones (DC-14 and DC-25) and four tetraploid clones (TC-13, TC-16, TC-17 and TC-35) were isolated from DC 8, and their DNA content as assessed by flow cytometry with Hoechst staining is shown (passage 3).
F) Family tree depicting all diploid clones (blue) and tetraploid clones (red) used in this study.

In order to generate tetraploid clones that had arisen within a specific time frame, a second generation of diploid and tetraploid clones was isolated from DC 8 (diploid clones DC-14 and DC-25 and tetraploid clones TC-13, TC-16, TC-17 and TC-35, Figure 3.3E). The tetraploid clones derived from DC 8 must have arisen from a single diploid cell within the time frame of the experiment, and could not have been cycling in the parental population for an unknown period of time, as is theoretically possible for TC 3 and TC4, the two tetraploid clones derived from the HCT-116 cell line. The two generations of diploid and tetraploid clones (three diploids and six

tetraploids, Figure 3.3F) were then continually passaged once a week for over 18 months, so that the effects of a genome-doubling event on genome evolution could be assessed.

In order to ascertain whether the formation of tetraploid cells in HCT-116 may be due to their microsatellite instability, a clone of HCT-116 was obtained (provided by Dr Francois Praz), which has a full length wildtype cDNA of the gene *hMLH1* reinserted in a plasmid under the control of the cytomegalovirus (CMV) promoter (referred to throughout as HCT-116_MLH1, Jacob et al., 2001). Since these cells are no longer mismatch repair defective, they were used to assess whether tetraploid cells can also arise in a microsatellite stable background and distinguish whether experimental observations were mismatch-repair deficient phenomena. Using the same cloning procedures as were used to isolate diploid and tetraploid clones from HCT-116, clones could also be isolated from HCT-116_MLH1 cells (Figure 3.4A and B).

Further, diploid and tetraploid clones could also be isolated from another MSI CRC cell line RKO (Figure 3.4C and D), showing that being able to isolate diploid and tetraploid clones from a cell line considered to be chromosomally stable and diploid is not confined to only HCT-116.

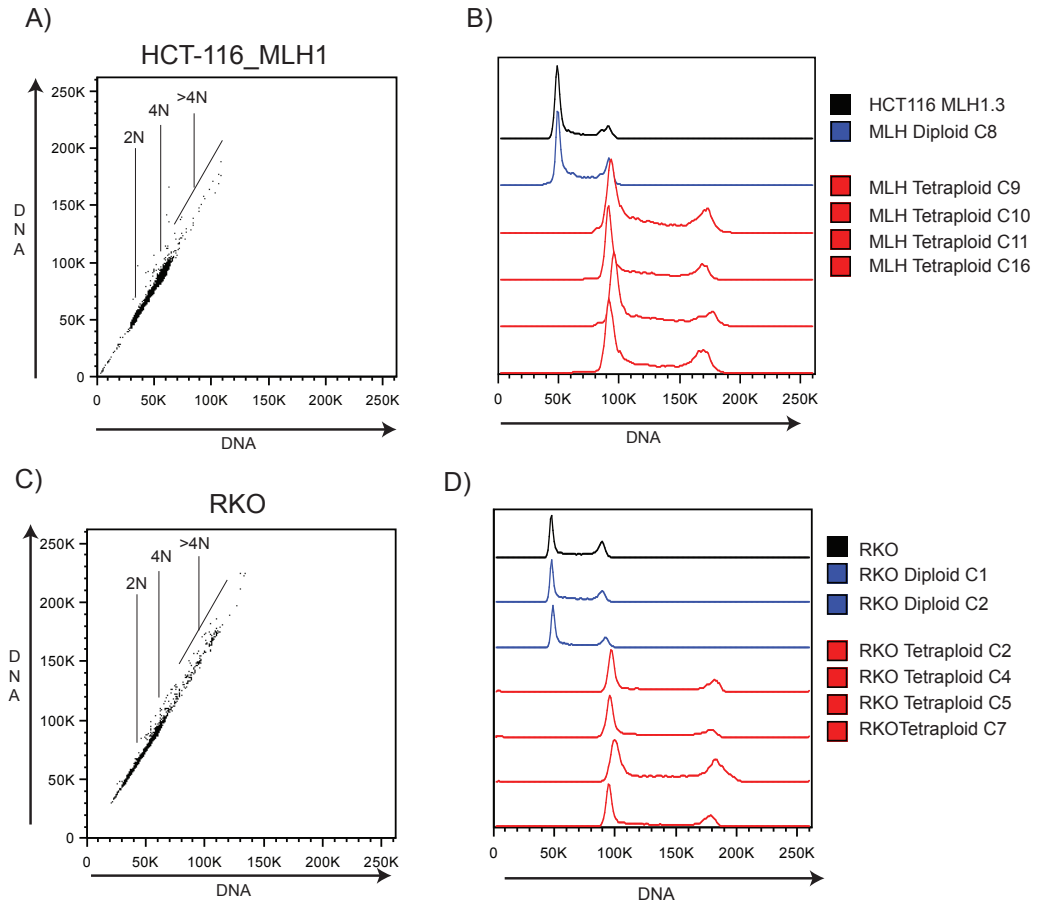

Figure 3.4: Diploid and tetraploid clones derived from HCT-116_MLH1 and RKO

A) Flow cytometry of a microsatellite competent clone of HCT-116_MLH1, with 2N, 4N and >4N populations depicted. Single cell sorting for DNA content was used to isolate diploid and tetraploid clones from this cell line.
B) Flow cytometry analysis with Propidium Iodide (PI) shows the ploidy of the parental cell line HCT-116_MLH1, as well as one diploid clone (MLH Diploid C8), and four tetraploid clones (MLH Tetraploids C9, C10, C11 and C16) derived from HCT-116_MLH1.
C) Flow cytometry of the MIN CRC cell line RKO also shows a >4N population. Single 2N and >4N clones were isolated using FACS.
D) DNA histograms of RKO and two diploid clones (RKO Diploid C1 and C2), and four tetraploid clones (RKO Tetraploid C2, C4, C5 and C7) derived from RKO.

3.2.3 Numerical instability in tetraploid clones

To assess the level of numerical chromosomal instability in diploid and tetraploid clones derived from HCT-116, clonal fluorescence *in-situ* hybridisation (FISH) was carried out (Figure 3.5A). The amount of cells that have chromosome copy

numbers deviating from the modal chromosome number of each colony gives an indication of the cell-to-cell variation within each colony that has likely occurred during colony expansion (Figure 3.5B). Fluorescent probes for chromosomes 2 and 8 were chosen, as these chromosomes are not commonly subjected to copy number changes in colorectal cancer and therefore are more likely to represent on-going chromosomal instability. An automated microscope system was used to analyse this data (see Methods). Colonies were selected from an initial low magnification scan (5X), and then scanned at 40X. The data was analysed using an automated assay with manual curation (see Methods). The percentage of cell-to-cell variation within individual colonies was significantly greater in tetraploid clones compared to diploid clones at both passage 5 (approximately 1 month of culture, Figure 3.5C, diploid mean=7% [0-23%]; tetraploid mean=28% [5-57%], $P<0.0001$, Student's T-test) and at passage 50 (approximately 1 year of culture, Figure 3.5D, diploid mean=13% [3-34%]; tetraploid mean=33%, [7-68%] $P<0.0001$, Student's T-test). The level of cell-to-cell variation observed in the parental cell line HCT-116 is similar to results from other laboratories carrying out this assay in the same cell line (Thompson and Compton, 2008).

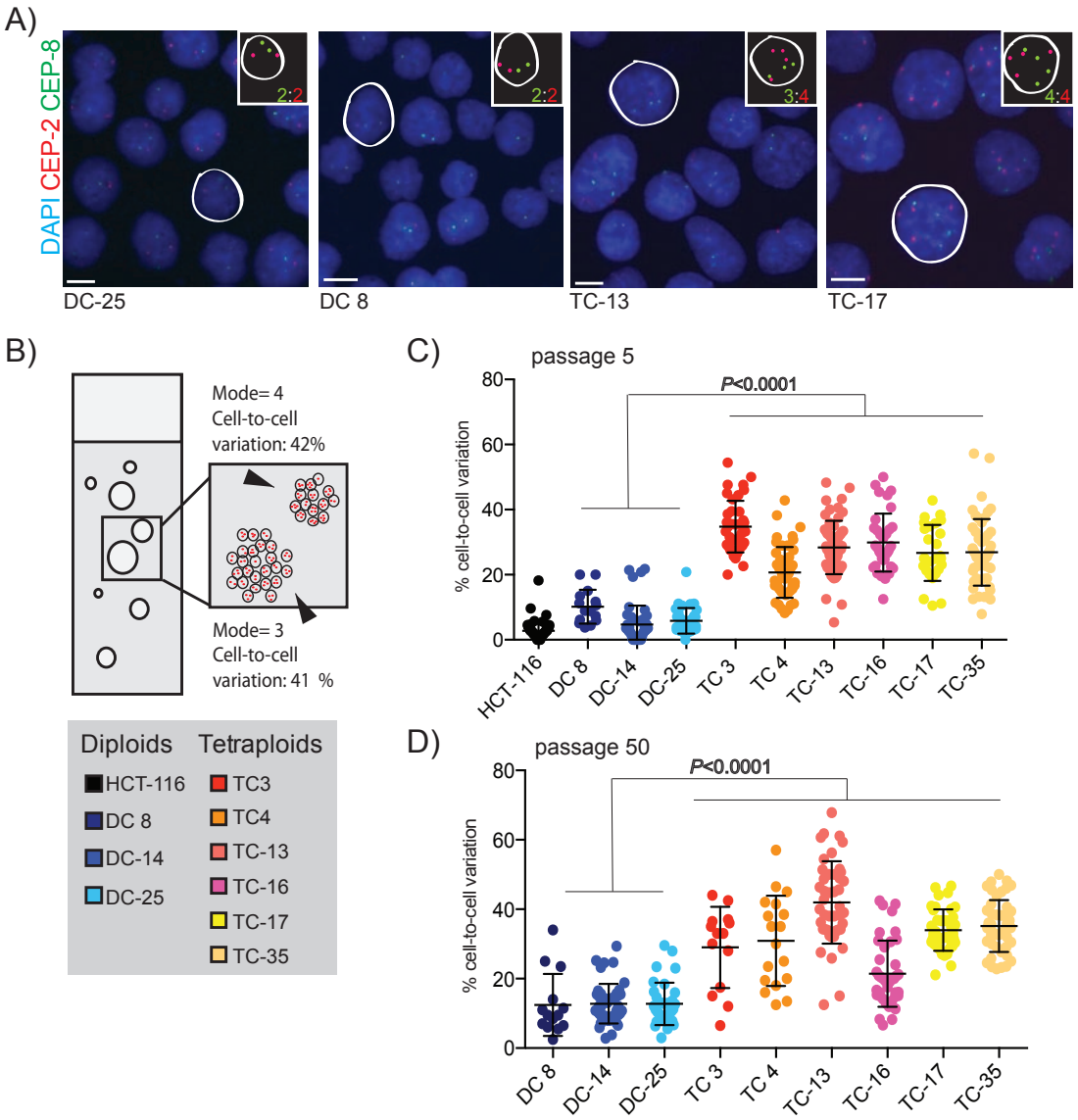

Figure 3.5: Tetraploid clones show increased cell-to-cell variation in chromosome number

A) Example images of clonal FISH. Two diploid clones DC-25 and DC 8, and two tetraploid clones TC-13 and TC-17 are shown. Chromosome 2 (CEP-2) is shown in red, and Chromosome 8 (CEP-8) is shown in green. One cell in each image is highlighted, and the copy number state for these two chromosomes is shown in the inset. Scale bar (in white) = 10µm.
B) A diagram of a clonal FISH slide is shown, depicting the two measures of chromosomal instability that can be measured in this assay. Cell-to-cell variation is the number of cells within one colony that vary from the overall modal chromosome copy number for each chromosome in that colony (also referred to as deviation from the mode). Colony-to-colony variation is the difference in modal chromosome number between colonies, also referred to as deviation of the mode.
C) Cell-to-cell variation in chromosome number between diploid and tetraploid clones at passage 5. The average deviation for both of the chromosomes analysed (2 and 8) is shown. Each point represents one colony. All passage 5 clones were

scored using the Ariol microscope system (see Methods). Colonies with <10 cells were excluded from analysis. Median number of cells scored = 2479.
D) Cell-to-cell variation of chromosomes 2 and 8 at passage 50. All clones were scored on the Ariol microscope system, apart from DC 8, TC3 and TC4, which were scored on a Deltavision microscope. Median number of cells scored = 2105.
NB: passage numbers depicted throughout this thesis are correct to within 4 passages.

Clonal FISH was also carried out on HCT-116_MLH1 diploid and tetraploid clones. Tetraploid clones from HCT-116_MLH1 also showed a significant increase in cell-to-cell variation compared to the diploid clone, with a similar magnitude of difference between diploid and tetraploids as was observed in MMR deficient clones (diploid average 11% [3-29%], tetraploid average 26% [2-61%] *P*<0.0001, Student's T-test Figure 3.6). This indicates that the increased numerical instability in tetraploid clones derived from HCT-116 is not likely to be due to their microsatellite instability phenotype.

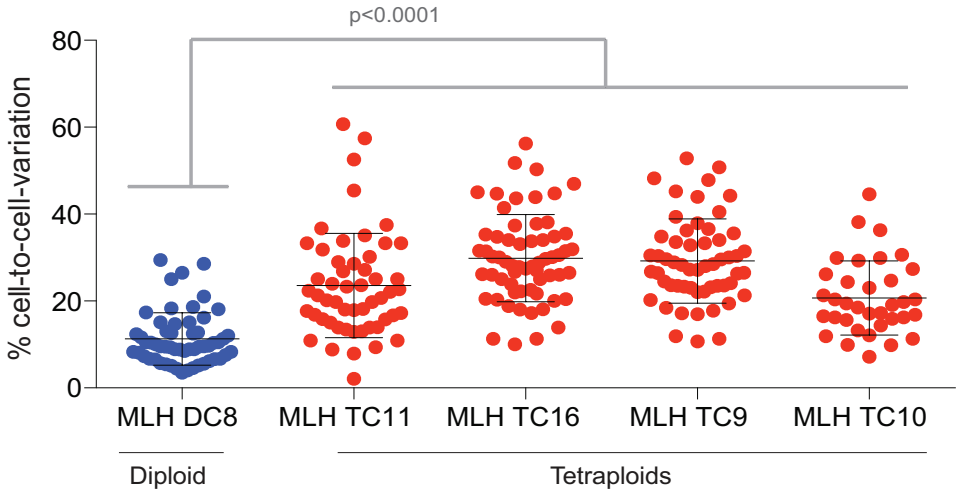

Figure 3.6: HCT-116_MLH1 tetraploid clones also show increased cell-to-cell variation in chromosome number

Clonal FISH in one diploid (DC8), and four tetraploid clones (TC11, TC16, TC9 and TC10) derived from HCT-116_MLH1 at passage 5. Each point represents one colony. Average cell-to-cell variation for chromosome 2 and 8 is shown. Median number of cells scored = 4227.

The increase in cell-to-cell variation in chromosome number observed in tetraploid clones using clonal FISH could be explained by a higher rate of chromosome missegregation occurring in tetraploid cells. To assess this, the frequency of

anaphase segregation errors in all clones was analysed using immunofluorescence (Figure 3.7A). Tetraploid clones had significantly higher frequencies of anaphase segregation errors than diploid clones at all 3 passages analysed (passage 5 *P*=0.0001, passage 5 *P*=0.0025, passage *P*=0.0047, Student's T-test, diploid mean=19% [11-26%]; tetraploid mean=42% [32-55%]). The frequency of segregation errors on a per chromosome basis was then calculated using the number of chromosomes calculated from SNP6.0 data (see Section 4.2.3 and Methods). The number of segregation errors per chromosome was not significantly increased in tetraploid clones (Figure 3.7A). This suggests that the increased frequency of anaphase segregation errors in tetraploid clones may simply be a consequence of the increased number of chromosomes.

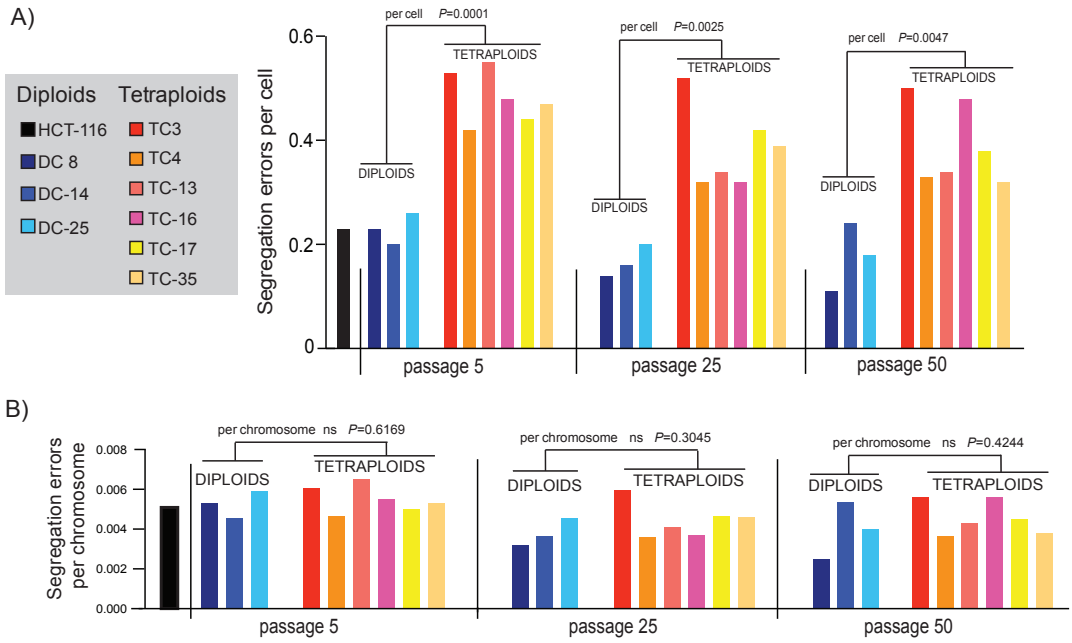

Figure 3.7: Frequency of segregation errors in diploid and tetraploid clones

A) Chromosome segregation errors between diploid and tetraploid clones at passage 5, 25 and 50. Segregation errors per cell are shown. Fifty anaphases were scored for each clone, only bipolar anaphases are shown. *P*-values above each graph refer to comparisons between all diploid and all tetraploid clones at each passage (Student's T-test).
B) The frequency of segregation errors on a per chromosome basis for each passage, using modal chromosome numbers for each clone calculated from SNP6.0 analysis (see Methods). *P*-values are shown above the graph.

3.2.4 Centriole number and spindle polarity in tetraploid clones

Given the relatively high level of segregation errors in the diploid clones and in the parental cell line, it is possible that the tetraploid cells were formed initially through a cytokinesis failure, which has been shown to occur after segregation errors cause regression of the cleavage furrow (Shi and King, 2005). A failure to undergo cytokinesis would result in tetraploid cells with supernumerary centrioles (see Section 1.5.1). Given previously published work, which has demonstrated a likely causative role between extra centrioles and increased chromosome segregation errors the number of centrioles in tetraploid clones was examined (Ganem et al., 2009 and see Section 1.8.2.1).

The number of centrioles in prophase cells was scored using immunofluorescence for centrin-3, a mammalian centrin that is associated with the centrosome. Representative images of prophase cells with centrin-3 antibody staining are shown in Figure 3.8A. Histograms showing the percentage frequency of centriole numbers at both passage 5 and passage 50 are presented in Figure 3.8B and C. The percentage of supernumerary centrioles (% of cells with >4 centrioles) is shown in Figure 3.8D and E. Tetraploid clones showed significantly more supernumerary centrioles at passage 5 (diploids mean = 31% [12-44%], tetraploid mean = 72% [43-85%] P=0.0046, Student's T-test) and passage 50 (diploids mean = 30% [25-38%] tetraploid mean = 75% [67-93%] P=0.0002, Student's T-test). Furthermore there was no significant difference in the percentage of supernumerary centrioles between passage 5 and passage 50 for diploid or tetraploid clones (P=0.6087, Paired T-test). Interestingly this indicates that there is no selective pressure over time for these cells to lose extra centrioles, which would be expected if the extra centrioles were causing the increase in the frequency of segregation errors observed in tetraploid clones (Figure 3.7).

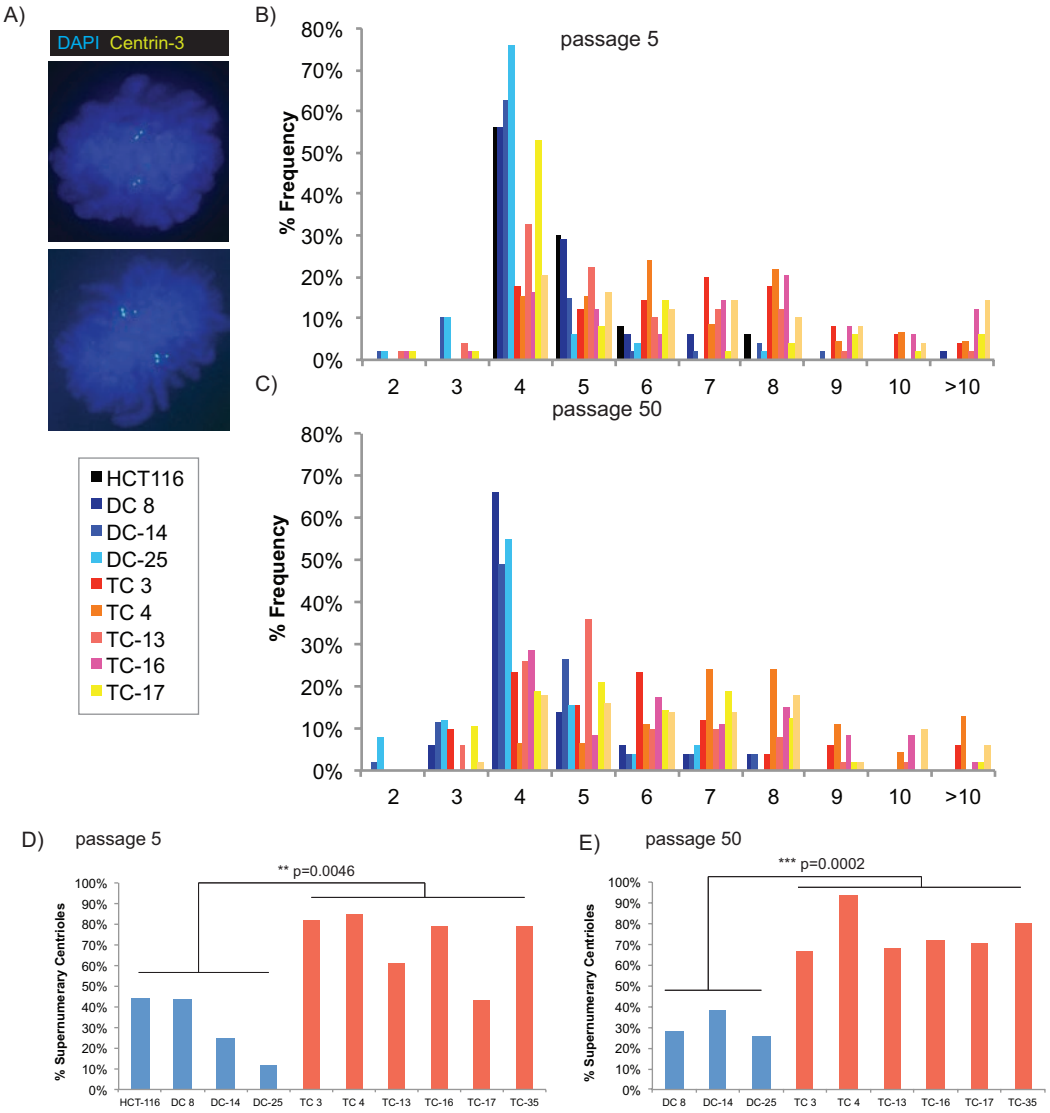

Figure 3.8: Maintenance of supernumerary centrioles over time in tetraploid clones

A) Representative images of two cells stained with DAPI (blue) and immunofluorescence against centrin-3 (green).
B) Frequency histogram of the percentage of cells scored displaying the indicated centriole number for diploid and tetraploid clones at passage 5. Median number of cell scored n=49.
C) Frequency histogram of centriole number for passage 50 diploid and tetraploid clones. Median number of cells scored n=50.
D) Percentage of cells with supernumerary (>4) centrioles at passage 5.
E) As above, for passage 50 cells.

As extra centrioles are thought to cause increased segregation errors via the formation of transient multipolar spindle intermediates (Ganem et al., 2009), the polarity of spindles was scored in pre-anaphase cells using immunofluorescence for β-tubulin and centrin-3 (Figure 3.9A).

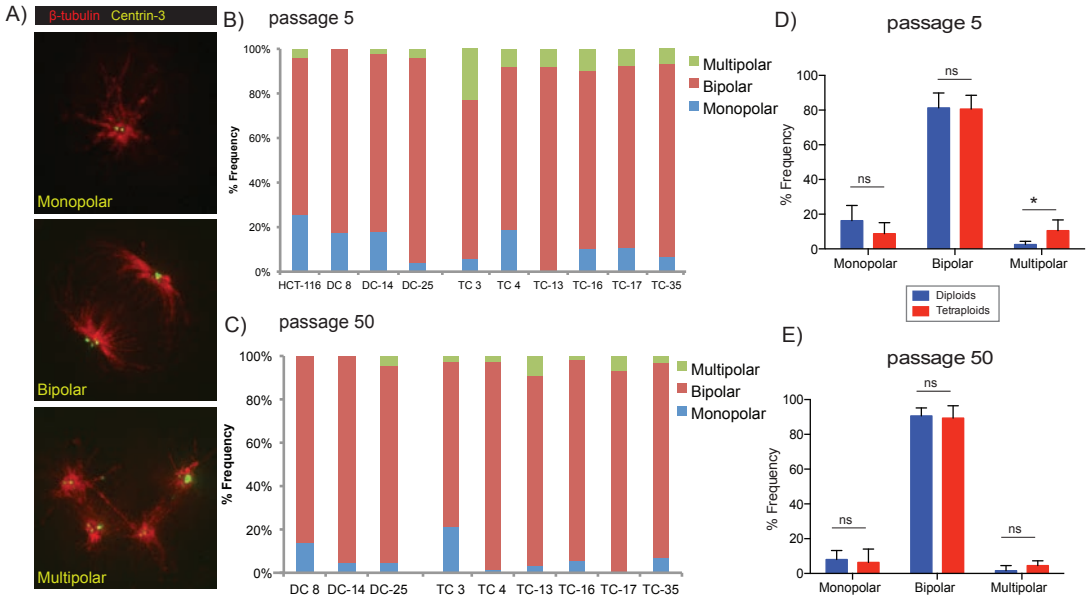

Figure 3.9: Pre-anaphase spindle polarity in diploid and tetraploid clones

A) Representative images of monopolar, bipolar and multipolar spindles that were scored using immunofluorescence for β-tubulin and centrin-3 in this analysis.
B) Quantification of percentage frequency of each spindle configuration in passage 5 cells.
C) As above for passage 50 cells.
D) Comparison of each spindle configuration between diploid and tetraploids at passage 5 (ns = not significant, * = P<0.05, Student's T-test).
E) As above, for clones at passage 50.

DAPI staining was used to identify pre-anaphase cells. The percentage frequency of each spindle configuration is shown in Figure 3.9B for passage 5 and Figure 3.9C for passage 50. There was no significant difference at either passage between the percentages of monopolar or bipolar spindles (Figure 3.9D and E, Student's T-test). Tetraploid clones showed a slight but significant increase in multipolar spindles at passage 5 (P=0.0399, Students T-test), but at passage 50 there was no significant difference. Interestingly these data suggest that the supernumerary centrioles in tetraploid cells only result in a slight increase in multipolar spindles in pre-anaphase compared to diploid cells (multipolar spindles: passage 5 diploid mean = 3% [0-4%] tetraploid mean = 11% [7-23%], passage 50 diploid mean =2% [0-5%], tetraploid mean = 4% [2-9%]). Previous studies have shown that multipolar divisions often result in non-viable progeny (Ganem et al., 2009, Kuffer et al., 2013), suggesting a selective pressure for cells to be able to

divide in a bipolar fashion. This is supported by the fact that the percentage of multipolar spindles decreases over time in tetraploid clones.

As discussed in Section 1.8.2.1, cells with supernumerary centrioles can divide in a bipolar fashion if they have efficient centriole clustering (Kwon et al., 2008). Since HCT-116 and diploid clones do have supernumerary centrioles (average 31% of cells with >4 centrioles Figure 3.8D), but few multipolar spindle configurations (average 3% multipolar spindles, Figure 3.9B and D) this suggests that efficient centriole clustering mechanisms are likely to already exist in diploid cells. The cloning process used to derive to tetraploid clones is likely to have positively selected for tetraploid cells that had efficient clustering mechanisms despite an increase in centriole number. This can also help explain why a change in centriole number over time was not observed in tetraploid clones. Without a selective pressure to lose centrioles (i.e. a detrimental effect on cell viability caused by their presence), there would be no reason for tetraploid cells to lose extra centrioles over continued passaging. This is in contrast to similar cell line systems where tetraploid cells have been shown to lose centrioles over time (Ganem et al., 2009).

3.2.5 Types of segregation error in tetraploid clones

Extra centrioles are thought to cause an increase specifically in lagging centric chromosomes (Ganem et al., 2009). In order to ascertain whether the increased centriole number in tetraploid clones has an effect on the type of segregation errors, anaphase segregation errors were classified using immunofluorescence. A CREST antibody was used to identify the centromeric regions of chromosomes in immunofluorescence (see insets, Figure 3.10A). This makes it possible to classify segregation errors into different types, in particular separating lagging chromosomes into either centric or acentric lagging chromosomes. Segregation error classification can shed light on likely mechanisms driving instability, as different mechanisms are thought to be responsible for causing different types of error (see Section 1.8). The profile of segregation error types for each individual diploid and tetraploid clone at passage 5 and passage 50 is shown in Figure 3.10B and C. There was no significant difference in the profile of segregation error types

between diploid and tetraploid clones (Figure 3.10D, *P*=0.178, Chi-squared test). There was no increase in lagging centric chromosomes in tetraploid clones, which is consistent with the fact that there was only a very small increase in pre-anaphase spindle multi-polarity (Figure 3.9G) despite the increased levels of supernumerary centrioles (Figure 3.8).

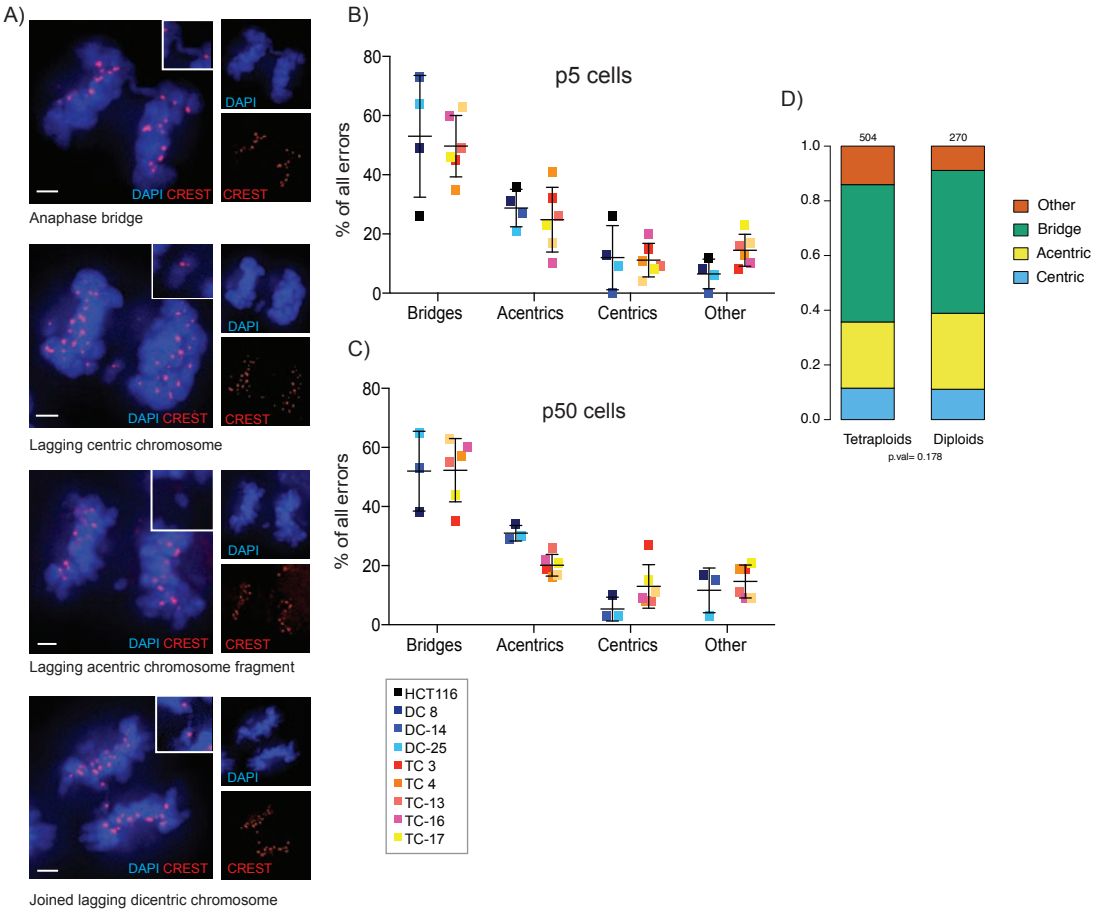

Figure 3.10: Tetraploid and diploid clones make a similar spectrum of segregation errors

A) Representative merged images of the different types of segregation error that were classified in diploid and tetraploid clones using DAPI staining and CREST immunofluorescence. Inset shows close up of the error, and side panels show each channel separately. Scale bar (in white) = approximately 3μm.
B) Quantification of the percentage of each type of error (only cells with errors were scored for this analysis) in passage 5 cells. Median number of cells with errors scored = 39.
C) Quantification of segregation error types in passage 50 cells. Median number of cells with errors scored = 37.

D) Comparison of the proportions of different types of error between diploids and tetraploids (at both passage 5 and passage 50) shows no difference in the proportion of different types of error (*P*=0.178, Chi-squared test).

The fact that tetraploid clones display a similar spectrum of segregation errors to diploid clones suggests that there is no 'tetraploid-specific' mechanism driving increases in any one type of segregation error.

3.2.6 Structural instability in tetraploid clones

Previous data has shown that tetraploid cells display elevated numerical chromosomal instability on a per cell, but not a per chromosome basis. To assess the relationship between ploidy and structural chromosomal instability, the level of structural chromosome abnormalities in all clones was analysed using metaphase spreads hybridised with a pan-centromeric probe (Figure 3.11A). The number of structural chromosome abnormalities in each cell was significantly increased in tetraploid clones at all three passages analysed (passage 5 *P*=0.0160, passage 25 *P*=0.0067, passage 50 *P*=0.0301, diploid mean: 0.39 [0.26-0.58] abnormalities per cell; tetraploid mean: 0.93 [0.60-1.62] abnormalities per cell, Figure 3.11B). The number of chromosomes was also counted from each metaphase spread analysed, and the number of structural chromosome abnormalities on a per chromosome basis was then calculated. The number of structural abnormalities per chromosome was not significantly different between diploid and tetraploid clones at any passage analysed (Figure 3.11C, diploid mean=0.0088 [0.0058-0.0130]; tetraploid mean=0.0108 [0.0073-0.0180], *P*=0.1093, Student's T-test). These data suggest that the increased level of structural chromosomal instability in tetraploid cells results from the increased number of chromosomes.

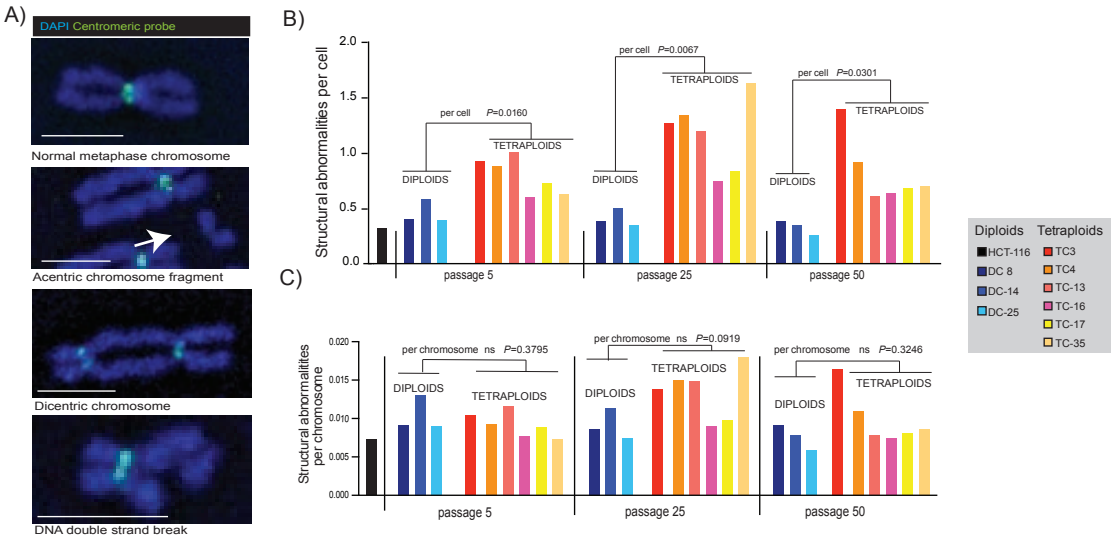

Figure 3.11: Structural chromosome abnormalities in diploid and tetraploid clones

A) Representative images of chromosomal abnormalities observed in metaphase spreads hybridised with a pan-centromeric probe (green) and stained with DAPI. Scale bar (in white) = approx. 2.5µm.
B) A comparison of the number of structural abnormalities observed per cell between diploid and tetraploid clones at passage 5, 25 and 50. Median number of metaphase spreads scored for each passage: passage 5 = 25, passage 25 = 29, passage 50 =27 and HCT-116 n = 37.
C) Number of structural abnormalities per chromosome, calculated from the number of chromosomes counted for each metaphase spread.

The different types of structural abnormalities scored included dicentric chromosomes, acentric chromosome fragments and double strand breaks (Figure 3.11A). The most common type of abnormality observed in both diploid and tetraploid clones was acentric chromosome fragments, accounting for a median of 56% (27-90%) of abnormalities (average % of abnormalities in all passage 5 and passage 50 diploids and tetraploids), followed by dicentric chromosomes, which accounted for 14% (0-62%) of abnormalities on average. Double strand breaks were less frequently observed, at 10% (0-43%) of abnormalities on average. Occasionally other types of abnormality that were less common were observed, for example ring chromosomes and fragmented chromosomes. These were considered in a single category of “other” in this analysis, which accounted for a median of 15% (0-40%) of all abnormalities.

In two tetraploid clones, TC3 and TC4, some particular chromosome abnormalities appeared to be conserved as they were observed on the majority of spreads. These appeared to be dicentric chromosomes, but with no sister chromatid cohesion between one pair of centromeres. Examples of these chromosomes are shown in Figure 3.12. These conserved structural abnormalities could possibly represent chromosome fusion events where one pair of centromeres has been inactivated. This has been shown to occur in fission yeast (Sato et al., 2012).

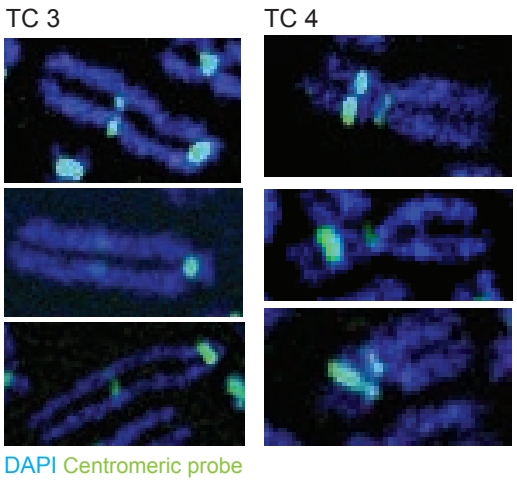

Figure 3.12: Conserved structurally abnormal chromosomes in TC 3 and TC 4

Examples of the same type of abnormal chromosomes that were observed across multiple metaphase spreads in TC 3 and TC 4. Images are from metaphase spreads stained with DAPI (blue), and hybridised to a centromeric probe.

An analysis of the percentage of each different type of abnormality between diploids and tetraploids was carried out (Figure 3.13). There were no significant differences in the frequencies of each type of structural abnormality between diploid and tetraploid clones at either passage 5 or passage 50 (Student's T-test). However the frequencies of dicentric chromosomes are higher in tetraploids at both passages. This is likely due to the presence of the conserved dicentric chromosomes shown in Figure 3.12.

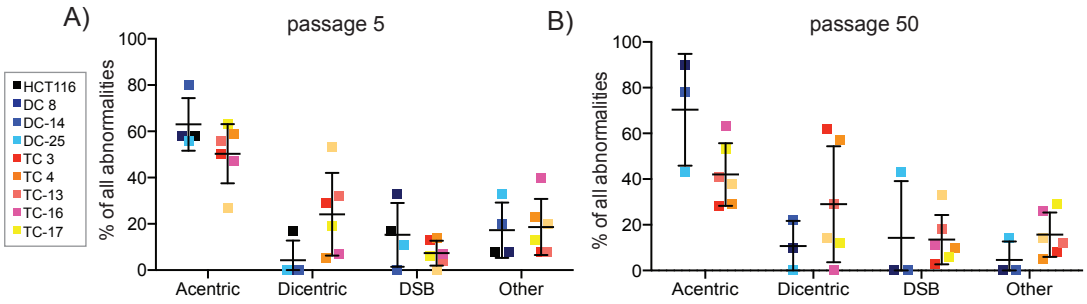

Figure 3.13: Diploid and tetraploid clones have similar frequencies of different structural abnormalities

A) A comparison of the proportion of different types of structural chromosome abnormalities observed on metaphase spreads between diploid and tetraploid clones at passage 5 (DSB = double strand break).
B) As above, for passage 50 clones.

3.2.7 Interphase DNA damage in diploid and tetraploid clones

Structural chromosome abnormalities are most likely to arise as a result of DNA double-strand breaks (DSBs) that have been erroneously corrected leading to chromosome fusions, or that have failed to be corrected leading to acentric chromosome fragments (Thompson and Compton, 2011b, Gisselsson, 2008, see Section 1.8.4). To assess the contribution of DNA damage to the increase in structurally abnormal chromosomes in tetraploid cells, the amount of basal DNA damage was analysed using indirect immunofluorescence for the DSB response proteins γH2AX and 53BP1. Examples of the images used to score these foci are shown in Figure 3.14A. Interphase nuclei were selected randomly using DAPI staining, and the number of co-localised γH2AX and 53BP1 foci per nucleus was scored.

The percentage frequency for different categories of foci number (0-2, 3-4, 5-6, 7-8 and >8) was calculated for both passage 5 (Figure 3.14B) and passage 50 (Figure 3.14C). To compare between diploid and tetraploids at both passages, summary graphs are presented in Figure 3.14D and E. At passage 5 there is a significant difference between diploid and tetraploids in the frequency of cells with 3-4 foci (diploid average 7%, tetraploid average 13%, *P*=0.0147, Student's T-test). There are no significant differences between any of the other categories (Student's T-

Test). This could suggest that tetraploid cells are subject to a greater frequency of low level DNA damage.

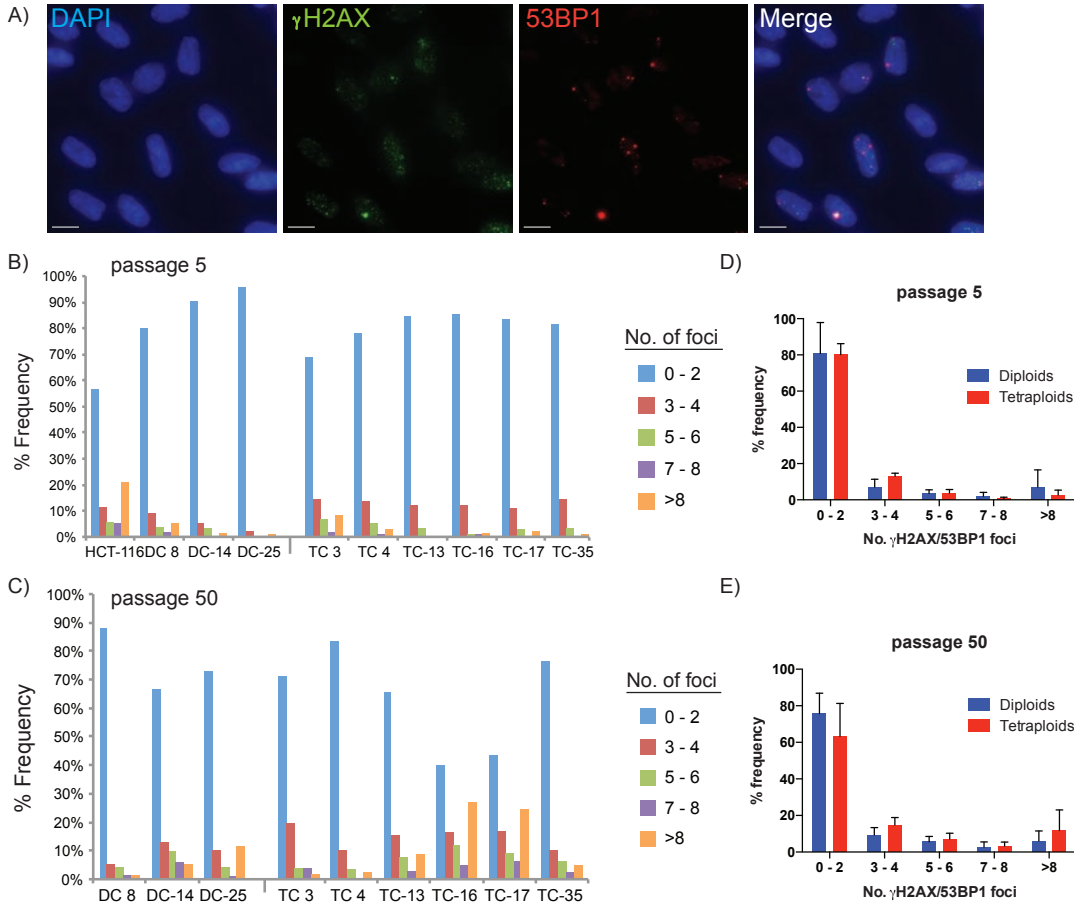

Figure 3.14: Levels of interphase DNA damage in diploid and tetraploid clones

A) Representative images used to score interphase DNA damage. Indirect immunofluorescence was carried out to detect γH2AX and 53BP1. The number of co-localised foci per nucleus was counted.
B) The percentage frequency of different numbers of foci in passage 5 diploid and tetraploid clones. The key shows the colours indicating different numbers of foci. Median number of nuclei scored = 248, range 191-429.
C) As for B), but in passage 50 clones. Median number of nuclei scored = 314, range 200-405.
D) A comparison of percentage frequency of different numbers of foci between all diploid and tetraploid clones at passage 5.
E) As above, but for passage 50 clones.

At passage 50 there are no significant differences between any of the categories (Student's T-test, Figure 3.14E). However, in every group apart from 0-2 foci, there is a slight increase in the mean number of foci in tetraploids compared to diploids.

This suggests that there may be modest increases in the levels of DNA damage in tetraploid clones. However, these differences in passage 50 cells seem to be mainly driven by two clones, TC-16 and TC-17, which seem to have a different profile of numbers of DNA damage foci, with an increase in the number of cells with more than 8 foci (Figure 3.14C). Neither of these clones had noticeably higher frequencies of segregation errors or structural abnormalities that could explain these differences (Figure 3.7, Figure 3.11). This analysis could be improved by carrying out an automated analysis of basal DNA damage that does not involve scoring by immunofluorescence images by eye, which could have introduced artefactual errors. Using a comet-assay could achieve this, as automated image software can calculate the length of the tail-moment.

All tetraploid clones have significant increases in the levels of segregation errors per cell (Figure 3.7), which are known to result in DNA damage (Janssen et al., 2011, Crasta et al., 2012), as well as an increase in the levels of structural chromosome abnormalities (Figure 3.11), which themselves result from DNA damage, and therefore it is surprising that there is not a more substantial increase in interphase DNA damage in tetraploid clones. As tetraploid cells have twice as much DNA, it would be expected that they would also sustain twice as much spontaneous DNA damage. No large differences in the frequency of DNA damage foci were observed between diploids and tetraploids, which could suggest that either tetraploid cells are not subject to as much DNA damage, or that more efficient DNA repair processes operate in tetraploid cells. There is a more obvious difference between diploid and tetraploids across multiple categories at passage 50 compared to passage 5, which would fit a model of gradual accumulation of DNA damage over time in culture, likely due to the increase in segregation errors and structural chromosome abnormalities.

3.2.8 Replication stress in tetraploid clones

It has been previously shown that replication stress is likely to be a major cause of segregation errors and structural chromosome abnormalities in chromosomally unstable CRC cell lines (Burrell et al., 2013). To see if tetraploid clones were

subject to replication stress the speed of DNA replication was assessed using DNA fibre assays. If cells are experiencing replication stress, a decrease in the progression of replication forks would be expected. To directly measure DNA replication rates, DNA fibre labelling was used. Briefly, exponentially growing cells were pulsed sequentially with two thymidine analogues 5-Chlorodeoxyuridine (CldU) and Iododeoxyuridine (IdU) that are incorporated into nascent DNA strands. These different analogues can be detected using immunofluorescence, and the speed of DNA replication can be inferred from the length of the fibres.

Representative fibres from all passage 5 cells are shown in Figure 3.15A. Fork speed was measured from the green CldU labelled fibres only, as these were detected more strongly by the secondary antibody used. Conversion of fibre length into fork speed in kilobases of DNA replicated per minute (kb/min) is shown in Figure 3.15B. To compare fork speed between diploid and tetraploids data is shown as a histogram (Figure 3.15C). Tetraploid clones have a slight but significant reduction in fork speed compared to diploid clones at passage 5 (diploid mean 1.095 ± 0.01436 kb/min [SEM] N=701, tetraploid mean 0.9746 ± 0.01095 kb/min [SEM] N=819, $P<0.0001$, Student's T-test, Figure 3.15C). The mean fork speed of the parental cell line HCT-116 is 1.07 ± 0.02788 kb/min, which is comparable to data from published studies (Burrell et al., 2013 Petermann et al., 2008). An average reduction in fork speed of just 0.12 kb/min between diploids and tetraploids is probably not significantly affecting the ability of tetraploid clones to synthesise DNA in a timely fashion.

The replication rate was also analysed for diploid and tetraploid clones at passage 50, after almost a year in culture (Figure 3.15D). Comparing between diploid and tetraploid clones at this passage revealed there was no significant difference in fork rate (diploid mean 1.009 ± 0.01646 [SEM] N=521, tetraploid mean 1.015 ± 0.009971 [SEM] N=1161, $P=0.734$, Student's T-test, Figure 3.15E). The changes in fork rate between passage 5 and passage 50 are very small, -0.086 kb/min for diploids, and +0.0404 kb/min for tetraploid clones. These small differences are unlikely to represent biological changes, and more likely is due to experimental variation. The fact that there is no significant change in tetraploid clones over time

supports the assumption that at passage 5 the slight reduction noted in fork rate compared to diploids is unlikely to be biologically relevant.

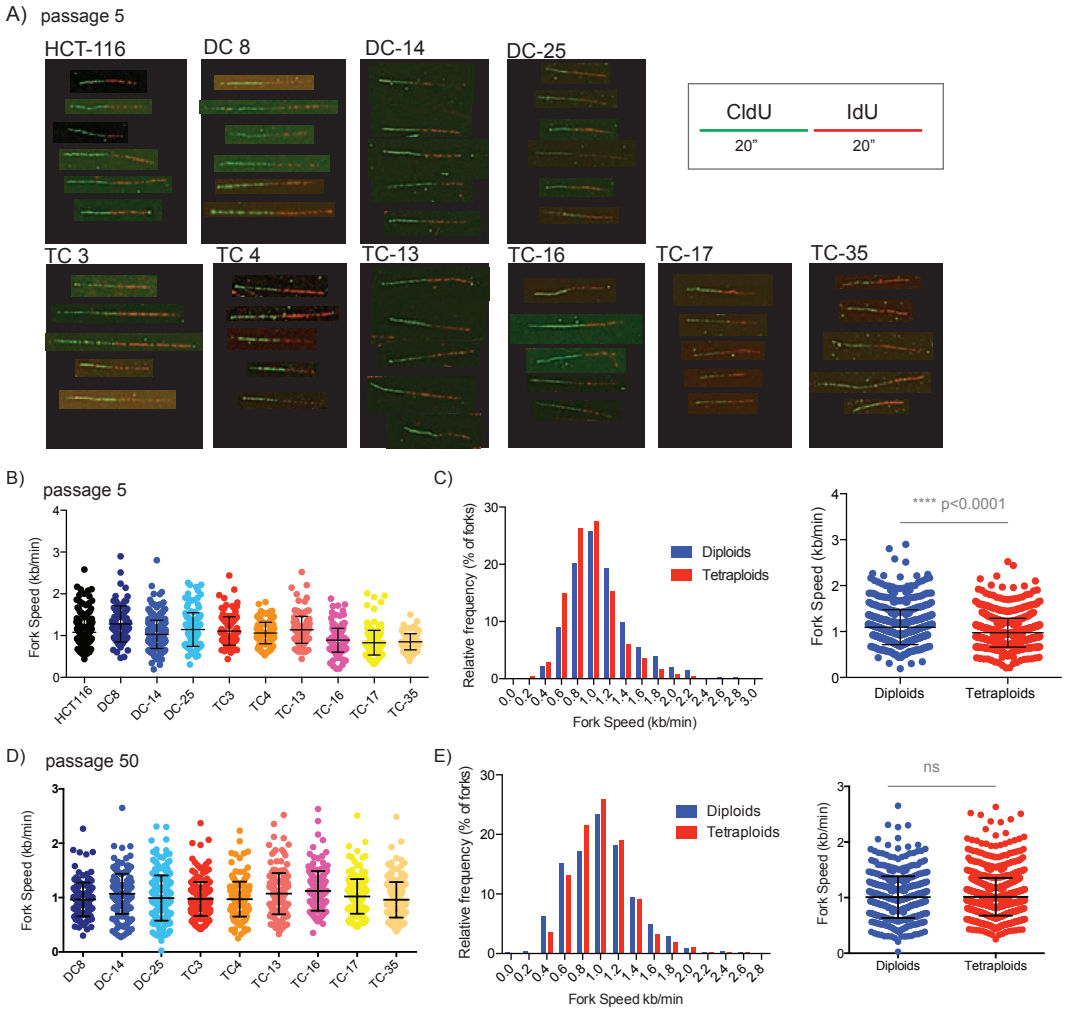

Figure 3.15: DNA replication rate is similar between diploid and tetraploids

A) Representative images from DNA fibres obtained from passage 5 diploid and tetraploid cells. Inset box indicates timing of CldU and IdU pulses (see Methods).
B) Quantification of fork speed (kb/min) between diploid and tetraploid clones at passage 5. Median number of fibres scored for each clone =137 (range 92-304).
C) Comparison of fork speed between passage 5 clones on a frequency histogram and quantification of fork speed differences.
D) Fork speed of diploid and tetraploid clones at passage 50 (kb/min). Median number of fibres scored = 183 (range 149-220).
E) Frequency histogram showing fork speed for all passage 50 clones, and quantification of fork speed differences.

It could be of interest to use DNA combing to improve this analysis. The use of combing allows more accurate recognition of particular fork structures that can be

indicative of specific problems during DNA replication, including stalled forks and asymmetric fork progression. However, since only a very slight difference was noted between diploid and tetraploid clones with respect to fork speed, it was deemed unnecessary to extend this analysis.

Replication stress has been shown to be linked to structural chromosomal instability (Burrell et al., 2013). Replication stress can result in a reduction in fork speed, however it does not appear that tetraploid cells are affected by replication stress to a great extent. This is in accordance with previous data (Figure 3.10) showing the spectrum of segregation errors in tetraploids is not significantly different from either the parental cell line or the diploid clones. Replication stress would likely result in an increase in acentric lagging chromosomes and anaphase bridges (Burrell et al., 2013).

3.2.9 Cell cycle timing and proliferation rate in diploid and tetraploid clones

Tetraploidy seems to have an effect on the levels of both numerical and structural chromosomal instability on a per cell, but not per chromosome basis. Next the effect of a doubled genome on cell cycle timing was investigated. Cell cycle duration in all diploid and tetraploid clones was assessed from live cell imaging of cells expressing a plasmid containing histone 2b tagged to red fluorescent protein (pH2B-mRFP) (Figure 3.16A). Cells were transfected with the H2B-mRFP expressing plasmid and sorted using FACS for RFP expression after selection in antibiotic (see Methods). Cells were imaged for approximately 6 hours on a climate-controlled microscope. A full cell cycle was defined as the time from mitosis to the next mitosis in resulting daughter cells. Only cells that underwent a normal mitosis with no visible segregation error defects were included in this analysis.

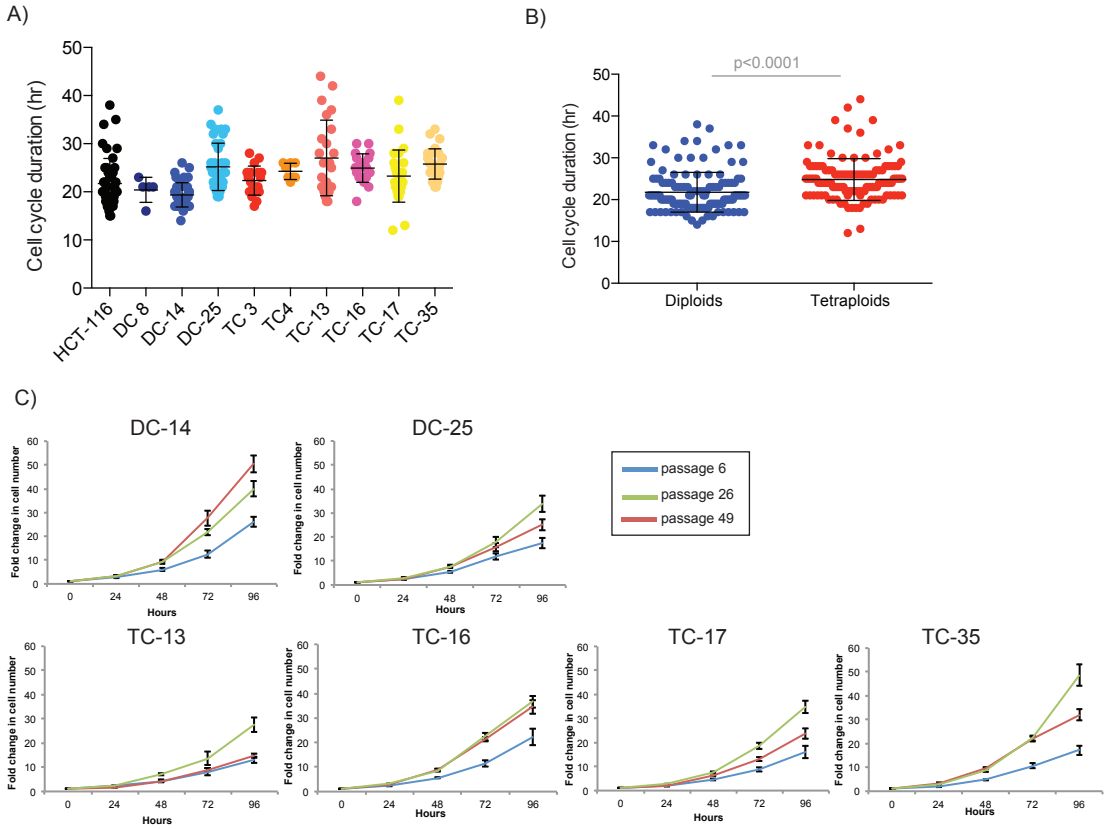

Figure 3.16: Tetraploid clones have a longer cell cycle duration than diploid clones

A) Quantification of cell cycle length from live-cell imaging of diploid and tetraploid clones expressing H2B-mRFP. Median number of cells scored = 26 (range 5-45). Approximate passage number of all clones after transfection was passage 15.
B) Comparison of cell cycle duration between diploid and tetraploid clones.
C) A fixed cell analysis of proliferation rate over 96 hours for second-generation clones at passage 6, passage 26 and passage 49. Five replicate wells were plated for each clone, from which standard deviations were calculated, and shown on graphs as error bars.

Cell cycle movies were captured between passage 6 and passage 11 (indicating the passage of cells at time of H2B-mRFP transfection). Although the cell cycle length was not remarkably different between all the clones (diploid range: 14 – 38 hours, tetraploid range: 12 – 44 hours), taken together there was a significant increase in cell cycle length in tetraploid clones (Figure 3.16B, $P<0.0001$, Student's T-test, diploid mean: 22 hours, tetraploid mean: 25 hours). In an analysis of fixed cells at three different passage numbers, all second generation clones showed a clear trend for an increase in proliferation rate over time (Figure 3.11C). It is likely that this is due to the selection pressure of passaging cells continuously, which will select for more rapidly growing cells over time.

3.2.10 Tetraploid clones have an increased mitotic duration

It has been previously reported that the number of chromosomes and presence of extra centrioles can increase the length of mitosis (Yang et al., 2008). The length of mitosis was analysed using live-cell imaging of H2B-mRFP expressing clones ranging between passage 6 and passage 11 (Figure 3.17A). Mitotic duration was significantly increased in tetraploid compared to diploid cells (diploid mean = 28 minutes, tetraploid mean = 38 minutes, $P<0.0001$, Student's T-test). The standard deviation also indicates that there is more variation in the tetraploid cells compared to the diploid cells (diploid SD = 7.6, tetraploid SD = 15.3). Mitotic duration can be split into two distinct phases using H2B-mRFP expressing cells (Figure 3.17B). The time from nuclear envelope breakdown (NEBD) until the last chromosome has congressed (LCC) to the metaphase plate is shown in Figure 3.17B. The length of this phase of mitosis is shortly but significantly increased in tetraploid clones compared to diploid clones (diploid mean =19 minutes, tetraploid mean = 23 minutes, $P<0.0001$, Student's T-test, Figure 3.17D). Similarly, the time between the last chromosome having congressed and anaphase onset (ANA) is also significantly increased in tetraploid clones (diploid mean = 9 minutes, tetraploid mean = 13 minutes, $P=0.004$, Student's T-test, Figure 3.17E and 9F).

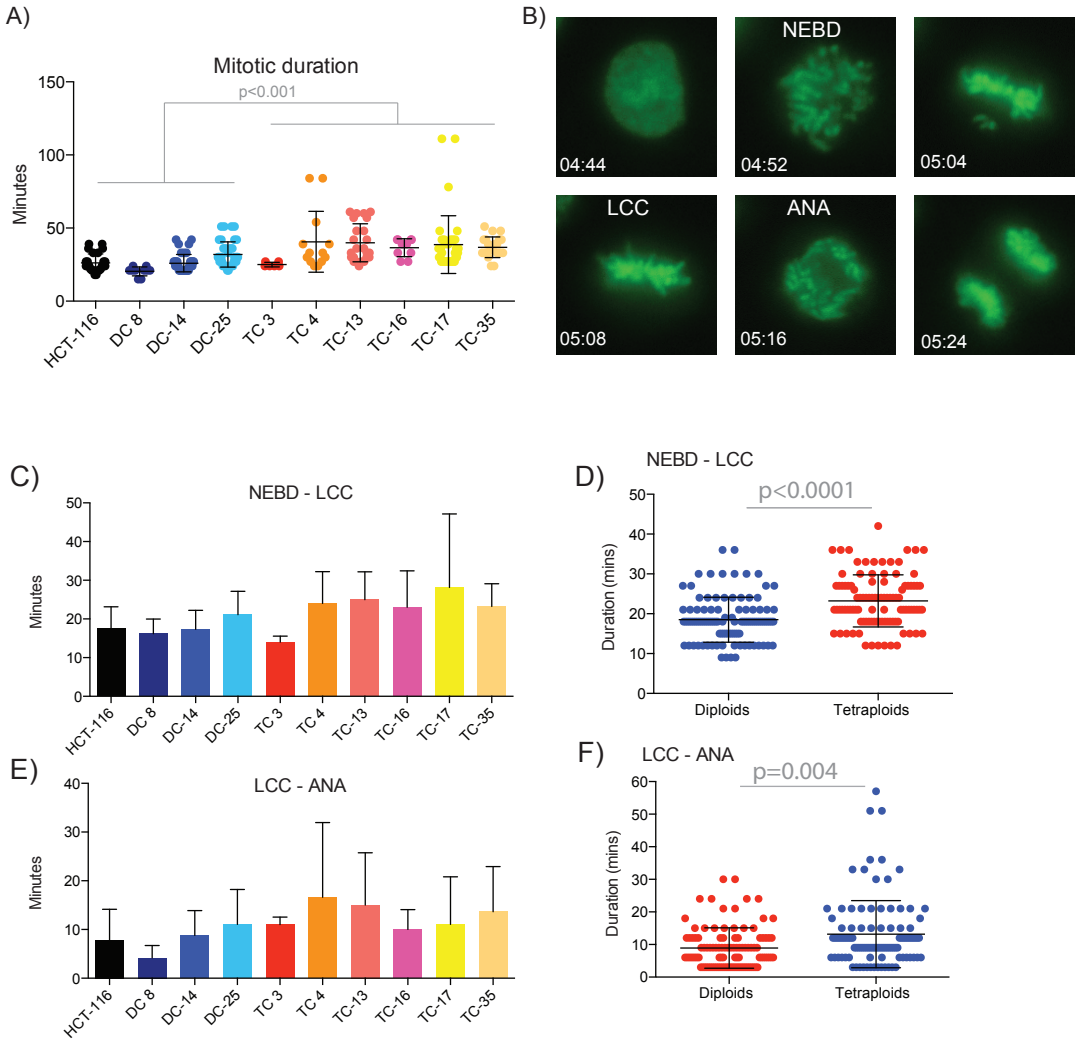

Figure 3.17: Increased mitotic duration in tetraploid clones

A) Mitotic duration calculated from live-cell imaging of H2B-mRFP expressing clones from approximately passage 15. Mitotic duration is defined as the time from nuclear envelope breakdown (NEBD) to anaphase. Median number of cells scored for this and subsequent analysis = 26 cells.
B) Images show the different phases of mitosis in H2B-mRFP expressing cells; time from start of movie is shown on each panel in the form hh:mm. NEBD, last chromosome congressed (LCC) and anaphase onset (ANA) are indicated.
C) Quantification of duration between NEBD and LCC in individual diploid and tetraploid clones.
D) Comparison of duration from NEBD-LCC between diploid and tetraploid clones.
E) Quantification of duration between LCC and ANA in individual diploid and tetraploid clones.
F) Comparison of duration from LCC-ANA between diploid and tetraploid clones.

A delay in NEBD to LCC is likely to represent a delay while all chromosomes are correctly aligned to the metaphase plate, and a LCC to ANA delay is likely to be caused by prolonged signalling of the spindle assembly checkpoint (SAC) (see

Section 1.4.2). As discussed for yeast (see Section 1.10), polyploidy has been suggested to cause geometric defects in spindle pole body (SPB) and microtubule formation that could be responsible for the increase in syntelic attachments observed in polyploid yeast (Storchova et al., 2006). It is not yet clear whether these same geometric constraints occur in tetraploid mammalian cells. However, there may well be physical constraints that arise due to a doubled chromosome number, and if these cause an increase in mal-attached chromosomes, this might lead to an increase in mitotic duration as the cell attempts to correct these. As has been previously shown, extra chromosomes and centrioles do result in an increased mitotic duration due to a delay in satisfying the spindle assembly checkpoint (Yang et al., 2008).

3.2.11 S-phase duration in tetraploid clones

Having only noted a small delay in mitosis in tetraploid cells, the length of S phase was then assessed. To explore the length of S-phase, a pulse-chase assay followed by flow cytometry analysis was used. Exponentially growing cells were exposed to the synthetic nucleoside analogue of thymidine Bromodeoxyuridine (BrdU), which is incorporated into newly forming DNA in cells during S-phase. After the pulse of BrdU treatment, cells are fixed at regular intervals and the BrdU positive cells can be tracked through subsequent phases of the cell cycle using a DNA stain (Figure 3.18A). These experiments were carried out in second-generation clones at passage 11. After 24 hours from the initial BrdU pulse there was no significant difference in cell cycle phase of the BrdU positive cells between the diploid and tetraploid clones (percentage of diploids vs. tetraploids in G1 after 24 hours: P=0.3118, S phase: P=0.1487, G2 phase: P=0.6544, Student's T-test, Figure 3.18B). These data indicate that there is no difference in the length of S phase between diploid and tetraploid clones.

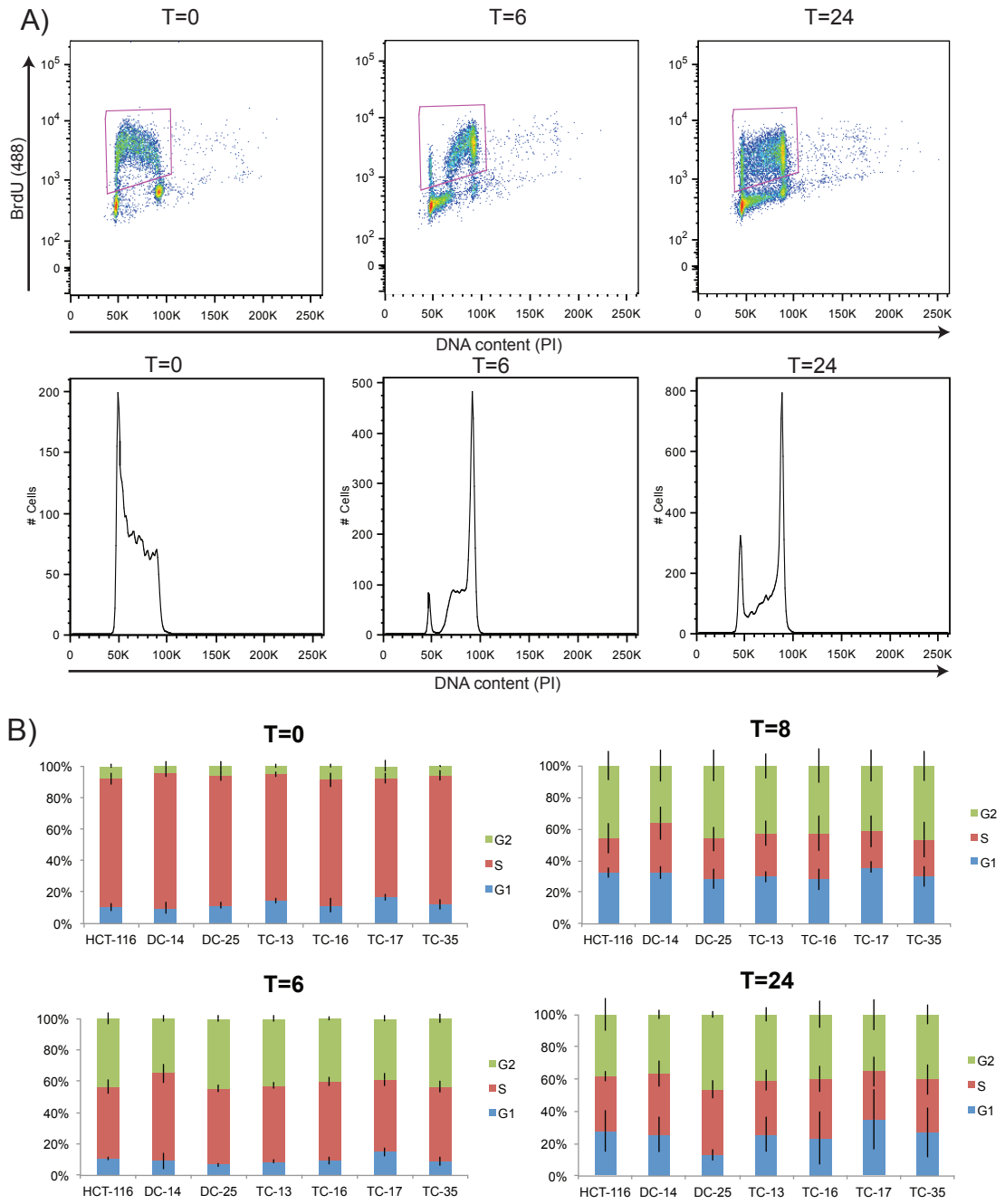

Figure 3.18: S phase duration is similar in diploid and tetraploid clones

A) Representative flow cytometry plots of a diploid clone pulsed with BrdU at different time points (T=0, T=6 and T=24 hours after BrdU pulse). Top panels compare DNA content (PI) on x-axis (linear scale) to BrdU positivity (green channel-488) on the y-axis (log scale). BrdU positive cells are demarcated by pink box at each time point (positivity was determined against a BrdU untreated control). Bottom panel shows a DNA histogram of the BrdU positive cells from the corresponding top panel.
B) The percentage of BrdU positive cells in cell cycle phase at the indicated time points after the BrdU pulse in passage 12 diploid and tetraploid clones. Cell cycle phases were defined from an algorithm in the flow cytometry analysis software

FlowJo (Watson pragmatic – see Methods). Time points T=0, T=6, T=8 have standard deviations derived from three independent experiments, T=24 has error bars from two independent experiments.

Taken together the data on cell cycle length has shown delayed cell cycle duration in tetraploid clones (Figure 3.16). However this delay (on average 3 hours longer in tetraploid clones) cannot be fully explained by the small increases in mitotic duration (on average 8 minutes longer, Figure 3.17). Furthermore, there does not appear to be systematic delay in the duration of S phase (Figure 3.18). It is possible that heterogeneity between different cells experiencing cell specific delays in different phases could account for the differences between diploid and tetraploids.

It is interesting as there are not significant changes in replication fork speed in tetraploid clones (Figure 3.15), given that they have an S phase of similar duration (Figure 3.18). This means that DNA in tetraploid cells is being replicated within the same time frame as half the amount of DNA in diploid cells with no increase in the speed of replication. This could suggest that twice as much replication machinery is present in each cell to achieve the same rate of origin firing from each chromosome.

3.3 Conclusions

In this chapter an isogenic system of diploid and tetraploid clones derived from HCT-116 has been used to study the effects of a naturally occurring tetraploidisation event on chromosomal instability. The long-term impact on chromosomal instability was investigated by continual passage of all clones over more than a year. Tetraploid cells at passage 5 (approximately 1 month after isolation) were compared to those at passage 25 (approximately 6 months in culture) and at passage 50 (after a year in culture).

Tetraploid clones demonstrated significantly higher levels of numerical chromosomal instability as evidenced by their increase in cell-to-cell variation in chromosome number and increase in the frequency of anaphase segregation errors per cell. However, there was no difference in the frequency of segregation

errors per chromosome, suggesting that the increase in segregation errors per cell results from the fact that there are more chromosomes in tetraploid cells. Despite tetraploid clones having a significant increase in the percentage of cells with extra centrioles, there was only a small difference in the number of cells undergoing a transient multipolar spindle intermediate in prophase between diploid and tetraploids, which has been suggested as a mechanism that drives increases in lagging chromosomes in cells with supernumerary centrioles (Ganem et al., 2009). These data are supported by the fact that there is no difference in the frequency of lagging centric chromosomes between diploid and tetraploid cells.

Tetraploid clones also displayed increased levels of structural chromosomal instability, as evidenced by structurally abnormal chromosomes observed on metaphase spreads. Similarly to numerical instability, this structural instability was only observed on a per cell, and not per chromosome basis. No evidence of replication stress was noted for tetraploid cells at either passage 5 or passage 50, and only small increases were observed at passage 50 when assessing interphase DNA damage. Differences in cell cycle phases and duration were also investigated between diploid and tetraploid clones. Despite a small increase in cell cycle duration in tetraploid cells, no systematic defect in S phase or mitosis was observed that could account for this. It is likely that heterogeneous cell cycle profiles of different cells within the population account for the small increase in cell cycle duration.

Taken together, these data indicate that tetraploidisation does not cause an increase in chromosomal instability above that which would be expected given the increase in the number of chromosomes in tetraploid cells. However a strong correlation was observed across multiple cancer types in TCGA between ploidy and chromosomal instability, which indicates that polyploid cells are able to maintain a high level of chromosomal instability that is positively selected for. In the next chapter, the ability of tetraploid cells to propagate chromosomal instability and segregation errors is investigated.

Chapter 4. Results 2: Tetraploid clones tolerate and propagate CIN

4.1 Introduction

An isogenic system of diploid and tetraploid clones has been described that was derived from the MIN CRC cell line HCT-116. Tetraploid clones exhibit increased numerical and structural chromosomal instability that seemed to remain at a constant level over the course of continual passaging for more than a year. Careful analysis showed that levels of chromosomal instability were not increased in tetraploids if their additional chromosome count was used to compare instability on a per chromosome basis. Chromosomal instability is a high-risk clinical phenotype, being associated with poor patient prognosis across a range of cancer types. Given that genome doubling events are noted to be associated with increased chromosomal instability across a range of cancer types, it was investigated how the increased chromosomal instability in tetraploid cells could affect the stability of the genome over time. It is clearly of clinical relevance to better understand how highly unstable cancers arise.

All bioinformatics analyses presented in this chapter were informed from the in vitro studies carried out in Chapter 3, and carried out in collaboration with Nicholas McGranahan.

4.2 Results

4.2.1 Tetraploid cell lines can propagate aneuploidy in clonal FISH assays

Clonal FISH assays can be used to assess a second measure of chromosomal instability as well as the cell-to-cell variation previously presented (see Section 3.2.3). This is the modal chromosomal variation between colonies, or colony-to-colony variation. An aneuploid modal chromosome number implies that an initial founding cell was aneuploid and has been able to grow into a colony. The number of colonies with colony modes differing from the expected modal chromosome number (2 for diploid and 4 for tetraploid colonies) gives information about the ability of a cell line to propagate an unbalanced, or aneuploid, chromosome number.

At both passage 5 and passage 50, aneuploid colonies were observed in tetraploid clones (Figure 4.1A and B) for either chromosome 2 or chromosome 8 (passage 5 mean=25% of colonies [8-44%]; passage 50 mean=30% [18-43%]).

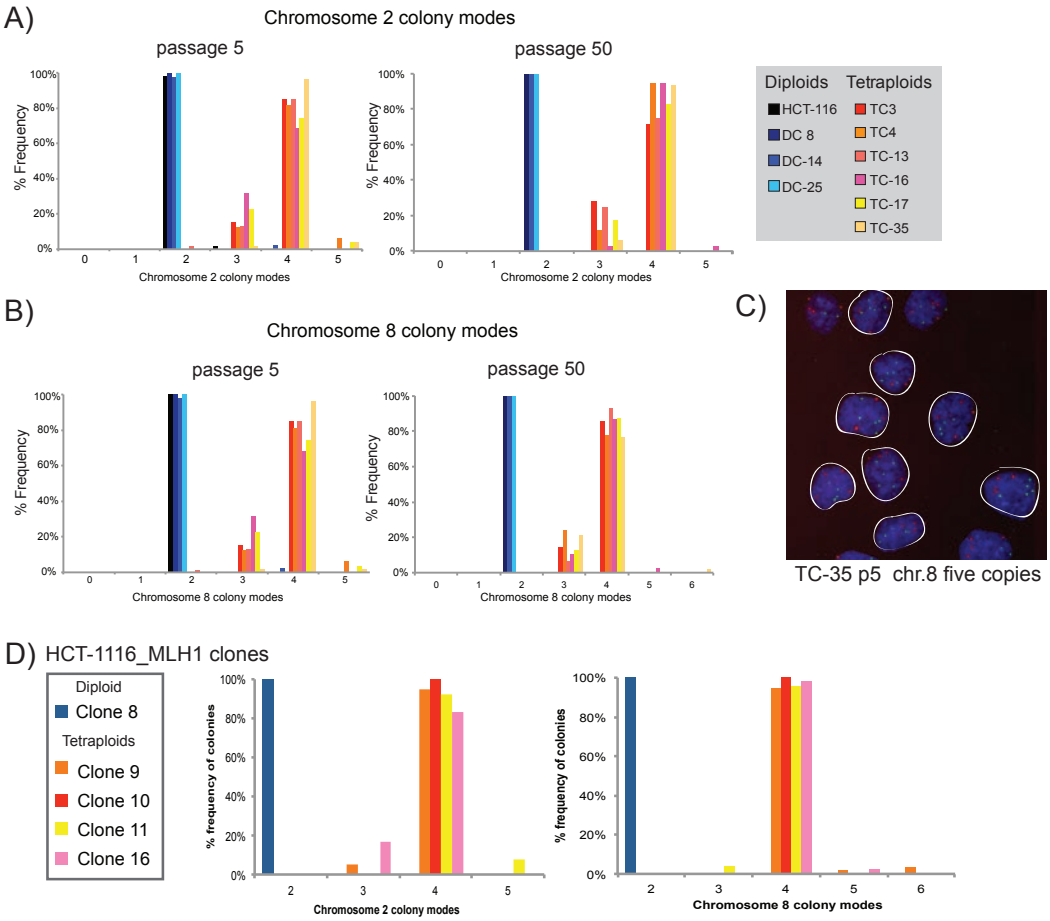

Figure 4.1: Increased colony-to-colony variation in tetraploid clones

A) Colony-to-colony variation (or deviation of the mode) of chromosome 2 analysed from clonal FISH data in both passage 5 and passage 50 diploid and tetraploid clones. Data is shown as percentage frequency of colonies with indicated modal chromosome numbers. Median numbers of colonies analysed: passage 5= 44, passage 50 = 39.
B) Colony-to-colony variation of chromosome 8 for both passage 5 and passage 50.
C) Representative image of a pentaploid colony, observed in the tetraploid clone TC-35. Cells with five copies of chromosome 8 are outlined in white.
D) Clonal FISH of HCT-116_MLH1 clones at passage 5 for both chromosome 2 and chromosome 8.

An example of an aneuploid colony that was observed in TC-35 is shown in Figure 4.1C. Only one aneuploid colony was found in HCT-116 (1.7% of all colonies), and

no aneuploid colonies were found in the other diploid clones. One tetraploid colony was observed in DC-14, consistent with the observation that diploid clones can tolerate tetraploidisation as a rare event (Figure 4.1A and B).

These data suggest that tolerance of aneuploidy is a rare event in diploid clones, but common in tetraploid cells. Further, the four tetraploid clones derived from a microsatellite competent clone of HCT-116 (HCT-116_MLH1) also displayed several aneuploid colonies in clonal FISH assays (Figure 4.1D). Taken together, these data suggest that tetraploid cells are better able to propagate aneuploidy than their diploid counterparts.

This result is intriguing as it suggests tetraploid cells may have an aneuploidy tolerance mechanism that is not present in diploid cells. It has previously been suggested that chromosomal instability may be a composite phenotype involving not only increased genome stability, but also tolerance and propagation of genome instability. In fact, HCT-116 has been previously used to demonstrate that CIN cannot be artificially induced in cell lines just by increasing the segregation error rate (Thompson and Compton, 2010).

4.2.2 Tetraploid clones can propagate segregation errors in live-cell imaging analysis

Since clonal FISH gives an indirect measure of the ability of cells to tolerate aneuploidy, a more direct assay to measure tolerance to chromosome missegregation was carried out. Using the H2B-mRFP expressing diploid and tetraploid clones described previously (see Section 3.2.9), daughter cell fate after both normal cell division and divisions with segregation errors was assessed. Images were taken every 3 minutes for the first six hours of acquisition so dividing cells could be scrutinised for segregation errors. Further images were taken at 15-minute intervals so that cell fate could be assessed over the next 60 hours. Daughter cell fate was split into three categories: mitosis, cell cycle arrest or cell death. Figure 4.2A-F show examples of the different cell fates analysed. Daughter cells were defined as arrested if they did not enter a subsequent mitosis within 48

hours of the first mitosis. Multipolar cell divisions were excluded from this analysis, as they are known to mainly result in unviable progeny (Ganem et al., 2009, Kuffer et al., 2013). Figure 4.2G shows the results of individual cell lines, indicating differences in cell fate after a normal division (no error), or an error. A summary of the number of daughter cells scored for each cell line is shown in Figure 4.2H. Data represented comes from an amalgamation of different passage numbers (see figure legend for details). Combining all the data from diploid and tetraploid clones shows that tetraploid cells have a significantly different response to segregation errors than diploid cells (Figure 4.2I). In diploid cells that made a segregation error in the first mitosis, the majority of daughter cells underwent cell cycle arrest or cell death (death and/or arrest- diploid mean: 58% - HCT-116: 43%, DC 8: 68%, DC-14: 55%, DC-25: 68%). In comparison in tetraploid cells that made a segregation error, significantly fewer daughter cells died or arrested (death and/or arrest – tetraploid mean: 16%, TC 3: 18%, TC 4: 12%, TC-13: 11%, TC-16: 10%, TC-17: 34%, TC-35: 12%, P=0.0002, Students T-test). This indicates that tetraploid cells have a specific ability to tolerate segregation errors, and supports the observation made from the clonal FISH data that tetraploid cells are able to propagate aneuploidy more efficiently than diploid cells (Figure 4.1).

Interestingly although an average of 42% of diploid cells continued cycling after a segregation error, observing aneuploid colonies was extremely rare, if not absent in the majority of diploid clones in the clonal FISH analysis (Figure 4.1). It is hard to discern using these live-cell imaging techniques whether a lagging chromosome was segregated into the correct or incorrect daughter cell, which can influence subsequent cell fate (Huang et al., 2012). It has been shown that in the majority of cells, a lagging chromosome will segregate to the correct daughter cell (Thompson and Compton, 2011a, Huang et al., 2012). This could explain why some diploid cells still manage to continue to a next mitosis after being classified as undergoing a segregation error. Additionally, this could be due to the fact that it was only possible to analyse cells for 60 hours, given the constraints of imaging live cells. A longer analysis would have allowed tracking of cells through more than one generation, and may have revealed that although some diploid cells do survive one division after a segregation error, they do not propagate for multiple generations.

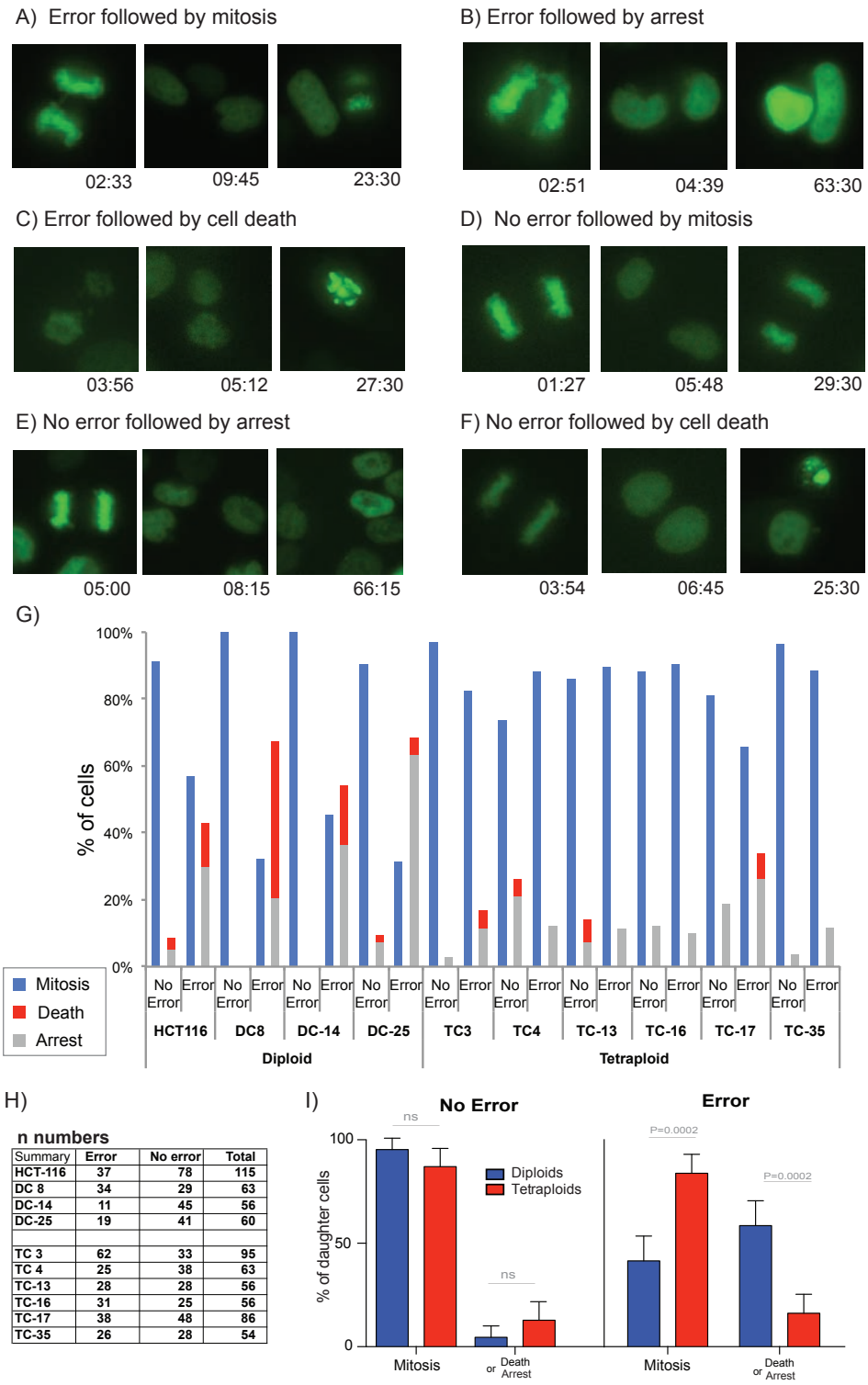

Summary	Error	No error	Total
HCT-116	37	78	115
DC 8	34	29	63
DC-14	11	45	56
DC-25	19	41	60
TC 3	62	33	95
TC 4	25	38	63
TC-13	28	28	56
TC-16	31	25	56
TC-17	38	48	86
TC-35	26	28	54

Figure 4.2: An increased tolerance to segregation errors in tetraploid clones

A-F) Example images to represent the different cell fates scored in this analysis. Time since start of movie is shown in the form hh:mm.
G) Cell fate both after a normal mitosis (no error) and after a segregation error is shown for each diploid and tetraploid clone. Data shown is an amalgamation of the following passage numbers: passage 6, 14 and 56 (three experiments) for DC 8,

TC 3 and TC 4, passage 10 and 20 (two experiments) for DC-14, DC-25, TC-13, TC-16 and TC-35, passage 10, 12 and 20 for TC-17, three experiments for HCT-116.
H) N numbers (number of daughter cells scored) for each clone.
I) Comparison of cell fate between diploid and tetraploid clones after a normal mitosis or after a segregation error. *P*-values from a Student's T-test are shown over the relevant comparisons.

4.2.3 Chromosomal instability emerges in tetraploid clones over time

Based on both the clonal FISH colony analysis and the live cell imaging data, which indicate tetraploid clones have an increased tolerance to segregation errors and a greater ability to propagate aneuploidy than diploid clones, genomic changes in all diploid and tetraploid clones over 18 months of continual passaging were assessed using CGH (comparative genome hybridisation). DNA from clones at different time points during the continuous culture was subjected to Affymetrix SNP6.0 analysis to see whether these phenotypes manifested themselves over time in changes to the genome of the whole population in tetraploid clones.

Figure 4.3 shows genomic changes over time in both diploid and tetraploid clones. Red represents gain relative to median ploidy, whereas blue represents loss. It is clear that tetraploid clones at all passages have greater levels of genomic aberrations than diploid clones. To quantify the level of genomic alterations between different clones, the wGII was calculated (Figure 4.4). All the diploid clones had similar wGII scores to the parental cell line at every passage analysed (passage 5, 25 and 50 for all clones, plus passage 75 for second generation clones). In comparison, tetraploid clones had significantly higher wGII scores at every passage, as well as showing a trend in the majority of clones for increasing wGII over time (averages for passage 5: diploids=0.066, tetraploids=0.122, passage 25: diploids=0.066 tetraploids=0.21, passage 50 diploids=0.067 tetraploids=0.30, passage 75 diploids=0.067 tetraploids=0.33).

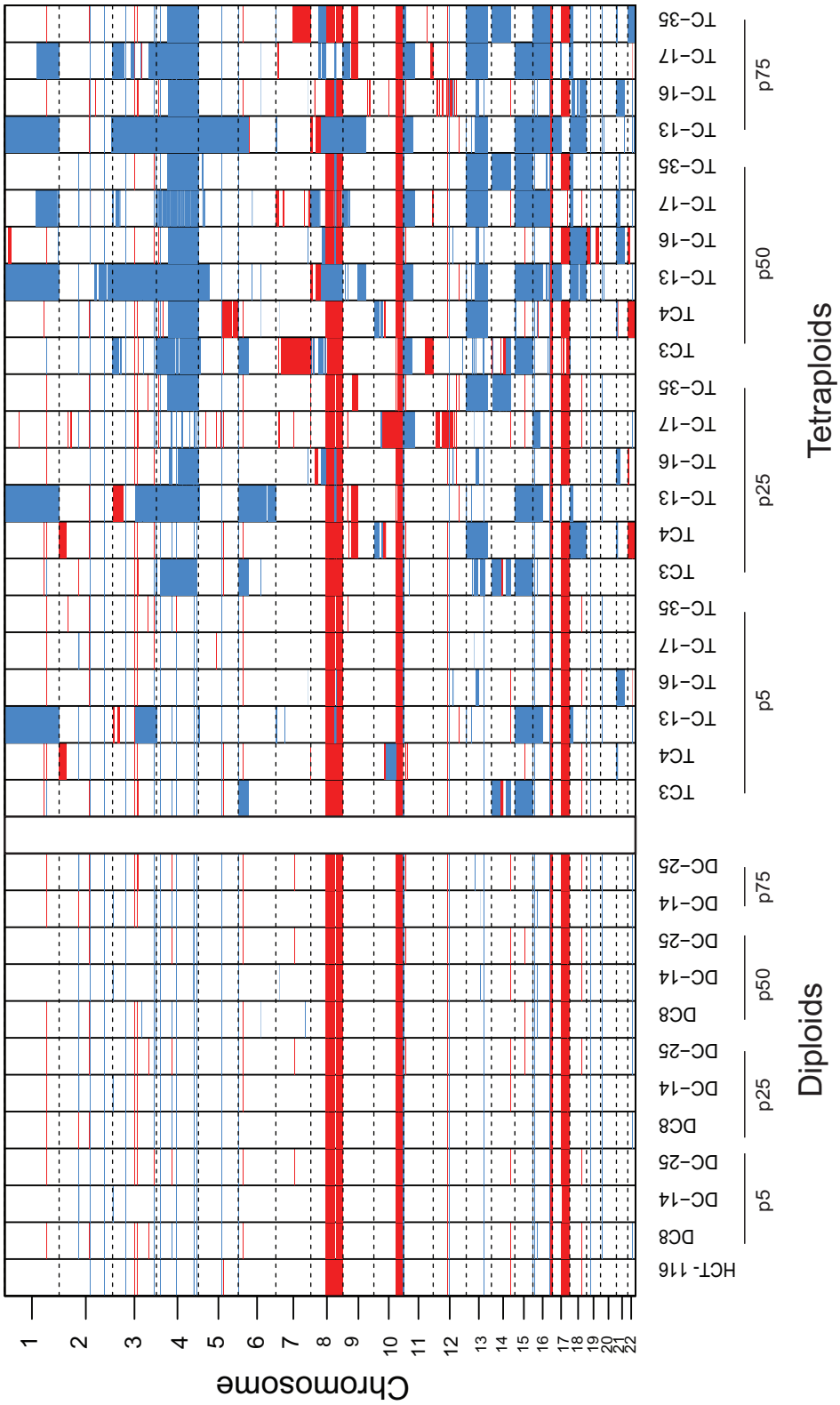

Figure 4.3: Genomic changes in all clones over time

CGH analysis of all diploid and tetraploid clones at passage 5, 25 and 50 (and also passage 75 for DC-25, DC-14, TC-13, TC-16, TC-17 and TC-35). Gains (shown in red) and losses (in blue) are calculated relative to median ploidy (see Methods).

Strikingly all tetraploid clones by passage 50 had wGII greater then 0.2, a threshold which has been shown to accurately separate CRC tumours into CIN- (or MIN) and CIN+ (Lee et al., 2011), whereas diploid clones remained chromosomally stable. Continuous culture of tetraploid clones for a year has changed the genomic subtype of these cancer cells from chromosomally stable to chromosomally unstable.

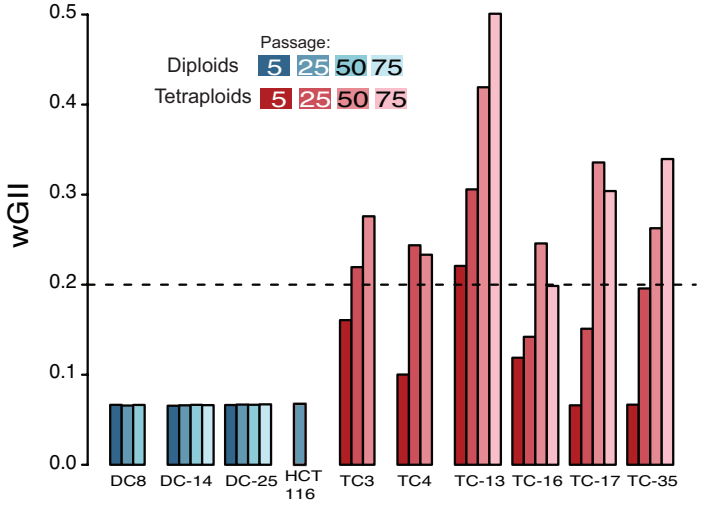

Figure 4.4: wGII increases over time in tetraploid clones

wGII scores for all clones calculated from SNP6.0 arrays (see Methods). Lighter colours indicate later passages, blue showing diploid clones and red showing tetraploid clones (see key in Figure). Dashed line indicates a wGII score of 0.2, which has been shown to separate CRC tumours into CIN- (<0.2) and CIN+ (>0.2) (Lee et al., 2011).

Strikingly there are genomic regions subjected to recurrent loss in all of the tetraploid clones (see Figure 4.3). A large but non-contiguous region of chromosome 4q was found to be lost to three copies in all the tetraploid clones by passage 50. This likely represents selection for loss of this region over prolonged culture. To assess the relevance of this genomic loss, CRC data from TCGA was sorted according to wGII score (Figure 4.5). The copy number state of this genomic region of chromosome 4 (schematically represented in Figure 4.5) was calculated. The correlation between loss of the genes on this region and increasing wGII is highly significant (P<0.001). This statistical analysis was tested for significance using simulations, which take into account the increased likelihood for genomic losses to occur in tumours with high wGII scores (see Methods). This result

suggests that there could be a beneficial phenotypic outcome for a genomically unstable tumour to lose copies of any or all of the 362 genes in this region. An alternative, but untested, hypothesis is that this region may be more likely to be subjected to copy number loss due to a unknown mechanism that makes it easier to lose genomic material from this region.

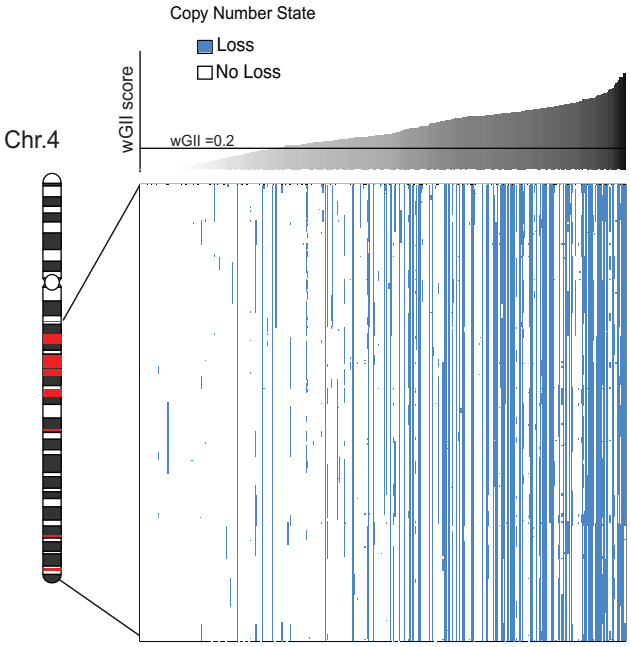

Figure 4.5: Association of chromosome 4q loss with increasing wGII in CRC

A relationship between the genes on chromosome 4q and highly unstable CRCs. CRC tumours from TCGA are ranked from left to right according to increasing wGII, and the copy number state for the genes on the regions of chromosome 4q (excluding regions in red) is shown as either white (no loss) or blue (loss).

CGH analysis of the diploid and tetraploid clones derived from HCT116_MLH1 revealed a very similar pattern of genomic loss (Figure 4.6). The wGII scores in the two tetraploid clones increased between passage 5 and passage 25 (0.07 to 0.13 in MLHC11, 0.12 to 0.17 in MLHC16), whereas the diploid clone remained stable (0.1 to 0.09 in MLHC8). Similar to the HCT-116 tetraploid clones, tetraploid HCT116_MLH1 clones also showed loss of chromosome 4q (Figure 4.6). This data show that the specific loss of chromosome 4q is not a result of the microsatellite instability phenotype of HCT-116 tetraploid clones.

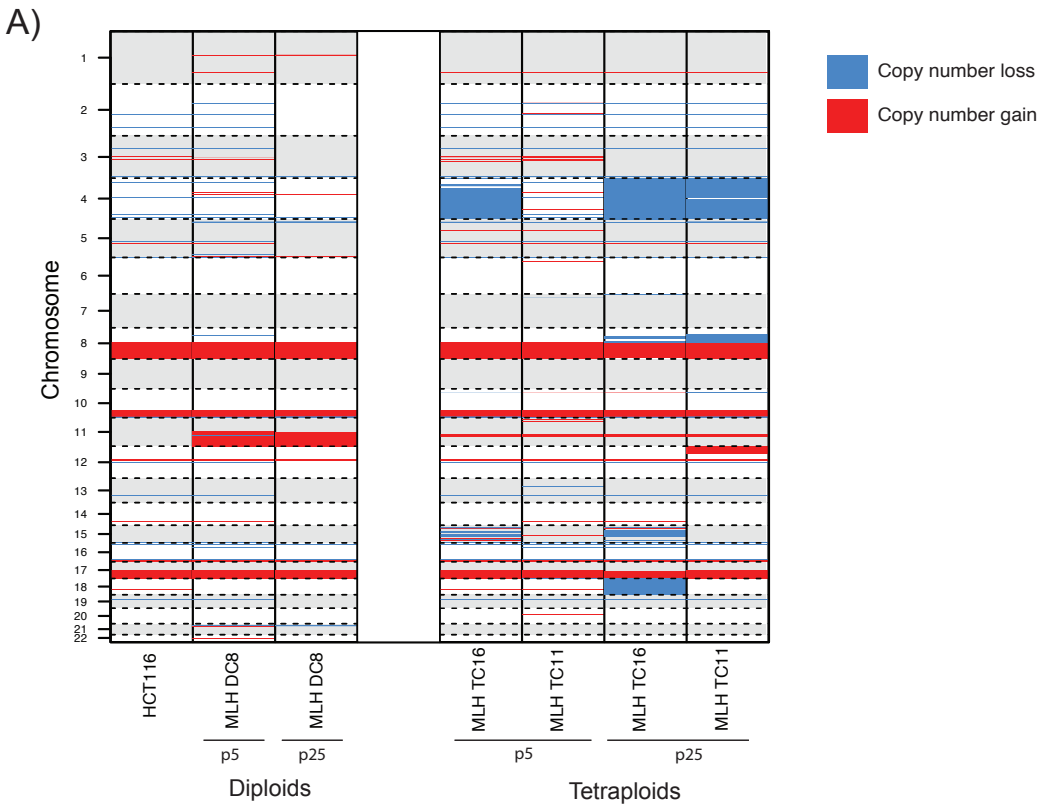

Figure 4.6: Copy number changes in microsatellite-competent HCT-116 clones

A) CGH analysis of copy number changes in HCT-116_MLH1 clones (MLH Diploid C8 and MLH Tetraploid C16 and C11) at passage 5 and passage 25. Blue shows copy number loss and red shows copy number gain (relative to median ploidy).

4.2.4 Genomic evolution of tetraploid clones over time reveals the origin of some unstable CRC tumours

Using the genomic data from CGH analysis, it was possible to compare the evolution of tetraploid clones over time to CRC data from TCGA. When the wGII scores and ploidy of HCT-116 clones at different passage numbers were compared to wGII and ploidy of TCGA tumours, a striking pattern emerges (Figure 4.7A). With increasing passage number, tetraploid clones tend to become more genomically unstable, and also tend to lose genomic material, becoming closer in genotype to the near-triploid, highly unstable, genome-doubled CRC tumours that were observed in the initial analysis of TCGA data (Figure 3.1).

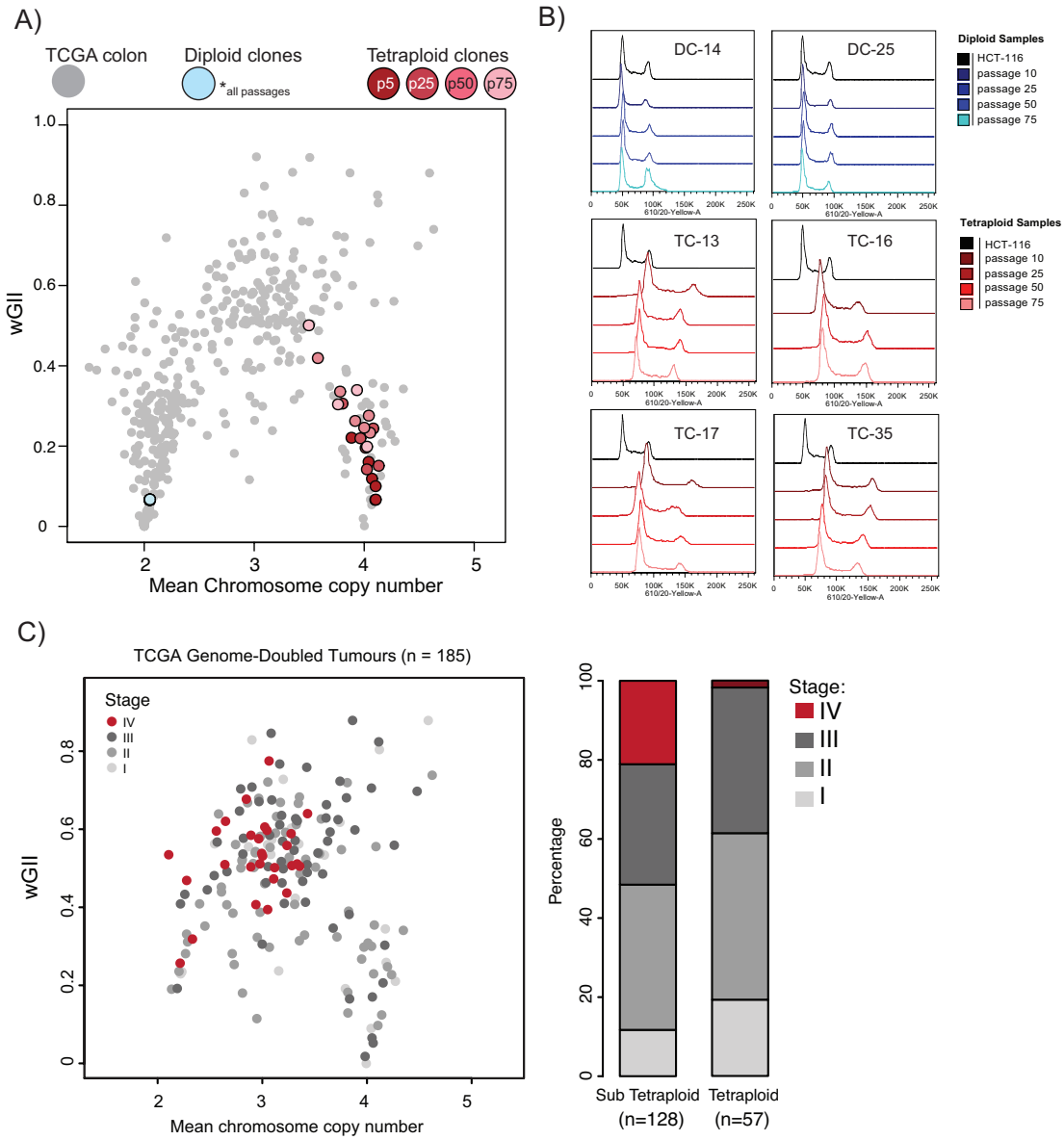

Figure 4.7: Comparison of tetraploid clones to TCGA data reveals route of evolution of some unstable CRCs

A) A comparison of wGII scores and mean chromosome copy number of diploid and tetraploid clones of HCT-116 and CRC tumours from TCGA. TCGA CRC tumours are shown as grey dots, and tetraploid HCT-116 clones are shown in different shades of red. Lighter red indicates later passage number (see key). All diploid clones (blue dots) at all passage numbers overlay the same point.
B) Flow cytometry analysis of second-generation diploid and tetraploid clones at passage 10, 25, 50 and 75. All clones were stained with PI at the same cell number to dye concentration.
C) Depiction of tumour stage specifically in TCGA CRC tumours that have been classified as genome doubled n=185. The bar plot shows percentage of tumours at stage I-IV in tetraploid and sub-tetraploid tumours.

The loss of genomic material over time is consistent with flow cytometry data of the tetraploid clones at different passage numbers (Figure 4.7B). These data fit a model whereby some CRC tumours are able to become highly genomically unstable through an initial genome-doubling event, which then results in the emergence of chromosomal instability over time. To assess whether this could be true of the TCGA tumours analysed here, the stage of all genome-doubled TCGA tumours was compared to their ploidy. Comparing sub-tetraploid (ploidy<4) to tetraploid tumours showed that sub-tetraploid tumours were more genomically complex and also enriched for Stage IV tumours (*P*=0.0062, Cochran-Armitage test, Figure 4.7C). This indicates that genome doubling is likely to be an early event in the evolution of high-stage (and hence metastatic), chromosomally unstable CRC.

4.2.5 Genome doubling is a predictive marker of poor outcome in CRC

Due to the known association between high chromosomal instability and poor outcome for patients, not just in CRC, but also in multiple cancer types (Lee et al., 2011, McGranahan et al., 2012), the utility of using the genome doubling algorithm as a predictive marker for patient outcome was tested. Available survival data from TCGA was obtained for 150 patients with Stage 1-3 CRC. Using the genome doubling algorithm as described (see section 3.2.1 and Methods), it was found that patients whose tumours were likely to have undergone a genome doubling event suffered a poorer outcome in a 2 year analysis of relapse-free survival (Figure 4.8A, *P*=0.019, hazard ratio [HR]=5.1, 95% confidence interval [CI] 1.1-22.8). A 2-year cut-off for relapse free survival was used, since the majority of CRCs relapse within this period (Hellinger and Santiago, 2006). An uncensored relapse free survival curve is shown in Figure 4.9A. To confirm the initial findings from the TCGA discovery cohort, a larger validation cohort of 389 Stage 2-3 CRC patients was obtained. In this cohort genome doubling was also predictive of poor relapse-free survival (Figure 4.8B, *P*=0.0022, HR=1.80, 95% CI 1.2-2.8, and full survival curves in Figure 4.9B). This data concurs with that of Carter and colleagues, who showed that presence of genome doubling predicted worse recurrence free incidence in high-grade serous ovarian carcinoma (Carter et al., 2012).

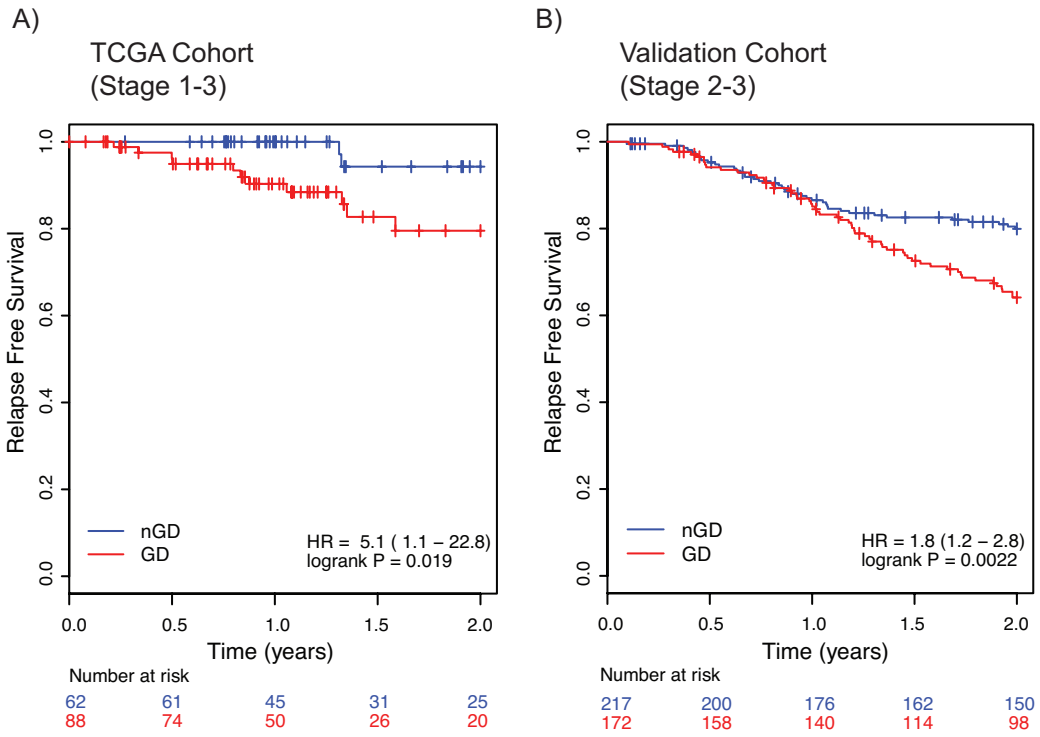

Figure 4.8: Genome doubling predicts worse relapse-free survival in two independent CRC cohorts

A) Kaplan-Meier relapse-free survival curves for genome doubled (GD, red line) and non-genome doubled (nGD, blue line) TCGA CRC tumours (n=150) censored at 2 years. *P*=0.019 log-rank test.
B) Kaplan-Meier relapse-free survival curves for GD (red line) and nGD (blue line) colorectal cancer patients in the validation cohort (n=389). *P*=0.0022, log-rank test.

Previous data has indicated that genome doubling is likely to be an early event in CRC occurring before the onset of chromosomal instability (see sections 3.2.1 and 4.2.4). It was therefore hypothesised that use of the genome doubling algorithm may have better predictive power to identify patients at higher risk of relapse than other markers such as stage and age. Indeed, in a multivariate analysis including MSI status, stage and age, genome doubling remained a significant predictor of outcome (Table 4.1, TCGA data: *P*= 0.045, HR=4.70, 95% CI 1.04-21.37, validation data: *P*=0.028, HR=1.59, 95% CI 1.05-2.42). Conversely, using wGII alone as a predictor of outcome was only significant in one of the cohorts in univariate analysis (TCGA data: *P*=0.1296, HR=6.09, 95% CI 0.57-64.93; validation data: *P*=0.00649, HR=3.81, 95% CI 1.44-10.03), and not significant in multivariate analysis when including age, stage and MSI status (Table 4.1). This suggests that

the reason genome doubling is predictive of outcome is not simply because it identifies tumours that are more genomically unstable.

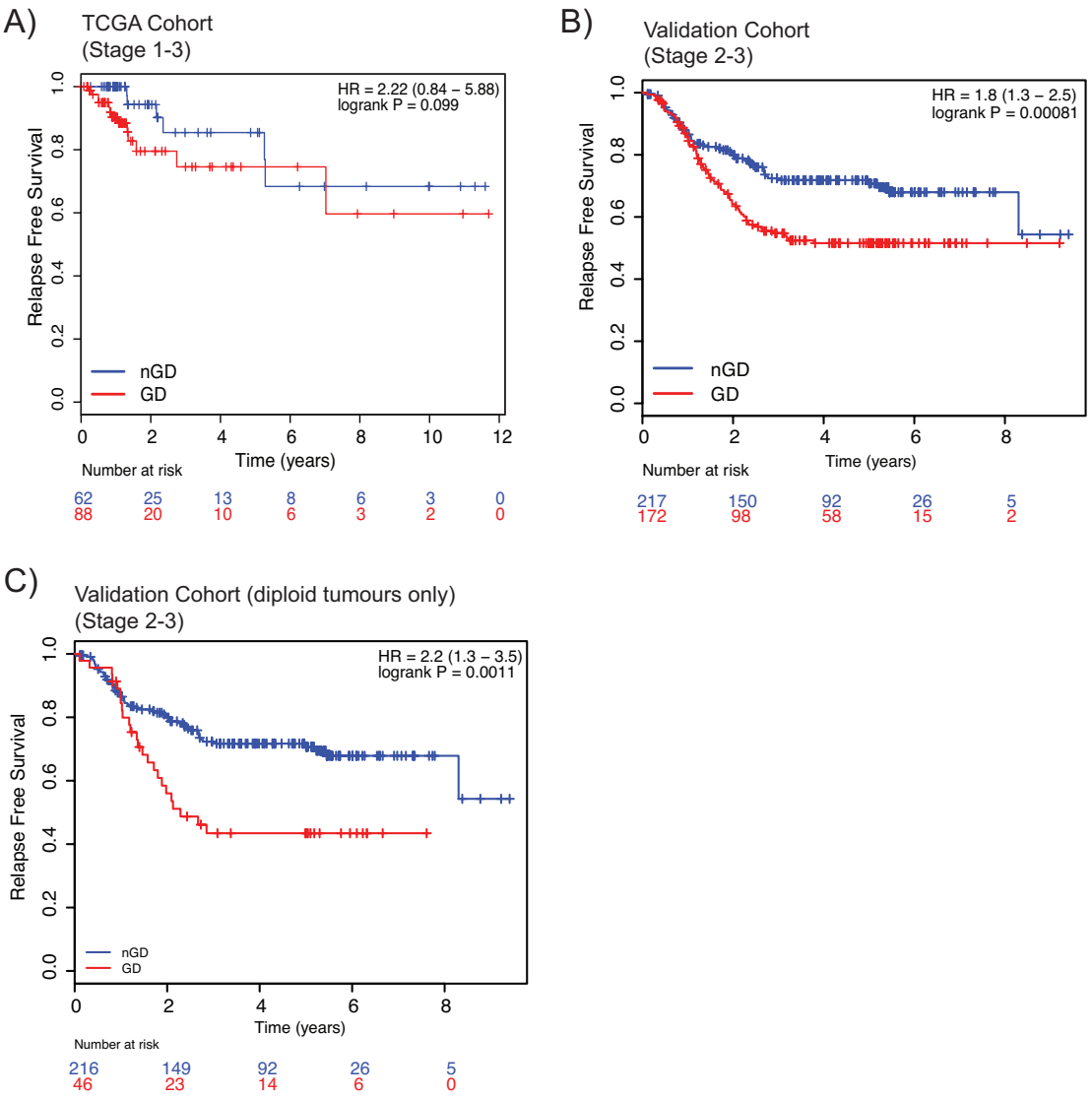

Figure 4.9: Full survival curves, and survival curves for only diploid tumours

A) Full Kaplan-Meier relapse free survival curves for CRC patients from TCGA cohort (n=150). Blue = non-genome doubled (nGD), red = genome doubled (GD). *P*=0.099 long-rank test.
B) Full Kaplan-Meier relapse free survival curves for CRC patients from the validation cohort (n=389). Blue = non-genome doubled (nGD), red = genome doubled (GD). *P*=0.00081, log-rank test.
C) Full Kaplan-Meier survival curves for diploid tumours from the validation cohort. Blue = non-genome doubled (nGD), red = genome doubled (GD). (n=262).

In addition, genome doubling remained a significant predictor of outcome when including ploidy (ploidy ≥ 3) in the multivariate analysis (Table 4.1). Indeed, when only considering diploid tumours from the validation cohort, genome doubling was still a strong predictor of outcome (*P*=0.0011, HR=2.2 95% CI 1.3-3.5, Figure 4.9C).

Table 4.1: Multivariate analysis of survival in TCGA and validation cohorts

A) Univariate and Multivariate analysis in TCGA cohort incorporating genome doubling and excluding wGII

	Relapse Free Survival, censor at 2 years, TCGA (Stage 1-3)			
	Univariate		Multivariate	
Variable	**HR (95%)**	**p.val (log-rank)**	**HR (95%)**	**p.val (Wald)**
GD	5.052 (1.118 -22.84)	0.0193	4.703e+00 (1.03533-21.366)	0.045
MSI	0.3173 (0.04124 - 2.441)	0.2443	2.938e-01 (0.03609-2.392)	0.252
Age	1.005 (0.9623-1.05)	0.813	9.998e-01 (0.95735-1.044)	0.993
Stage (highest vs. lowest)	97328732 (0- Inf)	0.3251	8.692e+07 (0.00000- Inf)	0.998

B) Univariate and Multivariate analysis in TCGA cohort incorporating wGII and excluding genome doubling

	Relapse Free Survival, censor at 2 years, TCGA (Stage 1-3)			
	Univariate		Multivariate	
Variable	**HR (95%)**	**p.val (log-rank)**	**HR (95%)**	**p.val (Wald)**
wGII	6.086 (0.570 -64.93)	0.135	3.72 (0.307 - 45.036)	0.302
MSI	0.3173 (0.04124 - 2.441)	0.2443	0.313 (0.0374-2.617)	0.284
Age	1.005 (0.9623-1.05)	0.813	0.997 (0.952-1.044)	0.897
Stage (highest vs. lowest)	97328732 (0- Inf)	0.3251	8.952e+07 (0.00000- Inf)	0.998

C) Univariate and Multivariate analysis in Validation cohort incorporating genome doubling and excluding wGII

	Relapse Free Survival, censor at 2 years, Validation (Stage 2-3)			
	Univariate		Multivariate	
Variable	**HR (95%)**	**p.val (log-rank)**	**HR (95%)**	**p.val (Wald)**
GD	1.85 (1.24- 2.76)	0.00221	1.594 1.052- 2.415)	0.0279
MSI	0.394 (0.1912- 0.8118)	0.00886	0.544 (0.255-1.158)	0.1141
Age	1.012 (0.9954-1.03)	0.153	1.019 (1.001-1.036)	0.0389
Stage (highest vs. lowest)	2.403 (1.484-3.89)	0.00023	2.238 (1.375-3.642)	0.00119

D) Univariate and Multivariate analysis in Validation cohort incorporating wGII and excluding genome doubling

	Relapse Free Survival, censor at 2 years, Validation (Stage 2-3)			
	Univariate		Multivariate	
Variable	**HR (95%)**	**p.val (log-rank)**	**HR (95%)**	**p.val (Wald)**
wGII	3.805 (1.44- 10.03)	0.00648	2.32 (0.795-7.013)	0.12182
MSI	0.394 (0.1912- 0.8118)	0.00886	0.566 (0.255-1.254)	0.16079
Age	1.012 (0.9954-1.03)	0.153	1.018 (1.000-1.036)	0.0466
Stage (highest vs. lowest)	2.403 (1.484-3.89)	0.00023	2.264 (1.391-3.684)	0.00101

E) Univariate and Multivariate analysis in Validation cohort incorporating ploidy and genome doubling

Relapse Free Survival, censor at 2 years, Validation (Stage 2-3)

	Univariate		Multivariate	
Variable	**HR (95%)**	**p.val (log-rank)**	**HR (95%)**	**p.val (Wald)**
GD	1.85 (1.24- 2.76)	0.00221	1.922 (1.104-3.347)	0.0209
Ploidy (>= 3)	1.39 (0.929 – 2.08)	0.11	0.765 (0.442-1.324)	0.338
MSI	0.394 (0.1912- 0.8118)	0.00886	0.539 (0.253-1.148)	0.109
Age	1.012 (0.9954-1.03)	0.153	1.019 (1.001-1.036)	0.0412
Stage (highest vs. lowest)	2.403 (1.484-3.89)	0.00023	2.238 (1.362-3.611)	0.00136

F) Univariate and Multivariate analysis in TCGA low stage cohort incorporating wGII and genome doubling

Overall Survival, censored at 5 years, TCGA (Stage 1-2)

	Univariate		Multivariate	
Variable	**HR (95%)**	**p.val (log-rank)**	**HR (95%)**	**p.val (Wald)**
GD	9.612 (1.165-79.32)	0.01088	10.76 (1.065175-108.649)	0.0441
MSI	1.239e-08 (0-Inf)	0.3436	2.264e-08 (0.0000-Inf)	0.9986
Age	1.043 (0.9751-1.116)	0.2158	1.034 (0.970241-1.101)	0.3051
Stage (highest vs. lowest)	1.512 (0.1836-12.45)	0.6989	2.911 (0.36- 23.42)	0.7722
wGII	9.354 (0.3339-262.1)	0.1798	1.376 (0.158539-11.943)	0.7755

Taken together these data indicate the genome doubling is a strong and independent indicator of patient outcome. Further, using genome doubling as a prognostic marker may be of greater clinical utility than using aneuploidy to predict high-risk tumours, at it appears to have more sensitivity than ploidy and wGII to predict patient outcome.

4.3 Conclusions

In this chapter the isogenic system of diploid and tetraploid clones described in Chapter 3 were tested for their ability to propagate chromosomal instability. Tetraploid clones were frequently shown to exhibit aneuploid colonies in clonal FISH assays, suggesting that they had an increased tolerance to aneuploidy. This was shown directly in live cell imaging analyses, where tetraploid cells were better able to continue cycling after a segregation error than their diploid counterparts. It would be interesting to assess whether tetraploid cells are also better able to tolerate induced segregation errors as well as endogenous missegregation events. Over time in culture this tolerance to chromosome missegregation has led to strikingly altered genome architecture in tetraploid clones. The genome duplication

event in HCT-116 cells has led to a cell line usually characterised as chromosomally stable to become chromosomally unstable based on wGII score. In patients with CRC, chromosomally unstable tumours (CIN+) have a worse prognosis than CIN- tumours (Walther et al., 2008, Mettu et al., 2010). It was therefore tested whether using an algorithm to identify tumours with genome duplication could be predictive of worse patient prognosis, as it had been observed that genome duplication in HCT-116 could lead to chromosomal instability. In two independent cohorts of CRC patients, genome doubling was found to be a strong predictor of worse relapse free survival. In these cohorts, genome doubling was a better prognostic marker than others that are used in this disease type such as MSI status, stage and age. Interestingly genome doubling also outperforms wGII as a predictive marker suggesting its prognostic value is greater than its tendency to associate with highly unstable tumours. Unfortunately, due to limitations in clinical data available from TCGA, it was not possible to compare genome doubling to other commonly used pathological markers, such as presentation with bowel obstruction, and immune cell infiltrate. It would be of interest to expand this analysis into a larger independent cohort, particularly of early stage patients, that had complete pathological annotation, to see whether genome doubling has predictive power over these pathology indicators.

The data presented in this chapter suggest that tetraploidy can be permissive for the development of chromosomal instability, a high-risk clinical phenotype. Data in the next chapter explores the functional consequences of tetraploidy in tumour relevant conditions, as well as seeking a mechanistic basis for the tolerance of chromosome segregation errors that seems coincident with genome doubling.

Chapter 5. Results 3: Functional consequences and mechanistic basis of CIN tolerance in tetraploid cells

5.1 Introduction

In Chapter 3 data were presented characterising an isogenic system of diploid and tetraploid clones derived from HCT-116. In Chapter 4 evidence was presented suggesting that tetraploid cells have an increased ability to tolerate and propagate chromosome missegregation events. Over the course of more than a year in continuous culture the tetraploid genome became increasingly genomically unstable. In this chapter, the functional consequences of the chromosomal instability evident in tetraploid clones were investigated, including the relationship between tetraploidy, chromosomal instability and drug resistance, and also the link between tetraploidy and metastatic potential. Finally, experiments that were designed to find a mechanism for the segregation error tolerance detailed in Chapter 4 are presented.

5.2 Results

5.2.1 Investigating drug resistance in tetraploid clones

Chromosomal instability has been linked with poor patient prognosis in many different cancer types (McGranahan et al., 2012). It has also been shown that CIN+ cell lines display increased resistance to a panel of kinase inhibitors (Lee et al., 2011). However the relationship between tetraploidy and drug resistance is seemingly more complex, with some studies reporting increased resistance to drugs, and others reporting increased sensitivity (see Section 1.7.3). Furthermore, in Chapter 4, genome doubling was shown to predict worse patient outcome in CRC, an association that has already been shown for ovarian cancer (Carter et al., 2012). Hence, finding a drug that could target tetraploid cells specifically could have significant clinical utility. To try to identify drugs that could specifically target tetraploid cells, all second-generation diploid and tetraploid clones were treated with an extensive panel of targeted kinase inhibitors at different passage numbers. A combination of Calbiochem Kinase Inhibitor Libraries I and II were used to treat diploid and tetraploid cell lines (a total of 160 inibitors).

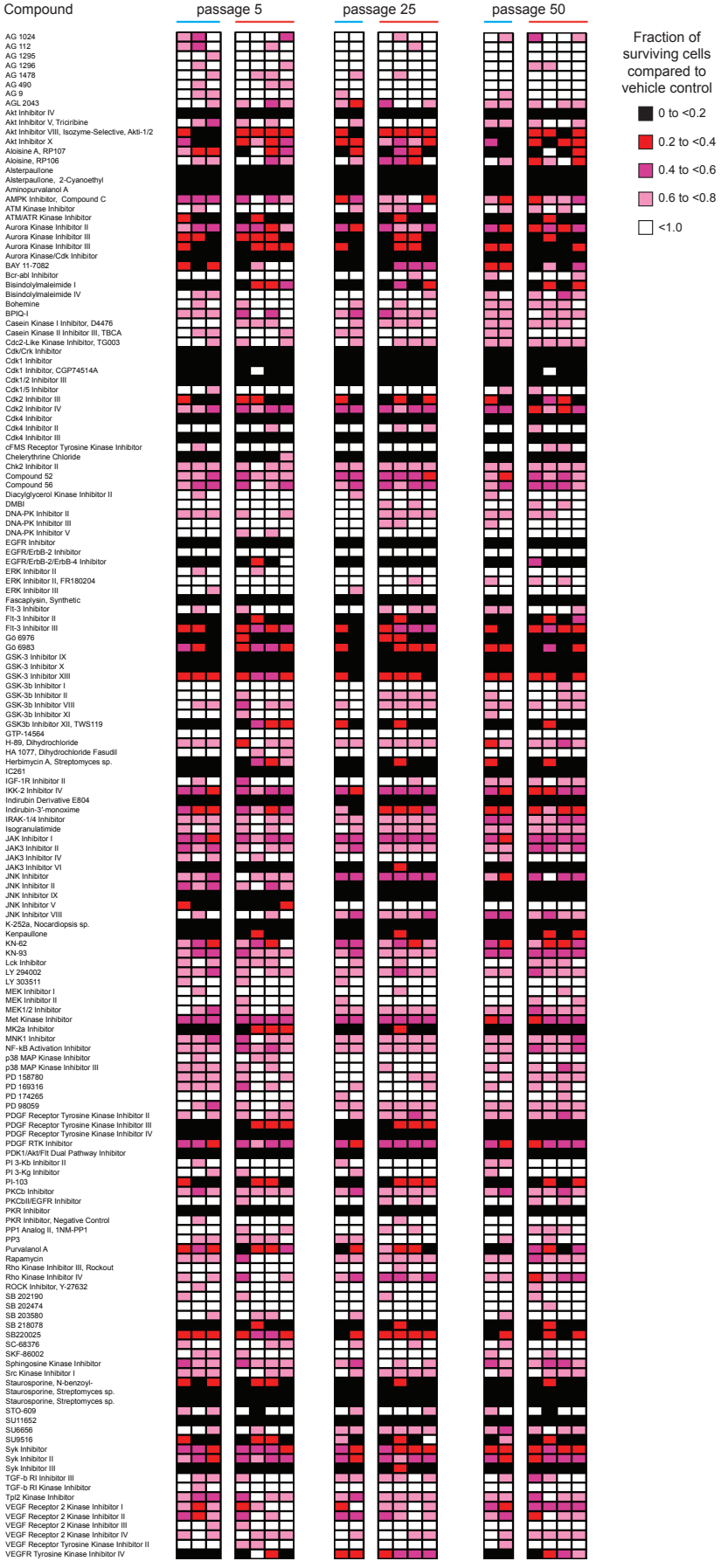
Compound
passage 5
passage 25
passage 50
AG 1024
AG 112
AG 1295
AG 1296
AG 1478
AG 490
AG 9
AGL 2043
Akt Inhibitor IV
Akt Inhibitor V, Triciribine
Akt Inhibitor VIII, Isozyme-Selective, Akti-1/2
Akt Inhibitor X
Aloisine A, RP107
Aloisine, RP106
Alsterpaullone
Alsterpaullone, 2-Cyanoethyl
Aminopurvalanol A
AMPK Inhibitor, Compound C
ATM Kinase Inhibitor
ATM/ATR Kinase Inhibitor
Aurora Kinase Inhibitor II
Aurora Kinase Inhibitor III
Aurora Kinase Inhibitor III
Aurora Kinase/Cdk Inhibitor
BAY 11-7082
Bcr-abl Inhibitor
Bisindolylmaleimide I
Bisindolylmaleimide IV
Bohemine
BPIQ-I
Casein Kinase I Inhibitor, D4476
Casein Kinase II Inhibitor III, TBCA
Cdc2-Like Kinase Inhibitor, TG003
Cdk/Crk Inhibitor
Cdk1 Inhibitor
Cdk1 Inhibitor, CGP74514A
Cdk1/2 Inhibitor III
Cdk1/5 Inhibitor
Cdk2 Inhibitor III
Cdk2 Inhibitor IV
Cdk4 Inhibitor
Cdk4 Inhibitor II
Cdk4 Inhibitor III
cFMS Receptor Tyrosine Kinase Inhibitor
Chelerythrine Chloride
Chk2 Inhibitor II
Compound 52
Compound 56
Diacylglycerol Kinase Inhibitor II
DMBI
DNA-PK Inhibitor II
DNA-PK Inhibitor III
DNA-PK Inhibitor V
EGFR Inhibitor
EGFR/ErbB-2 Inhibitor
EGFR/ErbB-2/ErbB-4 Inhibitor
ERK Inhibitor II
ERK Inhibitor II, FR180204
ERK Inhibitor III
Fascaplysin, Synthetic
Flt-3 Inhibitor
Flt-3 Inhibitor II
Flt-3 Inhibitor III
Go 6976
Go 6983
GSK-3 Inhibitor IX
GSK-3 Inhibitor X
GSK-3 Inhibitor XIII
GSK-3b Inhibitor I
GSK-3b Inhibitor II
GSK-3b Inhibitor VIII
GSK-3b Inhibitor XI
GSK3b Inhibitor XII, TWS119
GTP-14564
H-89, Dihydrochloride
HA 1077, Dihydrochloride Fasudil
Herbimycin A, Streptomyces sp.
IC261
IGF-1R Inhibitor II
IKK-2 Inhibitor IV
Indirubin Derivative E804
Indirubin-3'-monoxime
IRAK-1/4 Inhibitor
Isogranulatimide
JAK Inhibitor I
JAK3 Inhibitor II
JAK3 Inhibitor IV
JAK3 Inhibitor VI
JNK Inhibitor
JNK Inhibitor II
JNK Inhibitor IX
JNK Inhibitor V
JNK Inhibitor VIII
K-252a, Nocardiopsis sp.
Kenpaullone
KN-62
KN-93
Lck Inhibitor
LY 294002
LY 303511
MEK Inhibitor I
MEK Inhibitor II
MEK1/2 Inhibitor
Met Kinase Inhibitor
MK2a Inhibitor
MNK1 Inhibitor
NF-kB Activation Inhibitor
p38 MAP Kinase Inhibitor
p38 MAP Kinase Inhibitor III
PD 158780
PD 169316
PD 174265
PD 98059
PDGF Receptor Tyrosine Kinase Inhibitor II
PDGF Receptor Tyrosine Kinase Inhibitor III
PDGF Receptor Tyrosine Kinase Inhibitor IV
PDGF RTK Inhibitor
PDK1/Akt/Flt Dual Pathway Inhibitor
PI 3-Kb Inhibitor II
PI 3-Kg Inhibitor
PI-103
PKCb Inhibitor
PKCbII/EGFR Inhibitor
PKR Inhibitor
PKR Inhibitor, Negative Control
PP1 Analog II, 1NM-PP1
PP3
Purvalanol A
Rapamycin
Rho Kinase Inhibitor III, Rockout
Rho Kinase Inhibitor IV
ROCK Inhibitor, Y-27632
SB 202190
SB 202474
SB 203580
SB 218078
SB220025
SC-68376
SKF-86002
Sphingosine Kinase Inhibitor
Src Kinase Inhibitor I
Staurosporine, N-benzoyl-
Staurosporine, Streptomyces sp.
Staurosporine, Streptomyces sp.
STO-609
SU11652
SU6656
SU9516
Syk Inhibitor
Syk Inhibitor II
Syk Inhibitor III
TGF-b RI Inhibitor III
TGF-b RI Kinase Inhibitor
Tpl2 Kinase Inhibitor
VEGF Receptor 2 Kinase Inhibitor I
VEGF Receptor 2 Kinase Inhibitor II
VEGF Receptor 2 Kinase Inhibitor III
VEGF Receptor 2 Kinase Inhibitor IV
VEGF Receptor Tyrosine Kinase Inhibitor II
VEGFR Tyrosine Kinase Inhibitor IV
Fraction of surviving cells compared to vehicle control
0 to <0.2
0.2 to <0.4
0.4 to <0.6
0.6 to <0.8
<1.0

Figure 5.1: Extensive kinase inhibitor screen in diploid and tetraploid clones

Results of drug screen using Calbiochem Kinase Inhibitor Libraries I and II in diploid and tetraploid clones at the indicated passage numbers. The legend shows the different colours that represent different fractions of surviving cells (measured using CellTiter-Blue) in drug treated wells compared to DMSO treated control wells. Different cell lines are shown as columns. Blue line over column indicates a diploid cell line (ordered as follows: HCT-116 [passage 5 only], DC-14 and DC-25), and red line indicates a tetraploid cell line (ordered as follows: TC-13, TC-16, TC-17 and TC-35).

The parental cell line HCT-116 has previously been treated with this library at a 10μM concentration (Lee et al., 2011), and therefore the same concentration of drug was used to treat the diploid and tetraploid clones derived from HCT-116. Cells were seeded and then treated 24 hours later with the drug panel. After 72 hours of drug treatment the cells were assayed with CellTiter-Blue to assess cell viability. The results of this drug screen are shown in Figure 5.1. The plot shows the fraction of surviving cells left in each well, relative to wells treated with the vehicle control dimethyl sulfoxide (DMSO). The key displays different colours representing these different fractions, with darker colours indicating higher toxicity of a drug (black representing a 0 - 0.2 fraction of surviving cells compared to control). The three distinct blocks indicate different passage numbers. Second-generation clones at passage 5, 25 and 50 were tested. From the broad similarity of the plots, it appears that the response to these different drugs is fairly uniform between diploids and tetraploids.

In order to compare the relative resistance of diploid and tetraploid clones across the whole panel of kinase inhibitors, cumulative distribution frequency graphs were prepared. These graphs, presented in Figure 5.2, were prepared with bioinformatics and statistical help from Dr Pierre Martinez.

These comparisons show that there is a small but significant increase *(P*=0.032) in resistance in tetraploid cell lines at passage 5 (Figure 5.2A). However, there is no significant difference in relative resistance between diploids and tetraploids at either passage 25 (*P*=0.3) or passage 50 (*P*=0.11) (Figure 5.2B and C). In Chapter 3, the proliferation rates of diploid and tetraploid clones were assessed (Figure 3.16). These data indicate that early passage tetraploid clones grow marginally

slower than diploid clones. It has been previously shown that there is a correlation between slower growth rate and increased drug resistance for CIN+ cell lines (Lee et al., 2011), which could explain why only the early passage tetraploid cell lines display a slight increase in relative resistance.

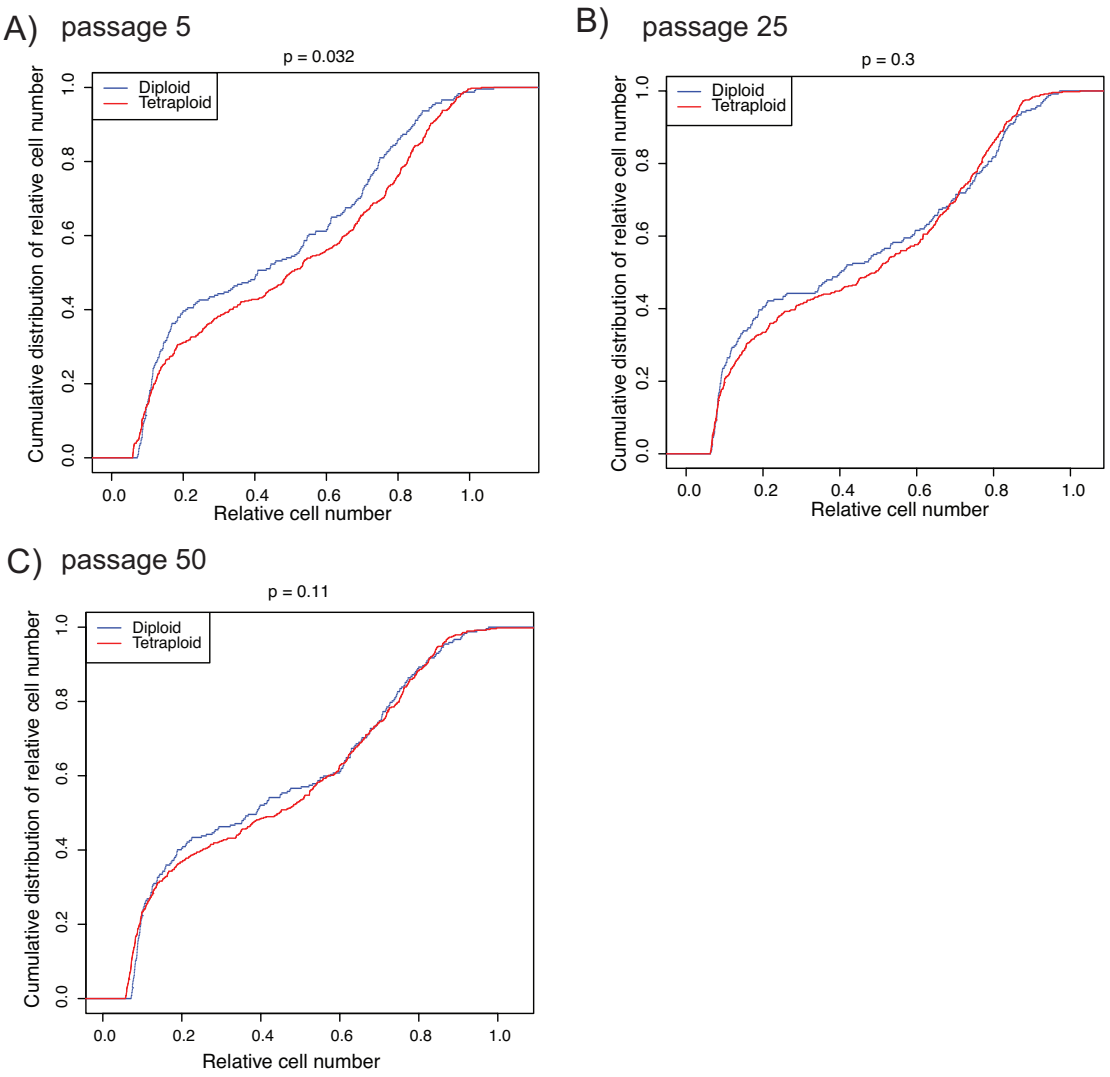

Figure 5.2: Only early passage tetraploid clones show a slight increase in drug resistance

A) Cumulative distribution of relative resistance to 160 kinase inhibitors between diploid (blue lines) and tetraploid (red lines) cell lines at passage 5.
B) As above, for passage 25 clones.
C) As above, for passage 50 clones.

To search for drugs displaying a differential effect between diploids and tetraploids, the average fold change between surviving cell fraction between diploids and

tetraploids was calculated. Drugs that had a significant (P<0.05) fold change difference between diploid and tetraploid clones are shown in Table 5.1.

Table 5.1: Drugs with differential effects on diploid and tetraploid clones

Compound	log FC
Cdk4 Inhibitor II, NSC 625987	0.175279366
SU9516	-0.053476514
TGF-b RI Inhibitor III	-0.057149269
GSK3b Inhibitor XII, TWS119	-0.084596466
MK2a Inhibitor	-0.086524098
Aurora Kinase Inhibitor III	-0.089075077
Gö 6976	-0.089515638
Met Kinase Inhibitor	-0.093726118
SB220025	-0.098634217
Gö 6983	-0.101923337
Src Kinase Inhibitor I	-0.108409306
JNK Inhibitor V	-0.110767403
PD 169316	-0.120949154
VEGF Receptor 2 Kinase Inhibitor III	-0.132491271
IGF-1R Inhibitor II	-0.142376615
Syk Inhibitor II	-0.178415499
AMPK Inhibitor, Compound C	-0.201234992
Indirubin-3′-monoxime	-0.213204362
Sphingosine Kinase Inhibitor	-0.241125979
VEGFR Tyrosine Kinase Inhibitor IV	-0.299888443

The only drug exerting a negative effect specifically in tetraploid clones was the compound Cdk4 Inhibitor II. The average surviving fraction for this drug was 0.93 in diploid clones and 0.85 in tetraploid clones, so although significant, this drug does not have a potent selective effect on tetraploid clones. The other significant drugs from this analysis were all more effective at targeting diploid compared to tetraploid cells.

Taken together these data indicate that in a system of isogenic cell lines, ploidy does not exert a large effect on resistance to kinase inhibitors. Relative resistance was increased slightly only in tetraploid clones at early passage numbers which could be explained by a decrease in growth rate. Furthermore, even at late passages, when tetraploid clones display high levels of chromosomal instability (see Chapter 4), they are not more resistant than their diploid counterparts. This

could in part be due to the fact that a targeted kinase library was used, to which resistance or sensitivity is likely to be mainly due to defects in cell signalling pathways that are likely to be similar to the parental cell line used to derive the clones.

To address this concern, drugs with more general mechanisms of action were used. The drug sensitivity of a select panel of diploid and tetraploid clones was assessed in response to three therapeutic agents used to target CRC: camptothecin, paclitaxel and cisplatin. Camptothecin is a quinolone alkaloid that inhibits Topoisomerase I, resulting in DNA complexes that cause replication fork collapse in S phase. Paclitaxel stabilises microtubules, thereby disrupting cell cycle progression. Cisplatin binds to DNA bases, resulting in DNA crosslinks, and subsequent DNA damage. It has previously been reported that tetraploid clones have increased resistance to camptothecin, amongst other DNA damaging agents (Castedo et al., 2006).

A difference in sensitivity to camptothecin was not observed between the two diploid and two tetraploid cell lines analysed (Figure 5.3A). There was also no difference in sensitivity between diploid and tetraploids treated with paclitaxel or cisplatin (Figure 5.3B, C and D).

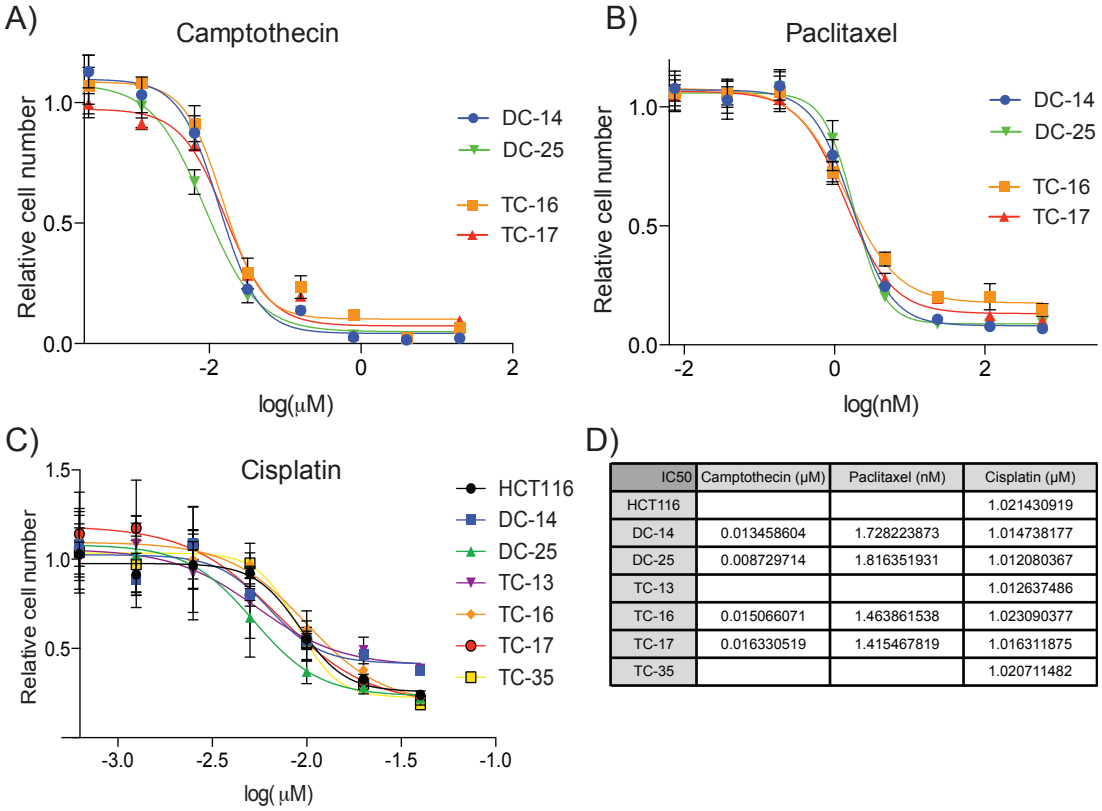

IC50	Camptothecin (μM)	Paclitaxel (nM)	Cisplatin (μM)
HCT116			1.021430919
DC-14	0.013458604	1.728223873	1.014738177
DC-25	0.008729714	1.816351931	1.012080367
TC-13			1.012637486
TC-16	0.015066071	1.463861538	1.023090377
TC-17	0.016330519	1.415467819	1.016311875
TC-35			1.020711482

Figure 5.3: Comparing the response of diploid and tetraploid clones to chemotherapeutic agents

A-B) Two diploid cell lines (DC-14 and DC-25) and two tetraploid cell lines (TC-16 and TC-17) were treated with increasing concentrations of either camptothecin (A) or paclitaxel (B). The relative cell number compared to DMSO treated controls is shown.
C) Dose response curve to increasing concentrations of cisplatin for all second-generation clones.
D) IC50 values for each cell line treated with the indicated drug, calculated using GraphPad prism software. All cell lines used were at passage 10.

This system of tetraploid clones was not found to exhibit the same resistance to camptothecin that has been previously reported (Castedo et al., 2006). Although only four clones were used to test the sensitivity against camptothecin, all second-generation clones were used to investigate the sensitivity to cisplatin. Cisplatin has a similar mechanism of action to oxaliplatin, another Platinum based DNA cross-linking agent reported to have increased efficacy against tetraploid cell lines (Castedo et al., 2006). No differential effect of cisplatin on diploid and tetraploid clones was observed (Figure 5.3C). In the previous report by Castedo and colleagues, tetraploid cell lines derived from HCT-116 were shown to have a 5.2

fold increase in IC50 compared to diploid cell lines when treated with oxaliplatin (Castedo et al., 2006). The average IC50 of diploids to cisplatin was 1.016μM, and the average IC50 of tetraploids was 1.018μM (Figure 5.3D). Possible explanations for these differing results are discussed in the conclusion to this chapter.

Taken together, these data indicate that in this isogenic system of diploid and tetraploid clones, there was no systematic increase or decrease in drug resistance based on ploidy status. Further, no increase in drug resistance was observed in later passages of tetraploid clones, despite higher levels of chromosomal instability. This could possibly suggest that in this cell line system, the nature of chromosomal instability is not the same as the chromosomal instability observed in CIN+ cell lines, which did show increased resistance to the same targeted panel of kinase inhibitors (Lee et al., 2011). This system may not recapitulate these findings due to the fact that HCT-116 derived tetraploid clones are not only chromosomally unstable, but also exhibit microsatellite instability. These two types of genetic instability do not commonly overlap in the clinical setting (see Section 1.11). It could be the case that having two different drivers of genetic diversity is not beneficial to cancer cells in the presence of environmental stress, such as that experienced under drug selection.

5.2.2 Growth of diploid and tetraploid cell lines in 3D environments

As discussed in Section 1.3, tetraploidy can occur as both an early or late event in tumourigenesis. In the HCT-116 cell line, it has been shown that the tetraploid fraction is continually generated (see Figure 3.3). However, this fraction remains at a constantly low percentage of the total population (as over many passages HCT-116 remains a predominantly diploid cell line), likely due to a selection pressure against tetraploid cells. This could be accounted for by their poor cloning efficiency (see Figure 3.3), or possibly by the slight reduction in growth rate in tetraploid cells (Figure 3.16). However, as genome doubling appears to be a common event in CRC (Figure 3.1), it is of interest to ascertain which culture conditions favour the expansion of a tetraploid population.

In order to try to better mimic the tumour environment diploid and tetraploid clones were grown in three-dimensional spheroid culture, which may better represent the environment of tissues compared to two-dimensional culture techniques (Pampaloni et al., 2007, Fennema et al., 2013). It has been shown previously using Chinese hamster V-79-171 cells, which spontaneously form spheroids in culture, that the fraction of tetraploid cells increases as the spheroids get larger (Olive et al., 1982). HCT-116 cells have also previously been grown in spheroid culture (McIntyre et al., 2012).

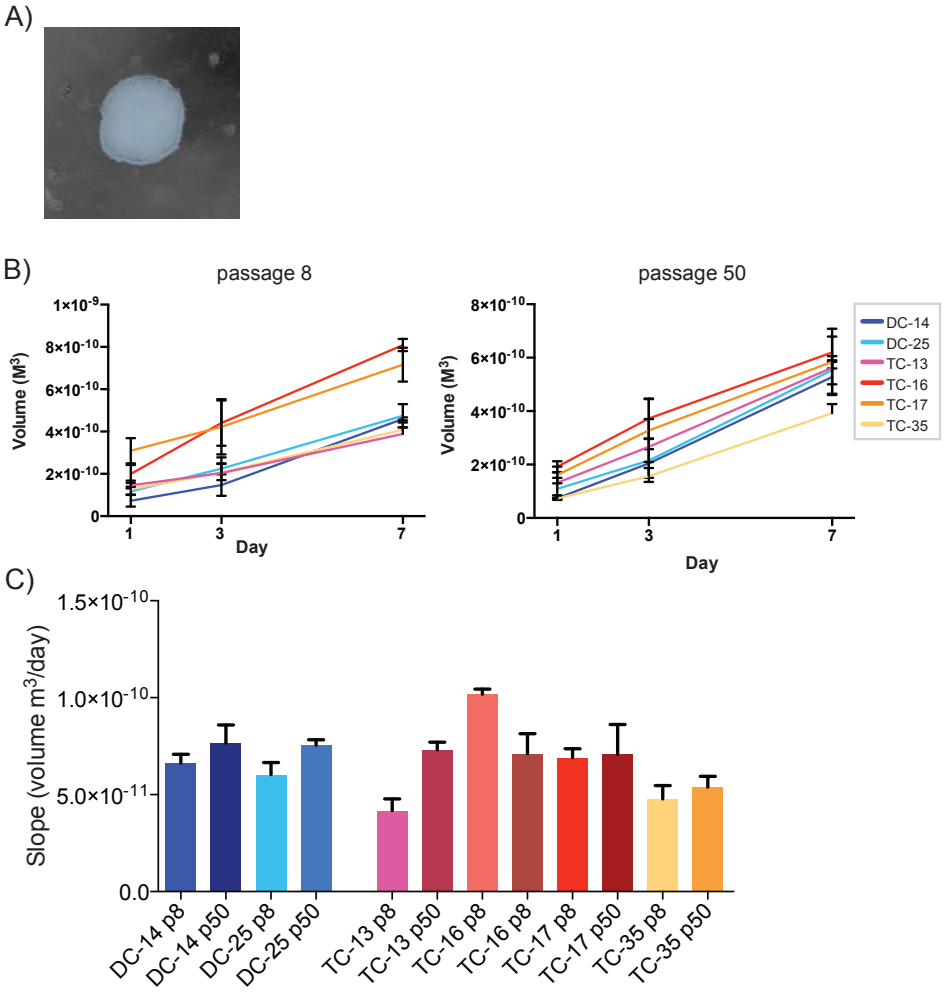

Figure 5.4: Growth of diploid and tetraploid clones in spheroid culture

A) Example of microscope image used to calculate volume of spheroids. Blue colouring indicates area that is used to calculate volume (see Methods).
B) Growth curves of diploid and tetraploid spheroids imaged on Days 1, 3 and 7. Data is from three independent experiments.
C) Slope of graphs shown in B) was calculated in order to compare between cell lines.

Spheroids were formed by seeding cells in ultra low attachment round-bottomed plates with 2.5% Matrigel and spinning the plates to condense the cells into a sphere at the bottom of the well (see Methods). In order to assess differences in growth between the diploid and tetraploid clones in spheroids, the growth rate of spheroids was determined. The spheroids were scanned using a phase-contrast microscope, and the total volume was calculated (Figure 5.4A, and see Methods). The growth curves for passage 8 and passage 50 are shown in Figure 5.4B. In order to compare between the growth curves, the slope of each line was calculated. Data shown is from three independent experiments, and the error bars indicate that the growth rate was fairly consistent in each cell line across different experiments (Figure 5.4C).

There is no difference in the growth rate of spheroids derived from diploid or tetraploid clones at passage 8 (diploid average slope 6.3e-11, tetraploid average 6.8e-11, *P*=0.8151, Student's T-test, Figure 5.4C). There is also no difference in spheroid growth rate at passage 50 (diploid average slope 7.0e-11, tetraploid average slope 6.7e-11, *P*=0.7351, Student's T-test, Figure 5.4C). Some cell lines exhibited growth in spheroids that appeared consistently faster than other cell lines (for example TC-16 passage 8, slope = 1.03e-10), whilst others showed consistently slower growth across all three experiments (for example TC-13 passage 8, slope = 4.2e-11). These clone specific differences indicate that enhanced growth in spheroid culture is unlikely to be a phenotype that is intrinsically linked to the genotypes of either tetraploidy or chromosomal instability. There are many factors that could influence a cell lines ability to grow specifically in three-dimensional culture, such as signalling from cell-to-cell attachment. Although investigating the molecular mechanisms determining variations in spheroid growth could help gain new insights into tumour growth, it was unfortunately beyond the scope of this investigation.

5.2.3 Investigating the role of tetraploidy in metastasis

Several studies using artificially generated tetraploid cells (through a variety of different mechanisms), have demonstrated that tetraploid cells have increased

tumorigenic capacity compared to diploid cells (see Section 1.7.1). As well as a link between tetraploidy and carcinogenic onset that has been described for example in Barrett's Oesophagus (Galipeau et al., 1996), tetraploidy can also occur later in tumourigenesis. Intriguingly recent work from this laboratory showed that the region of a primary renal cell carcinoma most likely to have seeded the metastasis was tetraploid (Gerlinger et al., 2012). It was therefore investigated using the system of diploid and tetraploid clones derived from HCT-116 whether tetraploid clones had an enhanced metastatic potential. It is well known that HCT-116 cells form tumours when injected into the tail-vein of nude mice (Langlois et al., 2010, Long et al., 2013, Lu et al., 2013, Wu et al., 2012b, Fan et al., 2011), with the most common metastatic location being the lungs. Therefore this system was used to investigate whether tetraploid clones had increased metastatic potential in comparison to their diploid counterparts.

By using bioluminescence imaging it is possible to effectively monitor and compare tumour growth in vivo. Given that HCT-116 cells are known to be tumorigenic in a metastatic tail-vein assay, it was reasoned that the best way to assess differences in growth between different clones was by using bioluminescence, since both diploid and tetraploid cells are likely to have tumour-forming capacity. One diploid clone (DC-14) and one tetraploid clone (TC-13) were infected using retroviruses expressing the Firefly (*Photinus pyralis*) luciferase gene. The pBabe-Hygromycin-Luciferase-Poly-A plasmid was used with the kind permission of Dr Miguel M. Murillo (manuscript in preparation). The two cell lines were infected at passage seven. After selection and in vitro testing the cells had been passaged a further four times, and were therefore at passage 11 when injected into mice.

The in vitro luciferase activity was confirmed by plating cells in a 96-well plate and treating with the substrate of luciferase, luciferin. The activity of luciferase was assessed by calculating photons emitted per second per cell, based on a range of cell seeding densities (Figure 5.5A). The bioluminescence activity was similar between DC-14 and TC-13. The data presented are from two independent experiments. In the first experiment, two different cell doses of 0.5×10^6 and 1.5×10^6 were chosen, as the majority of studies using HCT-116 in tail-vein injections have used 1×10^6 cells (Langlois et al., 2010, Long et al., 2013, Lu et al., 2013, Wu

et al., 2012b, Fan et al., 2011). However when DC-14 and TC-13 were injected at a dose of 1.5 x 10^6 cells, only one out of three mice developed tumours and only one mouse injected with 0.5 x 10^6 TC-13 cells developed a tumour (Figure 5.5B). The cell dose was increased in the second experiment to 3 x 10^6 and 6 x 10^6 cells per mouse. At 3 x 10^6 cells, 3 out of 4 (DC-14) and 2 out of 4 (TC-13) mice developed tumours. At the higher cell dose, all mice injected developed tumours, predominantly at either the tail base, or in the lungs (Figure 5.5C).

A)

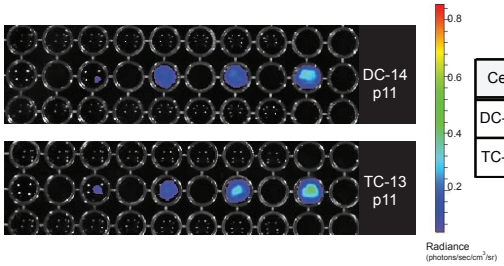

Cell Line	Photons/sec/cell
DC-14 p11	1230.076
TC-13 p11	1398.74

B)

	DOSE	DC-14 p11	TC-13 p11
EXPT 1	**5.00E+05**	0/3	1/3
	1.50E+06	1/3	1/3
EXPT 2	**3.00E+06**	3/4	2/4
	6.00E+06	4/4	3/3

C)

	DOSE	DC-14 p11				TC-13 p11			
EXPT 1	**5.00E+05**					lungs			
	1.50E+06	tail base				tail base			
EXPT 2	**3.00E+06**	tail base	lungs & tail base	tail base		lung	tail base		
	6.00E+06	lungs	tail base	LN/back	tail base	tail base	tail base	tail base	

D)

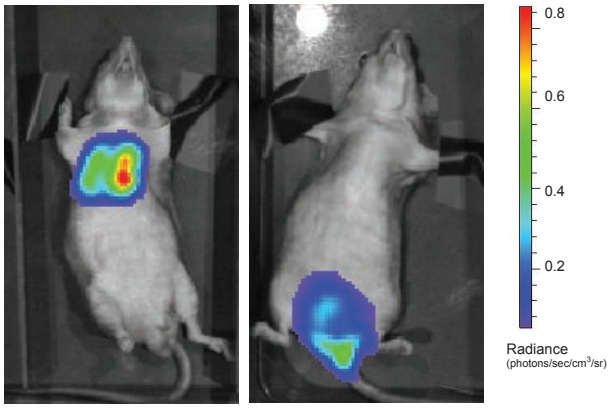

E)

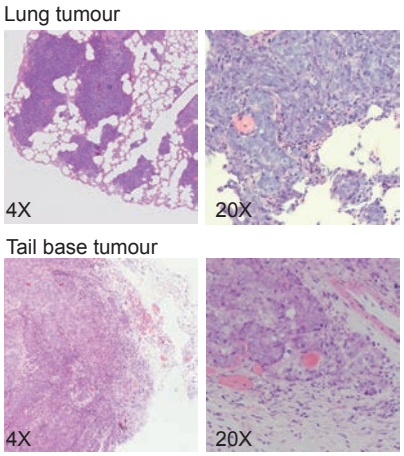

Figure 5.5: Tail-vein injection of DC-14 and TC-13 into nude mice

A) Representative image of in vitro analysis of DC-14 p11 and TC-13 p11 expressing luciferase. Photons per second per cell for each cell line was calculated from a range of cell numbers.
B) Tumour forming capacity of each cell line is shown as number of mice with detectable tumours/number of mice injected for two experiments (EXPT1 and 2) using four different cell doses.

C) Tumour location for each mouse that developed a tumour in two different experiments with DC-14 p11 and TC-13 p11 at two different cell doses. LN = lymph node. In the first experiment 3 mice per cell dose were injected, and in the second four mice per cell dose were injected, apart from TC-13 p11 (6×10^6 cells) where one mouse died as a result of the injection.
D) Example images of nude mice injected with luciferase expressing cell lines that formed either a lung tumour (left image) or a tumour at the base of the tail (right image).
E) Example H&E staining of the lungs and tail base tumours that developed in nude mice after tail-vein injection of these two cell lines. Both 4X and 20X images are shown.

From this data there does not seem to be a difference in the ability of either DC-14 or TC-13 to form tumours, with both cell lines producing less tumours than has been reported for the parental cell line HCT-116. This could in part be due to the fact that both DC-14 and TC-13 are derived from single cell clones from a heterogeneous HCT-116 parental population, and therefore the heterogeneity and frequency of tumour-forming cells is likely to be reduced compared to the parental cell line. Further, DC-14 and TC-13 are second-generation clones, and were derived themselves from a clone of HCT-116, DC 8. This diploid clone might also have a lower tumour forming capacity than the parental cell line.

The different locations of tumours arising in the two experiments are shown in Figure 5.5C. Many animals developed large tumours close to the tail base. Examples of bioluminescent signals arising from these tail base tumours, and also from lung tumours are shown in Figure 5.5D. In the first experiment tumour material was collected and fixed with 10% neutral buffered formalin (NBF) and subjected to haematoxylin and eosin (H&E) staining for pathological review.

All pathology reviews were carried out by Professor Gordon Stamp.

The tail base tumour shown in Figure 5.5D was described as fatty connective tissue containing a large mass of undifferentiated epithelial tumour, with intravascular tumour present at the peripheries. To ascertain the origin of these tail base tumours, one mouse was subjected to a whole body autopsy. The tail base tumour in this mouse was described as having multiple separate areas composed of differing morphologies, including an area of undifferentiated spindle cells, and another with a more epithelioid appearance. There was invasion into both soft

tissue and skeletal muscle, but the tumour did not appear to involve bone, although it extended close to the periosteum. The tumour displayed substantial intravascularisation. This morphology is consistent with the tumour having formed directly from injected cells that have become trapped in the pelvic venous system, and subsequently invaded the surrounding tissue. This mouse also had lung tumours displaying intravascular undifferentiated morphology and early invasion into the lung parenchyma. It could not be determined whether the tail base tumour had given rise to the lung tumours. Future experiments could utilise bioluminescent imaging immediately after cell injection to determine whether injected cells trafficked directly from the tail-vein to the lung, or whether they were all trapped in the venous system. Similar techniques have been used before with B-16 melanoma cell lines (Craft et al., 2005).

To measure the growth rate of all tumours arising in both experiments, mice were subjected to bioluminescent imaging once a week. Mice were anaesthetised using Isoflurane and injected intraperitoneally with 100µl of Luciferin substrate at 300µg/mL. Images were taken at regular intervals until a plateau of luminescent signal was reached (see Methods). The maximal bioluminescence signal for the whole body of each mouse was recorded. Only mice that developed tumours are shown in Figure 5.6. Figure 5.6A shows the three mice from experiment one that developed tumours. Both mice that developed tumours at the higher dose (1.5×10^6) had rapidly growing tumours and therefore had to be sacrificed in accordance with Home Office regulations (see Methods). The only mouse to develop a tumour at the lower dose (TC-13, 0.5×10^6 cells) showed slower tumour growth. In the second experiment the difference between the two doses (3×10^6 and 6×10^6 cells) is even more apparent, with the majority of mice injected with the higher dose sacrificed before 60 days, but the mice injected with the lower dose tending to have a reduced tumour growth rate. A notable exception was one mouse injected with TC-13 at the lower dose, which had to be sacrificed at Day 34 (Figure 5.6B).

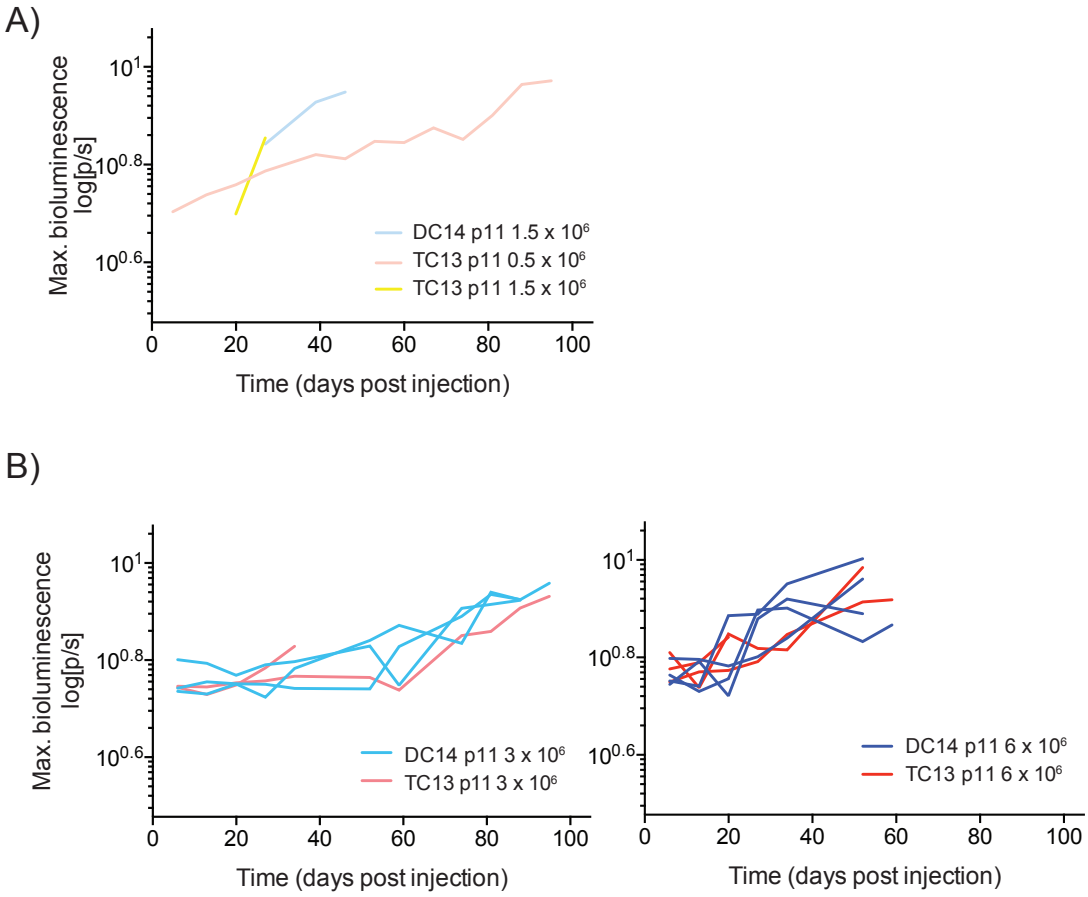

Figure 5.6: Growth rates of tumours derived from DC-14 and TC-13

A) Bioluminescent maximal signals (log transformed) from mice injected with 0.5x 10^6 or 1.5 x 10^6 cells of DC-14 and TC-13.
B) Bioluminescent maximal signals (log transformed) from mice injected with either 3 x 10^6 or 6 x 10^6 cells of DC-14 and TC-13.

Analysis of tumour growth rates was carried out with statistical help from Stuart Horswell.

The growth rate between tumours arising from diploid and tetraploid cells in the second experiment was compared using a multiple regression model. Using ANOVA to compare growth rates between DC-14 and TC-13 derived tumours is significant (*P*=0.028928), with an estimated increase in bioluminescence of 0.59712 log units for TC-13 derived tumours. However, the standard error of this prediction (1.27548 log bioluminescence units) results in a confidence interval that crosses 0 (95% interval -1.94 to +3.1385). These data therefore do not provide strong statistical evidence that tumours derived from TC-13 have higher

luminescence, although increasing the numbers of tumours analysed could potentially resolve this issue.

These data indicate that there is not a great statistical difference in the growth rate between DC-14 and TC-13 cells when they form metastatic tumours in nude mice. Given this result, the analysis was not extended into a larger panel of diploid and tetraploid cell lines. There are no reports in the literature regarding HCT-116 cells making similar tumours to those that were observed forming at the tail-base of the mice. This is most likely because most reports seem to use a lower cell dose (Langlois et al., 2010, Long et al., 2013, Lu et al., 2013, Wu et al., 2012b, Fan et al., 2011). As discussed, the lower tumour forming capability could be due to the fact that the diploid and tetraploid cell lines used are derived from single cell clones. The higher cell dose used, coupled with the fact that the cells are epithelial in origin and quite large, is likely to have caused the trapping in the venous system of the pelvis. Although the cells still had to invade from this area to form tumours, it is not as stringent as a metastatic assay using fewer cells, as the cells are being kept in one location by physical blockage that may allow the invasion of more than one cell. This may not be analogous to what occurs during the metastatic process in humans, where although clumps of cells have been found circulating together in the blood stream (Cho et al., 2012), their contribution to metastasis is not yet well defined. Lower cell numbers were used in an experiment using NSG (NOD-scid-gamma) mice (data not shown), but these mice have an extremely diminished immune capacity, so although tumours were formed more frequently, this system also does not model the metastatic process in humans very well. In summary, using nude mice and the high numbers of cells that had to be injected in order to achieve high penetrance of metastatic tumours is unlikely to represent a good method for comparing metastatic potential between these cell lines. Given this, no other diploid and tetraploid cell lines were tested in this way.

5.2.4 Ploidy differences between primary and metastatic tumours

Due to the difficulties and caveats of using tail-vein injections to model and compare metastatic potential between diploid and tetraploid cell lines, an analysis of material from patient tumours was carried out. A cohort of 64 matched colorectal

cancer samples (52 microsatellite stable, MSS, and 12 MSI+) and their liver metastases was provided by Dr Marcell Szasz (Department of Pathology, Semmelweis University, Hungary). The clinical features of this cohort are detailed in Table 5.2.

Table 5.2: Clinical characteristics of CRC patient cohort

Where available, clinical data is presented for patients in this cohort. Information for grade and TNM (Tumour, Node, Metastasis) staging, as well as MSI status (as defined by IHC staining) is shown. * Indicates samples where no data from IHC was provided, so MSI status was checked using PCR fragment analysis (see Methods). ** Indicates samples where there was a discrepancy in MSI status between the primary and the metastatic sample, and so MSI status was checked using PCR fragment analysis.

ID	Gender	Age	Grade:	T:	N:	M:	MSI status (IHC)
431	male	75	II	3	0	x	MSI+
3271	male	52	II	4	1	1	MSI+
7225	male	49	II	4	1	x	MSI+
10197	female	66	II	4	1	x	MSI+
12105	female	46	II	3	0	x	MSI+
12379	female	70	II	3	1	x	MSI+
15703	male	66	II	2a	0		MSI+
617	male	58		3	0	x	MSI+
3986	male	78	I	3	0	1	MSI+
4823	male	78	II	3	0	1a	MSI+
13598	male	57	III	3	1	1	MSI+
15764	female	53	II	1	0	x	MSI+ *
53	female	69					MSS
217	male	40	II	3	1	1	MSS
759	male	75	III				MSS
2736	male	66	III	3	2a	1	MSS
2950	male	67	II	3	0		MSS
3038	male	48	II	4	2	x	MSS
3217	female	60	II	3	1	1	MSS
3710	female	45	I	3	1	x	MSS
4182	male	64	II	3	1	1	MSS
4937	male	70	III	3	2		MSS
5262	female	53	II	3	2b	x	MSS
5690	male	41	II	3	2	x	MSS
5887	female	72	II	4	2	x	MSS
6648	male	68	II	3	2	x	MSS
7430	male	63	II	3	1	x	MSS
7605	male	62	II	3	0	x	MSS
8045	female	56	II	3	1	x	MSS
9607	female	56	II	3	0	x	MSS

10306	male	60	II	4a	1b		MSS
11752	male	43	III	3	2	x	MSS
12080	male	71	II	3	1	x	MSS
12435	male	74	II	3	1b		MSS
12961	male	61	II	3	0	x	MSS
13856	female	66	II	3	1	x	MSS
15539	male	52	II	3	2a		MSS
1892	female	75		3	2	1	MSS
2393	female	80	III	3	x	1	MSS
2714	female	47	II	4	1	1	MSS
3962	female	56	II	3	1	1	MSS
4785	female	76	III	3	2b	1a	MSS
6405	female	51	II	3	x	1	MSS
6744	male	70	II	3	1	0	MSS
7732	female	54		3	0	1	MSS
7906	male	61	II	4	2	1	MSS
9070	male	64					MSS
9240	female	49	II	4	0	1	MSS
10043	male	57	II	3	x	1	MSS
10067	female	80	II	4a	2a	1a	MSS
10814	female	61	II	4a	2b	1	MSS
11984	male	70	II	3	0	1	MSS
14642	male	49	III	3	1	1	MSS
15648	female	63	III	3	1		MSS
9438	female	45					MSS
11508	male	48	II	3	1a		MSS *
13487	female	73	II	3	0	x	MSS *
2900	female	71	II	3	2	1	MSS *
3737	male	59	II	3	1	1	MSS *
4129	male	69	II	3	0	1	MSS *
15144	female	44	II	3	2	1	MSS *
2383	male	74	II	3	1	x	MSS **
8681	male	67	III	3	2a	x	MSS **

Image cytometry was performed by Dahmane Oukrif (UCL Pathology).

The ploidy of each sample and its matched metastasis was assessed using image cytometry, where nuclei are isolated from a tissue scroll from a paraffin block and stained with Feulgen stain, before analysis on an image cytometer (see Methods). This method provides information on DNA index, a measure of the ratio of G1/G0 in the tumour sample compared to reference normal cells. Figure 5.7A shows example image cytometry plots from a diploid, aneuploid and tetraploid tumour sample. DNA indices are indicated for each sample.

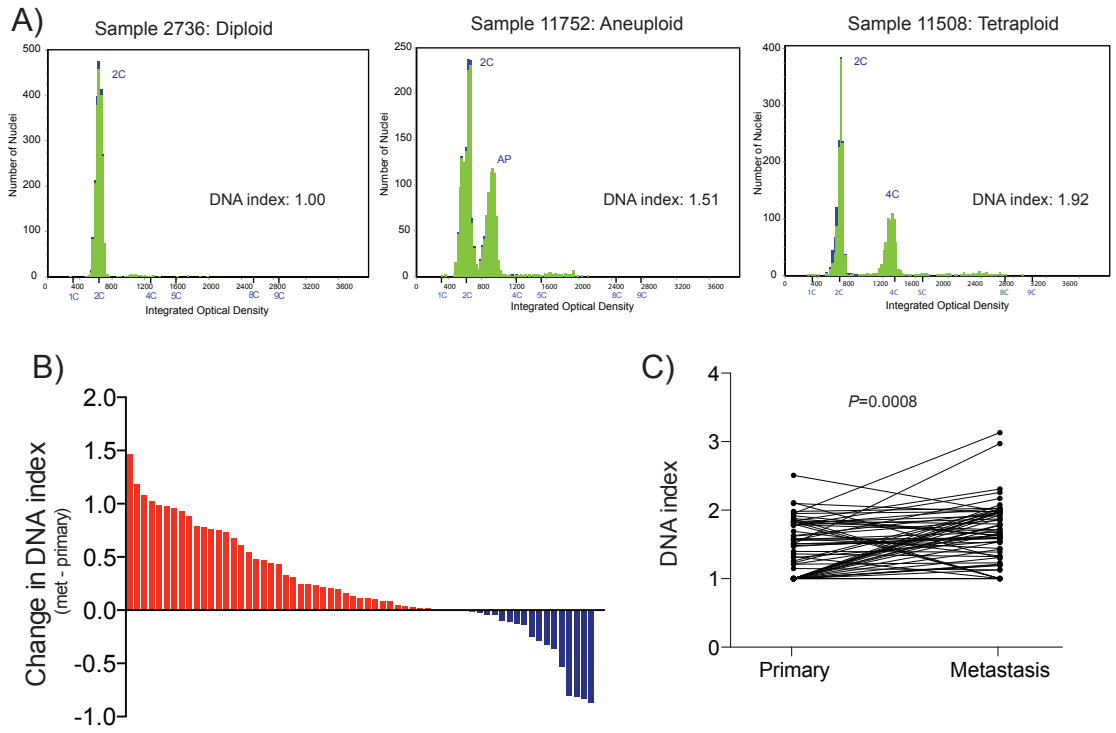

Figure 5.7: DNA index increases from primary to metastatic lesion in a CRC cohort

A) Examples of image cytometry histograms from a diploid, aneuploid and tetraploid tumour. Labels at 2C indicate diploid peaks, 4C tetraploid peaks, and AP = aneuploid peak. DNA index is indicated on each graph.
B) The change in DNA index between primary and metastasis is shown. Each bar represents one patient, red bars are positive values where DNA index increases from primary to metastasis, and blue bars are negative values where DNA index decreases between primary and metastatic samples.
C) DNA index changes plotted as a paired graph.

To assess changes in DNA index between each primary tumour and metastasis, the difference in DNA index between the primary tumour and metastasis was calculated (Figure 5.7B). These data show that there is an increase in DNA index from the primary tumour to the metastatic site in the majority of patients (*P*=0.008, Paired T-test, Figure 5.7C).

These data could potentially indicate a beneficial effect of increasing DNA index on the formation of metastasis. This increase in DNA index may be due to increases in ploidy, or an increase in the degree of aneuploidy in each tumour. Although these data show a clear trend towards an increasing DNA index, the magnitude of the

change is only infrequently close to 1 (i.e. from 1 in primary to 2 in the metastasis, Figure 5.7B), suggesting that a change from a diploid primary tumour to a polyploid metastasis is quite rare within this cohort. However there are frequent changes that are only slightly less than 1, and since previous data in this thesis has shown that after a genome duplication there is a trend towards loss of genomic material and increasing genomic aberrations (Figure 4.3, Figure 4.7), it may be that these smaller changes have resulted from a genome-doubling event and subsequent loss of genetic material. Genome doubling could not be assessed directly using copy number analysis in this cohort due to the poor quality of DNA that was available from the paraffin embedded tissue blocks.

To confirm that an increase in ploidy can influence metastasis, it would be of interest to increase the size of the dataset to see whether there was a trend for primary tumours that present with metastasis (M1 in Tumour, Node, Metastasis staging) to have an increased DNA index. However, this analysis would not necessarily be able to discern a trend unless there were multiple tumour regions analysed from the same primary tumour, as it has been previously shown that different regions of a primary tumour can have variations in ploidy (Gerlinger et al., 2012). Further, it would be interesting to use FISH for multiple chromosomes to assess the levels of chromosomal instability in these samples, in order to see if there was a correlation of increasing chromosomal instability with increasing DNA index.

5.2.5 A mutational basis for the tolerance of chromosomal instability in tetraploid clones

Chapter 4 demonstrated that tetraploid cells derived from HCT-116 could tolerate chromosome missegration events, and consequently their genomes become genomically unstable over time. Uncovering a mechanism by which cells could proliferate in a tetraploid state and tolerate chromosome missegregation events remained a priority.

All second-generation diploid and tetraploid clones at passage 4 and passage 50, plus parental HCT-116 cells were subject to whole-exome sequencing (WES) to search for somatic events common to all tetraploid clones. Alignment and variant calling from exome sequencing data, and mutation prediction analysis was carried out by Harshil Patel.

No coding mutations were found in *TP53*, *CDKN1A* or *RB1,* genes known to influence tolerance to chromosome missegregation and/or polyploidy (see Section 1.6). Additionally no common mutations were found in a list of genes relevant to the p53/p21 pathway, which is known to allow tolerance to chromosome missegregation (Table 5.3). Two individual tetraploid clones each had a mutation in one of the listed genes: a mutation in *MYC* in TC-16 and a mutation in *PCNA* in TC-35.

Table 5.3: p53/p21 pathway genes

No common mutations were found in any of the following genes. A mutation in *MYC* was found in TC-16, and a mutation in *PCNA* in TC-35 at passage 50. An *ID1* mutation was present in HCT-116.

RHOD	CCND1
E2F4	CDKN1
ID1*	CCCNE1
E2F1	CDKN1B
MYC *	CDK4
CDK2ND	CDKN2A
PCNA *	CDK2
CDK2NC	CDKN1A
RB1	E2F5
CDKN2B	TP53

Since no common mutation was found in members of the p53/p21 pathway, any mutations common to multiple tetraploid clones were collated. Only non-synonymous mutations were considered. Mutations present in any diploid sample were excluded. A full list of mutations found in multiple tetraploid clones, but not present in any diploid sample is shown in Table 5.4. Mutations listed in Table 5.4 are not necessarily the same amino acid change in all samples as all non-synonymous mutations for each gene were considered.

Table 5.4: Mutations common to 2 or more tetraploid clones

Gene Name	Mutated tetraploid samples		
ALDH5A1	TC-16 p50	TC-17 p50	
ALDOB	TC-17 p50	TC-35 p50	
ALG2	TC-35 p50	TC-17 p50	
ALS2CR11	TC-16 p50	TC-17 p50	
APOBEC3F	TC-17 p50	TC-35 p4	
ASB6	TC-16 p50	TC-17 p4 and p50	
ATP6V0A1	TC-17 p50	TC-16 p4 and p50	
CACNA1F	TC-35 p50	TC-13 p4 and p50	
CACNA1I	TC-35 p50	TC-13 p50	
CAPN14	TC-17 p50	TC-13 p50	
CBX2	TC-16 p50	TC-17 p4 and p50	
CELSR3	TC-17 p50	TC-16 p4 and p50	
CNTN3	TC-35 p50	TC-13 p4 and p50	
DAZAP1	TC-16 p50	TC-35 p50	
ELFN2	TC-35 p50	TC-17 p50	TC-35 p50
ESR1	TC-13 p50	TC-17 p4 and p50	
EXOC3L4	TC-13 p50	TC-17 p4 and p50	TC-17 p4 and p50
FAM135A	TC-13 p50	TC-16 p50	
FAM179B	TC-17 p50	TC-35 p4 and p50	
FASN	TC-13 p4 and p50	TC-16 p4 and p50	
FBXO18	TC-16 p50	TC-17 p4 and p50	
G6PC2	TC-13 p50	TC-16 p50	
GAA	TC-13 p50	TC-16 p4 and p50	
GRAMD2	TC-13 p50	TC-16 p50	
HSPH1	TC-13 p50	TC-17 p4 and p50	
IGSF10	TC-13 p50	TC-17 p50	
INADL	TC-17 p50	TC-13 p4 and p50	
KCNT1	TC-35 p50	TC-16 p4 and p50	
KIAA0317	TC-13 p50	TC-16 p50	
KIAA1239	TC-35 p50	TC-17 p50	
LIMK1	TC-17 p50	TC-35 p4 and p50	
LRP5	TC-16 p50	TC-17 p4 and p50	
MAN2B1	TC-13 p50	TC-16 p4 and p50	
MAPK3	TC-35 p50	TC-16 p50	
MYO18A	TC-35 p50	TC-13 p4 and p50	TC-13 p4 and p50
NAA30	TC-16 p50	TC-13 p50	
NDUFAF5	TC-17 p50	TC-16 p50	
NEFM	TC-13 p50	TC-17 p50	
NKD2	TC-16 p50	TC-35 p50	
NLN	TC-17 p50	TC-16 p4 and p50	
NOX3	TC-35 p50	TC-13 p50	
NSMAF	TC-17 p50	TC-13 p50	
NTN1	TC-13 p4 and p50	TC-17 p4 and p50	
NTRK1	TC-16 p50	TC-17 p50	
OR51B6	TC-35 p50	TC-16 p50	
PAGR1	TC-17 p50	TC-13 p4 and p50	
PAN2	TC-35 p50	TC-16 p50	
PKD2	TC-16 p4 and p50	TC-17 p4 and p50	
PLCG2	TC-13 p50	TC-16 p4 and p50	
PLXNB3	TC-13 p50	TC-17 p50	
PTPN21	TC-16 p50	TC-17 p4 and p50	
RBM47	TC-13 p50	TC-17 p4 and p50	
RERE	TC-35 p50	TC-16 p50	
SLIT1	TC-13 p50	TC-16 p4 and p50	
ST3GAL1	TC-16 p50	TC-17 p50	
STRN	TC-13 p4 and p50	TC-16 p4 and p50	
SYNE1	TC-13 p50	TC-17 p50	TC-16 p50
TACC2	TC-13 p4 and p50	TC-17 p4 and p50	
TMEM229A	TC-35 p50	TC-35 p4 and p50	
TNS1	TC-17 p50	TC-13 p4 and p50	
TRPM3	TC-16 p50	TC-35 p4 and p50	
TTC-21A	TC-16 p50	TC-17 p4 and p50	
TUBGCP6	TC-13 p50	TC-17 p50	
UROC1	TC-13 p4 and p50	TC-17 p4 and p50	
VWA5B1	TC-35 p50	TC-17 p50	

WDR52	TC-17 p50	TC-16 p50	TC-35 p4 and p50
ZBED4	TC-13 p50	TC-17 p50	
ZFPM2	TC-17 p50	TC-13 p50	
ZNF518B	TC-17 p50	TC-17 p4 and p50	
ZNF568	TC-35 p50	TC-16 p50	
ZNF574	TC-35 p50	TC-16 p50	
ZNF619	TC-17 p50	TC-17 p4 and p50	

Only two genes were mutated in more than two different tetraploid clones. These genes are *SYNE1* (Spectrin repeat containing nuclear envelope protein 1) and *WDR52* (WD repeat containing protein 52/ cilia and flagella associated protein 44). SYNE1 is a nuclear membrane protein involved in linking the nucleoskeleton with the cytoskeleton and maintaining subcellular spatial organisation. WDR52 has no known function. Furthermore, neither of these genes are categorised as driver genes, or are mutated at high frequency in any cancer type (Intogen database, (Gundem et al., 2010). An analysis of the predicted outcome of each individual mutation was carried out for these two genes using three different algorithms (SIFT, PolyPhen and Mutation-taster, see Methods). The results of this analysis are shown in Table 5.5. Mutations were considered as damaging overall if they had 2 or more predictions as damaging mutations from the three algorithms. These mutations are highlighted in grey in Table 5.5. Two of the mutations in *SYNE1* are predicted to be damaging based on this analysis. None of the mutations in *WDR52* are predicted to be damaging.

Table 5.5: Predicted outcome of mutations in more than 2 tetraploid clones

Mutation outcome as predicted by three different algorithms; SIFT output (D = damaging, T = tolerated), PolyPhen output (D =damaging, P= possibly damaging, B = benign) and Mutation-taster output (D =disease causing, A = disease causing [automatic], N = polymorphism, P = polymorphism [automatic]). NA = not applicable.

GENE	CLONES	SIFT predictor	POLY-PHEN predictor	Mutation-taster	Total damaging
SYNE1	TC-17 p50	D	D	D	3
SYNE1	TC-16 p50	D	P	N	1
SYNE1	TC-13 p50	D	D	D	3
WDR52	TC-35 p4 and p50	T	B	N	0
WDR52	TC-16 p50	T	D	N	1
WDR52	TC-17 p50	NA	NA	NA	0

Since tetraploid clones have been shown to tolerate chromosome missegregation at early passage (see Chapter 4, Figure 4.2), any mutation resulting in chromosome segregation error tolerance, or indeed tetraploid cell proliferation, should be present in early passage cells. Only 6 genes were mutated in more than one early passage clone. These genes are listed in Table 5.6. No gene was mutated in more than two early passage tetraploid samples. Of the six genes mutated in two tetraploid samples at early passage, none has a known role in chromosome segregation error tolerance. Further, there are no gene ontology pathways that link these 6 genes (Ashburner et al., 2000).

Table 5.6: Function of genes with multiple mutations in early tetraploid clones

Gene	Protein Name	Function
FASN	fatty acid synthase	Mainly catalyses palmitate synthesis
NTN1	netrin1	Unknown - in family of laminin related secreted proteins
PKD2	polycystin-2 (aka TRPP2)	Unknown
STRN	striatin	Unknown - possibly calmodulin binding
TACC2	transforming acidic coiled coil domain 2	In large family of centrosome and MT interacting proteins
UROC1	urocanate hydratase	Histidine catabolism

The functional outcome of these mutations was also tested using the algorithms SIFT, PolyPhen and Mutation-taster (see Methods and Table 5.7). The only gene to be consistently classed as damaging across all the tetraploid samples was *FASN*. None of the mutations in *NTN1* or *STRN* were consistently classed as damaging, and only one of the mutations in *PKD2*, *TACC2* and *UROC1* were classed as damaging using these methods. This suggests that these gene mutations may have occurred in multiple tetraploid samples by chance, as there does not appear to be selection for loss of function of these genes.

Table 5.7: Predicted outcome of mutations in early tetraploid samples

GENE	CLONES	SIFT predictor	POLY-PHEN predictor	Mutation-taster	Total damaging
FASN	TC-16 p4 and p50	T	D	D	2
FASN	TC-13 p4 and p50	T	D	D	2
NTN1	TC-17 p4 and p50	T	P	D	1
NTN1	TC-13 p4 and p50	T	B	D	1
PKD2	TC-17 p4 and p50	D	D	D	3
PKD2	TC-16 p4 and p50	NA	NA	A	0
STRN	TC-16 p4 and p50	T	P	D	1
STRN	TC-13 p4 and p50	NA	NA	A	0
TACC2	TC-17 p4 and p50	D	D	N	2
TACC2	TC-13 p4 and p50	NA	NA	NA	0
UROC1	TC-17 p4 and p50	D	D	D	3
UROC1	TC-13 p4 and p50	T	B	N	0

These data suggest that there is no common somatic mutational mechanism present in all the tetraploid clones that is responsible for the tolerance to chromosome segregation errors. It is however possible that different mutational mechanisms exist in different clones. Given the high mutational load present in all samples due to their microsatellite instability phenotype, it is also possible that mutations in genes common to more than one tetraploid sample occurred by chance. None of the genes in Table 5.6 are described as driver genes or have high mutational frequencies in any cancer type (Intogen database, Gundem et al., 2010). It is therefore unlikely that the mutations in these genes represent common mechanisms for cells to tolerate chromosomal instability.

5.2.6 A functional p53 pathway in tetraploid clones

No mutations were found in p53, or in members of the p53 pathway (Table 5.3). However, as the p53 pathway is one of the few mechanisms known to allow tolerance to chromosome segregation errors, the functionality of the pathway was further tested.

Diploid and tetraploid clones were treated with the DNA damaging agent Doxorubicin for an hour, and then allowed to recover in fresh media for 7 hours.

Lysates were prepared and probed for p53 and its downstream target p21 (Figure 5.8). All early passage diploid and tetraploid clones up-regulated p53 and p21 after Doxorubicin treatment, suggesting that the main axis of this pathway is indeed functional, at least in response to DNA damage.

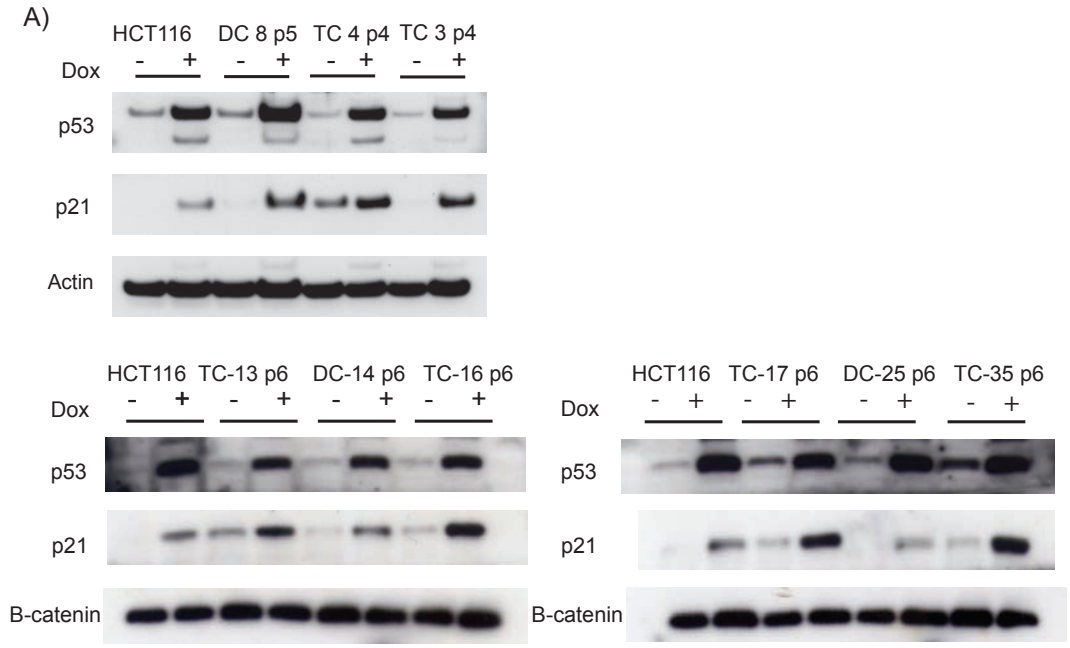

Figure 5.8: Up-regulation of p53 and p21 after DNA damage in all clones

A) Western blots for p53 and p21 with (+) and without (-) Doxorubicin (Dox) treatment for 1 hour at 1μM, followed by a 7 hour recovery in fresh media. Passage numbers are indicated for each clone. Either Actin or β-catenin was used as a loading control.

5.2.7 Changes in gene expression in tetraploid clones

Since tetraploid clones have no common mutations to explain their tolerance to chromosome missegregation events, and appear to have a functional p53 axis, a genome wide analysis of gene expression was carried out using microarrays, in order to investigate if tetraploid cells had epigenetically regulated any pathways that could explain their chromosome missegregation tolerance phenotype.

RNA was extracted from all second-generation diploid and tetraploid clones at both early passage (passage 6) and late passage (passage 49), as well as the parental HCT-116 cell line, and subjected to a microarray analysis using Affymetrix Human Gene 1.0 ST Arrays. Microarray profiling was carried out by the Affymetrix Microarray Service at the Cancer Research UK Manchester Institute. Microarray clustering and preparation of the graphs in Figure 5.9 was carried out by Dr Tejal Joshi and Dr Nicolai Birkbak.

A genome wide comparison of mean expression between early passage diploid and tetraploids showed very similar global patterns of gene expression (Figure 5.9A). There is a very good correlation in global gene expression between diploids and tetraploids. Genes that showed a significant difference in expression between diploid and tetraploids are shown in the adjacent table. The log fold change is shown for each significant gene (positive values are genes that are more highly expressed in tetraploid samples). A very similar pattern was observed in the comparison between late passage diploid and tetraploid clones (Figure 5.9B). In both early and late passage, the majority of genes that are significantly differentially expressed are down-regulated in tetraploids compared to diploids.

Figure 5.9C shows a comparison between all diploid and tetraploid clones at both early and late passage. Again, there are very similar global gene expression patterns between all diploid and tetraploid clones. Only one gene has a log fold change of greater than 2 fold (SYT1, Figure 5.9C).

A)

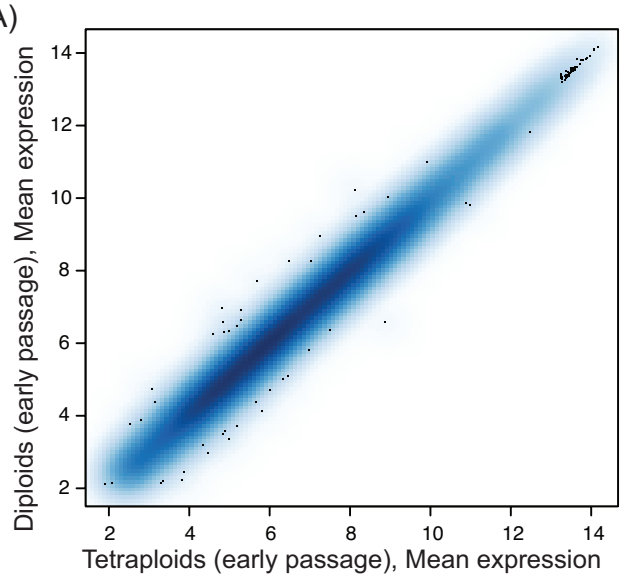

GENE NAME	logFC
KLK7	1.12
KLK5	1.12
NR2F2	1.09
IFITM1	-1.06
NR4A2	-1.07
ANTXR2	-1.11
SPOCK3	-1.16
KLRC2	-1.39
KLRC3	-1.44
CD24	-1.57
KLRC4-KLRK1	-1.85
KLRC4	-1.86
KLRK1	-2.02
TNFSF18	-2.4

B)

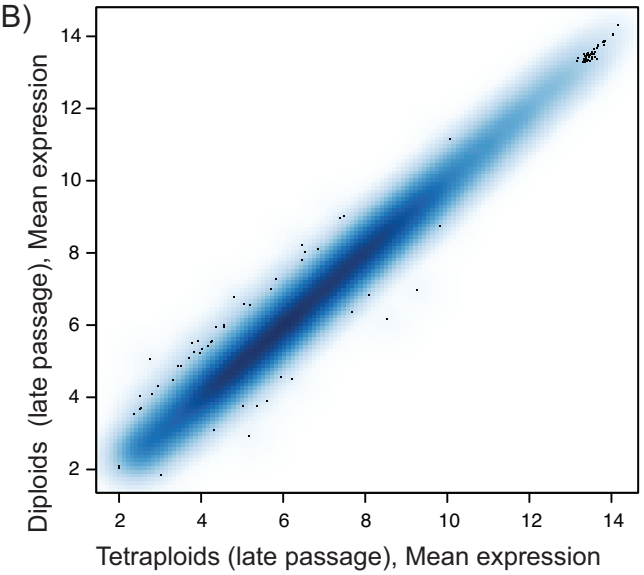

GENE NAME	logFC
FLJ32742	1.28
SPTSSB	-1.01
CASP6	-1.01
NPNT	-1.2
HNF4G	-1.24
CYP4F11	-1.34
EDNRA	-1.58
SAMD9	-1.97
EHF	-2.01
CNTN1	-2.12

C)

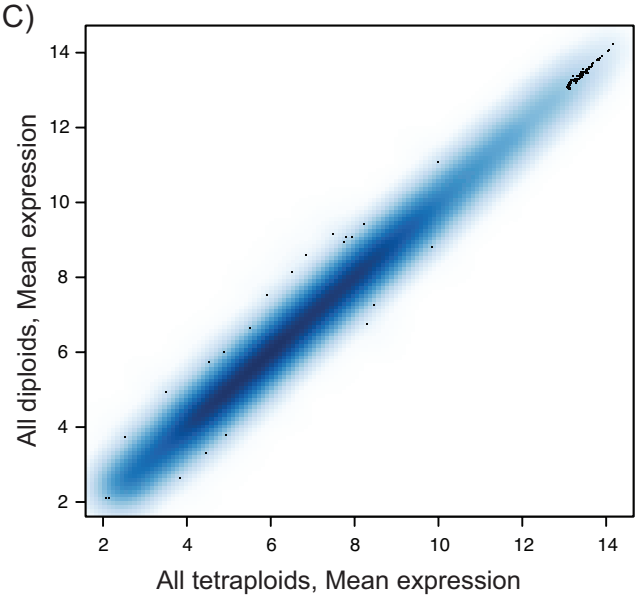

GENE NAME	logFC
SPOCK3	-1.01
NPNT	-1.01
TMEM200A	-1.02
SOX4	-1.09
KLRC4	-1.13
ZBED2	-1.25
KLRK1	-1.3
CD24	-1.47
ANXA10	-1.64
SYT1	-2.01

Figure 5.9: Microarray profiling results in diploid and tetraploid clones

A) Comparison of global gene expression patterns between early passage diploid and tetraploid clones. A list of significantly differentially expressed genes (P<0.05) is shown adjacent to the graph, with logFC (fold change) values indicated.
B) As in A), but for late passage clones.
C) Comparison between all diploid and tetraploid clones (both early and late passage).

To see if the most differentially expressed genes in all the samples were related to the ploidy status of the sample the 250 most variable probes were selected, and hierarchical clustering was performed. This analysis was carried out by Nicholas McGranahan.

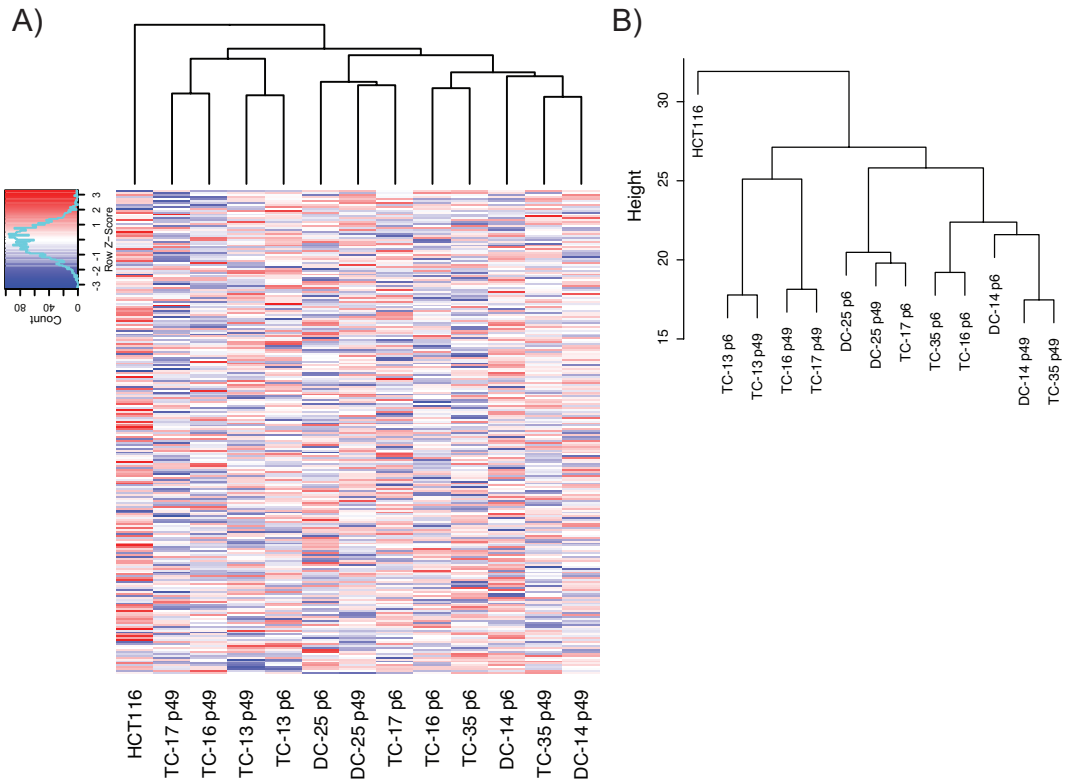

Figure 5.10: Clustering of the 250 most variable microarray probes

A) Graphical representation of the 250 most variable probes in the microarray analysis. Colours represent a z-score scale for each gene (red = overexpressed, blue = under-expressed). Each gene is scaled to have a mean of 0 and standard deviation of 1.
B) Hierarchical clustering shows the relationship between the samples for the 250 most variable probes.

The graph in Figure 5.10A shows that there are no obvious trends separating diploids and tetraploids when comparing even the most differentially expressed

genes. Furthermore the clustering in Figure 5.10B shows that diploid and tetraploid samples do not cluster together in this analysis.

These data indicate that there are no clear genome wide transcriptional changes associated with tetraploidy in this system. This result is consistent with the results of Kroemer and colleagues who also found few transcriptional changes between a panel of diploid cell lines derived from HCT-116 and RKO (Castedo et al., 2006). However comparing microarray data from tetraploid clones from both of these cell lines only resulted in a list of 29 genes that were altered as a function of ploidy (Castedo et al., 2006). Analysis of the differential expression of 15 of these 29 genes that had adequate annotation from the microarray analysis described above is shown in Figure 5.11. This analysis again shows that there is no separation of diploid and tetraploids based on the expression of these genes. This analysis was carried out by Dr Nicolai Birkbak.

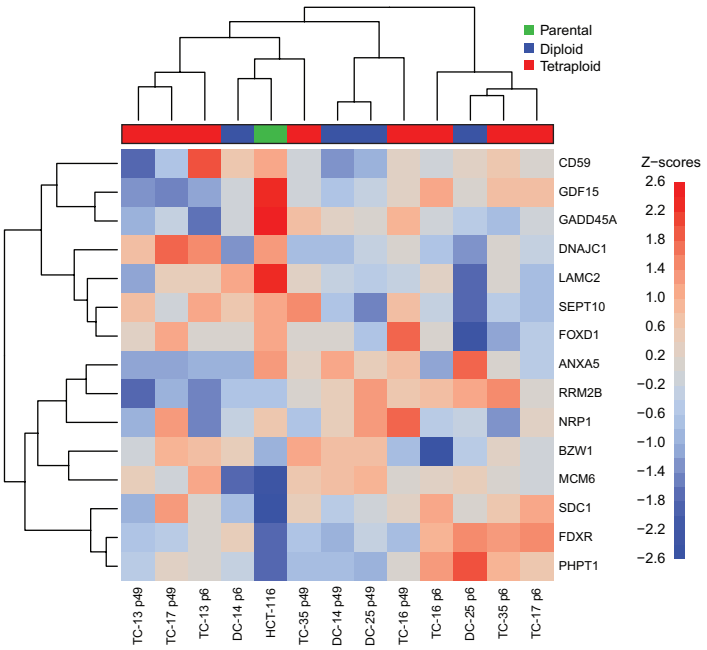

Figure 5.11: Analysis of 15/29 genes shown previously to have altered expression based on ploidy

Hierarchical clustering of expression of 15 genes from a list of 29 genes previously shown to have altered expression based on ploidy (Castedo et al., 2006). Blue colours in grid show under-expression compared to median expression, red colours indicate over-expressed genes (z-score). Clustering of different samples is shown

above graph, and ploidy status is indicated (red = tetraploid, blue = diploid, green = HCT-116 parental cell line).

It is surprising that there are also few differences in late passage tetraploid clones compared to diploid clones, as late passage tetraploid clones show higher levels of genomic instability (Figure 4.3). Previous studies have shown that there may be a common transcriptional response to chromosome imbalances in cells (Sheltzer et al., 2012, Durrbaum et al., 2014). However, at late passage numbers, there are no obvious transcriptional changes in tetraploid clones, which exhibit many chromosome imbalances (Figure 4.3). This could indicate that in the context of tetraploidy, additional chromosome imbalances do not result in a typical transcriptional response. Many of the genes that have been shown to be altered as a general response to aneuploidy are linked to cellular stress (Sheltzer et al., 2012, Durrbaum et al., 2014). However, in late passage tetraploid clones, loss or gain of chromosomes (for example the loss of chromosome 4q that occurs in all tetraploid clones, Figure 4.3) is unlikely to have resulted in an anti-proliferative or stress response, as these chromosomal changes have been selected in the whole population. It is possible that different chromosomal changes have occurred during the passaging of tetraploid clones, but have not been selected for as they resulted in this stress response. The degree of stress initiated after a chromosome missegregation could be due to the size and number of genes on the aneuploid chromosome, which could explain why cancer cells have been shown to more frequently lose small chromosomes (Duijf et al., 2013).

5.3 Conclusions

Although tetraploid clones derived from HCT-116 do exhibit hallmarks of chromosomal instability, including increased levels of segregation errors and structurally abnormal chromosomes (Chapter 3), they do not exhibit increased drug resistance to an extensive panel of kinase inhibitors. This would not have been predicted based on previous work showing that CIN+ cells were more resistant than CIN- cells to the same panel of drugs (Lee et al., 2011). This may indicate fundamental differences in the type of chromosomal instability generated by a tetraploidisation event in a microsatellite unstable cell line and the CIN+ cell lines

that were tested in the previous study. It could also indicate that chromosomal instability coupled with microsatellite instability is detrimental to cell survival under stressful conditions. Indeed, CIN and MIN are rarely observed together in CRC (see Section 1.11). This may suggest that there is a threshold level of genetic instability that can be tolerated by cells. This idea is consistent with recent studies that have shown that high levels of CIN can be beneficial for patients treated with certain chemotherapeutics (Birkbak et al., 2011, Jamal-Hanjani et al., 2015).

Additionally, no differences in sensitivity to a range of DNA damaging agents, some of which have previously shown to be less effective in tetraploid cells were observed (Castedo et al., 2006). These discrepancies may be due to different mechanisms that were used to generate tetraploid cells between this and the previous study. Tetraploid clones used in this study are naturally occurring in the parental HCT-116 population, but Castedo and colleagues used nocodazole or cytochalasin D to induce cytokinesis failure to generate tetraploid cells in HCT-116 (Castedo et al., 2006). The frequency of surviving cells after this treatment was extremely low (1 in 10,000), which may indicate that this study selected tetraploid cells that had already altered key survival pathways that meant that they were more resistant to multiple drug treatments, including the DNA damaging agents that they later tested (Castedo et al., 2006). Additionally different protocols of drug treatment could affect the outcome of these experiments. Preliminary data generated by a colleague Andrew Crockford, has demonstrated that tetraploid clones from HCT-116 are more resistant to some chemotherapeutic agents, but only in long-term, and not short-term assays. This could suggest that it is heterogeneity within the tetraploid population (for example the increase in cell-to-cell variation in chromosome number, Figure 3.5) that allows tetraploid cells to survive over long-term treatment, rather than an inherent drug resistance.

The ability of tetraploid cells to grow in 3D environments was investigated using spheroid culture. There were no significant differences in growth rate between diploid and tetraploid clones, and a large variation between clones. Using this system of clones has demonstrated that there is likely to be significant heterogeneity in phenotypes within the parental HCT-116 and DC-8 populations. This is probably due to the microsatellite instability inherent in HCT-116 cells, which

will continually be generating new mutations within cells of the population. Using bioluminescence imaging in mice revealed that there was no difference in metastatic potential between one diploid and one tetraploid clone. There was a small increase in tumour growth rate in the tetraploid clone TC-13, but the statistical evidence for this increase was ambiguous. It is difficult to assess the impact that tetraploidy has on metastatic potential using tetraploid clones derived from a cell line that is already metastatic in a tail-vein injection. If appropriate models of primary tumours that spontaneously metastasised in the mouse were available, it would be of greater interest to assess whether ploidy of the primary tumour changed the location, frequency or growth rate of metastases. This would be especially interesting given that in a cohort of matched primary CRC and their liver metastases, there was a significant increase in DNA index from the primary to the metastatic site. This could suggest that increasing ploidy is favourable for the formation of metastatic lesions. This would be an interesting area for further research.

An extensive analysis of mutations in tetraploid clones failed to identify any mutation common to all tetraploid clones that can explain their ability to propagate segregation errors (Chapter 4). Furthermore, very few mutations were shared between more than two tetraploid clones at early passages, which suggests there is no common mutational mechanism in these tetraploid clones that allowed them to survive tetraploidisation and single-cell cloning, which appeared to be a barrier to tetraploid cell survival (Figure 3.3B). There were no mutations found in either diploid or tetraploid clones in p53 or p21, and the p53 pathway appeared to be active in response to DNA damage. There were also very few global changes in gene expression between diploid and tetraploid clones, at either late or early passage. Although surprising given the extensive genomic changes at later passages (Figure 4.3), this is similar to previous work which showed across a panel of diploid and tetraploid clones derived from HCT-116 and RKO that there were very few transcriptional alterations based on ploidy (Castedo et al., 2006). However, preliminary data has indicated that there may be specific genes that are de-regulated at the mRNA level between diploid and tetraploid clones (Andrew Crockford, personal communication). It is likely that carrying out a large-scale

global analysis by using microarrays is not sensitive enough to pick up subtle but potentially important changes in gene expression.

A proteomics analysis between one diploid and one tetraploid clone has also been carried out by a colleague, Andrew Crockford, to assess changes in proteomic regulation between diploid and tetraploids. This analysis has resulted in a list of proteins that are up or down regulated in tetraploids that are currently being validated in the panel of tetraploid clones and followed up with functional analysis.

Given the data presented in this Chapter, which failed to reveal common changes in DNA sequence or gene expression that could explain the tolerance to chromosomal instability in tetraploid clones, a different approach to uncover genetic regulators of tetraploid cell survival was adopted in the next chapter.

Chapter 6. Results 4: A screen for regulators of cell cycle re-entry after cytokinesis failure

6.1 Introduction

In Chapter 5 the functional consequences of tetraploidy in the isogenic system of clones derived from diploid HCT-116 cells was explored. No inherent drug resistance was observed in tetraploid clones when treated with a large panel of kinase inhibitors, or a selection of clinically relevant DNA damaging agents. Although there was no difference in the ability of one diploid and one tetraploid clone to form tumours when injected into nude mice, some tetraploid cell lines showed an enhanced ability to grow in 3D culture. Analysis of patient data also revealed an intriguing correlation of increasing DNA index in metastatic compared to primary tumour samples. Surprisingly there were no common mutations in tetraploid clones that are likely to account for their ability to propagate chromosome missegregation events. Additionally there did not appear to be global changes in gene expression common to tetraploid clones. It may be that in this system of diploid and tetraploid clones there is no singular mechanism that can explain their tolerance to chromosome missegregation. Tetraploid cells could propagate segregation errors due to a buffering of chromosomal content. If one chromosome is missegregated into the incorrect daughter cell the other daughter cell will still have three chromosomes present that might compensate for alterations in gene dosage. If this is indeed the case then there may be no mutation or change in gene expression that does allow tolerance to chromosome missegregation.

Given the possibility that tetraploidy itself may allow the propagation of segregation errors, it is relevant to investigate the mechanisms by which tetraploid cells can initially proliferate. As discussed in Section 1.6, several studies have shown that after cytokinesis failure most primary cells undergo a p53 dependent cell cycle arrest. In this study it has also been shown that tetraploid cells are harder to clone than diploid cells (Figure 3.3B). As many tumours show evidence of whole genome doublings during their evolutionary histories (Carter et al., 2012, Zack et al., 2013

2014), it is likely that cells have found mechanisms to bypass this proliferative checkpoint. Although mutations in p53 occur frequently in GD tumours, a significant proportion (43%) of GD tumours (from a pan-cancer analysis) do not have p53 mutations (McGranahan et al., 2015). This suggests that alternative mechanisms for bypassing this checkpoint do exist in cancer cells. A recent study by Pellman and colleagues used this logic to design a screen for regulators of cell cycle arrest after cytokinesis failure (Ganem et al., 2014). Ganem and colleagues identified LATS2 (large tumour suppressor 2), a member of the Hippo signalling pathway, which is activated in response to cytokinesis failure. In this chapter a similar screening protocol is used to assay genes that are more frequently mutated in genome-doubled tumours to ascertain if they have a role in allowing the initial proliferation of tetraploid cells.

6.2 Results

6.2.1 Selection of genes to screen

The lists of genes in this analysis were provided by Nicholas McGranahan, using the data sets and criteria detailed below.

In order to establish a list of candidate genes contributing to cell cycle arrest after cytokinesis failure when silenced, publically available data from TCGA were utilised. SNP6.0 and somatic variant data from breast cancer, bladder cancer, lung adenocarcinoma, lung squamous cell carcinoma, melanoma, glioblastoma multiforme, colon adenocarcinoma and head and neck cancer was obtained from TCGA. All tumours were assessed for evidence of genome doubling using the algorithm described in Chapter 3. All non-silent mutations in all samples for each tumour type were used to assess whether a difference in prevalence of somatic aberrations was observed in specific genes in genome doubled (GD) compared to non-genome-doubled (nGD) tumours (see Methods). A graphical illustration of this analysis for colon adenocarcinoma is shown in Figure 6.1.

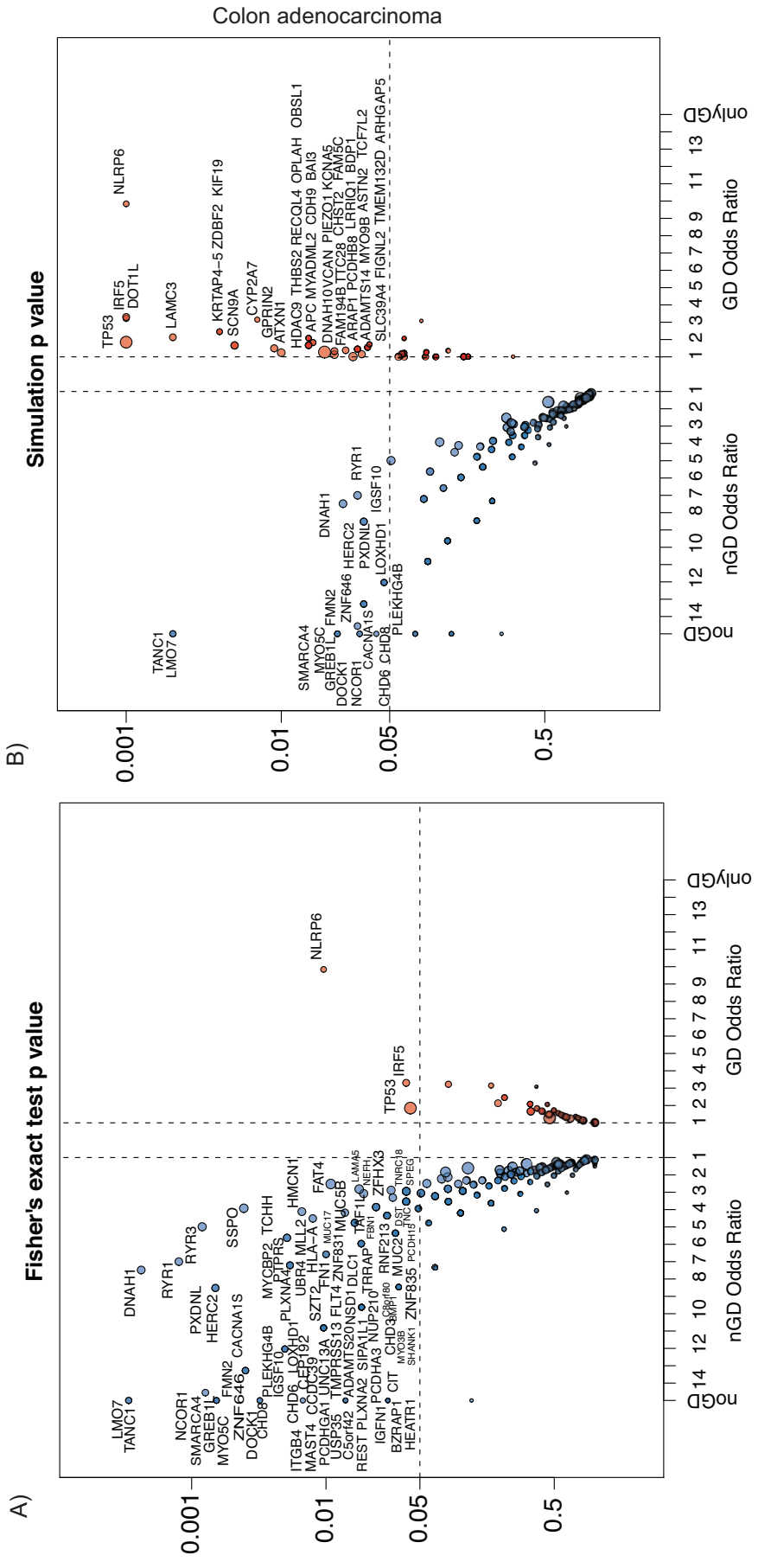
Colon adenocarcinoma
A)
Fisher's exact test p value
B)
Simulation p value
0.001
0.01
0.05
0.5
nGD Odds Ratio
GD Odds Ratio
noGD
onlyGD
TP53
IRF5
NLRP6
DNAH1
RYR1
RYR3
PXDNL
HERC2
SSPO
CACNA1S
ZNF646
FMN2
TANC1
LMO7
LAMC3
DOT1L
KRTAP4−5
ZDBF2
KIF19
SCN9A
CYP2A7
GPRIN2
ATXN1
HDAC9
THBS2
RECQL4
OPLAH
OBSL1
APC
MYADML2
CDH9
BAI3
DNAH10
VCAN
PIEZO1
KCNA5
FAM194B
TTC28
CHST2
FAM5C
ARAP1
PCDHB8
LRRIQ1
BDP1
ADAMTS14
MYO9B
ASTN2
TCF7L2
SLC39A4
FIGNL2
TMEM132D
ARHGAP5
SMARCA4
MYO5C
GREB1L
DOCK1
NCOR1
CHD6
CHD8
PLEKHG4B
LOXHD1
IGSF10

Figure 6.1: Relationship between mutations and genome doubling status of colon adenocarcinoma

A) Analysis of relationship between individual mutations and genome doubling status of colon adenocarcinoma. Mutations plotted according to Fisher's exact-test *P*-value and odds ratio.
B) Mutations plotted according to a simulated *P*-value and odds ratio (see Methods and text). NB: not all mutations in A) could be named on the graph due to space constraints.

All genes with at least five non-silent mutations are represented as circles. To assess whether any genes harboured an enrichment or depletion of non-silent mutations in GD compared to nGD tumours, a Fisher's exact-test was implemented for each gene, yielding an odds ratio – reflecting the association between mutations in that gene and the likelihood of the tumour having undergone GD – and an associated *P*-value. Genes depicted on the right hand side of each graph have a higher odds ratio, and hence occur more frequently in GD tumours.

The second graph presented depicts the simulated *P*-value for each mutation (Figure 6.1B). This simulated *P*-value was calculated from a permutation-based analysis, which takes into account the mutational load of each tumour. As most of the nGD tumours in colon adenocarcinoma are likely to be diploid and microsatellite unstable they are likely to have a high mutational burden, and in the Fisher's exact-test analysis many genes pass the threshold for being significantly mutated. However when the total number of mutations in each sample is taken into account using the simulated *P*-value then fewer mutations pass the significance threshold of $P<0.05$ (Figure 6.1B). This analysis was repeated across breast cancer, bladder cancer, lung adenocarcinoma, lung squamous cell carcinoma, melanoma, glioblastoma multiforme, and head and neck cancer samples from TCGA. To develop a list of genes to screen, only genes with a positive odds ratio for occurring more frequently in genome doubled samples were selected. All genes that had significant Fisher's exact test *P*-values or significant simulated *P*-values were taken forward.

The bioinformatics tool MutSigCV was developed at the Broad Institute to find significantly mutated genes in large datasets whilst avoiding false positive results that may stem from, among other factors, gene size or replication timing (Lawrence

et al., 2013). MutSigCV analysis was applied to all genes that were mutated significantly more frequently in GD tumours, and only those genes which passed a threshold of $P<0.05$ were taken forward for screening analysis.

Any genes that were discarded following the MutSigCV analysis were reanalysed to investigate if they overlapped with any of the four following relevant gene lists. These four gene lists were: the list of genes mutated in more than one tetraploid clone derived from HCT-116 (presented in Chapter 5, Table 5.4), a list of genes that are mutated specifically in aneuploid tumours from a cohort of colorectal cancers (used with the kind permission of Dr Carlos Lopez-Garcia, data not shown, manuscript in preparation), a list of hits from a reversine screen for regulators of segregation error tolerance (used with the kind permission of Dr Laurent Sansregret, data not shown, manuscript in preparation), and the list of significant genes from the original two screens found in the recent publication by Pellman and colleagues (DNA damage and tetraploidy tolerance) (Ganem et al., 2014). Any genes that were found to overlap with any of these gene lists were included if they had an odds ratio associated with GD of greater than 4. A schematic detailing the gene selection process is shown in Figure 6.2.

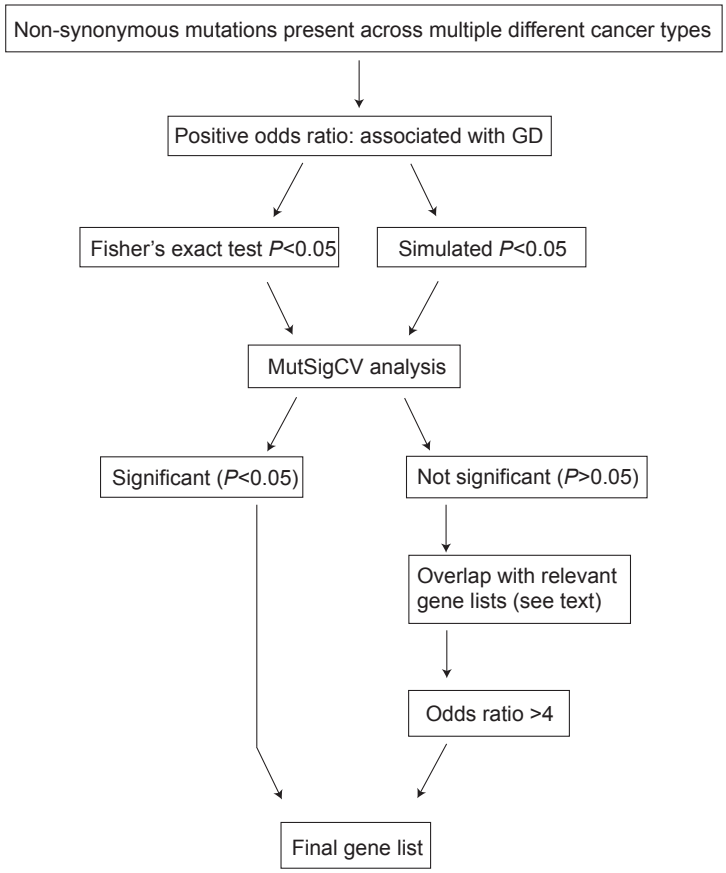

Figure 6.2: Schematic of gene selection for screen

An outline of how genes were selected for inclusion in a screen for regulators of cell cycle arrest after cytokinesis failure.

A complete list of all genes used in the screen is shown in Table 6.1. This list indicates from which cancer type the genes were selected and also whether each gene overlapped with any of the gene lists described above. Control genes selected as positive controls are also included. A complete list of all the siRNA sequences used for these genes is shown in Appendix Section 8.2.

Table 6.1: Full list of genes included in screen

Abbreviations for cancer types: BLCA: bladder cancer, LUAD: lung adenocarcinoma, LUSC: lung squamous cell carcinoma, SKCM: melanoma, GBM: glioblastoma multiforme, COAD: colon adenocarcinoma, HNSC: head and neck cancer. * indicates 3 additional genes included as they were found to be mutated in p53 WT but wGII high tumours (see Methods).

GENE	Significantly Mutated Cancer Type	TP clones mutation?	Aneuploid CRC mutation?	Pellman screen hit (all)	Reversine screen top hits
ZFPM2	LUAD	yes			yes
LGR5	SKCM	yes			
LRP5	SKCM	yes			
TG	LUAD	yes			
TP53	ALL!		yes	yes	yes
DNAH5	HNSC		yes		yes
INHBA	SKCM			yes	yes
SORCS1	LUAD			yes	
CNGB3	LUAD				yes
ELTD1	LUSC				yes
LILRB2	LUAD				yes
NRXN1	LUAD				yes
OR51B5	SKCM				yes
RB1	GBM				yes
RGS7	LUAD				yes
SALL4	LUAD				yes
SCN1A	LUSC				yes
SIGLEC6	SKCM				yes
ZNF208	LUAD				yes
ABCA13	LUAD				
APC	COAD				
ARHGAP5	COAD				
ARID1A	BLCA				
ATXN1	COAD				
BCAM	SKCM				
C12orf50	SKCM				
CCDC11	SKCM				
CD2	SKCM				
CDH10	LUAD, LUSC				
CDH9	COAD				
CHD2	SKCM				
COL11A1	HNSC, LUSC				
COL14A1	LUAD				
COL1A2	LUAD				
COL22A1	SKCM				
COL3A1	LUAD				
COL6A3	LUAD, BLCA				
CSMD2	LUAD				
FAM171B	LUAD				
FAM194B	COAD				
FSHR	LUSC				
GFRAL	LUAD				
HEATR7B2	HNSC, LUAD				
IDH1	GBM				
INSRR	LUAD				

ITGAX	LUAD				
KCNA5	COAD				
KIR2DL1	SKCM				
KLHL1	LUAD				
KRTAP4-5	COAD				
LRRIQ4	SKCM				
MUC7	LUAD				
MYADML2	COAD				
NAV3	LUAD				
NBAS	LUAD				
NCKAP1L	LUSC				
NID1	LUAD				
NOTCH4	LUAD				
PON1	SKCM				
PTEN	GBM				
PXDNL	LUAD				
PZP	LUAD				
RUNX1T1	LUAD				
SCN9A	COAD				
SELP	LUSC				
SLC13A1	LUSC				
SLC18A2	SKCM				
SLITRK1	LUAD				
SLITRK3	LUAD				
SNTG1	SKCM				
ST6GAL2	LUAD				
TCF7L2	COAD				
TPO	LUAD				
TRPS1	LUAD				
VCAN	LUAD				
DGKI*	COAD				
DMXL1*	COAD				
SATB2*	COAD				
DCP1A				yes	
CDKN1A				yes	
LATS2				yes	
PTBP1				yes	
SPINT2				yes	

The positive control genes used were TP53 and CDKN1A (p21) as knockdown of these genes will allow cells to bypass cell cycle checkpoints. Four genes were also included that were strong hits in the Ganem et al., 2014 paper: LATS2, SPINT2, PTPB1 and DCP1A. A custom 96-well plate format of pooled On-Target-Plus (OTP) small interfering RNAs (siRNAs) from Dharmacon were ordered for each gene. Separately ordered control siRNAs were also added to the plate layout. The non-targeting OTP Controls 1-4, si-Genome Control-5 and RISC-free siRNAs were

used. In addition to the positive controls within the plate layout, separate p53 and p21 siRNAs were also used (four individual OTP siRNAs for p53 [14-17] and one additional OTP siRNA for p21 [12]). The sequences of these additional siRNAs can be found in Methods Table 2.4.

6.2.2 Outline of screening procedure

The protocol for screening for genes regulating cell cycle re-entry after cytokinesis failure was followed from Ganem et al., 2014. The primary hTERT immortalised cell line RPE (retinal pigment epithelium) that expresses two fluorescent markers from the FUCCI (fluorescent ubiquitin based cell-cycle indicator) system was used to distinguish between cells in G1, S and G2 phases (Sakaue-Sawano et al., 2008). The RPE-FUCCI cell line was kindly provided by Dr Laurent Sansregret. These cells express a fragment of human Geminin tagged to the Venus protein and a fragment of human Cdt1 tagged to mCherry protein. As these two proteins are degraded in distinct phases of the cell cycle (Geminin in M and G1, Cdt1 in S and G2/M) by ubiquitination and proteasome targeting, cells express different fluorescent markers in the different phases of the cell cycle (mCherry in G1, Venus in S, G2 and M) (Sakaue-Sawano et al., 2008).

A schematic of the screening procedure is shown in Figure 6.3A. The purpose of the screen was to identify siRNAs that increase the fraction of cells re-entering the cell cycle after cytokinesis failure. Briefly, cells were treated with the actin polymerisation inhibitor dihydrocytochalasin B (DCB), which inhibits cytokinesis, as cells are unable to form a contractile ring around the cleavage furrow. Cells were then treated with the DNA dye Hoechst so that cells that had undergone cytokinesis failure and subsequently had a 4N DNA content could be identified. The FUCCI system was then used to distinguish between normal diploid cells in G2, and binucleated tetraploid cells in G1. This method of using FUCCI in flow cytometry to distinguish between cells in different cell cycle phases has been used previously (Wu et al., 2010). Cells with a 4N DNA content, but expressing the mCherry Cdt1 gene fragment (G1 cells) were selected and sorted. Cells were then reverse transfected with siRNA in 96-well plates, and the plates fixed 96 hours later. The plates were stained with DAPI and automatically scanned so the fraction of

Venus expressing cells (identifying cells in S/G2) could be calculated. This allows the identification of siRNAs which increase the fraction of cycling cells after cytokinesis failure, as the majority of untreated cells remain in G1 for the duration of the experiment.

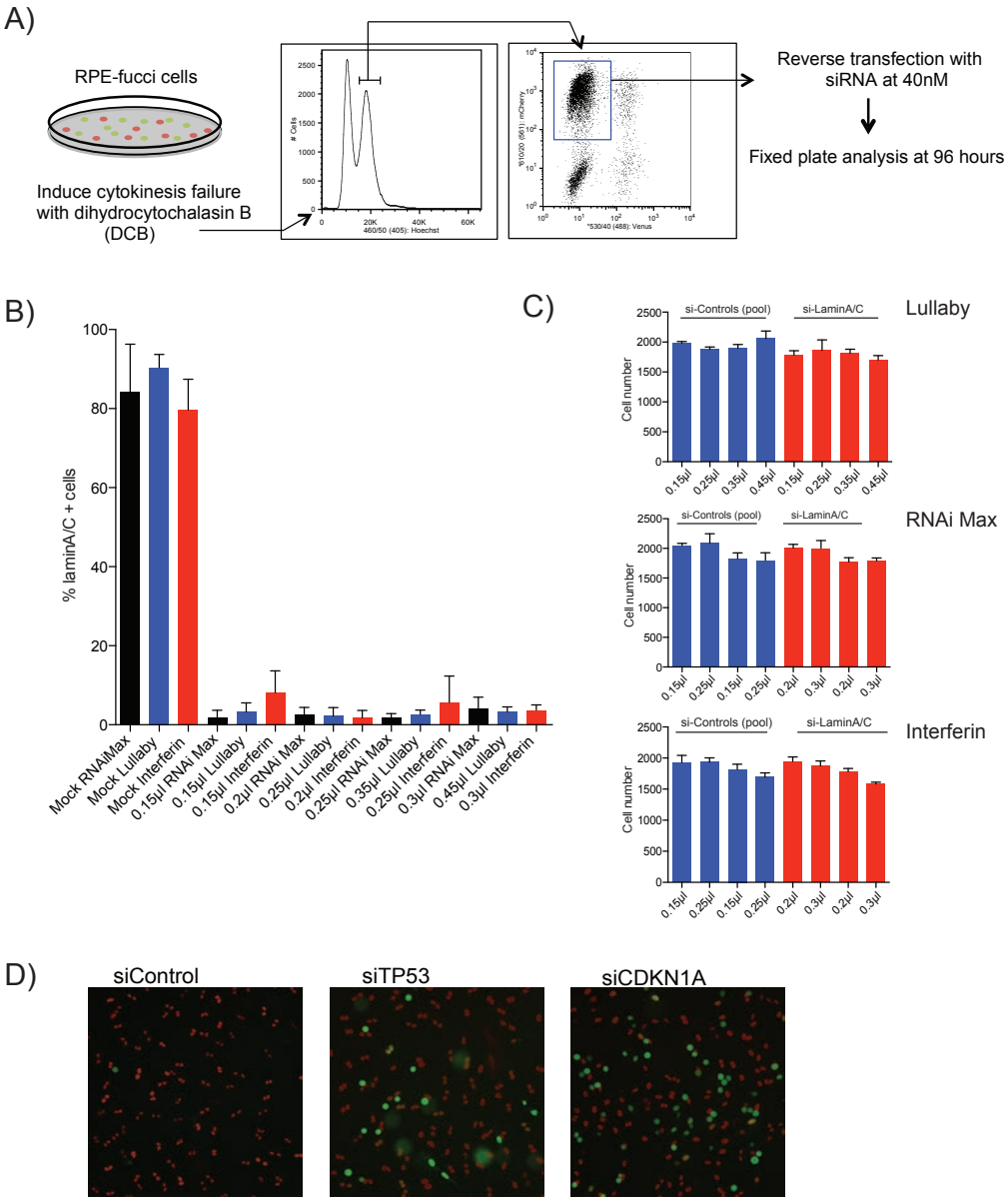

Figure 6.3: Outline and set-up of screening protocol

A) Outline of screening procedure followed from Ganem et al., 2014.
B) A transfection test using siRNA targeting LaminA/C and different concentrations of three different transfection reagents (RNAi Max, Lullaby and Interferin). Amount of reagent indicated is quantity used per well of a 96-well plate.
C) Effect of increasing concentration of the different transfection reagents on cell number.

D) Example images of control transfected cells, as well as the two positive controls p53 and p21 are shown from fixed plate analysis at 96 hours

Extensive optimisation was carried out on RPE-FUCCI cells to maximise transfection efficiency and viability after the sorting procedure detailed in Figure 6.3A. Using three different transfection reagents (RNAi Max, Lullaby and Interferin), cells were transfected with a pool of Control siRNAs (OTP Controls 1-4, Dharmacon), or si-LaminA/C at differing concentrations of transfection reagent per well. After 72 hours cells were fixed and the knockdown of LaminA/C was assessed using indirect immuno-fluorescence. Plates were scanned using a Cellomics ArrayScan Vti machine and the percentage of LaminA/C expressing cells was calculated using the target Activation Cellomics Bioapplication (see Methods). The results of the optimisation are presented in Figure 6.3B. Compared to mock transfected wells, all reagents resulted in a significant reduction in LaminA/C staining. However Interferin resulted in a less efficient knockdown than either RNAi Max or Lullaby reagents. To test the toxicity of the transfection reagent the number of cells per well was calculated for both the control and LaminA/C transfected wells using DAPI to count total cell number. Figure 6.3C shows the cell number after 72 hours for different concentrations of each reagent. Interferin showed the most obvious reduction in cell number at increasing concentrations, and RNAi max also showed a decrease in cell number (indicating toxicity) at the highest concentrations of reagent used. Lullaby did not have a striking effect on cell number at increasing concentrations. The reagent Lullaby was therefore chosen to use in the screen, at a concentration of 0.15µL per well, as this resulted in a significant reduction in LaminA/C staining. Example images of control, p53 and p21 transfected cells after the cell sort using these transfection conditions are shown in Figure 6.3D, showing that very few control cells start cycling after cytokinesis failure, whereas p53 or p21 siRNA transfection resulted in an increase in the number of cycling cells.

6.2.3 First two screen repeats

The screen was carried out twice in triplicate in two independent experiments. The results of these first two screens are shown in Figure 6.4. The siRNAs are ordered from left to right as decreasing percentages of cycling cells at 96 hours. All control

siRNAs for p53 and p21 are highlighted by blue and red bars respectively. In the first screen the average percentage of Venus positive cycling cells for all control siRNAs was 2.3% (standard deviation, SD 0.7%) (Figure 6.4A). The average percentage of cycling cells for p53 siRNAs was 15.5% (SD 7.2%), and for p21 siRNAs the average percentage of cycling cells was 22% (SD 9.8%), suggesting that technically the screen procedure had worked (Figure 6.4A). No siRNAs from the gene list appeared to increase the percentage of cycling cells above background levels.

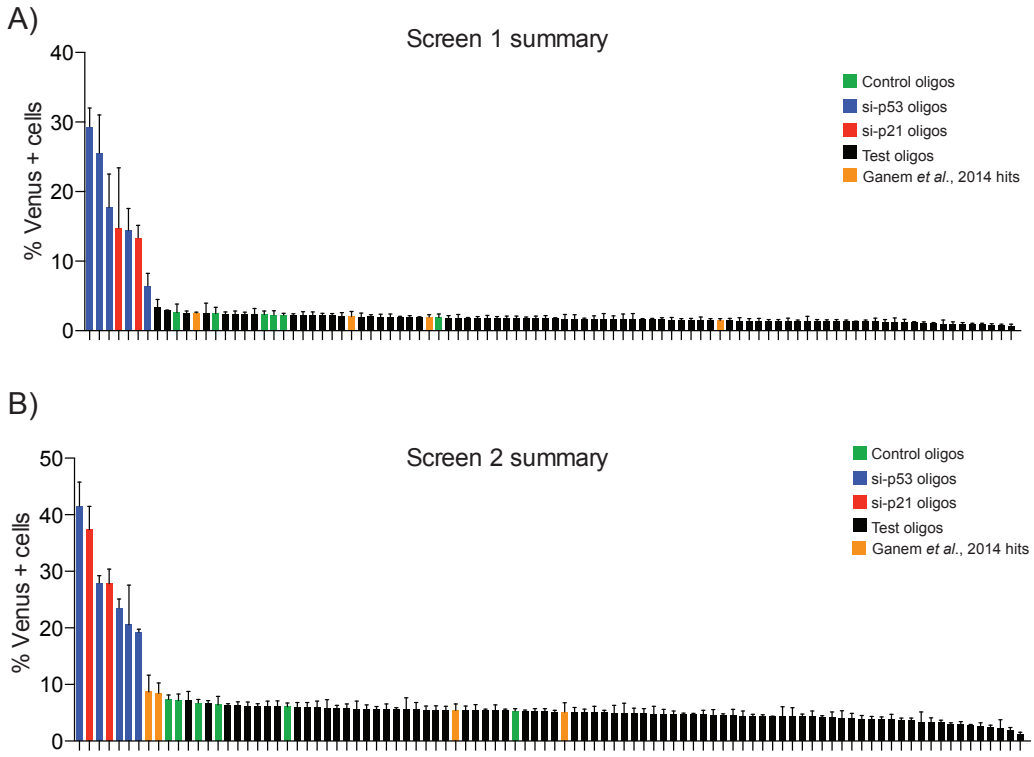

Figure 6.4: Two independent screen repeats

A) The percentage of Venus positive cells from the first screen is shown. The screen was carried out in triplicate (error bars are standard deviations from plate replicates). All p53 siRNAs are shown as blue bars, and p21 siRNAs as red bars. Six control siRNAs are shown in green (OTP Controls-1-4, si-Genome Control-5 and RISC-free). Positive controls chosen from Ganem et al., 2014 are shown as orange bars (LATS2, PTBP1, SPINT2 and DCP1A). All other siRNAs tested are shown as black bars.
B) As above, for the second screen repeat.

A second repeat of the screen was carried out, again in triplicate plates. The results of this second screen are shown in Figure 6.4B. In this repeat the average

percentage of cycling cells in control siRNAs was higher than in the initial experiment, at 6.5% (SD 1%). The average of all p53 siRNAs was 26.6% (SD 8.9%), and p21 siRNAs averaged 32.6% (SD 6%) (Figure 6.4B). This is comparable to the results obtained by Ganem and colleagues. Similarly to the first repeat, no test siRNAs (including positive controls from Ganem et al., 2014) increased the percentage of cycling cells significantly above the levels in control siRNAs, although siRNAs targeting PTBP1 and LATS2 resulted in the highest percentages of cycling cells after si-p53 and si-p21.

To investigate further the control siRNAs used from the Ganem et al., 2014 screen, individual plate data from the second experiment was examined. The percentage of cycling cells from each siRNA from each plate is shown in Figure 6.5A-C. The positive control siRNAs used from the Ganem et al., 2014 screen are each highlighted. For plates one and two there did not appear to be an effect of any of the positive control siRNAs (Figure 6.5A and B). However, in the third plate, two of the positive control siRNAs from the Ganem et al., 2014 screen appeared higher than the majority of controls. These two siRNAs were targeting LATS2 and PTPB1. The control siRNA average in the third plate was 6.9% cycling cells. LATS2 knockdown increased the percentage of cycling cells to 10.5%, and PTPB1 knockdown increased the percentage of cycling cells to 11.8%. Representative images from LATS2 and PTPB1 knockdown wells in the third plate are shown in Figure 6.5D. Although the percentage of cycling cells was not as high as the results reported in the Ganem et al., 2014 paper, the fact that two of their strongest hits were the top two siRNAs above the control siRNAs lead to speculation that the screen set up may not be optimal.

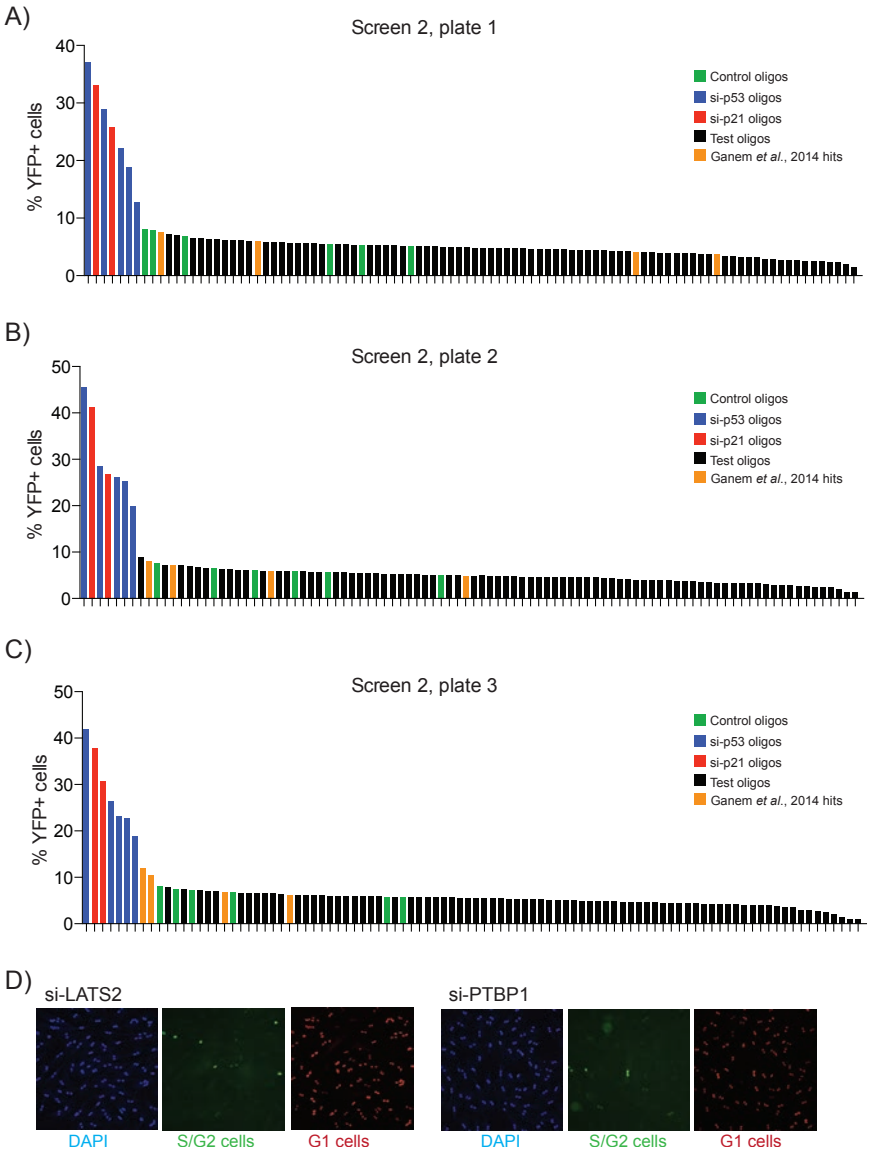

Figure 6.5: Data from each individual plate from screen 2

A-C) Data from the three plate replicates for screen 2. Control siRNAs are shown as green bars, p53 siRNAs as blue bars, p21 siRNAs as red bars and the Ganem et al., 2014 screen hits as orange bars.
D) Representative images from the plate scans of wells for LATS2 and PTPB1 siRNAs, showing the channels for DAPI, Venus (S-G2/M cells) and Cherry (G1 cells).

6.2.4 Modification of screening protocol

A further test of transfection efficiency using different transfection reagents was carried out. To assess the knockdown of genes that are relevant for the experimental set-up, knockdown efficiency of the positive control p53 and p21

siRNAs was checked after DCB treatment and the cell sorting procedure detailed in Figure 6.3A. The protein levels of p53 and p21 were examined using indirect immuno-fluorescence after 72 hours, and the average intensity of the secondary antibody compared to a control siRNA is shown (Figure 6.6). Across different concentrations of transfection reagent, the poorest knockdown was observed using Lullaby, which was the reagent used in the first two screen repeats. The most consistent knockdown for both p53 and p21 was obtained using RNAi Max reagent (Figure 6.6A and B). Furthermore, RNAi Max is the same reagent used in the Ganem et al., 2014 paper, and so it was chosen to replace Lullaby in subsequent experiments at a concentration of 0.2µL per well.

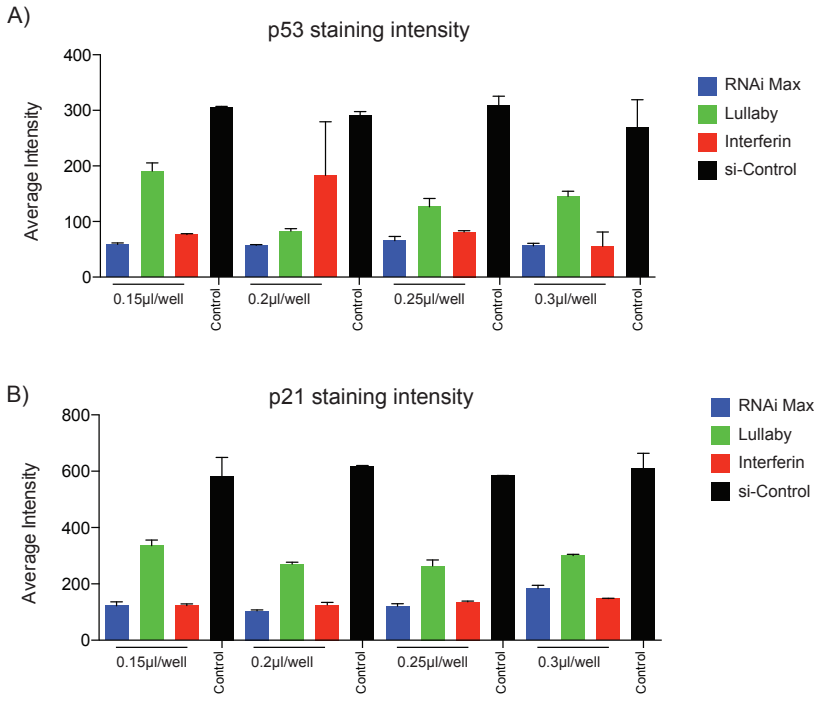

Figure 6.6: Knockdown efficiency of p53 and p21 with different reagents

A) The knockdown of p53 in 96-well plates was assessed by indirect immuno-fluorescence after 72 hours. The average intensity of p53 staining compared to control siRNAs is shown.
B) The knockdown of p21 was assessed by indirect immuno-fluorescence after 72 hours. The average intensity of p21 staining compared to control siRNAs is shown.

An additional concern with the original experimental set up was the length of the assay. After 96 hours the wells containing control p53 and p21 siRNAs were quite confluent as the cells were dividing rapidly after the cell sorting procedure.

Furthermore, the potency of some siRNAs may be diminished after 96 hours. The Incucyte imaging system (Essen Bioscience) was used to identify the best time point to fix cells after transfection. This device allows continued phase-contrast imaging at regular intervals within a tissue-culture incubator and has capability to image in the green fluorescence channel. It was therefore used to assess when RPE-FUCCI cells started to enter S phase based on Geminin-Venus expression. Importantly, it allowed temporal dissection of the effects of each siRNA, as described below.

Figure 6.7 shows at what time point after sorting and transfection individual cells started expressing Venus protein, and were hence entering S phase and subsequently G2. Each line on the graph indicates a single cell. It should be noted that because RPE cells are relatively motile, it was not possible to track individual cells for the duration of the movie and hence distinguish when an individual cell had completed G2 and stopped expressing Venus protein. Therefore although the green lines for every cell extend to the final time point (84 hours) the cell may not have been expressing Venus for the complete duration that the line depicts. RPE-FUCCI cells that had been treated with DCB but not sorted (and therefore including some G1 and G2 diploid cells as well as G1 tetraploid cells) were imaged as a control to check that the drug washout was working, and that treatment with DCB had not arrested all cells, regardless of their ploidy status. This is clearly not the case, as DCB treated but unsorted cells steadily started to enter S/G2 after 24 hours (Figure 6.7). Transfection with p21 siRNA had a striking effect, with cells synchronously entering S/G2 just 12 hours after sorting. siRNA targeting p53 had a slightly delayed effect compared to si-p21, with cells beginning to enter S/G2 after 24 hours. As expected, very few cells transfected with a control siRNA entered S/G2 after sorting, and those that did enter S/G2 did so randomly throughout the duration of imaging (Figure 6.7).

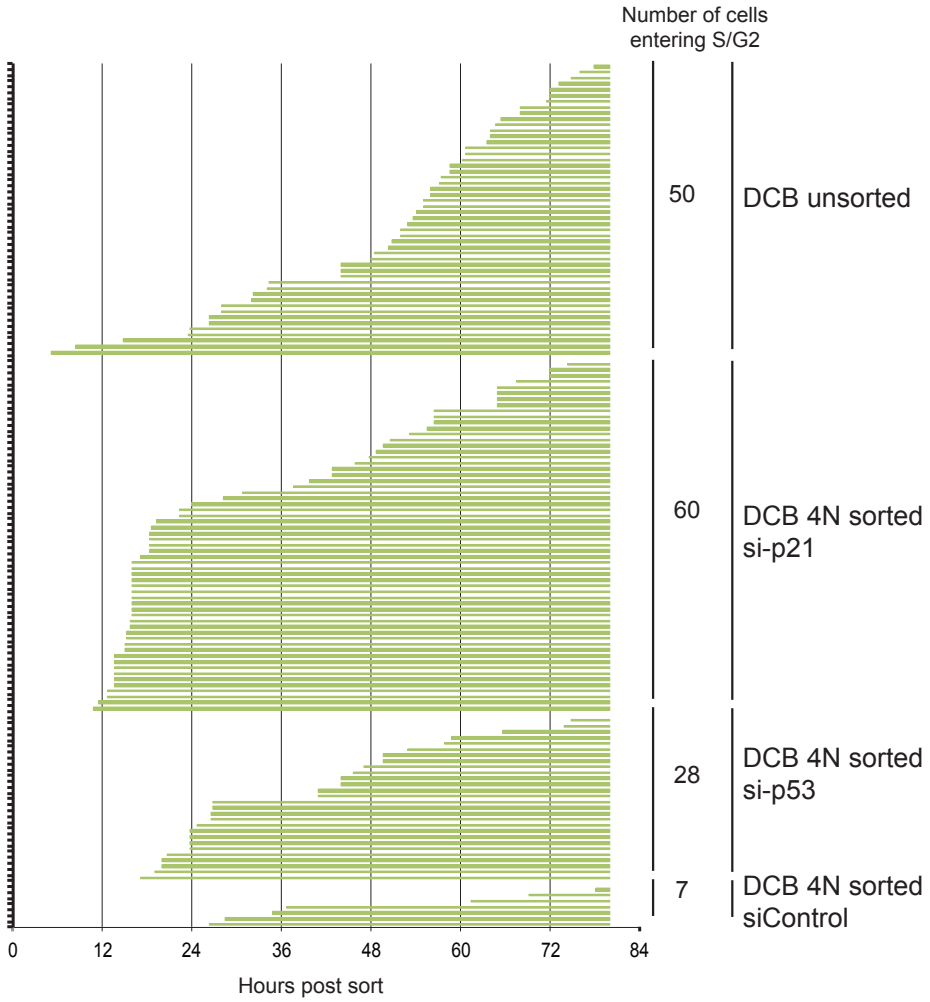

Figure 6.7: Scoring S-phase entry by live-cell imaging after cytokinesis failure

Depiction of when cells enter S phase or G2 after transfection with different siRNAs (si-p53, si-p21, si-Control) or unsorted cells that had been treated with DCB. Each horizontal line represents a single cell. The total number of cells entering S/G2 phase for the field of view scored is shown on the right hand side. Cells were imaged every 30 minutes after transfection using the Incucyte imaging system. Results were obtained by visualising the resulting movies and noting when cells start expressing Venus protein.

These results suggest that if a test siRNA has a significant effect it is likely to result in a pattern of S/G2 phase entry that is somewhere between the S/G2 phase entry patterns obtained from si-p21 and si-p53 cells and control transfected cells. If the knockdown of a particular test siRNA was having a substantial effect in a large proportion of cells, the cells should enter S/G2 in a more synchronised manner compared to control cells (since the cells begin the assay synchronised in G1). However, this is unlikely to occur as quickly as it does for p21 and p53 knockdown.

A further concern with the original screening set up used was that no test siRNAs had an effect because the arrest imposed by the DCB treatment was too harsh, and only knockdown of the two most potent cell cycle regulators (p53 and p21) could overcome it. This issue was addressed in Figure 6.7, where DCB treated, but not sorted, cells were imaged and observed to enter S/G2 after 24 hours. However previous studies have indicated that arrest after cytokinesis failure can be overcome by changing cell culture conditions and the concentration of the drug used to induce the failure (Uetake and Sluder, 2004, Wong and Stearns, 2005, and see Section 1.6). Specifically it was shown that the drugs used to induce cytokinesis failure were responsible for the damage that resulted in cell cycle arrest (Wong and Stearns, 2005), and that reducing the concentrations of those drugs or changing the culture conditions by coating the culture surface with Fibronectin could abrogate the arrest (Uetake and Sluder, 2004). To address these points in the cell line system that was being used for the screen, an experiment was carried out to see whether DCB concentration or Fibronectin coating of the plates would affect cell cycle arrest.

Cells were treated with three different concentrations of DCB (4, 2 and 0.5μM) and either sorted using Hoechst staining for 4N tetraploid cells in G1 (as described in Figure 6.3A) or not sorted (therefore containing a mixture of diploid cells in G1 and G2, as well as 4N G1 tetraploid cells). Cells were plated into normal uncoated plates, or plates coated with Fibronectin. The Incucyte imaging system was used to assess when cells entered S/G2, and it was noted whether those cells were mononucleated or binucleated using the phase contrast images. The total number of cells for each field of view was also noted, and so the number of cycling cells is expressed as a percentage in Figure 6.8A and B.

The addition of Fibronectin did not result in a clear abrogation of the arrest after cytokinesis failure in binucleated cells (Figure 6.8B). Although in some conditions it did increase the percentage of cycling binucleated cells, this was not consistent across all the different combinations (for example there was a decrease in cycling cells in the 4μM sorted condition with Fibronectin). Furthermore the increases observed in the other conditions were quite modest, and do not indicate that Fibronectin can completely rescue cell cycle arrest after cytokinesis failure, as had

been previously reported (Uetake and Sluder, 2004). Due to difficulties in controlling for the even coating of Fibronectin across multiple plates, and its modest effect on the percentage of cycling cells, plates were left uncoated in subsequent experiments.

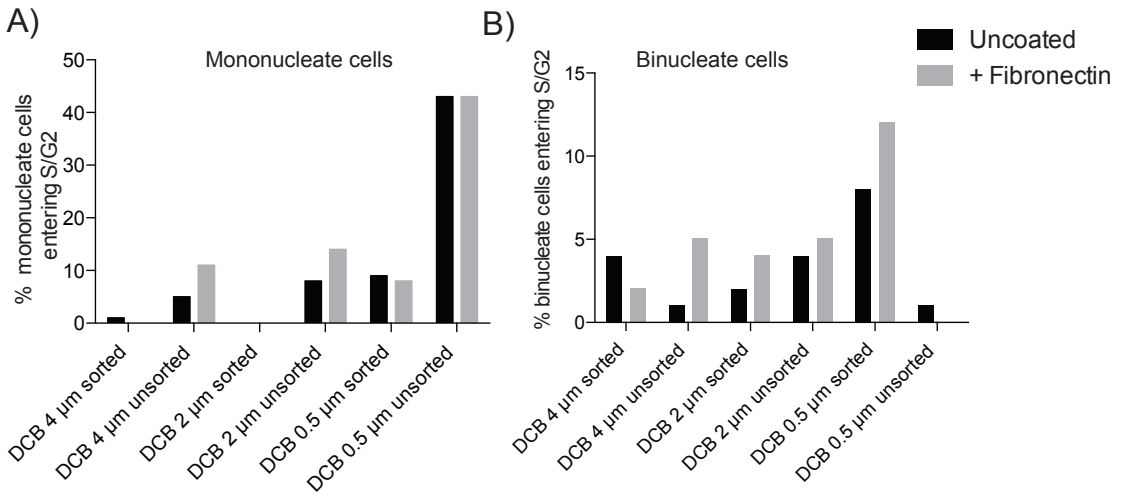

Figure 6.8: Effect of DCB concentration and Fibronectin coating on cell cycle arrest

A) Different concentrations of DCB were used to arrest cells. Cells were either sorted for only 4N G1 tetraploids, or unsorted, and plated into uncoated plates or plates coated with Fibronectin (indicated by the colour of the bars – see key). The percentage of mononucleate cells entering S/G2 is shown.
B) The percentage of binucleated cells entering S/G2 in the same conditions is shown.

The different drug concentrations also did not have markedly differing effects in terms of their ability to arrest cells. The difference in percentage of cycling binucleated cells between 4µM and 2µM DCB was only 2%. Only 0.5µM treated cells had a slight increase of 4% compared to 4µM (Figure 6.8B). However, the formation of binucleated tetraploid G1 cells was very inefficient when treating with 0.5µM DCB (as evidenced by the high percentage of mononucleated cycling cells in the unsorted condition), and therefore this concentration could not be used in subsequent experiments. The differences in cycling mononucleated cells between the different drug concentrations in unsorted cells are more likely to reflect the differences in number of mononucleated cells after the treatment, as opposed to higher concentrations of drug inhibiting cell cycle re-entry (Figure 6.8A). Taken

together, these results suggest that lowering the concentration of DCB does not completely abrogate the cell cycle arrest. However, in order to mitigate against this possibility, 2μM DCB was used for subsequent experiments, as binucleated cells still underwent cell cycle arrest with the same efficiency as 4μM treated cells (Figure 6.8B).

6.2.5 Screen repeat using new conditions

After the above modifications to the screening protocol the screen was repeated. Cells were treated with 2μM DCB, and the transfection reagent used was RNAi Max instead of Lullaby. In order to be sure that no positive hits were missed due to fixation at 96 hours, plates were continuously imaged using the Incucyte system, and plates were fixed at intervals throughout the screening. In this screen OTP Control siRNAs 1-4 and si-Genome Control-5 were used. In addition, new pooled siRNAs were ordered for LATS2, the strongest tetraploid specific hit in the Ganem et al., 2014 screen. The results of this screen repeat are shown in Figure 6.9. The three plates were fixed at 36, 50 and 74 hours (Figure 6.9A-C). Again, siRNAs are ordered from left to right as the number of cycling cells decreased.

At 36 hours the highest number of cycling cells was found in wells transfected with si-p21 (Figure 6.9A). Although the Ganem et al., 2014 positive controls were towards the left hand side of the graph (more cycling cells), they were not significantly higher than the control siRNAs at this time point. At 50 hours the highest percentages of cycling cells were found in wells transfected with p53 siRNA (Figure 6.9B). These data confirm what was observed using live cell imaging; that p21 knockdown induces the most rapid cell cycle re-entry and p53 transfected cells are approximately 12 hours delayed compared to si-p21 transfected cells (Figure 6.7).

In the plate fixed at 50 hours, two of the Ganem et al., 2014 screen hits resulted in the highest percentage of cycling cells apart from p53 and p21 knockdown (si-LATS2 = 5.29% cycling cells, siPTBP1 = 4.47%), along with two siRNAs from the gene list. These two genes were KCNA5 (5.05%) and CNGB3 (4.96%). At the final time point of 74 hours, three of the Ganem et al., 2014 hits were the next highest in

terms of cycling cells after p53 and p21 knockdown (Figure 6.9C). However at this time point there was little difference between these siRNAs and other test siRNAs, with the graph showing a smooth decrease from left to right.

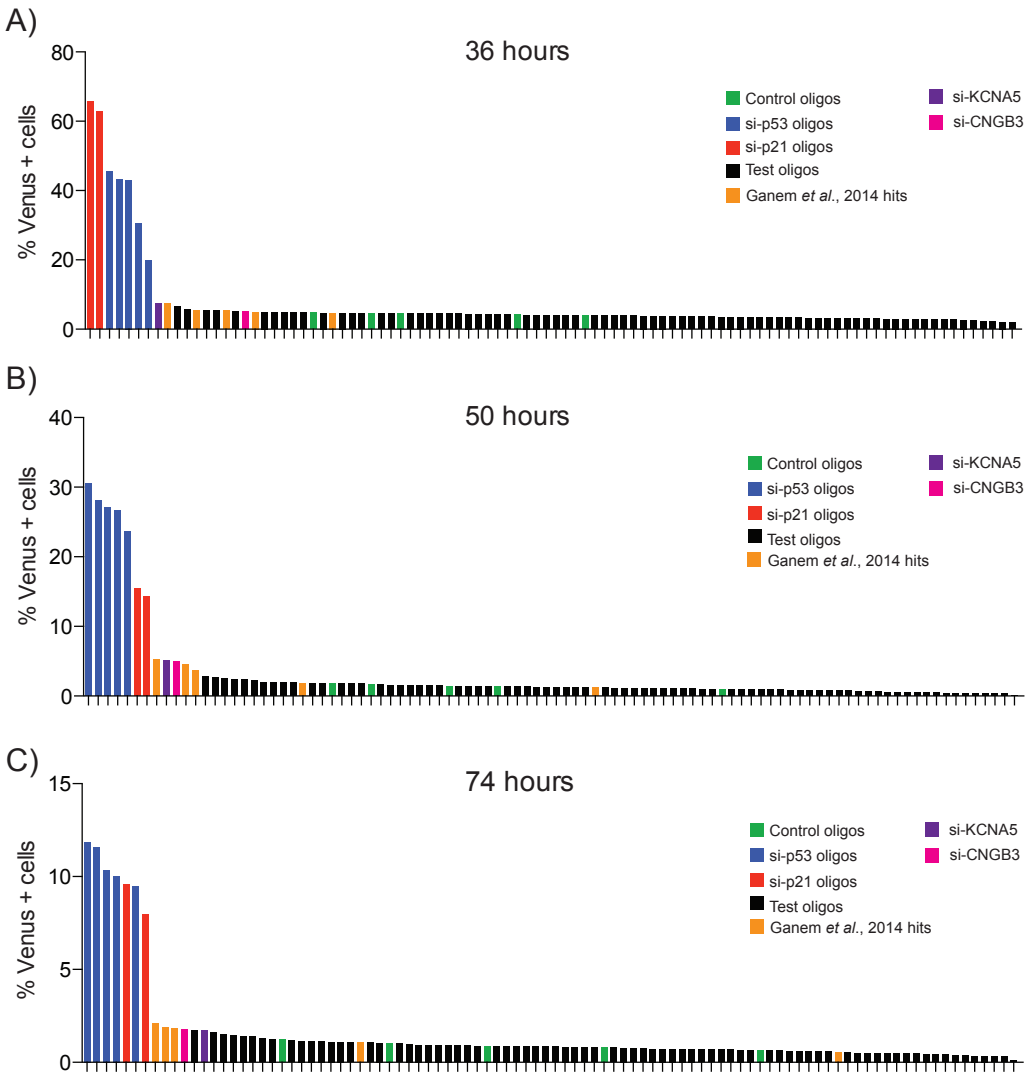

Figure 6.9: Screen repeat with new conditions

A) The percentage of Venus expressing cells for each siRNA at 36 hours. Control siRNAs are shown as green bars, p53 siRNAs as blue bars, p21 siRNAs as red bars and the Ganem et al., 2014 screen hits as orange bars. Two novel candidates, KCNA5 (purple bars) and CNGB3 (pink bars), are also shown.
B) As above, for the plate fixed at 50 hours.
C) Results for the plate fixed at 74 hours.

Images were obtained from the plate fixed at 50 hours, and examples from cells treated with a control siRNA, p53 and p21 siRNAs, as well as control siRNAs from the Ganem et al., 2014 paper, and images from si-CNGB3 and si-KCNA5 treated

cells are shown in Figure 6.10. It is clear from these images that siRNAs targeting KCNA5 and CNGB3 resulted in increases in cycling cells at least as great as the best positive controls from the Ganem et al., 2014 screen (LATS2 and PTPB1) (Figure 6.10B and C). Although the effects of gene knockdown of KCNA5 and CNGB3, as well as the Ganem et al., 2014 positive controls were modest, they all resulted in increases in the percentage of cycling cells above background levels. This prompted further investigation of these two novel candidates.

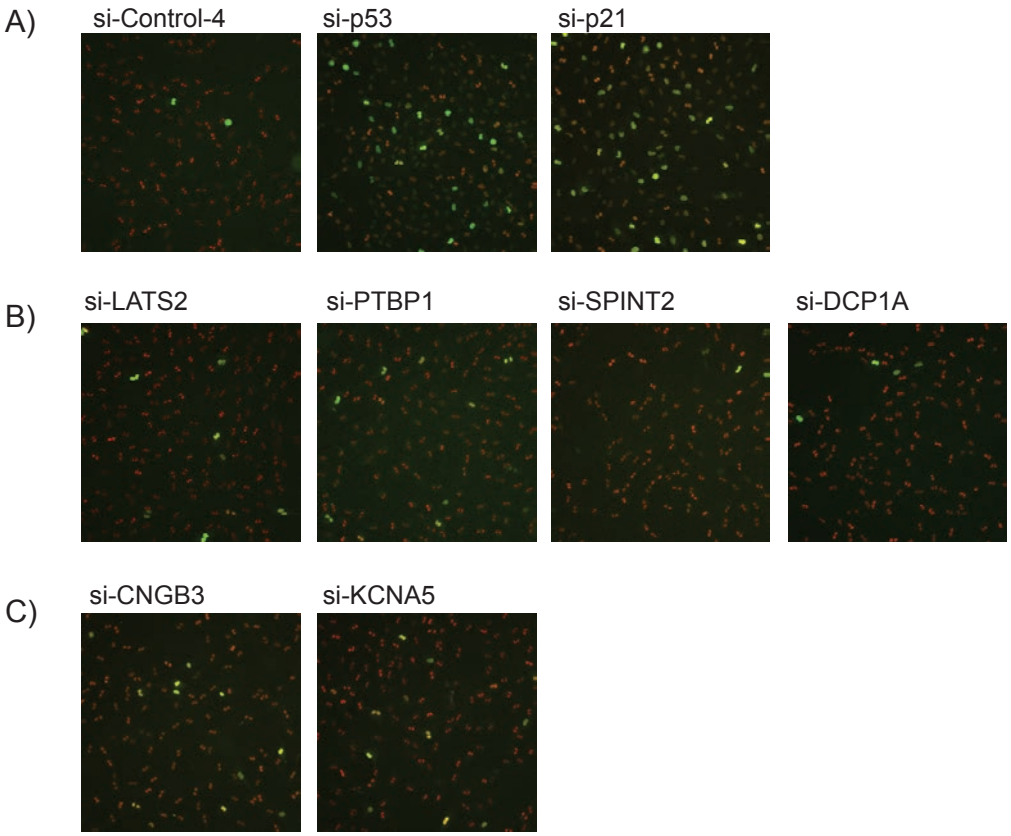

Figure 6.10: Images from screen repeat with new conditions, fixed at 50 hours

A) Representative images from control wells of plate fixed at 50 hours after transfection. G1 cells appear as red, and S/G2 cells appear green. The effects of using STLC to arrest mitotic cells can be clearly observed in the si-p21 panel, as many cells are arrested in mitosis (see Methods).
B) Images from positive controls taken from the Ganem et al., 2014 screen.
C) Images from CNGB3 and KCNA5 transfected cells at 50 hours.

6.2.6 Deconvolution of screen hits

Given these intriguing results, it was decided to take KCNA5 and CNGB3 forward for deconvolution screening. As the screen was carried out with a pool of 4 individual siRNAs, it was important to test these siRNAs individually to mitigate against off-target effects. Deconvolved siRNAs from these two genes were ordered from Dharmacon, and the screen was carried out again, this time fixing plates at 50 hours and 74 hours. The results of this experiment are shown in Figure 6.11.

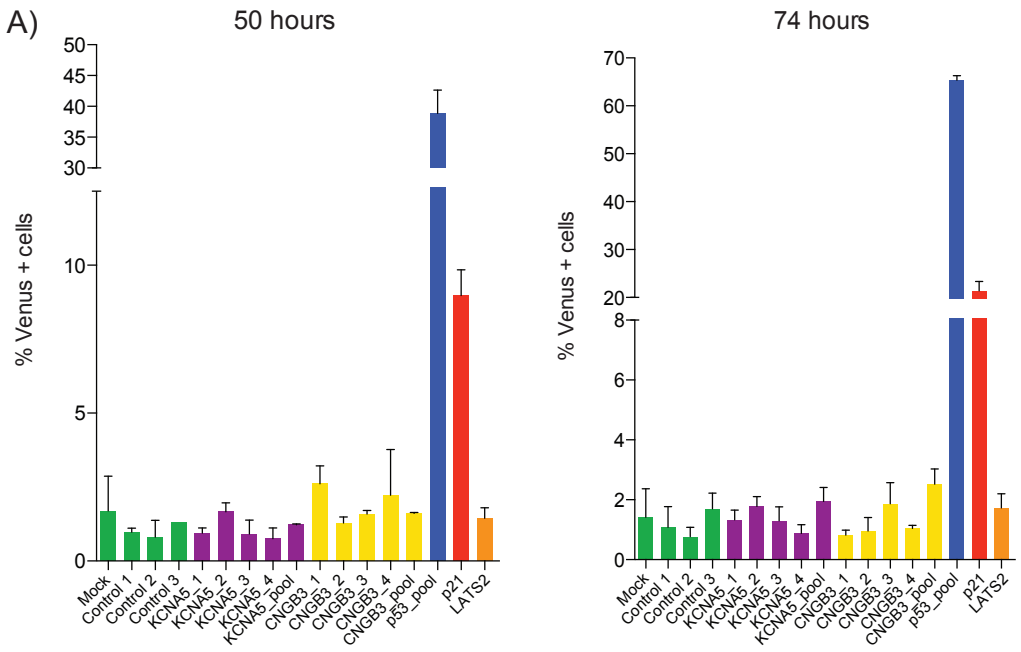

Figure 6.11: Deconvolution of KCNA5 and CNGB3

A) Analysis of percentage of Venus positive cycling cells 50 hours after siRNA transfection of two potential screen hits. Control siRNAs are shown in green, KCNA5 siRNAs in purple, CNGB3 siRNAs in yellow, p53 siRNAs in blue, p21 siRNAs in red, and LATS2, a positive control from the Ganem et al., 2014 screen, in orange. The y-axis is split as p53 results in a much higher percentage of cycling cells than the rest of the siRNAs.
B) As in A, but 74 hours after transfection. The y-axis is split as both p53 and p21 knockdown results in a much higher percentage of cycling cells than the rest of the siRNAs.

At 50 hours after siRNA transfection, the average percentage of cycling cells was 1.2% (SD 0.7%) for all control siRNAs, including a mock transfected well (Figure 6.11A). None of the KCNA5 siRNAs, including the pool, raised the percentage of cycling cells significantly. The largest increase was noted for KCNA5_siRNA2 that

resulted in 1.67% cycling cells. CNGB3 siRNAs resulted in slightly higher percentages of cycling cells, with siRNAs 1 and 4 increasing the percentage of cycling cells above 2%. LATS2 knockdown resulted in 1.44% of cycling cells. At 74 hours there was also little increase caused by either KCNA5 or CNGB3 siRNAs (Figure 6.11B). The average percentage of cycling cells for all control siRNAs (including mock transfected cells) was 1.24% (SD 0.7%). None of the KCNA5 siRNAs increased the percentage of cycling cells above 2%. Only the CNGB3 pool of siRNAs increased the percentage of cycling cells to 2.5%. LATS2 knockdown only increased the percentage of cycling cells to 1.7%. In order to make sure the knockdown of KCNA5 and CNGB3 was working efficiently in the conditions used, the levels of mRNA after transfection with siRNAs against each of these genes was assessed using qPCR (Figure 6.12).

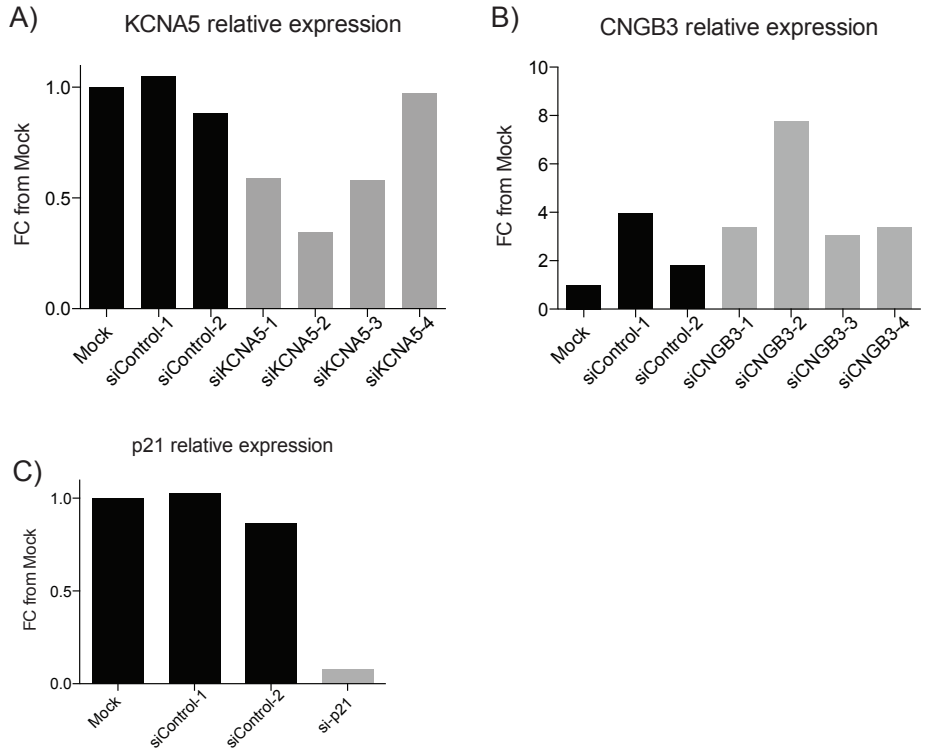

Figure 6.12: qPCR of mRNA levels after knockdown of target genes

A) Comparative qPCR of mRNA levels of KCNA5 relative to the housekeeping gene β-actin. Average cycle number for mock and control transfected samples: 34.8.
B) As in A) but for CNGB3. Average cycle number for mock and control transfected samples: 36.2.

C) Positive control showing relative p21 knockdown in the same experiment. Average cycle number for mock and control transfected samples: 19.9.

Figure 6.12A shows the relative expression of KCNA5 after knockdown with each of the individual siRNAs. Only KCNA5_siRNA2 results in a reduction in mRNA levels to less than 50% of the level observed in mock transfected wells. However this is the same siRNA that showed the greatest increase in the percentage of cycling cells in the deconvolution screen (Figure 6.11). These results suggest that KCNA5 could have a role in allowing cell cycle re-entry after cytokinesis failure, however the levels of knockdown achieved with the reagents available was likely not sufficient to result in large increases in the fraction of cycling cells. Only better knockdown conditions could help rule out an effect of KCNA5 on this cell cycle checkpoint.

The relative expression of CNGB3 after knockdown of each individual siRNA is shown in Figure 6.12B. This shows that no knockdown was achieved with any of the siRNAs used against CNGB3. This could be due to the apparently low expression of CNGB3 within RPE cells, as the cycle number in qPCR was almost 37 cycles. This low abundance could mean that the results obtained in Figure 6.12B represent noise rather than real changes in expression of CNGB3 after knockdown. A positive control of p21 expression after knockdown from the same experiment is also shown in Figure 6.12C.

In order to investigate the knockdown efficiency of LATS2 siRNAs, the positive control identified from the Ganem et al., 2014 screen, the levels of mRNA for this gene were also checked after 72 hours of siRNA mediated knockdown. The results of this analysis are shown in Figure 6.13A. Two out of four siRNAs (siRNAs 1 and 2) for LATS2 gave a fairly efficient knockdown, reducing the levels of mRNA to less than 20% of that found in control cells. These are the same two siRNAs reported by Ganem et al., 2014 to give the best knockdown in their screening procedure (Ganem et al., 2014). The knockdown of two positive controls p21 and p53 was also efficient in this experiment (Figure 6.13B).

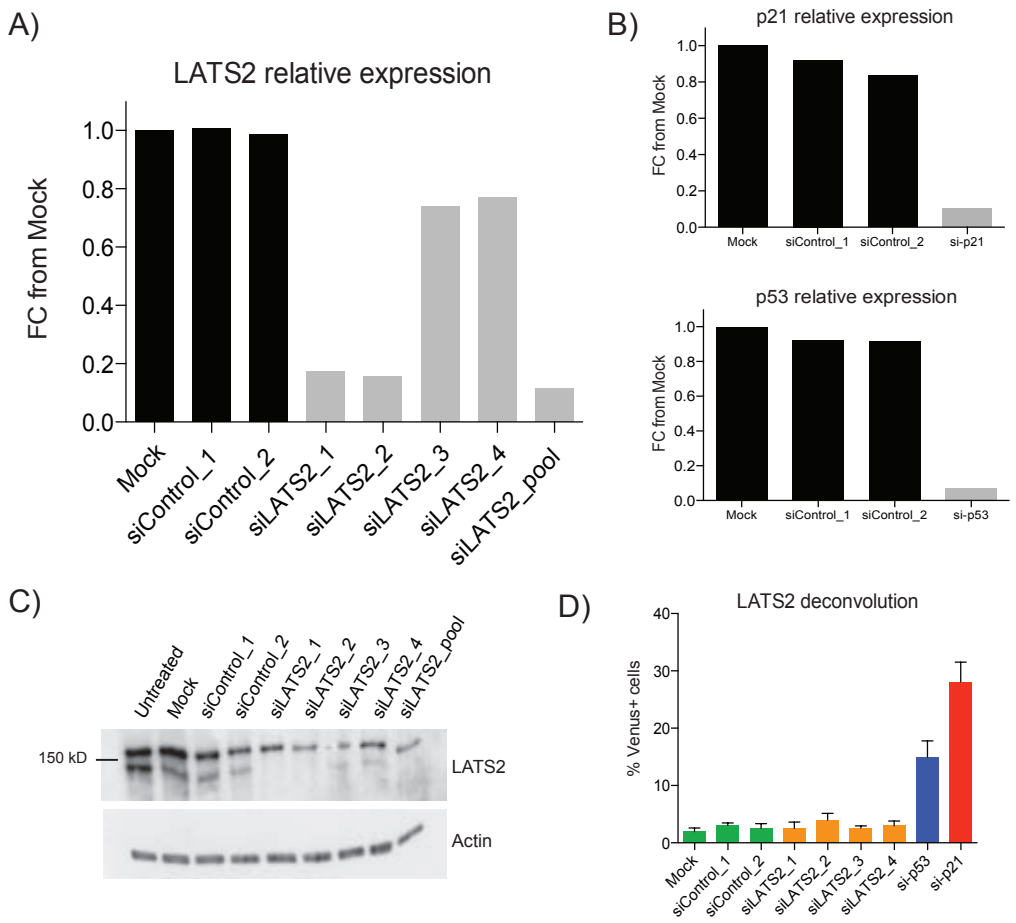

Figure 6.13: mRNA and protein validation of knockdown for LATS2

A) The expression of LATS2 relative to housekeeping gene β-actin after control transfection and transfection of the deconvolved pool of OTP LATS2 oligos. Average cycle number of LATS2 in control sample: 22.7.
B) Expression of two positive controls (relative to housekeeping gene β-actin), p21 and p53 after knockdown in the same experimental repeat as in A.
C) Detection of LATS2 protein after knockdown. Actin is used as a loading control.
D) Repeat of the screening procedure with each individual LATS2 oligo. The percentage of Venus positive cycling cells is shown after fixed plate analysis at 96 hours.

The knockdown efficiency was also examined by assessing LATS2 protein levels after 72 hours (Figure 6.13C). The lower band detected by the LATS2 antibody mirrors the results of the qPCR, with LATS2 siRNAs 1 and 2 resulting in the best knockdown. There is still residual protein visible for LATS2 siRNAs 3 and 4 at the level of the lower band. Each deconvoluted siRNA was used in a repeat of the original screening procedure as described in Figure 6.3A, but using RNAiMax as the transfection reagent. None of the individual LATS2 siRNAs increased the level of cycling cells significantly above that of control wells (Figure 6.13D).

6.3 Conclusions

Taken together these results suggest that the results of the screen were likely to have been influenced by two main factors. Firstly, the knockdown efficiency of each gene tested could not be controlled for within the screen. Although when setting up the transfection conditions three different approaches were taken (using LaminA/C, p53 and p21 knockdown followed by indirect immuno-fluorescence), the knockdown efficiency, even of control genes, could not be tested in every subsequent plate replicate. Furthermore, the knockdown of p53 and p21 is likely to be very efficient, as these genes are commonly targeted using siRNA, and therefore the siRNA sequences are being frequently modified and improved. Furthermore, both these proteins are turned over at a high rate, so knockdown using siRNA has a rapid effect. The results from the transfection efficiency test using these genes could therefore have given 'false positive' results. The knockdown efficiency of other genes, for example KCNA5, was not as efficient using the same transfection conditions (Figure 6.12). Secondly, the expression of some of the test genes in RPE cells might be low, and therefore knockdown is unlikely have a reproducible effect. This is possibly the case for both CNGB3 and KCNA5 (Figure 6.12).

Although the knockdown efficiency appeared good for two out of four siRNAs targeting LATS2, as well as the pool, this level of knockdown was not sufficient to elicit an effect on cell cycle re-entry after cytokinesis failure (Figure 6.13A and D). Even in three replicate plates, only one plate showed a significant difference in percentage of cycling cells after LATS2 knockdown and the other two plates did not (screen 2, Figure 6.5). This could suggest that LATS2 is a difficult gene to knock down consistently. However, both mRNA and protein levels suggested a reasonable level of knockdown with the reagents used in the screen, and although the knockdown could not be directly tested within the screen format, these results suggest that LATS2 is not a potent regulator of cell cycle arrest after cytokinesis failure.

Technically, the set up and screening procedure worked well. This is evidenced by the fact that knockdown of the positive controls p53 and p21 consistently resulted

in high numbers of cycling cells. As the initial screen, following the protocol as published in Ganem et al., 2014, did not result in any positive hits, the screen was modified in a logical fashion, following reports in previous papers regarding the use of cytokinesis inhibitors to arrest cells (Uetake and Sluder, 2004, Wong and Stearns, 2005). Only two weak positive hits were identified using the modified screening protocol, KCNA5 and CNGB3. *CNGB3* is an ion channel gene, encoding cyclic nucleotide gated channel beta 3. This gene was included in the screen as it is significantly mutated in GD lung adenocarcinoma, and overlapped with an extended list of genes identified in a screen for segregation error tolerance (Table 6.1). However, the knockdown of CNGB3 using deconvoluted siRNAs could not be validated, possibly due to low expression of CNGB3 in RPE cells.

KCNA5 encodes a potassium channel subunit (potassium channel, voltage gated shaker related subfamily member 5, Kv1.5). KCNA5 was included in the screen as it is significantly mutated in GD colon adenocarcinoma (Table 6.1). Intriguingly, the altered expression of potassium channels has been linked to various hallmarks of carcinogenesis, including increased proliferation and resistance to cell death (Huang and Jan, 2014). A recent study showed that KCNA5 expression was repressed in aggressive cancer cells due to polycomb protein epigenetic repression (Ryland et al., 2014). The repression of KCNA5 allowed cancer cells to survive under hypoxic stress conditions. These results implicate the Kv1.5 potassium channel as a mediator of apoptosis under hypoxic stress conditions (Ryland et al., 2014). The knockdown of KCNA5 using the available OTP siRNAs in the screen was potentially not sufficient to result in completely non-functional potassium channels. However, the deconvolved siRNAs that resulted in the best knockdown of the gene at the mRNA level also resulted in the greatest number of cycling cells after DCB treatment (Figure 6.11, Figure 6.12). Given the link between KCNA5 loss of expression and cancer cell survival under stressful conditions, it would be of interest to use different methods to impair potassium channel functionality (Ryland et al., 2014). This could include testing the efficacy of Kv1.5 specific inhibitors such as DPO-1 (diphenyl phosphine oxide-1) and 4'AP (4'aminopyridine) in allowing cells to start cycling after DCB treatment (Stump et al., 2005, Fedida et al., 1996).

In conclusion, from a gene list selected from tumour relevant mutations, no genes were found to have a significant or reproducible effect on cell cycle re-entry after cytokinesis failure. Despite this, the list of genes may still be relevant to the evolution of GD tumours. It may be that mutation of these genes occurs after genome duplication, rather than as a tolerance mechanism for the initial tetraploidisation event. Alternatively these gene mutations could be beneficial for the proliferation of tetraploid cells. Interestingly the list of gene mutations that were screened had a strong bias towards genes that were annotated as integral to membrane function or to the extracellular matrix. This is shown in Table 6.2, where the entire list of genes screened was subject to gene-set enrichment analysis (GSEA), using a publically available web-based tool from the Broad Institute (Subramanian et al., 2005, Mootha et al., 2003). This could indicate a deregulation of normal membrane function in genome-doubled tumours. It would be interesting to investigate this potential link further.

Table 6.2: GSEA of selected gene list

Gene Set Name	GO Term	# Genes in Gene Set (K)	# Genes in Overlap (k)	k/K	p-value
PLASMA_MEMBRANE_PART	GO:0044459	1158	14	0.0121	3.57E-09
PLASMA_MEMBRANE	GO:0005886	1426	15	0.0105	5.95E-09
MEMBRANE_PART	GO:0044425	1670	16	0.0096	6.41E-09
MEMBRANE	GO:0016020	1994	17	0.0085	1.12E-08
PROTEINACEOUS_EXTRACELLULAR_MATRIX	GO:0005578	98	6	0.0612	1.22E-08
EXTRACELLULAR_MATRIX	GO:0031012	100	6	0.06	1.38E-08
INTEGRAL_TO_MEMBRANE	GO:0016021	1330	14	0.0105	2.03E-08
INTRINSIC_TO_MEMBRANE	GO:0031224	1348	14	0.0104	2.40E-08
EXTRACELLULAR_MATRIX_PART	GO:0044420	57	5	0.0877	3.45E-08
INTEGRAL_TO_PLASMA_MEMBRANE	GO:0005887	977	12	0.0123	4.46E-08

Chapter 7. Discussion

Tetraploid cells have long been observed in pre-malignant conditions such as Barrett's oesophagus, and the theory that tetraploidy could result in the aneuploidy that is a hallmark of cancer has persisted for decades (Shackney et al., 1989, Galipeau et al., 1996). A landmark study by the Pellman laboratory was the first to show that experimental tetraploidisation could directly lead to tumourigenesis (Fujiwara et al., 2005). However, it is only over the last three years that the prevalence of tetraploidisation events across the majority of solid tumour types has begun to be appreciated (Carter et al., 2012, Zack et al., 2013). It appears that whole genome duplications can occur at many different points in a tumour's evolutionary history, and the relevance of these whole genome duplications are now the subject of intense study from many different laboratories. This thesis has contributed to the understanding of the consequences of tetraploidisation by demonstrating that tetraploid cells are able to propagate CIN and contribute to on-going tumour evolution. As such, it is likely that tetraploidy influences the development of intra-tumour heterogeneity, one of the major challenges facing cancer medicine.

7.1 Tetraploid cells exhibit chromosomal instability

In this thesis an isogenic system of diploid and tetraploid clones derived from the microsatellite unstable cell line HCT-116 has been used to investigate the effect of genome duplication on chromosomal stability over time. All tetraploid clones showed consistently increased levels of both numerical and structural chromosome aberrations compared to diploid clones over 18 months of continuous culture. Analysis of genomic copy number changes over time in diploid and tetraploid clones revealed that tetraploid cells developed high levels of instability, comparable to that which is observed in CIN+ CRC.

These results support previous studies that have shown that genomic instability emerges after experimentally induced tetraploidisation (Fujiwara et al., 2005, Davoli and de Lange, 2012). In contrast to these studies, the tetraploid cells examined in

this thesis were naturally occurring, and therefore the increased chromosomal instability is unlikely to have been caused by the experimental procedure used to generate tetraploid clones. Indeed, it has been shown that using cytochalasins to induce cytokinesis failure can result in DNA damage (Wong and Stearns, 2005). Although the mechanism by which the tetraploid cells arise in HCT-116 was not investigated, it is likely that tetraploid cells arise stochastically and at a low frequency in many tumour cell populations. Understanding the consequences of naturally occurring tetraploidisation events for genomic stability within a tumour cell population was one of the principal aims of this thesis.

The level of both segregation errors and structural aberrations was calculated on a per cell and per chromosome basis. This analysis has shown that tetraploidy does not initiate an increase in chromosomal instability above that which would be expected given the increased number of chromosomes in this cell line. The study by Fujiwara and colleagues shows a similar result using tetraploid MMECs, as diploid MMECs also had high levels of aneuploidy and translocations that increased over time, but the level of these aberrations was always higher in tetraploid MMECs (Fujiwara et al., 2005). Given that HCT-116 cells show evidence of segregation errors and structurally abnormal chromosomes, neither this nor the study by Fujiwara and colleagues directly addresses whether tetraploidy can induce CIN in a stable cell line (Fujiwara et al., 2005). It would be of great interest to extend this study to stable diploid cell lines in which the driving mechanisms of CIN were not already present. However this presents difficulties, as stable diploid cell lines are unlikely to contain naturally occurring tetraploid cells. A recently published study has used the approach of inducing cytokinesis failure to study the effects of tetraploidisation on a stable diploid cell line. Kuznetsova and colleagues treated the stable diploid cell line RPE-1 with cytochalasin D, and isolated rare clones that were tetraploid after this treatment (Kuznetsova et al., 2015). One out of three RPE-1 tetraploid clones showed an increase in segregation errors, suggesting that tetraploidy can also result in chromosomal instability in non-transformed diploid cells, albeit with lower frequency than in diploid cancer cells (Kuznetsova et al., 2015).

The frequency of different types of chromosome missegregation events was also compared between diploid and tetraploid cells. This analysis showed that there was no difference in the frequency of errors thought to arise through either mitotic (lagging centric chromosomes) or pre-mitotic (chromosome bridges and acentric chromosome fragments) mechanisms. This suggests that, in this system of diploid and tetraploid clones, there is not a tetraploid-specific mechanism that results in an increase in any one type of segregation error. The same result was obtained by Kuznetsova and colleagues in their analysis of segregation error profiles of tetraploid clones derived from cytochalasin D treatment of HCT-116 cells (Kuznetsova et al., 2015). However, the authors did find that the frequency of segregation errors in tetraploid HCT-116 clones was increased above the increase in chromosome number observed in tetraploid clones. This is in contrast to work presented in this thesis that shows that segregation error frequency in HCT-116 tetraploid clones is likely to be a consequence of the total increase in number of chromosomes. Interestingly the frequency of mitotic errors reported in parental HCT-116 cells in the above study is significantly lower than that reported in this thesis, as well as in other studies (Janssen et al., 2009, Bakhoum et al., 2014, Thompson and Compton, 2008). This potentially illustrates different sub-clones of HCT-116 that are used by different laboratories, as well as different scoring bias. Furthermore, the percentage of anaphases in cytochalasin D derived tetraploid cells displaying segregation errors is significantly lower than was observed in naturally occurring HCT-116 tetraploid cells. These differing results could suggest that different mechanisms of forming tetraploid cells result in different levels of chromosomal instability.

All tetraploid clones were found to have supernumerary centrosomes, the number of which was rather heterogeneous both within and between clones. Despite the increase in centrosomes no increase in lagging centric chromosomes was observed in tetraploid clones. This is in contrast to previous studies that have shown that extra centrosomes can cause chromosome segregation errors through the promotion of improper kinetochore-microtubule attachments (Ganem et al., 2009, Silkworth et al., 2009). As the parental cell line, HCT-116, also contains a relatively high frequency of cells with supernumerary centrosomes, it is likely that efficient mechanisms for clustering extra centrosomes already exist in this cell line,

and hence its tetraploid derivatives. The number of centrosomes were analysed at both early and late passage (after a year of continuous culture), and no difference in the frequency of supernumerary centrioles was observed in tetraploid cells over time. This further supports the assertion that supernumerary centrioles are not detrimental to tetraploid clones, as otherwise a selection for cells with lower numbers of centrioles would have been expected to occur over the culture period. Many cancer cells exhibit supernumerary centrioles (Nigg, 2002, Lingle et al., 1998, Pihan et al., 1998). However, whether the presence of extra centrioles always causes increases in chromosome missegregation in tumours is not yet known, although centriole number has been shown to correlate with CIN in cell lines and human tumours (Kramer et al., 2003, Koutsami et al., 2006, Levine et al., 1991, Pihan et al., 2001, Ghadimi et al., 2000). This study has shown that the presence of extra centrioles is not always linked to an increase in segregation errors. The ability of cells to efficiently cluster extra centrosomes without an increase in segregation errors may be required in MIN cell lines such as HCT-116, to restrain the amount of genetic instability. Indeed, it has been shown that increasing the number of centrioles in HCT-116 will only cause an increase in CIN when coupled with deregulation of the key mitotic kinase Aurora A (Lentini et al., 2007). Further, MIN diploid CRC tumours tend to have fewer supernumerary centrosomes than CIN+ CRC (Pihan et al., 2001, Ghadimi et al., 2000), suggesting that there may be selection against centrosome amplification in MIN tumours. The study by Kuznetsova and colleagues also showed that the number of centrosomes does not directly influence the level of chromosome missegregation, as two tetraploid RPE-1 clones had similar numbers of extra centrosomes, but only one clone displayed an increase in segregation errors (Kuznetsova et al., 2015). These intriguing data support the observations made in this thesis, and suggest that segregation errors are not an obligatory consequence of supernumerary centrosomes.

7.2 Tetraploid cells tolerate chromosome missegregation

Clonal FISH assays and live cell imaging using H2B-mRFP expressing cells have shown that HCT-116 tetraploid cells are better able to survive after segregation errors than diploid cells. This result sheds light on the frequent observation of

aneuploidy arising as a consequence of tetraploidisation in tumours as well as in vitro studies (Galipeau et al., 1996, Olaharski, Lv et al., 2012, Fujiwara et al., 2005, Davoli and de Lange, 2012). This result has recently been confirmed by Kuznetsova and colleagues, who also showed that tetraploid clones, derived from cytochalasin D treated HCT-116 cells also less frequently died or underwent cell cycle arrest after segregation errors than diploid cells (Kuznetsova et al., 2015).

Attempts to find a mutational mechanism for this segregation error tolerance did not reveal any mutations common to all tetraploid clones. It is possible that different mutational mechanisms for tolerating chromosome missegregation are present in different tetraploid clones. Using a cell line that was microsatellite unstable also complicated this analysis, as HCT-116 cells acquire mutations at a high frequency. Therefore many mutations that were identified are unlikely to have been positively selected for, but rather occurred by chance. It would be of great interest to repeat this sequencing analysis in tetraploid clones derived from a microsatellite stable diploid cell line. Future work will focus on profiling tetraploid cells derived from the microsatellite stable diploid colon cancer cell line C-99.

No mutations were found in either p53 or p21, which would be expected to allow tolerance to chromosome missegregation (Thompson and Compton, 2010, Li et al., 2010, Kumari et al., 2014). Surprisingly, no altered expression of p53, or p53 target genes was identified in tetraploid clones. This is in contrast to Kroemer and colleagues, who profiled expression differences between HCT-116 and RKO clones, and reported a slight de-regulation of the p53 pathway in tetraploid cells, as 41% of the genes that showed altered expression in tetraploids contained a p53 consensus binding site (Castedo et al., 2006). Similarly, HCT-116 and RPE-1 tetraploids were shown to have deregulation of 23% of 388 genes annotated as p53 interactors (Kuznetsova et al., 2015). These differing results suggest that deregulated expression of multiple p53 pathway genes may not be an obligatory consequence of tetraploidisation. It would be interesting to expand this to include a proteomics analysis of a panel of diploid and tetraploid cell lines, as regulation of different genes can be at the protein rather than the mRNA level.

Interestingly it has been shown that p53 is necessary for the clustering of extra centrosomes via its interaction with Aurora A (Nam and van Deursen, 2014, Vitale et al., 2010b, Wu et al., 2012a). It is possible that p53 mutations in these HCT-116 tetraploid cells are negatively selected as they could lead to an increase in the frequency of multipolar spindles and chromosome missegregation due to the increased numbers of centrioles in tetraploid cells. This could result in tetraploid cells passing the threshold for viable levels of chromosomal instability.

A plausible explanation for the increased tolerance to chromosome missegregation in tetraploid cells is that with a doubled genome the gain or loss of genetic material does not result in the same genetic imbalances as in diploid cells, and hence in the same cellular consequences. Aneuploidy, arising from imbalances in single chromosomes has been shown to lead to conserved transcriptional responses across different organisms (Donnelly and Storchova, 2014). It is possible that on a tetraploid background single chromosome aneuploidy will not cause a stress response, as there would still be one homologous chromosome remaining. In support of this theory, late passage tetraploid cells, which display distinct aneuploidy, did not show significant expression differences compared to diploid clones. Furthermore, the majority of the chromosome losses that developed in tetraploid clones were losses to three gene copies, rather than complete loss or loss to two gene copies that would result in loss of heterozygosity. This mirrors the genomic landscape of CRC, as the majority of GD tumours have a triploid karyotype. It has recently been shown that polyploidy can foster rapid adaptation in yeast (Selmecki et al., 2015). Polyploid yeast evolved quicker in response to a poor carbon source environment, and part of their adaptation involved increased frequencies of whole chromosome aneuploidy (Selmecki et al., 2015). Diploid and haploid yeast under the same conditions did not evolve whole chromosome aneuploidy, supporting the idea that polyploidy might be a permissive state for the acquisition of unbalanced karyotypes (Selmecki et al., 2015, Dewhurst et al., 2014). It is challenging to design experiments that could either prove or disprove the theory of buffering as a mechanism of segregation error tolerance in tetraploid cells. In transformed cell lines this is particularly difficult, as there are many pre-existing genetic aberrations that could alter the cellular response to a segregation error. It would be of great interest to know whether the non-transformed RPE-1 tetraploid

clones derived by Kuznetsova and colleagues also showed tolerance to segregation errors (Kuznetsova et al., 2015). Since RPE-1 cells make a low frequency of endogenous segregation errors, this could be achieved by experimentally inducing segregation errors and tracking cell fate.

It would also be of interest to explore whether tetraploid cells tolerate chromosome missegregation because of a difference in the molecular response to segregation errors compared to diploid cells. It is known that chromosome missegregation up-regulates p53, although the mechanism causing this up-regulation remains elusive (Thompson and Compton, 2010). This continues to be an active and important area of research. Live-cell imaging followed by immunofluorescence, or live cell imaging with a p53 or p21 reporter could shed light on whether tetraploid cells have dampened the response to segregation errors, and this is the mechanism by which they are able to continue proliferating. Preliminary experiments carried out by a colleague, Andrew Crockford and not presented in this thesis, would suggest that this is not the case, as tetraploid cells up-regulate p53 to the same extent as diploid cells in response to segregation errors induced with the Mps1 inhibitor reversine. However the response to endogenous segregation errors has not been profiled. This is a crucial area for future experiments.

7.3 Genome doubling predicts worse patient prognosis

The use of algorithms that can identify genome duplication in tumours from copy number data has shown that the majority of solid tumour types can be subject to genome duplications during their evolution (Carter et al., 2012, Zack et al., 2013). In this thesis the identification of genome duplication events in two different CRC cohorts was found to predict poor relapse free survival. The in vitro analysis of genomic instability arising after genome duplication presented herein is likely to explain the association of genome doubling with poor patient prognosis. This is likely because increased levels of chromosomal instability are associated with poor patient prognosis, and resistance to different drugs (McGranahan et al., 2012, Lee et al., 2011). However, tetraploid clones derived from HCT-116, even at late passage when they showed evidence of chromosomal instability, did not show

evidence of increased drug resistance. As discussed, this may be a caveat of using a cell line that already displays microsatellite instability. Alternatively, longer-term assays should be used to explore whether the cell-to-cell heterogeneity present in tetraploid clones leads to drug resistance over long periods of selective pressure rather than short-term assays. The ability of the GD algorithm to predict patient survival was most striking in the validation cohort of 239 patients, where GD also predicted uncensored relapse free survival and survival when only considering diploid GD tumours. These results are in accordance with those of Carter and colleagues, who demonstrated genome doubling to be predictive of poor survival in ovarian cancer (Carter et al., 2012), and also of the association in multiple studies of aneuploidy and poor patient prognosis (Araujo et al., 2007).

Further work still needs to be undertaken to ascertain whether genome doubling is a better prognostic marker than other pathological tumour characteristics, such as immune cell infiltrate, that could not be analysed in this thesis due to limitations in the completeness of clinical data available in both cohorts. It would be of interest to investigate the utility of genome doubling as a prognostic marker across different cancer types, as it has been shown to be a common occurrence in most solid tumours, albeit to different degrees (Zack et al., 2013). The differing prevalence of genome doubling between different cancer types could shed light on the environmental conditions in which genome doubling is beneficial for tumours, or the most likely route of whole genome duplication. It would also be of interest to dissect further the timing of genome doubling in different cancer types, especially pre- and post-therapy.

7.4 Genes selectively mutated in GD tumours do not contribute to the response to cytokinesis failure

A focussed approach for selecting genes that are more frequently mutated in genome doubled tumours was employed to create a shortlist of genes to screen for their potential involvement in allowing tetraploid cells to re-enter the cell cycle. Despite extensive optimisation and modification of a published screening protocol for genes which, when knocked down, allow cells to start cycling after cytokinesis

failure (Ganem et al., 2014), no novel gene was found to have a strong effect on this cell cycle checkpoint.

This could in part be due to technical limitations of the approach taken. Although the level of gene knockdown was optimised for specific genes, the efficacy of the knockdown of each different gene tested in the screen could not be validated. If the assumption is made that the reagents provided by Dharmacon are effective in knocking down the intended target, then it must be concluded that none of the genes tested in the screen have a strong effect on the tetraploidy checkpoint. This is even true of siRNAs against LATS2, which did result in gene knockdown at the mRNA and protein level, but which did not greatly influence the proportion of tetraploid cells re-entering the cell cycle.

An important factor to consider is whether any of the genes tested would be expected to be as efficient as knockdown of either p53 or p21. Since p53 and p21 are master regulators of this checkpoint, whose knockdown was shown to rapidly allow cells to re-enter the cell cycle (within 12 hours for si-p21 treated cells), it seems unlikely that any other gene would have an effect as striking as these two genes. Surprisingly Ganem and colleagues report that the knockdown of SPINT2 and PTPB1 resulted in greater percentages of cycling cells than p21 knockdown (Ganem et al., 2014). The strong effects of knockdown of these two genes could not be replicated in this study. The use of p53 and p21 as positive controls in the screen may have masked any other novel hits. For example KCNA5, which did increase the percentages of cycling cells during some experiments, was not a significant hit when compared to either p53 or p21. It is possible that some of the genes included in the screen do play a minor role in cell cycle arrest after cytokinesis failure, but the striking effects of p53 and p21 knockdown eclipse these. In future experiments, chemical inhibition of the potassium channel that KCNA5 is part of will be used to either confirm or exclude a role of KCNA5 in regulating cell cycle arrest after cytokinesis failure.

Furthermore, whether this screen has relevance for the cancer scenario that exists when genome duplication occurs should also be considered. Although genome doubling has been shown to occur as a relatively early event in colorectal cancer,

at this stage it is likely that several oncogenic mutations already exist, and cells are somewhat transformed. The existence of a tetraploidy checkpoint in transformed cells is debateable (Andreassen et al., 2001, Uetake and Sluder, 2004, Wong and Stearns, 2005). In this thesis, genes were selected for the screen based on their association with genome-doubled tumours in vivo. It is possible that these genes do provide a specific benefit for genome-doubled tumours, but this benefit may not be in altering the cell cycle response to the initial tetraploidisation event. It would be of interest to test the function of these genes in different assays that could mimic the tumour cell environment. In this regard, it is interesting that the final list of genes that were screened had strong gene set enrichment analysis (GSEA) associations with many terms that were related to membrane function and extracellular matrix function. This could indicate the genome-doubled tumours have a requirement, or selective pressure to de-regulate key membrane and/or extracellular matrix functions. It would be interesting to test the function of knockdown of the gene list in three-dimensional (3D) environments that more closely imitate the tumour microenvironment. This could be achieved by modelling the growth rate of spheroids formed from diploid and tetraploid cells after gene knockdown, to assess whether any of the genes normally restrain growth in a 3D environment specifically in polyploid cells.

Finally, the gene list that was screened was created from a pan-cancer analysis of mutations. It is possible that each cancer type has specific and differing requirements for cells to tolerate whole genome duplications. Repeating the screen in different cell lines in a tissue-specific matter could help address this question.

7.5 The role of tetraploidy in cancer evolution

In this thesis the tetraploidisation of a chromosomally stable diploid cell line has been shown to result in rapid genomic evolution. All tetraploid clones examined, even those derived from a microsatellite stable clone of HCT-116, displayed a similar loss of chromosome 4q. Chromosome 4q loss was also shown to occur in more genomically unstable colorectal cancers. This striking example of parallel evolution suggests that chromosome 4q loss is associated with chromosomal

instability. Whether the loss of chromosome 4q has a functional impact on the acquisition of chromosomal instability, or whether 4q loss is a consequence of chromosomal instability remains unknown. However, in the system of diploid and tetraploid clones analysed in this study, it seems unlikely that the loss of chromosome 4q has a functional impact on the ability of tetraploid cells to tolerate chromosome missegregation. This is because chromosome 4q is subject to copy number loss at late passage (after passage 25 in most clones), and tetraploid cells could already propagate aneuploidy before this time point. This suggests that chromosome 4q may be intrinsically easier to lose than other chromosomes, possibly due to the presence of particular fragile sites that make it prone to DNA damage and structural re-arrangements. Alternatively loss of the genes on chromosome 4q does not have a detrimental effect on cellular fitness, or may even be advantageous. The loss of chromosome 4q has been shown to be predictive of worse patient outcome in CRC (Brosens et al., 2011). This association could be due to the frequency of chromosome 4q loss in CIN+ CRCs, thus identifying patients with more unstable cancers. Taken together, the results in this thesis have shown that tetraploidisation can lead to the emergence of high-risk karyotypic alterations in CRC.

This study, as well as others, has shown that genomic instability seems to be an inherent consequence of tetraploidisation. An important question then arises of which phenotype is actually being subject to selection. Is tetraploidy so common in cancer merely because it provides a platform for genomic instability?

To answer this question, it will be important to understand whether tetraploidy results in additional benefits for cancer cells aside from an increase in genomic instability. Although no inherent drug resistance as a result of tetraploidisation was observed in this study, others have shown that tetraploid cells are more resistant to some drugs (Castedo et al., 2006, Kuznetsova et al., 2015). This may be a phenotypic consequence of tetraploidisation that is not related to the CIN+ phenotype of tetraploid cells, since RPE-1 tetraploid cells did not all display CIN, but were all generally more resistant to a small selection of drugs than RPE-1 parental cells (Kuznetsova et al., 2015). The observation that many normal mammalian tissues undergo polyploidisation when subject to stress also suggests

that tetraploidy can result in other cellular consequences apart from increasing genomic instability. Although the result of tetraploidisation under these circumstances is not fully understood, it has been suggested that tetraploidisation could result in more efficient use of energy (Lee et al., 2009). It would be interesting to explore metabolic differences between diploid and tetraploid cancer cells to understand whether tetraploidy affects energy utilisation.

Polyploidy has played a role in the evolution of many species (Otto and Whitton, 2000). It has been suggested that polyploids have an inherent advantage over diploids due to their ability to mask deleterious mutations (by virtue of having one intact gene copy still present). Indeed it has been shown that an increased mutation rate, coupled with a doubled genome in yeast can enhance adaptation to novel environments (Thompson et al., 2006). However recessive mutations will be slower to benefit a polyploid compared to a diploid organism, which could provide a selective pressure to reduce genome size after polyploidisation. This could explain the high prevalence of triploid karyotypes in CRC. Other work from this laboratory has indicated that polyploidy could act as a buffer to protect against deleterious mutations. In a multi-region sequencing analysis of a renal cell carcinoma, one tetraploid region had a lower ratio of synonymous to non-synonymous mutations than other diploid regions, which could indicate that non-synonymous mutations are buffered against in polyploid cells (Gerlinger et al., 2012). On-going efforts within this laboratory to carry out multi-region sequencing on different cancer types will hopefully be able to shed light on whether polyploid tumour regions consistently have a reduction in the ratio of synonymous to non-synonymous mutations.

In this study, naturally occurring tetraploid cells were found in the diploid MIN cell lines HCT-116 and RKO. Tetraploid sub-fractions were also found in the microsatellite stable cell line C-99, as well as in UO31, a renal cell carcinoma cell line (data not shown). The fact that tetraploid cells seem to be generated with high frequency in diploid cell lines, as well as the fact that a myriad of genetic defects have been shown to lead to tetraploidisation (see Introduction, Section 1.5) suggests that tetraploidisation will be a common event in tumours. However, it is not known which conditions favour the expansion of a tetraploid cell population. Future work will focus on uncovering environmental conditions that favour the

growth of tetraploid compared to diploid cells to understand when tetraploid cells become most relevant for tumour evolution. This work could also shed light on whether tetraploidy results in additional benefits to tumours other than increasing levels of genomic instability, which could lead to novel therapeutic strategies to target tetraploid cells.

7.6 Conclusion

It is clear from the work presented in this thesis that tetraploidy can lead to genomic instability and foster the evolution of unstable cancer genomes. In the absence of any mechanistic basis for the chromosome segregation error tolerance observed in tetraploid cells, the conclusion that tetraploid cells buffer chromosome changes by virtue of their doubled genetic content is favoured. This CIN tolerance phenotype in tetraploid cells meant that over 18 months in culture, tetraploid clones derived from HCT-116 cells began to resemble highly unstable CRC tumours. Likely due to the emergence of CIN in genome-doubled cells, observing genome doubling in two independent cohorts of CRC patients predicted poorer relapse free survival. Tetraploidy is likely to play a significant role in shaping the on-going evolution of cancers, and will likely contribute to the intra-tumour heterogeneity that has been observed in many cancer types. It will be of great clinical interest to develop novel ways to target tetraploid cancer cells in order to limit their contribution to genetic instability, evolution and adaptation in human tumours.

Chapter 8. Appendix

8.1 List of papers and reviews published during the production of this thesis

Primary research articles:

Tolerance of Whole-Genome Doubling Propagates Chromosomal Instability and Accelerates Cancer Genome Evolution. Sally M. Dewhurst*, Nicholas McGranahan*, Rebecca A. Burrell, Andrew J. Rowan, Eva Gronroos, David Endesfelder, Tejal Joshi, Dmitri Mouradov, Peter Gibbs, Robyn L. Ward, Nicholas J. Hawkins, Zoltan Szallasi, Oliver M. Sieber and Charles Swanton. *Cancer Discovery*, **4**(2): 175-185 (2014).
(Also included as a supplement at the back of this thesis).

Replication Stress Links Structural and Numerical Cancer Chromosomal Instability. Rebecca A. Burrell*****, Sarah E. McClelland*****, David Endesfelder, Petra Groth, Marie-Christine Weller, Nadeem Shaikh, Enric Domingo, Nnennaya Kanu, Sally M. Dewhurst, Eva Gronroos, Su Kit Chew, Andrew J. Rowan, Arne Schenk, Michal Sheffer, Michael Howell, Maik Kschischo, Axel Behrens, Thomas Helleday, Jiri Bartek, Ian P. Tomlinson and Charles Swanton. *Nature* **494**:492-496 (2013).

Reviews:

Cancer: Evolution within a lifetime. Marco Gerlinger*, Nicholas McGranahan*, Sally M. Dewhurst*, Rebecca A. Burrell, Ian P. Tomlinson and Charles Swanton. Annual Review of Genetics 48: 215-36 (2014).

* denotes shared first authorship

8.2 Full list of siRNA sequences used in screen for regulators of cell cycle arrest after cytokinesis failure

Well	Duplex Catalogue Number	Gene Symbol	Sequence
A01	J-003296-23	RB1	GAACAGGAGUGCACGGAUA
A01	J-003296-24	RB1	GGUUCAACUACGCGUGUAA
A01	J-003296-25	RB1	CAUUAAUGGUUCACCUCGA
A01	J-003296-26	RB1	CAACCCAGCAGUUCGAUAU
A02	J-009296-05	DNAH5	UAAAGGAACCUACGGACUA
A02	J-009296-06	DNAH5	GGACAUCACUGAAUAUUGA
A02	J-009296-07	DNAH5	GAAACUAAAUCGUCCAAUU
A02	J-009296-08	DNAH5	GGGCAAGGCUGUGCUAUUA
A03	J-006161-06	CNGB3	GCAAAUAGGAUGUUAAAGU
A03	J-006161-07	CNGB3	GUACUAAAGUUCUGGUUAC
A03	J-006161-08	CNGB3	CUAUUUGCCUGGUGACUUU
A03	J-006161-09	CNGB3	UCGAACAACUGGAUACUUG
A04	J-020017-05	LILRB2	CGAUAUGGCUGUCAGUAUU
A04	J-020017-06	LILRB2	UGACAGGAGCCUACCCAAA
A04	J-020017-07	LILRB2	GCAGACUCCACACUCAGUA
A04	J-020017-08	LILRB2	CGAAAUAACUAAUAUCCCU
A05	J-011941-17	NRXN1	GGGUAUGGUCGUUGGGAUA
A05	J-011941-18	NRXN1	GCUCAUACCAUGUGGACGA
A05	J-011941-19	NRXN1	GGCCAGUGAUCGAGCGCUA
A05	J-011941-20	NRXN1	CCAUUAUGUGGGCAGGUUA
A06	J-015720-05	RGS7	GAAGGAACCUGGACGAUAC
A06	J-015720-06	RGS7	UUAGAUAGACAUCGGUUAA
A06	J-015720-07	RGS7	GACUGGAGCUCGCAGACUA
A06	J-015720-08	RGS7	ACACAGAUUAUGCCGUUUA
A07	J-007033-06	SALL4	GAACCAACACAUCCAUUAA
A07	J-007033-07	SALL4	CCACCUCCGUUGUGAAUAA
A07	J-007033-08	SALL4	CAAGAUUGCGGUCAGCUAA
A07	J-007033-09	SALL4	GAACCGAGUCUUUCUUUAG
A08	J-012405-05	ZFPM2	CAGCUUUGGUGUACAACUA
A08	J-012405-06	ZFPM2	GAUACAGCCUACAACAAAU
A08	J-012405-07	ZFPM2	GAUGGCAGCAGAUGGCUAA
A08	J-012405-08	ZFPM2	CAAGCUGCCUUCCGAUGUA
A09	J-019511-17	ZNF208	AAUCCUAGCCAGAGAAUAA
A09	J-019511-18	ZNF208	GGAAUUAACUCCCUAUUUA
A09	J-019511-19	ZNF208	ACUCAUACAUGGAUGCUAA
A09	J-019511-20	ZNF208	CGAGAGACAAUGCAAAUAA
A10	J-021612-09	ELTD1	AGAGUCAUAUCUUCAGUAA
A10	J-021612-10	ELTD1	GAUGUGCAUUGAAGGCAUA
A10	J-021612-11	ELTD1	UGAUGGAACCGUCUGUAUA
A10	J-021612-12	ELTD1	GUACCUGGCUUCAGAUCCA
A11	J-006297-06	SCN1A	GCACUACUAUGUGGAAAUA
A11	J-006297-07	SCN1A	GAAAGACGAUUAAGACGAU
A11	J-006297-08	SCN1A	UGACGGACCAUUUCAAUAA
A11	J-006297-09	SCN1A	AGGAGUAGCUUAUGUGAAA
A12	J-011701-06	INHBA	GAACGGGUAUGUGGAGAUA
A12	J-011701-07	INHBA	GAGUGUGGGUGCUCAUAGA
A12	J-011701-08	INHBA	GGAUUUCUGUUGGCAAGUU
A12	J-011701-09	INHBA	GGAGUGAACUGUUGCUCUC
B01	J-032495-17	OR51B5	CAUUAUGAGCUAUGCCUAU
B01	J-032495-18	OR51B5	GUGCUGGAUUAUCUGAUUA
B01	J-032495-19	OR51B5	GAAAGCAGGUUCCACAUAU
B01	J-032495-20	OR51B5	GGGCCAAGGCUCUCAUUAC
B02	J-004226-10	SIGLEC6	GCAUACUUCUUUCGGUUGA
B02	J-004226-11	SIGLEC6	CACAAACGACCCAGACGAA
B02	J-004226-12	SIGLEC6	GCAAUGUACCACAAACCGA
B02	J-004226-13	SIGLEC6	GAACCAAAGGUCACCGACA

B03	J-006717-07	DGKI	AAGCAGGCGUUUCACAAUA
B03	J-006717-08	DGKI	GGGAGAUUGUGAAAUAUAU
B03	J-006717-09	DGKI	AAGAUGCGCUUGAAUUGUA
B03	J-006717-10	DGKI	GAACUAGUGCAGUCAUUUG
B04	J-012091-09	DMXL1	AGUAAUGAGAGUACGUUAA
B04	J-012091-10	DMXL1	CCUCAAAAUUAUAUCGCAA
B04	J-012091-11	DMXL1	GGGAUUAUAUAGAGCUGAA
B04	J-012091-12	DMXL1	CAUAUGAGCCUAACAGGAA
B05	J-023161-09	SATB2	UGUCUGAGAUUCUGCGUAA
B05	J-023161-10	SATB2	AGUUUGUCCUGGUGCGGAA
B05	J-023161-11	SATB2	UAAUAAGCCUGCUCGUUUA
B05	J-023161-12	SATB2	GCCAGAUCUUUGCGAAUUA
B06	J-003329-14	TP53	GAAAUUUGCGUGUGGAGUA
B06	J-003329-15	TP53	GUGCAGCUGUGGGUUGAUU
B06	J-003329-16	TP53	GCAGUCAGAUCCUAGCGUC
B06	J-003329-17	TP53	GGAGAAUAUUUCACCCUUC
B07	J-017263-05	ARID1A	GAAUAGGGCCUGAGGGAAA
B07	J-017263-06	ARID1A	AGAUGUGGGUGGACCGUUA
B07	J-017263-07	ARID1A	GCAACGACAUGAUUCCUAU
B07	J-017263-08	ARID1A	GGACCUCUAUCGCCUCUAU
B08	J-003869-09	APC	GAUGAUAUGUCGCGAACUU
B08	J-003869-10	APC	AUGAUAAGCUCCCAAAUAA
B08	J-003869-11	APC	GAGAAUACGUCCACACCUU
B08	J-003869-12	APC	GAACUAGAUACACCAAUAA
B09	J-009580-05	ARHGAP5	GUACGAAUUUGCAACCAUA
B09	J-009580-06	ARHGAP5	GCUGAUACAACCACAAUUA
B09	J-009580-07	ARHGAP5	GAUCAUGGCCGCUUAAGAU
B09	J-009580-08	ARHGAP5	GGAAUCAGUUAAACACAAU
B10	J-004510-06	ATXN1	GGGAAUAGGUUUACACAAA
B10	J-004510-07	ATXN1	GGUCUAAUGUAGGCAAGUA
B10	J-004510-08	ATXN1	CCAGCCAGCUCUUUGAUUU
B10	J-004510-09	ATXN1	GAAGAACGGCUCUGUUAAA
B11	J-013169-05	CDH9	CAACAACCCUCCUCGAUUU
B11	J-013169-06	CDH9	GGAAUCAGUUCUUCUUAUU
B11	J-013169-07	CDH9	UGUAAUGCCUGAAACUAUU
B11	J-013169-08	CDH9	GAGACUAAGAGGAUUGUUU
B12	J-018973-17	FAM194B	CGACAGAACUGCCGUAAAA
B12	J-018973-18	FAM194B	GAUUAAGAGGAGACGUGAA
B12	J-018973-19	FAM194B	GCUCAUCUUAUAUGCGAAA
B12	J-018973-20	FAM194B	CGAGAUAAGGAAUGGAUAC
C01	J-006215-06	KCNA5	CUAGAGAAGUGUAACGUCA
C01	J-006215-07	KCNA5	ACAGAGGAGUCCAGCGGAA
C01	J-006215-08	KCNA5	GAAAGGAGAUUCAGGCAGA
C01	J-006215-09	KCNA5	GAACCCAUUUCUCUAGCAU
C02	J-013660-25	KRTAP4-5	CUAAUGUCUCCUUGUGAUA
C02	J-013660-26	KRTAP4-5	CAGACAAUCACAUUCAUUA
C02	J-013660-27	KRTAP4-5	CAUUCAGAGUGGACAUUCA
C02	J-013660-28	KRTAP4-5	CAUUCGAAGGGGACACUAA
C03	J-022981-09	MYADML2	GCUAGAAGCAUUUGCGAGG
C03	J-022981-10	MYADML2	CAGGGGAGAUGAAGUACAA
C03	J-022981-11	MYADML2	GCUGGUCACUGGAACAUCA
C03	J-022981-12	MYADML2	CCAAGUACGGUGAGCCCAA
C04	J-006503-05	SCN9A	UUUAAGGGAUGGACGAUUA
C04	J-006503-06	SCN9A	GCACACAAAUUCUUGAUCU
C04	J-006503-07	SCN9A	CAGCUGAAAUGGUAUUAAA
C04	J-006503-08	SCN9A	CUAUGUGCCUUAUUGUUUA
C05	J-003816-05	TCF7L2	CAGCGAAUGUUUCCUAAAU
C05	J-003816-06	TCF7L2	CGAGACAAAUCCCGGGAAA
C05	J-003816-07	TCF7L2	ACACUUACCAGCCGACGUA
C05	J-003816-08	TCF7L2	GAUGUCGGCUCACUCCAUA
C06	J-010216-06	SPINT2	GAAGACCACUCCAGCGAUA
C06	J-010216-07	SPINT2	GCUCAAAGGUGGUGGUUCU
C06	J-010216-08	SPINT2	GCAAUAAUUACCUGACCAA
C06	J-010216-09	SPINT2	CCUGCCAGCUGUUUGUGUA
C07	J-008294-09	IDH1	UGUCAUAGAUAUCCCGUUU
C07	J-008294-10	IDH1	GCAUAAUGUUGGCGUCAAA
C07	J-008294-11	IDH1	GCUUGUGAGUGGAUGGGUA
C07	J-008294-12	IDH1	CCGCAGGAGAGUUUGGAAU
C08	J-003023-09	PTEN	GAUCAGCAUACACAAAUUA

C08	J-003023-10	PTEN	GACUUAGACUUGACCUAUA
C08	J-003023-11	PTEN	GAUCUUGACCAAUGGCUAA
C08	J-003023-12	PTEN	CGAUAGCAUUUGCAGUAUA
C09	J-003471-09	CDKN1A	CGACUGUGAUGCGCUAAUG
C09	J-003471-10	CDKN1A	CCUAAUCCGCCCACAGGAA
C09	J-003471-11	CDKN1A	CGUCAGAACCCAUGCGGCA
C09	J-003471-12	CDKN1A	AGACCAGCAUGACAGAUUU
C10	J-018452-17	MROH2B	UAGCUAAGAUUGUCAGUAA
C10	J-018452-18	MROH2B	UCGGAGAACUACCGGAUAA
C10	J-018452-19	MROH2B	AGGAAAUGCUGGACGGUCU
C10	J-018452-20	MROH2B	CUUCCAGAUCACUGCGAAA
C11	J-011614-07	COL11A1	AGAAUUUGGUCCAGGUGUA
C11	J-011614-08	COL11A1	GAUGUUACCGUUCCGUUAU
C11	J-011614-09	COL11A1	GAACGUGGGUCAGCAGGUA
C11	J-011614-10	COL11A1	GGAUUCUGAUCUUCUGGUA
C12	J-009032-09	ABCA13	CUGCAAGACAUGAUCGAAA
C12	J-009032-10	ABCA13	GACAAACGGUGCCGGGAAA
C12	J-009032-11	ABCA13	GCUUCAAUAUGGAGGAGUA
C12	J-009032-12	ABCA13	GCUGAUGGGUUCAAAUAUA
D01	J-025907-05	COL14A1	GAUCAAUGGUUAUCGAAUU
D01	J-025907-06	COL14A1	UAUAACCGGUUGCGCAUUA
D01	J-025907-07	COL14A1	GUACAAUGUUGCCGAAUUC
D01	J-025907-08	COL14A1	GCAUUGAUCUUGCAGGAUU
D02	J-004758-05	COL1A2	CAGAGGUCUUCCUGGCUUA
D02	J-004758-06	COL1A2	CAGGUUCACUUACACUGUU
D02	J-004758-07	COL1A2	GGAACUUUGCUGCUCAGUA
D02	J-004758-08	COL1A2	CCAAUGGGCUUAAUGGGAC
D03	J-011012-05	COL3A1	GGUCAGUCCUAUGCGGAUA
D03	J-011012-06	COL3A1	ACAAAUAGAAAGCCUCAUU
D03	J-011012-07	COL3A1	GAUGGUGGUUUUCAGUUUA
D03	J-011012-08	COL3A1	GGACACAGAGGCUUCGAUG
D04	J-007868-17	CSMD2	CUACAUAGAAAUCCGGAAU
D04	J-007868-18	CSMD2	CAAUAUAGGUGACAUCGUA
D04	J-007868-19	CSMD2	GGACCAUCACCGCGGAAGA
D04	J-007868-20	CSMD2	CAUUAAGUUCAGCGCCAAA
D05	J-018304-17	FAM171B	GUAGAAAGCUCGAGAGGGA
D05	J-018304-18	FAM171B	GGUUUAAGGCUCACUGAUA
D05	J-018304-19	FAM171B	CAAGCAGAGUAAAUGGUAA
D05	J-018304-20	FAM171B	GCUUCAAGAUGUUAGUUAU
D06	J-032083-17	GFRAL	AAACAUGCUUGGAGAGUAA
D06	J-032083-18	GFRAL	GUGAGGAAUCUUUGUGUAA
D06	J-032083-19	GFRAL	GCAACCACGUCAAGACAAC
D06	J-032083-20	GFRAL	CAGUUGGCCUCUUACCUUA
D07	J-005332-05	INSRR	GGGAGCAGAUCUCGAUAAU
D07	J-005332-06	INSRR	CGUAAUAGCAGCAGCAUAU
D07	J-005332-07	INSRR	GAUGGGAACUACACUCUCU
D07	J-005332-08	INSRR	CAGCGCCUCUGAUAUGUAU
D08	J-008009-07	ITGAX	GUUCAUACCUGCCGAGAUC
D08	J-008009-08	ITGAX	CCCAUUACCUUGCGUCUGA
D08	J-008009-09	ITGAX	GCACAGAUACCAGGUCAAU
D08	J-008009-10	ITGAX	CAACUUCUCUAGGUUUCAA
D09	J-010912-05	KLHL1	GGACAUUUGUAGCCAGUAU
D09	J-010912-06	KLHL1	CGAAAGAUACCUGCACAUA
D09	J-010912-07	KLHL1	GUUCCCGGCUACUGGAUUA
D09	J-010912-08	KLHL1	CAGCAACUUUGUGAUGUUA
D10	J-015885-09	MUC7	ACAGAAUUAUUGACGACAU
D10	J-015885-10	MUC7	GCUACUUGGUAUACGGAGA
D10	J-015885-11	MUC7	GAUCAUGAACUACGUCACA
D10	J-015885-12	MUC7	CCACAAGACCUAUUAACAA
D11	J-018348-05	NAV3	GGACUUAACCUAUAUACUA
D11	J-018348-06	NAV3	GAGAGGGUCUUCAGAUGUA
D11	J-018348-07	NAV3	CAGGGAGCCUCUAAUUUAA
D11	J-018348-08	NAV3	GCUGUUAGCUCAGAUAUUU
D12	J-020986-05	NBAS	GUAAAGAGAUGACUAGAAA
D12	J-020986-06	NBAS	UAUCAGUGCUUCACCAUUA
D12	J-020986-07	NBAS	GAAGACACUGGGAUUAUUA
D12	J-020986-08	NBAS	GGUCAACGUUGCUUCAAUU
E01	J-019674-05	NID1	CAACGGAGCUUAUAACAUA
E01	J-019674-06	NID1	GGGCGAACCUGCUAUGAUA

E01	J-019674-07	NID1	UAACCUGGAUCGAAUAGAA
E01	J-019674-08	NID1	CCUCCACUCUUACGUAGUA
E02	J-011883-05	NOTCH4	GCACGGACGGUGUCAGUAA
E02	J-011883-06	NOTCH4	GCAGGAGGGUCCACGUUGU
E02	J-011883-07	NOTCH4	GGUGAGACGUGCCAGUUUC
E02	J-011883-08	NOTCH4	GCCCAACCCUGCGAUAAUG
E03	J-008450-09	PXDNL	CUGAGAAAGUUGUACGGCU
E03	J-008450-10	PXDNL	GGAUUCAGUCUAUGCACGA
E03	J-008450-11	PXDNL	GCUACAACCCCAACGUGAA
E03	J-008450-12	PXDNL	UACCUGAACUGCAGCGAGA
E04	J-010105-09	PZP	GUGACAAAUCAGACGCUAA
E04	J-010105-10	PZP	CUACCAGUAUCUCGGUUAA
E04	J-010105-11	PZP	CUACAGAACCGCAGUAUAU
E04	J-010105-12	PZP	GAGCAGUAGGUCAAGGAUA
E05	J-011824-05	RUNX1T1	AAGCGACCAUGCACUAUUA
E05	J-011824-06	RUNX1T1	GAGAGUUGCUGGAAUUGUG
E05	J-011824-07	RUNX1T1	CGACAACGUUAACUAAUGG
E05	J-011824-08	RUNX1T1	CCGAUACUGUGGCUCAUUU
E06	J-021768-09	SLITRK1	GGGCAGAGGGAAGGCGAUA
E06	J-021768-10	SLITRK1	AGAUAGACCUCCACGGAAA
E06	J-021768-11	SLITRK1	CCGAAGUGCUGAUGAGCGA
E06	J-021768-12	SLITRK1	CUGAUAAGUUCCAUCGUAU
E07	J-020435-09	SLITRK3	CCUUAAUGGCAACGAUAUA
E07	J-020435-10	SLITRK3	AAGUGAUUACCUCGAGUUA
E07	J-020435-11	SLITRK3	UGGAAAGGACCUACGAGAA
E07	J-020435-12	SLITRK3	CUUCAAACCAAGCCGGAUU
E08	J-013422-05	SORCS1	GGACAUCGGUCGAGUCAUC
E08	J-013422-06	SORCS1	GAAUGGAGGACGCCAGUAA
E08	J-013422-07	SORCS1	CAAAUGAAGCUUCCGAAAU
E08	J-013422-08	SORCS1	CGGCUGAACUUCUACAUUC
E09	J-008402-09	ST6GAL2	CAGAGAGGUGCACGUGUAU
E09	J-008402-10	ST6GAL2	ACCCGGAGGAUGACGACUA
E09	J-008402-11	ST6GAL2	CGUCAUGUCUGCAGGCGCA
E09	J-008402-12	ST6GAL2	UACACGUGGUUAUGAGAAA
E10	J-009299-06	TG	ACUCAAAGCUGCACACAUA
E10	J-009299-07	TG	CAAUGGAAAUCAAUCACUA
E10	J-009299-08	TG	GGGAUUAGAUUCAAAUUCU
E10	J-009299-09	TG	CCACAGACAUGAUGAUUUU
E11	J-009863-05	TPO	CCAGAUGACUUGUGAGAAC
E11	J-009863-06	TPO	GGUUAUGGCCUGCACAGAA
E11	J-009863-07	TPO	GUACGUGGGUCCCUAUGAA
E11	J-009863-08	TPO	GCACGGGUAUGAGCUCCAA
E12	J-009644-05	TRPS1	GAAUGCAAAUGGCGGAUAU
E12	J-009644-06	TRPS1	CAACUCAUCCACCGAAUUA
E12	J-009644-07	TRPS1	GCUGGAAGCUCGCGAGUCA
E12	J-009644-08	TRPS1	CCACAGAUCUGAUUAAGCA
F01	J-016071-05	VCAN	CCACUACCCUUGAAGAUAU
F01	J-016071-06	VCAN	CCUAGAGGAUAUUGAUUUA
F01	J-016071-07	VCAN	GAAGGUAGUGGGUCAGUAA
F01	J-016071-08	VCAN	GAGCAUGACUUCCGUUGGA
F02	J-003646-06	COL6A3	CGACAUGGCUUUCAUCUUA
F02	J-003646-07	COL6A3	GAAGGAACUUGCAGGGAUU
F02	J-003646-08	COL6A3	GAGAUGUGGUCUUGAGUAU
F02	J-003646-09	COL6A3	UAGAGAGGCUGGUUGACUA
F03	J-013520-05	CDH10	CGAAAUGUCUGUUGUAGGU
F03	J-013520-06	CDH10	GGGUAUGCCUGCCACAUUU
F03	J-013520-07	CDH10	CAGCUAAUACAGACUAUAA
F03	J-013520-08	CDH10	GCCACAAGGCGAAUUGAUA
F04	J-005497-06	FSHR	CCAGUGAGCUGUCAGUCUA
F04	J-005497-07	FSHR	UUACAUACUUGUCCCUCUA
F04	J-005497-08	FSHR	UAUCACAACUAUGCCAUUG
F04	J-005497-09	FSHR	GGCAAGAAGUUGAUUAUAU
F05	J-019219-09	NCKAP1L	GGACCAGUACAUCGUGAAA
F05	J-019219-10	NCKAP1L	GAUUGAAGAUCGGCGGAUA
F05	J-019219-11	NCKAP1L	GUCAGAUGGUCUUGGAGUA
F05	J-019219-12	NCKAP1L	CGAAACAGCACGCAACAUU
F06	J-008079-05	SELP	GCUGAGAGGAGCCGAUAUA
F06	J-008079-06	SELP	GCUGAGAACUGGGCUGAUA
F06	J-008079-07	SELP	GUAAAGCUGUGCAGUGUCA

F06	J-008079-08	SELP	CUAGAGGGCCAGUUACUUA
F07	J-007391-09	SLC13A1	CUGACUAUCUUGCGGUAAU
F07	J-007391-10	SLC13A1	UAGAAGUGAGGAUGCGAAA
F07	J-007391-11	SLC13A1	AAUGAAAACUGCUGACGUA
F07	J-007391-12	SLC13A1	UCUUGUUGGUGGAGGGUUU
F08	J-003865-09	LATS2	GCACGCAUUUUACGAAUUC
F08	J-003865-10	LATS2	ACACUCACCUCGCCCAAUA
F08	J-003865-11	LATS2	AAUCAGAUAUUCCUUGUUG
F08	J-003865-12	LATS2	GAAGUGAACCGGCAAAUGC
F09	J-010608-05	BCAM	GCUAAAGACAGCGGAAAUA
F09	J-010608-06	BCAM	CGGGAACCCACGACCAUUA
F09	J-010608-07	BCAM	GAGGUGCGCUUGUCUGUAC
F09	J-010608-08	BCAM	CGAGGAAAGUCUGUCAUUC
F10	J-016856-17	C12orf50	ACGCAUGGGUCCUACAAUA
F10	J-016856-18	C12orf50	CCAGACAAAUAUACGUCAA
F10	J-016856-19	C12orf50	GGUCAUAUUUCUUGGAGUC
F10	J-016856-20	C12orf50	GAAAAUAUAUCACGACCCA
F11	J-016630-17	CCDC11	GUAACAACGCACAGAUUAA
F11	J-016630-18	CCDC11	CCGUACAGCGGGAGGUUAA
F11	J-016630-19	CCDC11	CAUUGAAGAAAGACGAAAU
F11	J-016630-20	CCDC11	GCUCCGUGUUGAAUUGUUA
F12	J-017854-05	CD2	CCAAAGAGAUUACGAAUGC
F12	J-017854-06	CD2	GAACUGACCCCGAAUUAAA
F12	J-017854-07	CD2	CCGAUGAUCAGGAUAUCUA
F12	J-017854-08	CD2	CCAAAGAUCUCCUGGACUU
G01	J-008948-22	CHD2	CCGAAGACUCAGCGUGGAA
G01	J-008948-23	CHD2	GACAAGAACCAUCGCGAUU
G01	J-008948-24	CHD2	ACAGCAAUGCAUCGAGUCA
G01	J-008948-25	CHD2	AGAGGAGGACAGUUCGCUA
G02	J-025842-17	COL22A1	GAUCAUAUGUCUUGGCCAA
G02	J-025842-18	COL22A1	CGGAAAAGUCAGAGGGUCA
G02	J-025842-19	COL22A1	CCAAGGGUCACCUGGGAAA
G02	J-025842-20	COL22A1	GGGACGUGCAUUUGGAAAA
G03	J-020683-05	KIR2DL1	CAACAGAUAUCAUCGUGUA
G03	J-020683-06	KIR2DL1	GAAACAGAACAGCGAAUAG
G03	J-020683-07	KIR2DL1	UCACAAUUCCAAACAUACA
G03	J-020683-08	KIR2DL1	CAACCUAACUGGCUUACUU
G04	J-005577-05	LGR5	CCUAGAGACUUUAGAUUUA
G04	J-005577-06	LGR5	GACAAUGCGUUAACAGAAA
G04	J-005577-07	LGR5	CCUCACAAAUAACUGAAUU
G04	J-005577-08	LGR5	UCAAUUAACUCUGAUGAUG
G05	J-003844-05	LRP5	CGUCAAAGCCAUCGACUAU
G05	J-003844-06	LRP5	CGUCAUGGGUGGUGUCUAU
G05	J-003844-07	LRP5	GGACGGACCUACGGAGGAU
G05	J-003844-08	LRP5	GUACAGGCCCUACAUCAUU
G06	J-023646-09	LRRIQ4	AGAUCUACCUGAAGCGAAA
G06	J-023646-10	LRRIQ4	CCCAGGAGAUUCAGCGUUU
G06	J-023646-11	LRRIQ4	GAAAUCGGGCUGAGCGGGA
G06	J-023646-12	LRRIQ4	AGUGUGUGCUGAAGGCAAU
G07	J-009229-05	PON1	CAUCAGAGGUGCUUCGAAU
G07	J-009229-06	PON1	GACAUAAACUUCUGCCUAA
G07	J-009229-07	PON1	GGUCGUAUGUUGUCUACUA
G07	J-009229-08	PON1	GUUGCUGGCUCAUAAGAUU
G08	J-007420-09	SLC18A2	GAAGAGAGAGGCAACGUCA
G08	J-007420-10	SLC18A2	GAUCACAACUGCCCUAUUA
G08	J-007420-11	SLC18A2	GGGAAUGAUAAUUGUUGGA
G08	J-007420-12	SLC18A2	GCUAGUAUCUCUUAUCUCA
G09	J-021231-05	SNTG1	GGAUUUGGAUUAAGCAUAA
G09	J-021231-06	SNTG1	GCUCAUGUCUCUACAAGUU
G09	J-021231-07	SNTG1	GCACAGGAUUUAUCUGCUU
G09	J-021231-08	SNTG1	UAAUGGGACUCACAAUUGA
G10	J-021242-05	DCP1A	GCAAGCUUGUCGAUAUAUA
G10	J-021242-06	DCP1A	ACUCAUGGCUGAUGUGGUA
G10	J-021242-07	DCP1A	ACAAGCAUCUGACGGUAGA
G10	J-021242-08	DCP1A	CCAAUUCAUUCCUACCAUU
G11	J-003528-06	PTBP1	CGUCAAAGGAUUCAAGUUC
G11	J-003528-07	PTBP1	GGCACAAGCUGCACGGGAA
G11	J-003528-08	PTBP1	GAACUUCCAGAACAUAUUC
G11	J-003528-09	PTBP1	GCAUCACGCUCUCGAAGCA

G12	J-003916-07	NF1	GAACAAACCAUAGCUAUAA
G12	J-003916-08	NF1	CAGAUAAUCCGUAUUCUUA
G12	J-003916-09	NF1	CGAAGUCGCUGCAGCCUAA
G12	J-003916-10	NF1	GCAAGUACUUACAUCAAUU
H01	J-003020-14	PIK3R1	AGUAAAGCAUUGUGUCAUA
H01	J-003020-15	PIK3R1	CCAACAACGGUAUGAAUAA
H01	J-003020-16	PIK3R1	GACGAGAGACCAAUACUUG
H01	J-003020-17	PIK3R1	UAUUGAAGCUGUAGGGAAA

Reference List

ABDEL-RAHMAN, W. M., KATSURA, K., RENS, W., GORMAN, P. A., SHEER, D., BICKNELL, D., BODMER, W. F., ARENDS, M. J., WYLLIE, A. H. & EDWARDS, P. A. 2001. Spectral karyotyping suggests additional subsets of colorectal cancers characterized by pattern of chromosome rearrangement. *Proc Natl Acad Sci U S A,* 98**,** 2538-43.

ABE, Y., OHSUGI, M., HARAGUCHI, K., FUJIMOTO, J. & YAMAMOTO, T. 2006. LATS2-Ajuba complex regulates gamma-tubulin recruitment to centrosomes and spindle organization during mitosis. *FEBS Lett,* 580**,** 782-8.

ANATSKAYA, O. V. & VINOGRADOV, A. E. 2007. Genome multiplication as adaptation to tissue survival: evidence from gene expression in mammalian heart and liver. *Genomics,* 89**,** 70-80.

ANATSKAYA, O. V. & VINOGRADOV, A. E. 2010. Somatic polyploidy promotes cell function under stress and energy depletion: evidence from tissue-specific mammal transcriptome. *Funct Integr Genomics,* 10**,** 433-46.

ANDALIS, A. A., STORCHOVA, Z., STYLES, C., GALITSKI, T., PELLMAN, D. & FINK, G. R. 2004. Defects arising from whole-genome duplications in Saccharomyces cerevisiae. *Genetics,* 167**,** 1109-21.

ANDREASSEN, P. R., LOHEZ, O. D., LACROIX, F. B. & MARGOLIS, R. L. 2001. Tetraploid state induces p53-dependent arrest of nontransformed mammalian cells in G1. *Mol Biol Cell,* 12**,** 1315-28.

ANDREWS, P. D., OVECHKINA, Y., MORRICE, N., WAGENBACH, M., DUNCAN, K., WORDEMAN, L. & SWEDLOW, J. R. 2004. Aurora B regulates MCAK at the mitotic centromere. *Dev Cell,* 6**,** 253-68.

ARAUJO, S. E., BERNARDO, W. M., HABR-GAMA, A., KISS, D. R. & CECCONELLO, I. 2007. DNA ploidy status and prognosis in colorectal cancer: a meta-analysis of published data. *Dis Colon Rectum,* 50**,** 1800-10.

ARTANDI, S. E., CHANG, S., LEE, S. L., ALSON, S., GOTTLIEB, G. J., CHIN, L. & DEPINHO, R. A. 2000. Telomere dysfunction promotes non-reciprocal translocations and epithelial cancers in mice. *Nature,* 406**,** 641-5.

ASHBURNER, M., BALL, C. A., BLAKE, J. A., BOTSTEIN, D., BUTLER, H., CHERRY, J. M., DAVIS, A. P., DOLINSKI, K., DWIGHT, S. S., EPPIG, J. T., HARRIS, M. A., HILL, D. P., ISSEL-TARVER, L., KASARSKIS, A., LEWIS, S., MATESE, J. C., RICHARDSON, J. E., RINGWALD, M., RUBIN, G. M. & SHERLOCK, G. 2000. Gene ontology: tool for the unification of biology. The Gene Ontology Consortium. *Nat Genet,* 25**,** 25-9.

AYLON, Y., MICHAEL, D., SHMUELI, A., YABUTA, N., NOJIMA, H. & OREN, M. 2006. A positive feedback loop between the p53 and Lats2 tumor suppressors prevents tetraploidization. *Genes Dev,* 20**,** 2687-700.

BAKHOUM, S. F., DANILOVA, O. V., KAUR, P., LEVY, N. B. & COMPTON, D. A. 2011. Chromosomal Instability Substantiates Poor Prognosis in Patients with Diffuse Large B-cell Lymphoma. *Clin Cancer Res,* 17**,** 7704-11.

BAKHOUM, S. F., GENOVESE, G. & COMPTON, D. A. 2009a. Deviant kinetochore microtubule dynamics underlie chromosomal instability. *Curr Biol,* 19**,** 1937-42.

BAKHOUM, S. F., KABECHE, L., MURNANE, J. P., ZAKI, B. I. & COMPTON, D. A. 2014. DNA-damage response during mitosis induces whole-chromosome missegregation. *Cancer Discov,* 4**,** 1281-9.

BAKHOUM, S. F., THOMPSON, S. L., MANNING, A. L. & COMPTON, D. A. 2009b. Genome stability is ensured by temporal control of kinetochore-microtubule dynamics. *Nat Cell Biol,* 11**,** 27-35.

BALBAS-MARTINEZ, C., SAGRERA, A., CARRILLO-DE-SANTA-PAU, E., EARL, J., MARQUEZ, M., VAZQUEZ, M., LAPI, E., CASTRO-GINER, F., BELTRAN, S., BAYES, M., CARRATO, A., CIGUDOSA, J. C., DOMINGUEZ, O., GUT, M., HERRANZ, J., JUANPERE, N., KOGEVINAS, M., LANGA, X., LOPEZ-KNOWLES, E., LORENTE, J. A., LLORETA, J., PISANO, D. G., RICHART, L., RICO, D., SALGADO, R. N., TARDON, A., CHANOCK, S., HEATH, S., VALENCIA, A., LOSADA, A., GUT, I., MALATS, N. & REAL, F. X. 2013. Recurrent inactivation of STAG2 in bladder cancer is not associated with aneuploidy. *Nat Genet,* 45**,** 1464-9.

BARBER, T. D., MCMANUS, K., YUEN, K. W., REIS, M., PARMIGIANI, G., SHEN, D., BARRETT, I., NOUHI, Y., SPENCER, F., MARKOWITZ, S., VELCULESCU, V. E., KINZLER, K. W., VOGELSTEIN, B., LENGAUER, C. & HIETER, P. 2008. Chromatid cohesion defects may underlie chromosome instability in human colorectal cancers. *Proc Natl Acad Sci U S A,* 105**,** 3443-8.

BARSKI, G. & CASSINGENA, R. 1963. Malignant transformation in vitro of cells from C57BL mouse normal pulmonary tissue. *J Natl Cancer Inst,* 30**,** 865-83.

BARTKOVA, J., HOREJSI, Z., KOED, K., KRAMER, A., TORT, F., ZIEGER, K., GULDBERG, P., SEHESTED, M., NESLAND, J. M., LUKAS, C., ORNTOFT, T., LUKAS, J. & BARTEK, J. 2005. DNA damage response as a candidate anti-cancer barrier in early human tumorigenesis. *Nature,* 434**,** 864-70.

BARTKOVA, J., REZAEI, N., LIONTOS, M., KARAKAIDOS, P., KLETSAS, D., ISSAEVA, N., VASSILIOU, L. V., KOLETTAS, E., NIFOROU, K., ZOUMPOURLIS, V. C., TAKAOKA, M., NAKAGAWA, H., TORT, F., FUGGER, K., JOHANSSON, F., SEHESTED, M., ANDERSEN, C. L., DYRSKJOT, L., ORNTOFT, T., LUKAS, J., KITTAS, C., HELLEDAY, T., HALAZONETIS, T. D., BARTEK, J. & GORGOULIS, V. G. 2006. Oncogene-induced senescence is part of the tumorigenesis barrier imposed by DNA damage checkpoints. *Nature,* 444**,** 633-7.

BENGTSSON, H., RAY, A., SPELLMAN, P. & SPEED, T. P. 2009. A single-sample method for normalizing and combining full-resolution copy numbers from multiple platforms, labs and analysis methods. *Bioinformatics,* 25**,** 861-7.

BEROUKHIM, R., MERMEL, C. H., PORTER, D., WEI, G., RAYCHAUDHURI, S., DONOVAN, J., BARRETINA, J., BOEHM, J. S., DOBSON, J., URASHIMA, M., MC HENRY, K. T., PINCHBACK, R. M., LIGON, A. H., CHO, Y. J., HAERY, L., GREULICH, H., REICH, M., WINCKLER, W., LAWRENCE, M. S., WEIR, B. A., TANAKA, K. E., CHIANG, D. Y., BASS, A. J., LOO, A., HOFFMAN, C., PRENSNER, J., LIEFELD, T., GAO, Q., YECIES, D., SIGNORETTI, S., MAHER, E., KAYE, F. J., SASAKI, H., TEPPER, J. E., FLETCHER, J. A., TABERNERO, J., BASELGA, J., TSAO, M. S., DEMICHELIS, F., RUBIN, M. A., JANNE, P. A., DALY, M. J., NUCERA, C., LEVINE, R. L., EBERT, B. L., GABRIEL, S., RUSTGI, A. K., ANTONESCU, C. R., LADANYI, M., LETAI, A., GARRAWAY, L. A., LODA, M., BEER, D. G., TRUE, L. D., OKAMOTO, A., POMEROY, S. L., SINGER, S., GOLUB, T. R., LANDER, E. S., GETZ, G., SELLERS, W. R. & MEYERSON, M. 2010. The landscape of somatic copy-number alteration across human cancers. *Nature,* 463**,** 899-905.

BESTER, A. C., RONIGER, M., OREN, Y. S., IM, M. M., SARNI, D., CHAOAT, M., BENSIMON, A., ZAMIR, G., SHEWACH, D. S. & KEREM, B. 2011. Nucleotide deficiency promotes genomic instability in early stages of cancer development. *Cell,* 145**,** 435-46.

BETTENCOURT-DIAS, M. & GLOVER, D. M. 2007. Centrosome biogenesis and function: centrosomics brings new understanding. *Nat Rev Mol Cell Biol,* 8**,** 451-63.

BIRKBAK, N. J., EKLUND, A. C., LI, Q., MCCLELLAND, S. E., ENDESFELDER, D., TAN, P., TAN, I. B., RICHARDSON, A. L., SZALLASI, Z. & SWANTON, C. 2011. Paradoxical relationship between chromosomal instability and survival outcome in cancer. *Cancer Res,* 71**,** 3447-52.

BONNER, W. M., REDON, C. E., DICKEY, J. S., NAKAMURA, A. J., SEDELNIKOVA, O. A., SOLIER, S. & POMMIER, Y. 2008. GammaH2AX and cancer. *Nat Rev Cancer,* 8**,** 957-67.

BOVERI, T. 2008. Concerning the origin of malignant tumours by Theodor Boveri. Translated and annotated by Henry Harris. *J Cell Sci,* 121 Suppl 1**,** 1-84.

BRANZEI, D. & FOIANI, M. 2010. Maintaining genome stability at the replication fork. *Nat Rev Mol Cell Biol,* 11**,** 208-19.

BRAY, F., REN, J. S., MASUYER, E. & FERLAY, J. 2013. Global estimates of cancer prevalence for 27 sites in the adult population in 2008. *Int J Cancer,* 132**,** 1133-45.

BRITO, D. A. & RIEDER, C. L. 2006. Mitotic checkpoint slippage in humans occurs via cyclin B destruction in the presence of an active checkpoint. *Curr Biol,* 16**,** 1194-200.

BROSENS, R. P., BELT, E. J., HAAN, J. C., BUFFART, T. E., CARVALHO, B., GRABSCH, H., QUIRKE, P., CUESTA, M. A., ENGEL, A. F., YLSTRA, B. & MEIJER, G. A. 2011. Deletion of chromosome 4q predicts outcome in stage II colon cancer patients. *Cell Oncol (Dordr),* 34**,** 215-23.

BUNZ, F., DUTRIAUX, A., LENGAUER, C., WALDMAN, T., ZHOU, S., BROWN, J. P., SEDIVY, J. M., KINZLER, K. W. & VOGELSTEIN, B. 1998. Requirement for p53 and p21 to sustain G2 arrest after DNA damage. *Science,* 282**,** 1497-501.

BURAKOV, A., NADEZHDINA, E., SLEPCHENKO, B. & RODIONOV, V. 2003. Centrosome positioning in interphase cells. *J Cell Biol,* 162**,** 963-9.

BURRELL, R. A., MCCLELLAND, S. E., ENDESFELDER, D., GROTH, P., WELLER, M. C., SHAIKH, N., DOMINGO, E., KANU, N., DEWHURST, S. M., GRONROOS, E., CHEW, S. K., ROWAN, A. J., SCHENK, A., SHEFFER, M., HOWELL, M., KSCHISCHO, M., BEHRENS, A., HELLEDAY, T., BARTEK, J., TOMLINSON, I. P. & SWANTON, C. 2013. Replication stress links structural and numerical cancer chromosomal instability. *Nature,* 494**,** 492-6.

CAHILL, D. P., LENGAUER, C., YU, J., RIGGINS, G. J., WILLSON, J. K., MARKOWITZ, S. D., KINZLER, K. W. & VOGELSTEIN, B. 1998. Mutations of mitotic checkpoint genes in human cancers. *Nature,* 392**,** 300-3.

CANCER GENOME ATLAS, N. 2012. Comprehensive molecular characterization of human colon and rectal cancer. *Nature,* 487**,** 330-7.

CARLTON, J. G., CABALLE, A., AGROMAYOR, M., KLOC, M. & MARTIN-SERRANO, J. 2012. ESCRT-III governs the Aurora B-mediated abscission checkpoint through CHMP4C. *Science,* 336**,** 220-5.

CARLTON, J. G. & MARTIN-SERRANO, J. 2007. Parallels between cytokinesis and retroviral budding: a role for the ESCRT machinery. *Science,* 316**,** 1908-12.

CARTER, S. L., CIBULSKIS, K., HELMAN, E., MCKENNA, A., SHEN, H., ZACK, T., LAIRD, P. W., ONOFRIO, R. C., WINCKLER, W., WEIR, B. A., BEROUKHIM, R., PELLMAN, D., LEVINE, D. A., LANDER, E. S., MEYERSON, M. & GETZ, G. 2012. Absolute quantification of somatic DNA alterations in human cancer. *Nat Biotechnol,* 30**,** 413-21.

CARTER, S. L., EKLUND, A. C., KOHANE, I. S., HARRIS, L. N. & SZALLASI, Z. 2006. A signature of chromosomal instability inferred from gene expression profiles predicts clinical outcome in multiple human cancers. *Nat Genet,* 38**,** 1043-8.

CASTEDO, M., COQUELLE, A., VIVET, S., VITALE, I., KAUFFMANN, A., DESSEN, P., PEQUIGNOT, M. O., CASARES, N., VALENT, A., MOUHAMAD, S., SCHMITT, E., MODJTAHEDI, N., VAINCHENKER, W., ZITVOGEL, L., LAZAR, V., GARRIDO, C. & KROEMER, G. 2006. Apoptosis regulation in tetraploid cancer cells. *EMBO J,* 25**,** 2584-95.

CASTILLO, A., MORSE, H. C., 3RD, GODFREY, V. L., NAEEM, R. & JUSTICE, M. J. 2007. Overexpression of Eg5 causes genomic instability and tumor formation in mice. *Cancer Res,* 67**,** 10138-47.

CELTON-MORIZUR, S., MERLEN, G., COUTON, D., MARGALL-DUCOS, G. & DESDOUETS, C. 2009. The insulin/Akt pathway controls a specific cell division program that leads to generation of binucleated tetraploid liver cells in rodents. *J Clin Invest,* 119**,** 1880-7.

CHAE, H. D., KIM, S. Y., PARK, S. E., KIM, J. & SHIN, D. Y. 2012. p53 and DNA-dependent protein kinase catalytic subunit independently function in regulating actin damage-induced tetraploid G1 arrest. *Exp Mol Med,* 44**,** 236-40.

CHEN, L., GILKES, D. M., PAN, Y., LANE, W. S. & CHEN, J. 2005. ATM and Chk2-dependent phosphorylation of MDMX contribute to p53 activation after DNA damage. *EMBO J,* 24**,** 3411-22.

CHIN, S. F., TESCHENDORFF, A. E., MARIONI, J. C., WANG, Y., BARBOSA-MORAIS, N. L., THORNE, N. P., COSTA, J. L., PINDER, S. E., VAN DE WIEL, M. A., GREEN, A. R., ELLIS, I. O., PORTER, P. L., TAVARE, S., BRENTON, J. D., YLSTRA, B. & CALDAS, C. 2007. High-resolution aCGH and expression profiling identifies a novel genomic subtype of ER negative breast cancer. *Genome Biol,* 8**,** R215.

CHO, E. H., WENDEL, M., LUTTGEN, M., YOSHIOKA, C., MARRINUCCI, D., LAZAR, D., SCHRAM, E., NIEVA, J., BAZHENOVA, L., MORGAN, A., KO, A. H., KORN, W. M., KOLATKAR, A., BETHEL, K. & KUHN, P. 2012. Characterization of circulating tumor cell aggregates identified in patients with epithelial tumors. *Phys Biol,* 9**,** 016001.

CHOI, C. M., SEO, K. W., JANG, S. J., OH, Y. M., SHIM, T. S., KIM, W. S., LEE, D. S. & LEE, S. D. 2009. Chromosomal instability is a risk factor for poor prognosis of adenocarcinoma of the lung: Fluorescence in situ hybridization analysis of paraffin-embedded tissue from Korean patients. *Lung Cancer,* 64**,** 66-70.

CHOI, S. H. & MCCOLLUM, D. 2012. A role for metaphase spindle elongation forces in correction of merotelic kinetochore attachments. *Curr Biol,* 22**,** 225-30.

CICCIA, A. & ELLEDGE, S. J. 2010. The DNA damage response: making it safe to play with knives. *Mol Cell,* 40**,** 179-204.

CIMINI, D., FIORAVANTI, D., SALMON, E. D. & DEGRASSI, F. 2002. Merotelic kinetochore orientation versus chromosome mono-orientation in the origin of lagging chromosomes in human primary cells. *J Cell Sci,* 115**,** 507-15.

CIMINI, D., HOWELL, B., MADDOX, P., KHODJAKOV, A., DEGRASSI, F. & SALMON, E. D. 2001. Merotelic kinetochore orientation is a major mechanism of aneuploidy in mitotic mammalian tissue cells. *J Cell Biol,* 153**,** 517-27.

COOPER, H. L. & BLACK, P. H. 1963. Cytogenetic studies of hamster kidney cell cultures transformed by the simian vacuolating virus (SV40). *J Natl Cancer Inst,* 30**,** 1015-43.

COSCHI, C. H., ISHAK, C. A., GALLO, D., MARSHALL, A., TALLURI, S., WANG, J., CECCHINI, M. J., MARTENS, A. L., PERCY, V., WELCH, I., BOUTROS, P. C., BROWN, G. W. & DICK, F. A. 2014. Haploinsufficiency of an RB-E2F1-Condensin II complex leads to aberrant replication and aneuploidy. *Cancer Discov,* 4**,** 840-53.

CRAFT, N., BRUHN, K. W., NGUYEN, B. D., PRINS, R., LIAU, L. M., COLLISSON, E. A., DE, A., KOLODNEY, M. S., GAMBHIR, S. S. & MILLER, J. F. 2005. Bioluminescent imaging of melanoma in live mice. *J Invest Dermatol,* 125**,** 159-65.

CRASTA, K., GANEM, N. J., DAGHER, R., LANTERMANN, A. B., IVANOVA, E. V., PAN, Y., NEZI, L., PROTOPOPOV, A., CHOWDHURY, D. & PELLMAN, D. 2012. DNA breaks and chromosome pulverization from errors in mitosis. *Nature*.

DAVOLI, T. & DE LANGE, T. 2011. The Causes and Consequences of Polyploidy in Normal Development and Cancer. *Annual Review of Cell and Developmental Biology,* 27**,** 585-610.

DAVOLI, T. & DE LANGE, T. 2012. Telomere-driven tetraploidization occurs in human cells undergoing crisis and promotes transformation of mouse cells. *Cancer Cell,* 21**,** 765-76.

DAVOLI, T., DENCHI, E. L. & DE LANGE, T. 2010. Persistent Telomere Damage Induces Bypass of Mitosis and Tetraploidy. *Cell,* 141**,** 81-93.

DELUCA, J. G., GALL, W. E., CIFERRI, C., CIMINI, D., MUSACCHIO, A. & SALMON, E. D. 2006. Kinetochore microtubule dynamics and attachment stability are regulated by Hec1. *Cell,* 127**,** 969-82.

DELUCA, J. G. & MUSACCHIO, A. 2012. Structural organization of the kinetochore-microtubule interface. *Curr Opin Cell Biol,* 24**,** 48-56.

DENCHI, E. L. & DE LANGE, T. 2007. Protection of telomeres through independent control of ATM and ATR by TRF2 and POT1. *Nature,* 448**,** 1068-71.

DEPRISTO, M. A., BANKS, E., POPLIN, R., GARIMELLA, K. V., MAGUIRE, J. R., HARTL, C., PHILIPPAKIS, A. A., DEL ANGEL, G., RIVAS, M. A., HANNA, M., MCKENNA, A., FENNELL, T. J., KERNYTSKY, A. M., SIVACHENKO, A. Y., CIBULSKIS, K., GABRIEL, S. B., ALTSHULER, D. & DALY, M. J. 2011. A framework for variation discovery and genotyping using next-generation DNA sequencing data. *Nat Genet,* 43**,** 491-8.

DEWHURST, S. M., MCGRANAHAN, N., BURRELL, R. A., ROWAN, A. J., GRONROOS, E., ENDESFELDER, D., JOSHI, T., MOURADOV, D., GIBBS, P., WARD, R. L., HAWKINS, N. J., SZALLASI, Z., SIEBER, O. M. & SWANTON, C. 2014. Tolerance of whole-genome doubling propagates chromosomal instability and accelerates cancer genome evolution. *Cancer Discov,* 4**,** 175-85.

DIKOVSKAYA, D., SCHIFFMANN, D., NEWTON, I. P., OAKLEY, A., KROBOTH, K., SANSOM, O., JAMIESON, T. J., MENIEL, V., CLARKE, A. & NATHKE, I. S. 2007. Loss of APC induces polyploidy as a result of a combination of defects in mitosis and apoptosis. *J Cell Biol,* 176**,** 183-95.

DING, S., XING, N., LU, J., ZHANG, H., NISHIZAWA, K., LIU, S., YUAN, X., QIN, Y., LIU, Y., OGAWA, O. & NISHIYAMA, H. 2011. Overexpression of Eg5 predicts unfavorable prognosis in non-muscle invasive bladder urothelial carcinoma. *Int J Urol,* 18**,** 432-8.

DJOS, A., FRANSSON, S., KOGNER, P. & MARTINSSON, T. 2013. Aneuploidy in neuroblastoma tumors is not associated with inactivating point mutations in the STAG2 gene. *BMC Med Genet,* 14**,** 102.

DONNELLY, N., PASSERINI, V., DURRBAUM, M., STINGELE, S. & STORCHOVA, Z. 2014. HSF1 deficiency and impaired HSP90-dependent protein folding are hallmarks of aneuploid human cells. *EMBO J,* 33**,** 2374-87.

DONNELLY, N. & STORCHOVA, Z. 2014. Dynamic karyotype, dynamic proteome: buffering the effects of aneuploidy. *Biochim Biophys Acta,* 1843**,** 473-81.

DUELLI, D. M., PADILLA-NASH, H. M., BERMAN, D., MURPHY, K. M., RIED, T. & LAZEBNIK, Y. 2007. A Virus Causes Cancer by Inducing Massive Chromosomal Instability through Cell Fusion. *Current Biology,* 17**,** 431-437.

DUESBERG, P., STINDL, R. & HEHLMANN, R. 2000. Explaining the high mutation rates of cancer cells to drug and multidrug resistance by chromosome reassortments that are catalyzed by aneuploidy. *Proc Natl Acad Sci U S A,* 97**,** 14295-300.

DUIJF, P. H., SCHULTZ, N. & BENEZRA, R. 2013. Cancer cells preferentially lose small chromosomes. *Int J Cancer,* 132**,** 2316-26.

DUKER, N. J. 2002. Chromosome breakage syndromes and cancer. *Am J Med Genet,* 115**,** 125-9.

DUNCAN, A. W., HANLON NEWELL, A. E., BI, W., FINEGOLD, M. J., OLSON, S. B., BEAUDET, A. L. & GROMPE, M. 2012. Aneuploidy as a mechanism for stress-induced liver adaptation. *J Clin Invest,* 122**,** 3307-15.

DUNCAN, A. W., TAYLOR, M. H., HICKEY, R. D., HANLON NEWELL, A. E., LENZI, M. L., OLSON, S. B., FINEGOLD, M. J. & GROMPE, M. 2010. The ploidy conveyor of mature hepatocytes as a source of genetic variation. *Nature,* 467**,** 707-710.

DURRBAUM, M., KUZNETSOVA, A. Y., PASSERINI, V., STINGELE, S., STOEHR, G. & STORCHOVA, Z. 2014. Unique features of the transcriptional response to model aneuploidy in human cells. *BMC Genomics,* 15**,** 139.

ELHAJOUJI, A., CUNHA, M. & KIRSCH-VOLDERS, M. 1998. Spindle poisons can induce polyploidy by mitotic slippage and micronucleate mononucleates in the cytokinesis-block assay. *Mutagenesis,* 13**,** 193-8.

ERTYCH, N., STOLZ, A., STENZINGER, A., WEICHERT, W., KAULFUSS, S., BURFEIND, P., AIGNER, A., WORDEMAN, L. & BASTIANS, H. 2014. Increased microtubule assembly rates influence chromosomal instability in colorectal cancer cells. *Nat Cell Biol,* 16**,** 779-91.

FALCK, J., MAILAND, N., SYLJUASEN, R. G., BARTEK, J. & LUKAS, J. 2001. The ATM-Chk2-Cdc25A checkpoint pathway guards against radioresistant DNA synthesis. *Nature,* 410**,** 842-7.

FAN, F., SAMUEL, S., GAUR, P., LU, J., DALLAS, N. A., XIA, L., BOSE, D., RAMACHANDRAN, V. & ELLIS, L. M. 2011. Chronic exposure of colorectal cancer cells to bevacizumab promotes compensatory pathways that mediate tumour cell migration. *Br J Cancer,* 104**,** 1270-7.

FEDEDA, J. P. & GERLICH, D. W. 2012. Molecular control of animal cell cytokinesis. *Nat Cell Biol,* 14**,** 440-7.

FEDIDA, D., BOUCHARD, R. & CHEN, F. S. 1996. Slow gating charge immobilization in the human potassium channel Kv1.5 and its prevention by 4-aminopyridine. *J Physiol,* 494 (Pt 2)**,** 377-87.

FENNEMA, E., RIVRON, N., ROUWKEMA, J., VAN BLITTERSWIJK, C. & DE BOER, J. 2013. Spheroid culture as a tool for creating 3D complex tissues. *Trends Biotechnol,* 31**,** 108-15.

FODDE, R., KUIPERS, J., ROSENBERG, C., SMITS, R., KIELMAN, M., GASPAR, C., VAN ES, J. H., BREUKEL, C., WIEGANT, J., GILES, R. H. & CLEVERS, H. 2001. Mutations in the APC tumour suppressor gene cause chromosomal instability. *Nat Cell Biol,* 3**,** 433-8.

FUJIWARA, T., BANDI, M., NITTA, M., IVANOVA, E. V., BRONSON, R. T. & PELLMAN, D. 2005. Cytokinesis failure generating tetraploids promotes tumorigenesis in p53-null cells. *Nature,* 437**,** 1043-7.

GAASENBEEK, M., HOWARTH, K., ROWAN, A. J., GORMAN, P. A., JONES, A., CHAPLIN, T., LIU, Y., BICKNELL, D., DAVISON, E. J., FIEGLER, H., CARTER, N. P., ROYLANCE, R. R. & TOMLINSON, I. P. 2006. Combined array-comparative genomic hybridization and single-nucleotide polymorphism-loss of heterozygosity analysis reveals complex changes and multiple forms of chromosomal instability in colorectal cancers. *Cancer Res,* 66**,** 3471-9.

GAILLARD, H., GARCIA-MUSE, T. & AGUILERA, A. 2015. Replication stress and cancer. *Nat Rev Cancer,* 15**,** 276-89.

GALIPEAU, P. C., COWAN, D. S., SANCHEZ, C. A., BARRETT, M. T., EMOND, M. J., LEVINE, D. S., RABINOVITCH, P. S. & REID, B. J. 1996. 17p (p53) allelic losses, 4N (G2/tetraploid) populations, and progression to aneuploidy in Barrett's esophagus. *Proc Natl Acad Sci U S A,* 93**,** 7081-4.

GANEM, N. J., CORNILS, H., CHIU, S. Y., O'ROURKE, K. P., ARNAUD, J., YIMLAMAI, D., THERY, M., CAMARGO, F. D. & PELLMAN, D. 2014. Cytokinesis failure triggers hippo tumor suppressor pathway activation. *Cell,* 158**,** 833-48.

GANEM, N. J., GODINHO, S. A. & PELLMAN, D. 2009. A mechanism linking extra centrosomes to chromosomal instability. *Nature,* 460**,** 278-82.

GANEM, N. J., STORCHOVA, Z. & PELLMAN, D. 2007. Tetraploidy, aneuploidy and cancer. *Current Opinion in Genetics & Development,* 17**,** 157-162.

GENTRIC, G., DESDOUETS, C. & CELTON-MORIZUR, S. 2012. Hepatocytes polyploidization and cell cycle control in liver physiopathology. *Int J Hepatol,* 2012**,** 282430.

GERLINGER, M., MCGRANAHAN, N., DEWHURST, S. M., BURRELL, R. A., TOMLINSON, I. & SWANTON, C. 2014. Cancer: evolution within a lifetime. *Annu Rev Genet,* 48**,** 215-36.

GERLINGER, M., ROWAN, A. J., HORSWELL, S., LARKIN, J., ENDESFELDER, D., GRONROOS, E., MARTINEZ, P., MATTHEWS, N., STEWART, A., TARPEY, P., VARELA, I., PHILLIMORE, B., BEGUM, S., MCDONALD, N. Q., BUTLER, A., JONES, D., RAINE, K., LATIMER, C., SANTOS, C. R., NOHADANI, M., EKLUND, A. C., SPENCER-DENE, B., CLARK, G., PICKERING, L., STAMP, G., GORE, M., SZALLASI, Z., DOWNWARD, J., FUTREAL, P. A. & SWANTON, C. 2012. Intratumor heterogeneity and branched evolution revealed by multiregion sequencing. *N Engl J Med,* 366**,** 883-92.

GERSTUNG, M., BEISEL, C., RECHSTEINER, M., WILD, P., SCHRAML, P., MOCH, H. & BEERENWINKEL, N. 2012. Reliable detection of subclonal single-nucleotide variants in tumour cell populations. *Nat Commun,* 3**,** 811.

GHADIMI, B. M., SACKETT, D. L., DIFILIPPANTONIO, M. J., SCHROCK, E., NEUMANN, T., JAUHO, A., AUER, G. & RIED, T. 2000. Centrosome amplification and instability occurs exclusively in aneuploid, but not in diploid colorectal cancer cell lines, and correlates with numerical chromosomal aberrations. *Genes Chromosomes Cancer,* 27**,** 183-90.

GIL, J. & PETERS, G. 2006. Regulation of the INK4b-ARF-INK4a tumour suppressor locus: all for one or one for all. *Nat Rev Mol Cell Biol,* 7**,** 667-77.

GISSELSSON, D. 2008. Classification of chromosome segregation errors in cancer. *Chromosoma,* 117**,** 511-9.

GISSELSSON, D., HAKANSON, U., STOLLER, P., MARTI, D., JIN, Y., ROSENGREN, A. H., STEWENIUS, Y., KAHL, F. & PANAGOPOULOS, I. 2008. When the genome plays dice: circumvention of the spindle assembly checkpoint and near-random chromosome segregation in multipolar cancer cell mitoses. *PLoS One,* 3**,** e1871.

GISSELSSON, D., JONSON, T., PETERSEN, A., STROMBECK, B., DAL CIN, P., HOGLUND, M., MITELMAN, F., MERTENS, F. & MANDAHL, N. 2001. Telomere dysfunction triggers extensive DNA fragmentation and evolution of complex chromosome abnormalities in human malignant tumors. *Proc Natl Acad Sci U S A,* 98**,** 12683-8.

GODINHO, S. A. & PELLMAN, D. 2014. Causes and consequences of centrosome abnormalities in cancer. *Philos Trans R Soc Lond B Biol Sci,* 369.

GORLA, G. R., MALHI, H. & GUPTA, S. 2001. Polyploidy associated with oxidative injury attenuates proliferative potential of cells. *J Cell Sci,* 114**,** 2943-51.

GRADY, W. M. & CARETHERS, J. M. 2008. Genomic and epigenetic instability in colorectal cancer pathogenesis. *Gastroenterology,* 135**,** 1079-99.

GREENMAN, C. D., BIGNELL, G., BUTLER, A., EDKINS, S., HINTON, J., BEARE, D., SWAMY, S., SANTARIUS, T., CHEN, L., WIDAA, S., FUTREAL, P. A. & STRATTON, M. R. 2010. PICNIC: an algorithm to predict absolute allelic copy number variation with microarray cancer data. *Biostatistics,* 11**,** 164-75.

GREGORY, T. R. 2001. Coincidence, coevolution, or causation? DNA content, cell size, and the C-value enigma. *Biol Rev Camb Philos Soc,* 76**,** 65-101.

GUASTADISEGNI, C., COLAFRANCESCHI, M., OTTINI, L. & DOGLIOTTI, E. 2010. Microsatellite instability as a marker of prognosis and response to therapy: a meta-analysis of colorectal cancer survival data. *Eur J Cancer,* 46**,** 2788-98.

GUNDEM, G., PEREZ-LLAMAS, C., JENE-SANZ, A., KEDZIERSKA, A., ISLAM, A., DEU-PONS, J., FURNEY, S. J. & LOPEZ-BIGAS, N. 2010. IntOGen: integration and data mining of multidimensional oncogenomic data. *Nat Methods,* 7**,** 92-3.

GUPTA, S. 2000. Hepatic polyploidy and liver growth control. *Semin Cancer Biol,* 10**,** 161-71.

HARTLERODE, A. J. & SCULLY, R. 2009. Mechanisms of double-strand break repair in somatic mammalian cells. *Biochem J,* 423**,** 157-68.

HATTORI, N., DAVIES, T. C., ANSON-CARTWRIGHT, L. & CROSS, J. C. 2000. Periodic expression of the cyclin-dependent kinase inhibitor p57(Kip2) in trophoblast giant cells defines a G2-like gap phase of the endocycle. *Mol Biol Cell,* 11**,** 1037-45.

HAU, P., SIU, W., WONG, N., LAI, P. & POON, R. 2006. Polyploidization increases the sensitivity to DNA-damaging agents in mammalian cells. *FEBS Letters,* 580**,** 4727-4736.

HAUF, S., COLE, R. W., LATERRA, S., ZIMMER, C., SCHNAPP, G., WALTER, R., HECKEL, A., VAN MEEL, J., RIEDER, C. L. & PETERS, J. M. 2003. The small molecule Hesperadin reveals a role for Aurora B in correcting kinetochore-microtubule attachment and in maintaining the spindle assembly checkpoint. *J Cell Biol,* 161**,** 281-94.

HELLINGER, M. D. & SANTIAGO, C. A. 2006. Reoperation for recurrent colorectal cancer. *Clin Colon Rectal Surg,* 19**,** 228-36.

HEMBERGER, M. 2008. IFPA award in placentology lecture - characteristics and significance of trophoblast giant cells. *Placenta,* 29 Suppl A**,** S4-9.

HERMAN, J. G., UMAR, A., POLYAK, K., GRAFF, J. R., AHUJA, N., ISSA, J. P., MARKOWITZ, S., WILLSON, J. K., HAMILTON, S. R., KINZLER, K. W., KANE, M. F., KOLODNER, R. D., VOGELSTEIN, B., KUNKEL, T. A. & BAYLIN, S. B. 1998. Incidence and functional consequences of hMLH1 promoter hypermethylation in colorectal carcinoma. *Proc Natl Acad Sci U S A,* 95**,** 6870-5.

HERNANDO, E., NAHLE, Z., JUAN, G., DIAZ-RODRIGUEZ, E., ALAMINOS, M., HEMANN, M., MICHEL, L., MITTAL, V., GERALD, W., BENEZRA, R., LOWE, S. W. & CORDON-CARDO, C. 2004. Rb inactivation promotes genomic instability by uncoupling cell cycle progression from mitotic control. *Nature,* 430**,** 797-802.

HERZOG, F., PRIMORAC, I., DUBE, P., LENART, P., SANDER, B., MECHTLER, K., STARK, H. & PETERS, J. M. 2009. Structure of the anaphase-promoting complex/cyclosome interacting with a mitotic checkpoint complex. *Science,* 323**,** 1477-81.

HOCKEMEYER, D., DANIELS, J. P., TAKAI, H. & DE LANGE, T. 2006. Recent expansion of the telomeric complex in rodents: Two distinct POT1 proteins protect mouse telomeres. *Cell,* 126**,** 63-77.

HOEIJMAKERS, J. H. 2009. DNA damage, aging, and cancer. *N Engl J Med,* 361**,** 1475-85.

HONDA, R., KORNER, R. & NIGG, E. A. 2003. Exploring the functional interactions between Aurora B, INCENP, and survivin in mitosis. *Mol Biol Cell,* 14**,** 3325-41.

HOWELL, B. J., MCEWEN, B. F., CANMAN, J. C., HOFFMAN, D. B., FARRAR, E. M., RIEDER, C. L. & SALMON, E. D. 2001. Cytoplasmic dynein/dynactin drives kinetochore protein transport to the spindle poles and has a role in mitotic spindle checkpoint inactivation. *J Cell Biol,* 155**,** 1159-72.

HSU, T. C., BILLEN, D. & LEVAN, A. 1961. Mammalian chromosomes in vitro. XV. Patterns of transformation. *J Natl Cancer Inst,* 27**,** 515-41.

HU, D. & CROSS, J. C. 2010. Development and function of trophoblast giant cells in the rodent placenta. *Int J Dev Biol,* 54**,** 341-54.

HU, L., PLAFKER, K., VOROZHKO, V., ZUNA, R. E., HANIGAN, M. H., GORBSKY, G. J., PLAFKER, S. M., ANGELETTI, P. C. & CERESA, B. P. 2009. Human papillomavirus 16 E5 induces bi-nucleated cell formation by cell-cell fusion. *Virology,* 384**,** 125-34.

HUANG, X. & JAN, L. Y. 2014. Targeting potassium channels in cancer. *J Cell Biol,* 206**,** 151-62.

HUANG, Y., JIANG, L., YI, Q., LV, L., WANG, Z., ZHAO, X., ZHONG, L., JIANG, H., RASOOL, S., HAO, Q., GUO, Z., COOKE, H. J., FENECH, M. & SHI, Q. 2012. Lagging chromosomes entrapped in micronuclei are not 'lost' by cells. *Cell Res,* 22**,** 932-5.

HURLEY, J. H. & HANSON, P. I. 2010. Membrane budding and scission by the ESCRT machinery: it's all in the neck. *Nat Rev Mol Cell Biol,* 11**,** 556-66.

IWAIZUMI, M., SHINMURA, K., MORI, H., YAMADA, H., SUZUKI, M., KITAYAMA, Y., IGARASHI, H., NAKAMURA, T., SUZUKI, H., WATANABE, Y., HISHIDA, A., IKUMA, M. & SUGIMURA, H. 2009. Human Sgo1 downregulation leads to chromosomal instability in colorectal cancer. *Gut,* 58**,** 249-60.

IWANAGA, Y., CHI, Y. H., MIYAZATO, A., SHELEG, S., HALLER, K., PELOPONESE, J. M., JR., LI, Y., WARD, J. M., BENEZRA, R. & JEANG, K. T. 2007. Heterozygous deletion of mitotic arrest-deficient protein 1 (MAD1) increases the incidence of tumors in mice. *Cancer Res,* 67**,** 160-6.

JACKSON, J. L., SANFORD, K. K. & DUNN, T. B. 1970. Neoplastic conversion and chromosomal characteristics of rat embryo cells in vitro. *J Natl Cancer Inst,* 45**,** 11-23.

JACOB, S., AGUADO, M., FALLIK, D. & PRAZ, F. 2001. The role of the DNA mismatch repair system in the cytotoxicity of the topoisomerase inhibitors camptothecin and etoposide to human colorectal cancer cells. *Cancer Res,* 61**,** 6555-62.

JALLEPALLI, P. V., WAIZENEGGER, I. C., BUNZ, F., LANGER, S., SPEICHER, M. R., PETERS, J. M., KINZLER, K. W., VOGELSTEIN, B. & LENGAUER, C. 2001. Securin is required for chromosomal stability in human cells. *Cell,* 105**,** 445-57.

JAMAL-HANJANI, M., A'HERN, R., BIRKBAK, N. J., GORMAN, P., GRONROOS, E., NGANG, S., NICOLA, P., RAHMAN, L., THANOPOULOU, E., KELLY, G., ELLIS, P., BARRETT-LEE, P., JOHNSTON, S. R., BLISS, J., ROYLANCE, R. & SWANTON, C. 2015. Extreme chromosomal instability forecasts improved outcome in ER-negative breast cancer: a prospective validation cohort study from the TACT trial. *Ann Oncol,* 26**,** 1340-6.

JANSSEN, A., KOPS, G. J. & MEDEMA, R. H. 2009. Elevating the frequency of chromosome mis-segregation as a strategy to kill tumor cells. *Proc Natl Acad Sci U S A,* 106**,** 19108-13.

JANSSEN, A. & MEDEMA, R. H. 2012. Genetic instability: tipping the balance. *Oncogene*.

JANSSEN, A., VAN DER BURG, M., SZUHAI, K., KOPS, G. J. & MEDEMA, R. H. 2011. Chromosome segregation errors as a cause of DNA damage and structural chromosome aberrations. *Science,* 333**,** 1895-8.

JAZAYERI, A., FALCK, J., LUKAS, C., BARTEK, J., SMITH, G. C., LUKAS, J. & JACKSON, S. P. 2006. ATM- and cell cycle-dependent regulation of ATR in response to DNA double-strand breaks. *Nat Cell Biol,* 8**,** 37-45.

JIN, Y., DAI, M. S., LU, S. Z., XU, Y., LUO, Z., ZHAO, Y. & LU, H. 2006. 14-3-3gamma binds to MDMX that is phosphorylated by UV-activated Chk1, resulting in p53 activation. *EMBO J,* 25**,** 1207-18.

KABECHE, L. & COMPTON, D. A. 2012. Checkpoint-independent stabilization of kinetochore-microtubule attachments by Mad2 in human cells. *Curr Biol,* 22**,** 638-44.

KALITSIS, P., EARLE, E., FOWLER, K. J. & CHOO, K. H. 2000. Bub3 gene disruption in mice reveals essential mitotic spindle checkpoint function during early embryogenesis. *Genes Dev,* 14**,** 2277-82.

KASTAN, M. B. & BARTEK, J. 2004. Cell-cycle checkpoints and cancer. *Nature,* 432**,** 316-23.

KIM, H., JEN, J., VOGELSTEIN, B. & HAMILTON, S. R. 1994. Clinical and pathological characteristics of sporadic colorectal carcinomas with DNA replication errors in microsatellite sequences. *Am J Pathol,* 145**,** 148-56.

KIM, Y., CHOI, J. W., LEE, J. H. & KIM, Y. S. 2014. MAD2 and CDC20 are upregulated in high-grade squamous intraepithelial lesions and squamous cell carcinomas of the uterine cervix. *Int J Gynecol Pathol,* 33**,** 517-23.

KING, R. W. 2008. When 2+2=5: The origins and fates of aneuploid and tetraploid cells. *Biochim Biophys Acta,* 1786**,** 4-14.

KLEIN, U. R., NIGG, E. A. & GRUNEBERG, U. 2006. Centromere targeting of the chromosomal passenger complex requires a ternary subcomplex of Borealin, Survivin, and the N-terminal domain of INCENP. *Mol Biol Cell,* 17**,** 2547-58.

KLEYMAN, M., KABECHE, L. & COMPTON, D. A. 2014. STAG2 promotes error correction in mitosis by regulating kinetochore-microtubule attachments. *J Cell Sci,* 127**,** 4225-33.

KOBOLDT, D. C., STEINBERG, K. M., LARSON, D. E., WILSON, R. K. & MARDIS, E. R. 2013. The next-generation sequencing revolution and its impact on genomics. *Cell,* 155**,** 27-38.

KOPS, G. J., FOLTZ, D. R. & CLEVELAND, D. W. 2004. Lethality to human cancer cells through massive chromosome loss by inhibition of the mitotic checkpoint. *Proc Natl Acad Sci U S A,* 101**,** 8699-704.

KOUTSAMI, M. K., TSANTOULIS, P. K., KOULOUKOUSSA, M., APOSTOLOPOULOU, K., PATERAS, I. S., SPARTINOU, Z., DROUGOU, A., EVANGELOU, K., KITTAS, C., BARTKOVA, J., BARTEK, J. & GORGOULIS, V. G. 2006. Centrosome abnormalities are frequently observed in non-small-cell lung cancer and are associated with aneuploidy and cyclin E overexpression. *J Pathol,* 209**,** 512-21.

KRAMER, A., SCHWEIZER, S., NEBEN, K., GIESECKE, C., KALLA, J., KATZENBERGER, T., BENNER, A., MULLER-HERMELINK, H. K., HO, A. D. & OTT, G. 2003. Centrosome aberrations as a possible mechanism for chromosomal instability in non-Hodgkin's lymphoma. *Leukemia,* 17**,** 2207-13.

KRONENWETT, U., HUWENDIEK, S., OSTRING, C., PORTWOOD, N., ROBLICK, U. J., PAWITAN, Y., ALAIYA, A., SENNERSTAM, R., ZETTERBERG, A. & AUER, G. 2004. Improved grading of breast adenocarcinomas based on genomic instability. *Cancer Res,* 64**,** 904-9.

KUERBITZ, S. J., PLUNKETT, B. S., WALSH, W. V. & KASTAN, M. B. 1992. Wild-type p53 is a cell cycle checkpoint determinant following irradiation. *Proc Natl Acad Sci U S A,* 89**,** 7491-5.

KUFFER, C., KUZNETSOVA, A. Y. & STORCHOVA, Z. 2013. Abnormal mitosis triggers p53-dependent cell cycle arrest in human tetraploid cells. *Chromosoma,* 122**,** 305-18.

KUMAGAI, A. & DUNPHY, W. G. 2000. Claspin, a novel protein required for the activation of Chk1 during a DNA replication checkpoint response in Xenopus egg extracts. *Mol Cell,* 6**,** 839-49.

KUMARI, G., ULRICH, T., KRAUSE, M., FINKERNAGEL, F. & GAUBATZ, S. 2014. Induction of p21CIP1 protein and cell cycle arrest after inhibition of Aurora B kinase is attributed to aneuploidy and reactive oxygen species. *J Biol Chem,* 289**,** 16072-84.

KUZNETSOVA, A. Y., SEGET, K., MOELLER, G. K., DE PAGTER, M. S., DE ROOS, J. A., DURRBAUM, M., KUFFER, C., MULLER, S., ZAMAN, G. J., KLOOSTERMAN, W. P. & STORCHOVA, Z. 2015. Chromosomal instability, tolerance of mitotic errors and multidrug resistance are promoted by tetraploidization in human cells. *Cell Cycle***,** 0.

KWON, M., GODINHO, S. A., CHANDHOK, N. S., GANEM, N. J., AZIOUNE, A., THERY, M. & PELLMAN, D. 2008. Mechanisms to suppress multipolar divisions in cancer cells with extra centrosomes. *Genes Dev,* 22**,** 2189-203.

LAMPSON, M. A., RENDUCHITALA, K., KHODJAKOV, A. & KAPOOR, T. M. 2004. Correcting improper chromosome-spindle attachments during cell division. *Nat Cell Biol,* 6**,** 232-7.

LANGLOIS, M. J., BERGERON, S., BERNATCHEZ, G., BOUDREAU, F., SAUCIER, C., PERREAULT, N., CARRIER, J. C. & RIVARD, N. 2010. The PTEN phosphatase controls intestinal epithelial cell polarity and barrier function: role in colorectal cancer progression. *PLoS One,* 5**,** e15742.

LARA-GONZALEZ, P., WESTHORPE, F. G. & TAYLOR, S. S. 2012. The spindle assembly checkpoint. *Curr Biol,* 22**,** R966-80.

LAWRENCE, M. S., STOJANOV, P., POLAK, P., KRYUKOV, G. V., CIBULSKIS, K., SIVACHENKO, A., CARTER, S. L., STEWART, C., MERMEL, C. H., ROBERTS, S. A., KIEZUN, A., HAMMERMAN, P. S., MCKENNA, A., DRIER, Y., ZOU, L., RAMOS, A. H., PUGH, T. J., STRANSKY, N., HELMAN, E., KIM, J., SOUGNEZ, C., AMBROGIO, L., NICKERSON, E., SHEFLER, E., CORTES, M. L., AUCLAIR, D., SAKSENA, G., VOET, D., NOBLE, M., DICARA, D., LIN, P., LICHTENSTEIN, L., HEIMAN, D. I., FENNELL, T., IMIELINSKI, M., HERNANDEZ, B., HODIS, E., BACA, S., DULAK, A. M., LOHR, J., LANDAU, D. A., WU, C. J., MELENDEZ-ZAJGLA, J., HIDALGO-MIRANDA, A., KOREN, A., MCCARROLL, S. A., MORA, J., LEE, R. S., CROMPTON, B., ONOFRIO, R., PARKIN, M., WINCKLER, W., ARDLIE, K., GABRIEL, S. B., ROBERTS, C. W., BIEGEL, J. A., STEGMAIER, K., BASS, A. J., GARRAWAY, L. A., MEYERSON, M., GOLUB, T. R., GORDENIN, D. A., SUNYAEV, S., LANDER, E. S. & GETZ, G. 2013. Mutational heterogeneity in cancer and the search for new cancer-associated genes. *Nature,* 499**,** 214-8.

LAZZERINI DENCHI, E., CELLI, G. & DE LANGE, T. 2006. Hepatocytes with extensive telomere deprotection and fusion remain viable and regenerate liver mass through endoreduplication. *Genes Dev,* 20**,** 2648-53.

LEE, A. J., ENDESFELDER, D., ROWAN, A. J., WALTHER, A., BIRKBAK, N. J., FUTREAL, P. A., DOWNWARD, J., SZALLASI, Z., TOMLINSON, I. P., HOWELL, M., KSCHISCHO, M. & SWANTON, C. 2011. Chromosomal instability confers intrinsic multidrug resistance. *Cancer Res,* 71**,** 1858-70.

LEE, H. O., DAVIDSON, J. M. & DURONIO, R. J. 2009. Endoreplication: polyploidy with purpose. *Genes & Development,* 23**,** 2461-2477.

LEHMAN, N. L., TIBSHIRANI, R., HSU, J. Y., NATKUNAM, Y., HARRIS, B. T., WEST, R. B., MASEK, M. A., MONTGOMERY, K., VAN DE RIJN, M. & JACKSON, P. K. 2007. Oncogenic regulators and substrates of the anaphase promoting complex/cyclosome are frequently overexpressed in malignant tumors. *Am J Pathol,* 170**,** 1793-805.

LEHMAN, N. L., VERSCHUREN, E. W., HSU, J. Y., CHERRY, A. M. & JACKSON, P. K. 2006. Overexpression of the anaphase promoting complex/cyclosome inhibitor Emi1 leads to tetraploidy and genomic instability of p53-deficient cells. *Cell Cycle,* 5**,** 1569-73.

LEIGHT, E. R. & SUGDEN, B. 2001. Establishment of an oriP replicon is dependent upon an infrequent, epigenetic event. *Mol Cell Biol,* 21**,** 4149-61.

LENGAUER, C., KINZLER, K. W. & VOGELSTEIN, B. 1997. Genetic instability in colorectal cancers. *Nature,* 386**,** 623-7.

LENGAUER, C., KINZLER, K. W. & VOGELSTEIN, B. 1998. Genetic instabilities in human cancers. *Nature,* 396**,** 643-9.

LENTINI, L., AMATO, A., SCHILLACI, T. & DI LEONARDO, A. 2007. Simultaneous Aurora-A/STK15 overexpression and centrosome amplification induce chromosomal instability in tumour cells with a MIN phenotype. *BMC Cancer,* 7**,** 212.

LEVINE, D. S., SANCHEZ, C. A., RABINOVITCH, P. S. & REID, B. J. 1991. Formation of the tetraploid intermediate is associated with the development of cells with more than four centrioles in the elastase-simian virus 40 tumor antigen transgenic mouse model of pancreatic cancer. *Proc Natl Acad Sci U S A,* 88**,** 6427-31.

LI, H. & DURBIN, R. 2009. Fast and accurate short read alignment with Burrows-Wheeler transform. *Bioinformatics,* 25**,** 1754-60.

LI, M., FANG, X., BAKER, D. J., GUO, L., GAO, X., WEI, Z., HAN, S., VAN DEURSEN, J. M. & ZHANG, P. 2010. The ATM-p53 pathway suppresses aneuploidy-induced tumorigenesis. *Proc Natl Acad Sci U S A,* 107**,** 14188-93.

LIM, S. & KALDIS, P. 2013. Cdks, cyclins and CKIs: roles beyond cell cycle regulation. *Development,* 140**,** 3079-93.

LINDAHL, T. & BARNES, D. E. 2000. Repair of endogenous DNA damage. *Cold Spring Harb Symp Quant Biol,* 65**,** 127-33.

LINGLE, W. L., LUTZ, W. H., INGLE, J. N., MAIHLE, N. J. & SALISBURY, J. L. 1998. Centrosome hypertrophy in human breast tumors: implications for genomic stability and cell polarity. *Proc Natl Acad Sci U S A,* 95**,** 2950-5.

LISSA, D., SENOVILLA, L., RELLO-VARONA, S., VITALE, I., MICHAUD, M., PIETROCOLA, F., BOILEVE, A., OBRIST, F., BORDENAVE, C., GARCIA, P., MICHELS, J., JEMAA, M., KEPP, O., CASTEDO, M. & KROEMER, G. 2014. Resveratrol and aspirin eliminate tetraploid cells for anticancer chemoprevention. *Proc Natl Acad Sci U S A,* 111**,** 3020-5.

LIU, D., VADER, G., VROMANS, M. J., LAMPSON, M. A. & LENS, S. M. 2009. Sensing chromosome bi-orientation by spatial separation of aurora B kinase from kinetochore substrates. *Science,* 323**,** 1350-3.

LIU, D., VLEUGEL, M., BACKER, C. B., HORI, T., FUKAGAWA, T., CHEESEMAN, I. M. & LAMPSON, M. A. 2010a. Regulated targeting of protein phosphatase 1 to the outer kinetochore by KNL1 opposes Aurora B kinase. *J Cell Biol,* 188**,** 809-20.

LIU, M., WANG, X., YANG, Y., LI, D., REN, H., ZHU, Q., CHEN, Q., HAN, S., HAO, J. & ZHOU, J. 2010b. Ectopic expression of the microtubule-dependent motor protein Eg5 promotes pancreatic tumourigenesis. *J Pathol,* 221**,** 221-8.

LONG, L., HUANG, G., ZHU, H., GUO, Y., LIU, Y. & HUO, J. 2013. Down-regulation of miR-138 promotes colorectal cancer metastasis via directly targeting TWIST2. *J Transl Med,* 11**,** 275.

LOTHSCHUTZ, D., JENNEWEIN, M., PAHL, S., LAUSBERG, H. F., EICHLER, A., MUTSCHLER, W., HANSELMANN, R. G. & OBERRINGER, M. 2002. Polyploidization and centrosome hyperamplification in inflammatory bronchi. *Inflamm Res,* 51**,** 416-22.

LU, J., YE, X., FAN, F., XIA, L., BHATTACHARYA, R., BELLISTER, S., TOZZI, F., SCEUSI, E., ZHOU, Y., TACHIBANA, I., MARU, D. M., HAWKE, D. H., RAK, J., MANI, S. A., ZWEIDLER-MCKAY, P. & ELLIS, L. M. 2013. Endothelial cells promote the colorectal cancer stem cell phenotype through a soluble form of Jagged-1. *Cancer Cell,* 23**,** 171-85.

LV, L., ZHANG, T., YI, Q., HUANG, Y., WANG, Z., HOU, H., ZHANG, H., ZHENG, W., HAO, Q., GUO, Z., COOKE, H. J. & SHI, Q. 2012. Tetraploid cells from cytokinesis failure induce aneuploidy and spontaneous transformation of mouse ovarian surface epithelial cells. *Cell Cycle,* 11**,** 2864-75.

MAILAND, N., FALCK, J., LUKAS, C., SYLJUASEN, R. G., WELCKER, M., BARTEK, J. & LUKAS, J. 2000. Rapid destruction of human Cdc25A in response to DNA damage. *Science,* 288**,** 1425-9.

MALEY, C. C. 2007. Multistage carcinogenesis in Barrett's esophagus. *Cancer Lett,* 245**,** 22-32.

MANNING, A. L., LONGWORTH, M. S. & DYSON, N. J. 2010. Loss of pRB causes centromere dysfunction and chromosomal instability. *Genes Dev,* 24**,** 1364-76.

MANNING, A. L., YAZINSKI, S. A., NICOLAY, B., BRYLL, A., ZOU, L. & DYSON, N. J. 2014. Suppression of genome instability in pRB-deficient cells by enhancement of chromosome cohesion. *Mol Cell,* 53**,** 993-1004.

MARGALL-DUCOS, G., CELTON-MORIZUR, S., COUTON, D., BREGERIE, O. & DESDOUETS, C. 2007. Liver tetraploidization is controlled by a new process of incomplete cytokinesis. *J Cell Sci,* 120**,** 3633-9.

MARXER, M., FOUCAR, C. E., MAN, W. Y., CHEN, Y., MA, H. T. & POON, R. Y. 2012. Tetraploidization increases sensitivity to Aurora B kinase inhibition. *Cell Cycle,* 11**,** 2567-77.

MAYER, V. W. & AGUILERA, A. 1990. High levels of chromosome instability in polyploids of Saccharomyces cerevisiae. *Mutat Res,* 231**,** 177-86.

MCCALL, M. N., BOLSTAD, B. M. & IRIZARRY, R. A. 2010. Frozen robust multiarray analysis (fRMA). *Biostatistics,* 11**,** 242-53.

MCGRANAHAN, N., BURRELL, R. A., ENDESFELDER, D., NOVELLI, M. R. & SWANTON, C. 2012. Cancer chromosomal instability: therapeutic and diagnostic challenges. 'Exploring aneuploidy: the significance of chromosomal imbalance' review series. *EMBO Rep*.

MCGRANAHAN, N., FAVERO, F., DE BRUIN, E. C., BIRKBAK, N. J., SZALLASI, Z. & SWANTON, C. 2015. Clonal status of actionable driver events and the timing of mutational processes in cancer evolution. *Sci Transl Med,* 7**,** 283ra54.

MCGRANAHAN, N. & SWANTON, C. 2015. Biological and therapeutic impact of intratumor heterogeneity in cancer evolution. *Cancer Cell,* 27**,** 15-26.

MCINTYRE, A., PATIAR, S., WIGFIELD, S., LI, J. L., LEDAKI, I., TURLEY, H., LEEK, R., SNELL, C., GATTER, K., SLY, W. S., VAUGHAN-JONES, R. D., SWIETACH, P. & HARRIS, A. L. 2012. Carbonic anhydrase IX promotes tumor growth and necrosis in vivo and inhibition enhances anti-VEGF therapy. *Clin Cancer Res,* 18**,** 3100-11.

MCPHERSON, J. P., TAMBLYN, L., ELIA, A., MIGON, E., SHEHABELDIN, A., MATYSIAK-ZABLOCKI, E., LEMMERS, B., SALMENA, L., HAKEM, A., FISH, J., KASSAM, F., SQUIRE, J., BRUNEAU, B. G., HANDE, M. P. & HAKEM, R.

2004. Lats2/Kpm is required for embryonic development, proliferation control and genomic integrity. *EMBO J,* 23**,** 3677-88.

MECKERT, P. C., RIVELLO, H. G., VIGLIANO, C., GONZALEZ, P., FAVALORO, R. & LAGUENS, R. 2005. Endomitosis and polyploidization of myocardial cells in the periphery of human acute myocardial infarction. *Cardiovasc Res,* 67**,** 116-23.

MENDOZA, M., NORDEN, C., DURRER, K., RAUTER, H., UHLMANN, F. & BARRAL, Y. 2009. A mechanism for chromosome segregation sensing by the NoCut checkpoint. *Nat Cell Biol,* 11**,** 477-83.

MERALDI, P., HONDA, R. & NIGG, E. A. 2002. Aurora-A overexpression reveals tetraploidization as a major route to centrosome amplification in p53-/- cells. *EMBO J,* 21**,** 483-92.

METTU, R. K., WAN, Y. W., HABERMANN, J. K., RIED, T. & GUO, N. L. 2010. A 12-gene genomic instability signature predicts clinical outcomes in multiple cancer types. *Int J Biol Markers,* 25.

MICHEL, L., DIAZ-RODRIGUEZ, E., NARAYAN, G., HERNANDO, E., MURTY, V. V. & BENEZRA, R. 2004. Complete loss of the tumor suppressor MAD2 causes premature cyclin B degradation and mitotic failure in human somatic cells. *Proc Natl Acad Sci U S A,* 101**,** 4459-64.

MIKULE, K., DELAVAL, B., KALDIS, P., JURCYZK, A., HERGERT, P. & DOXSEY, S. 2007. Loss of centrosome integrity induces p38-p53-p21-dependent G1-S arrest. *Nat Cell Biol,* 9**,** 160-70.

MITELMAN F, J. B. A. M. F. 2015. *Mitelman database of chromosome aberrations and gene fusions in cancer* [Online]. Available: http://cgap.nci.nih.gov/Chromosomes/Mitelman [Accessed 22/7/15 2015].

MITTAL, K. R., CHAN, W. & DEMOPOULOS, R. I. 1990. Sensitivity and specificity of various morphological features of cervical condylomas. An in situ hybridization study. *Arch Pathol Lab Med,* 114**,** 1038-41.

MOORHEAD, P. S. & SAKSELA, E. 1965. The sequence of chromosome aberrations during SV 40 transformation of a human diploid cell strain. *Hereditas,* 52**,** 271-84.

MOOTHA, V. K., LINDGREN, C. M., ERIKSSON, K. F., SUBRAMANIAN, A., SIHAG, S., LEHAR, J., PUIGSERVER, P., CARLSSON, E., RIDDERSTRALE, M., LAURILA, E., HOUSTIS, N., DALY, M. J., PATTERSON, N., MESIROV, J. P., GOLUB, T. R., TAMAYO, P., SPIEGELMAN, B., LANDER, E. S., HIRSCHHORN, J. N., ALTSHULER, D. & GROOP, L. C. 2003. PGC-1alpha-responsive genes involved in oxidative phosphorylation are coordinately downregulated in human diabetes. *Nat Genet,* 34**,** 267-73.

MORDES, D. A., GLICK, G. G., ZHAO, R. & CORTEZ, D. 2008. TopBP1 activates ATR through ATRIP and a PIKK regulatory domain. *Genes Dev,* 22**,** 1478-89.

MORGAN, D. O. 1997. Cyclin-dependent kinases: engines, clocks, and microprocessors. *Annu Rev Cell Dev Biol,* 13**,** 261-91.

MORITA, E., SANDRIN, V., CHUNG, H. Y., MORHAM, S. G., GYGI, S. P., RODESCH, C. K. & SUNDQUIST, W. I. 2007. Human ESCRT and ALIX proteins interact with proteins of the midbody and function in cytokinesis. *EMBO J,* 26**,** 4215-27.

MOURADOV, D., DOMINGO, E., GIBBS, P., JORISSEN, R. N., LI, S., SOO, P. Y., LIPTON, L., DESAI, J., DANIELSEN, H. E., OUKRIF, D., NOVELLI, M., YAU, C., HOLMES, C. C., JONES, I. T., MCLAUGHLIN, S., MOLLOY, P., HAWKINS, N. J., WARD, R., MIDGELY, R., KERR, D., TOMLINSON, I. P. & SIEBER, O. M. 2013. Survival in stage II/III colorectal cancer is independently predicted by chromosomal and microsatellite instability, but not by specific driver mutations. *Am J Gastroenterol,* 108**,** 1785-93.

MULLINS, J. M. & BIESELE, J. J. 1973. Cytokinetic activities in a human cell line: the midbody and intercellular bridge. *Tissue Cell,* 5**,** 47-61.

MULLINS, J. M. & BIESELE, J. J. 1977. Terminal phase of cytokinesis in D-98s cells. *J Cell Biol,* 73**,** 672-84.

MURAYAMA-HOSOKAWA, S., ODA, K., NAKAGAWA, S., ISHIKAWA, S., YAMAMOTO, S., SHOJI, K., IKEDA, Y., UEHARA, Y., FUKAYAMA, M., MCCORMICK, F., YANO, T., TAKETANI, Y. & ABURATANI, H. 2010. Genome-wide single-nucleotide polymorphism arrays in endometrial carcinomas associate extensive chromosomal instability with poor prognosis and unveil frequent chromosomal imbalances involved in the PI3-kinase pathway. *Oncogene,* 29**,** 1897-908.

NAGASAKI, A., DE HOSTOS, E. L. & UYEDA, T. Q. 2002. Genetic and morphological evidence for two parallel pathways of cell-cycle-coupled cytokinesis in Dictyostelium. *J Cell Sci,* 115**,** 2241-51.

NAM, H. J., NAYLOR, R. M. & VAN DEURSEN, J. M. 2015. Centrosome dynamics as a source of chromosomal instability. *Trends Cell Biol,* 25**,** 65-73.

NAM, H. J. & VAN DEURSEN, J. M. 2014. Cyclin B2 and p53 control proper timing of centrosome separation. *Nat Cell Biol,* 16**,** 538-49.

NGUYEN, H. G., MAKITALO, M., YANG, D., CHINNAPPAN, D., ST. HILAIRE, C. & RAVID, K. 2009. Deregulated Aurora-B induced tetraploidy promotes tumorigenesis. *The FASEB Journal,* 23**,** 2741-2748.

NIGG, E. A. 2002. Centrosome aberrations: cause or consequence of cancer progression? *Nat Rev Cancer,* 2**,** 815-25.

NIGG, E. A. 2006. Origins and consequences of centrosome aberrations in human cancers. *Int J Cancer,* 119**,** 2717-23.

NIJENHUIS, W., VON CASTELMUR, E., LITTLER, D., DE MARCO, V., TROMER, E., VLEUGEL, M., VAN OSCH, M. H., SNEL, B., PERRAKIS, A. & KOPS, G. J. 2013. A TPR domain-containing N-terminal module of MPS1 is required for its kinetochore localization by Aurora B. *J Cell Biol,* 201**,** 217-31.

NIK-ZAINAL, S., VAN LOO, P., WEDGE, D. C., ALEXANDROV, L. B., GREENMAN, C. D., LAU, K. W., RAINE, K., JONES, D., MARSHALL, J., RAMAKRISHNA, M., SHLIEN, A., COOKE, S. L., HINTON, J., MENZIES, A., STEBBINGS, L. A., LEROY, C., JIA, M., RANCE, R., MUDIE, L. J., GAMBLE, S. J., STEPHENS, P. J., MCLAREN, S., TARPEY, P. S., PAPAEMMANUIL, E., DAVIES, H. R., VARELA, I., MCBRIDE, D. J., BIGNELL, G. R., LEUNG, K., BUTLER, A. P., TEAGUE, J. W., MARTIN, S., JONSSON, G., MARIANI, O., BOYAULT, S., MIRON, P., FATIMA, A., LANGEROD, A., APARICIO, S. A., TUTT, A., SIEUWERTS, A. M., BORG, A., THOMAS, G., SALOMON, A. V., RICHARDSON, A. L., BORRESEN-DALE, A. L., FUTREAL, P. A., STRATTON, M. R. & CAMPBELL, P. J. 2012. The life history of 21 breast cancers. *Cell,* 149**,** 994-1007.

NIKONOVA, A. S., ASTSATUROV, I., SEREBRIISKII, I. G., DUNBRACK, R. L., JR. & GOLEMIS, E. A. 2013. Aurora A kinase (AURKA) in normal and pathological cell division. *Cell Mol Life Sci,* 70**,** 661-87.

NORDEN, C., MENDOZA, M., DOBBELAERE, J., KOTWALIWALE, C. V., BIGGINS, S. & BARRAL, Y. 2006. The NoCut pathway links completion of cytokinesis to spindle midzone function to prevent chromosome breakage. *Cell,* 125**,** 85-98.

OBEID, M., TESNIERE, A., GHIRINGHELLI, F., FIMIA, G. M., APETOH, L., PERFETTINI, J. L., CASTEDO, M., MIGNOT, G., PANARETAKIS, T., CASARES, N., METIVIER, D., LAROCHETTE, N., VAN ENDERT, P., CICCOSANTI, F., PIACENTINI, M., ZITVOGEL, L. & KROEMER, G. 2007. Calreticulin exposure dictates the immunogenicity of cancer cell death. *Nat Med,* 13**,** 54-61.

OLAHARSKI, A. J. 2006. Tetraploidy and chromosomal instability are early events during cervical carcinogenesis. *Carcinogenesis,* 27**,** 337-343.

OLAHARSKI, A. J., SOTELO, R., SOLORZA-LUNA, G., GONSEBATT, M. E., GUZMAN, P., MOHAR, A. & EASTMOND, D. A. 2006. Tetraploidy and chromosomal instability are early events during cervical carcinogenesis. *Carcinogenesis,* 27**,** 337-43.

OLIVE, P. L., LEONARD, J. C. & DURAND, R. E. 1982. Development of tetraploidy in V79 spheroids. *In Vitro,* 18**,** 708-14.

OTTO, S. P. & WHITTON, J. 2000. Polyploid incidence and evolution. *Annu Rev Genet,* 34**,** 401-437.

PAMPALONA, J., SOLER, D., GENESCA, A. & TUSELL, L. 2010. Whole chromosome loss is promoted by telomere dysfunction in primary cells. *Genes Chromosomes Cancer,* 49**,** 368-78.

PAMPALONI, F., REYNAUD, E. G. & STELZER, E. H. 2007. The third dimension bridges the gap between cell culture and live tissue. *Nat Rev Mol Cell Biol,* 8**,** 839-45.

PARKIN, D. M. 2006. The global health burden of infection-associated cancers in the year 2002. *Int J Cancer,* 118**,** 3030-44.

PAVELKA, N., RANCATI, G., ZHU, J., BRADFORD, W. D., SARAF, A., FLORENS, L., SANDERSON, B. W., HATTEM, G. L. & LI, R. 2010. Aneuploidy confers quantitative proteome changes and phenotypic variation in budding yeast. *Nature,* 468**,** 321-5.

PETERMANN, E., HELLEDAY, T. & CALDECOTT, K. W. 2008. Claspin promotes normal replication fork rates in human cells. *Mol Biol Cell,* 19**,** 2373-8.

PICARD, B. 2012. http://broadinstitute.github.io/picard/ [Online]. Available: http://broadinstitute.github.io/picard/.

PIHAN, G. A., PUROHIT, A., WALLACE, J., KNECHT, H., WODA, B., QUESENBERRY, P. & DOXSEY, S. J. 1998. Centrosome defects and genetic instability in malignant tumors. *Cancer Res,* 58**,** 3974-85.

PIHAN, G. A., PUROHIT, A., WALLACE, J., MALHOTRA, R., LIOTTA, L. & DOXSEY, S. J. 2001. Centrosome defects can account for cellular and genetic changes that characterize prostate cancer progression. *Cancer Res,* 61**,** 2212-9.

PINES, J. 2011. Cubism and the cell cycle: the many faces of the APC/C. *Nat Rev Mol Cell Biol,* 12**,** 427-38.

RAVID, K., LU, J., ZIMMET, J. M. & JONES, M. R. 2002. Roads to polyploidy: the megakaryocyte example. *J Cell Physiol,* 190**,** 7-20.

REDDY, S. K., RAPE, M., MARGANSKY, W. A. & KIRSCHNER, M. W. 2007. Ubiquitination by the anaphase-promoting complex drives spindle checkpoint inactivation. *Nature,* 446**,** 921-5.

REID, R. 1983. Genital warts and cervical cancer. II. Is human papillomavirus infection the trigger to cervical carcinogenesis? *Gynecol Oncol,* 15**,** 239-52.

REINA-SAN-MARTIN, B., NUSSENZWEIG, M. C., NUSSENZWEIG, A. & DIFILIPPANTONIO, S. 2005. Genomic instability, endoreduplication, and diminished Ig class-switch recombination in B cells lacking Nbs1. *Proc Natl Acad Sci U S A,* 102**,** 1590-5.

RELLO-VARONA, S., VITALE, I., KEPP, O., SENOVILLA, L., JEMAA, M., METIVIER, D., CASTEDO, M. & KROEMER, G. 2009. Preferential killing of tetraploid tumor cells by targeting the mitotic kinesin Eg5. *Cell Cycle,* 8**,** 1030-5.

RIEDER, C. L., COLE, R. W., KHODJAKOV, A. & SLUDER, G. 1995. The checkpoint delaying anaphase in response to chromosome monoorientation is mediated by an inhibitory signal produced by unattached kinetochores. *J Cell Biol,* 130**,** 941-8.

RIEDER, C. L. & MAIATO, H. 2004. Stuck in division or passing through: what happens when cells cannot satisfy the spindle assembly checkpoint. *Dev Cell,* 7**,** 637-51.

ROBERTS, P. C., MOTTILLO, E. P., BAXA, A. C., HENG, H. H., DOYON-REALE, N., GREGOIRE, L., LANCASTER, W. D., RABAH, R. & SCHMELZ, E. M. 2005. Sequential molecular and cellular events during neoplastic progression: a mouse syngeneic ovarian cancer model. *Neoplasia,* 7**,** 944-56.

ROBINSON, D. N. & SPUDICH, J. A. 2004. Mechanics and regulation of cytokinesis. *Curr Opin Cell Biol,* 16**,** 182-8.

ROSCHKE, A. V., TONON, G., GEHLHAUS, K. S., MCTYRE, N., BUSSEY, K. J., LABABIDI, S., SCUDIERO, D. A., WEINSTEIN, J. N. & KIRSCH, I. R. 2003. Karyotypic complexity of the NCI-60 drug-screening panel. *Cancer Res,* 63**,** 8634-47.

ROYLANCE, R., ENDESFELDER, D., GORMAN, P., BURRELL, R. A., SANDER, J., TOMLINSON, I., HANBY, A. M., SPEIRS, V., RICHARDSON, A. L., BIRKBAK, N. J., EKLUND, A. C., DOWNWARD, J., KSCHISCHO, M., SZALLASI, Z. & SWANTON, C. 2011. Relationship of extreme chromosomal instability with long-term survival in a retrospective analysis of primary breast cancer. *Cancer Epidemiol Biomarkers Prev,* 20**,** 2183-94.

RUCHAUD, S., CARMENA, M. & EARNSHAW, W. C. 2007. Chromosomal passengers: conducting cell division. *Nat Rev Mol Cell Biol,* 8**,** 798-812.

RYLAND, K. E., SVOBODA, L. K., VESELY, E. D., MCINTYRE, J. C., ZHANG, L., MARTENS, J. R. & LAWLOR, E. R. 2014. Polycomb-dependent repression of the potassium channel-encoding gene KCNA5 promotes cancer cell survival under conditions of stress. *Oncogene*.

SACRISTAN, C. & KOPS, G. J. 2015. Joined at the hip: kinetochores, microtubules, and spindle assembly checkpoint signaling. *Trends Cell Biol,* 25**,** 21-8.

SAKAUE-SAWANO, A., KUROKAWA, H., MORIMURA, T., HANYU, A., HAMA, H., OSAWA, H., KASHIWAGI, S., FUKAMI, K., MIYATA, T., MIYOSHI, H., IMAMURA, T., OGAWA, M., MASAI, H. & MIYAWAKI, A. 2008. Visualizing spatiotemporal dynamics of multicellular cell-cycle progression. *Cell,* 132**,** 487-98.

SALE, S., TUNSTALL, R. G., RUPARELIA, K. C., POTTER, G. A., STEWARD, W. P. & GESCHER, A. J. 2005. Comparison of the effects of the chemopreventive agent resveratrol and its synthetic analog trans 3,4,5,4'-tetramethoxystilbene (DMU-212) on adenoma development in the Apc(Min+) mouse and cyclooxygenase-2 in human-derived colon cancer cells. *Int J Cancer,* 115**,** 194-201.

SATO, H., MASUDA, F., TAKAYAMA, Y., TAKAHASHI, K. & SAITOH, S. 2012. Epigenetic Inactivation and Subsequent Heterochromatinization of a Centromere Stabilize Dicentric Chromosomes. *Curr Biol*.

SCHNEIDER, Y., DURANTON, B., GOSSE, F., SCHLEIFFER, R., SEILER, N. & RAUL, F. 2001. Resveratrol inhibits intestinal tumorigenesis and modulates host-defense-related gene expression in an animal model of human familial adenomatous polyposis. *Nutr Cancer,* 39**,** 102-7.

SCHWARTZ, M., ZLOTORYNSKI, E. & KEREM, B. 2006. The molecular basis of common and rare fragile sites. *Cancer Lett,* 232**,** 13-26.

SELMECKI, A. M., MARUVKA, Y. E., RICHMOND, P. A., GUILLET, M., SHORESH, N., SORENSON, A. L., DE, S., KISHONY, R., MICHOR, F., DOWELL, R. & PELLMAN, D. 2015. Polyploidy can drive rapid adaptation in yeast. *Nature,* 519**,** 349-52.

SENOVILLA, L., VITALE, I., MARTINS, I., TAILLER, M., PAILLERET, C., MICHAUD, M., GALLUZZI, L., ADJEMIAN, S., KEPP, O., NISO-SANTANO, M., SHEN, S.,

MARINO, G., CRIOLLO, A., BOILEVE, A., JOB, B., LADOIRE, S., GHIRINGHELLI, F., SISTIGU, A., YAMAZAKI, T., RELLO-VARONA, S., LOCHER, C., POIRIER-COLAME, V., TALBOT, M., VALENT, A., BERARDINELLI, F., ANTOCCIA, A., CICCOSANTI, F., FIMIA, G. M., PIACENTINI, M., FUEYO, A., MESSINA, N. L., LI, M., CHAN, C. J., SIGL, V., POURCHER, G., RUCKENSTUHL, C., CARMONA-GUTIERREZ, D., LAZAR, V., PENNINGER, J. M., MADEO, F., LOPEZ-OTIN, C., SMYTH, M. J., ZITVOGEL, L., CASTEDO, M. & KROEMER, G. 2012. An immunosurveillance mechanism controls cancer cell ploidy. *Science,* 337**,** 1678-84.

SHACKNEY, S. E., SMITH, C. A., MILLER, B. W., BURHOLT, D. R., MURTHA, K., GILES, H. R., KETTERER, D. M. & POLLICE, A. A. 1989. Model for the genetic evolution of human solid tumors. *Cancer Res,* 49**,** 3344-54.

SHELTZER, J. M., BLANK, H. M., PFAU, S. J., TANGE, Y., GEORGE, B. M., HUMPTON, T. J., BRITO, I. L., HIRAOKA, Y., NIWA, O. & AMON, A. 2011. Aneuploidy drives genomic instability in yeast. *Science,* 333**,** 1026-30.

SHELTZER, J. M., TORRES, E. M., DUNHAM, M. J. & AMON, A. 2012. Transcriptional consequences of aneuploidy. *Proc Natl Acad Sci U S A,* 109**,** 12644-9.

SHEN, H., MORAN, D. M. & MAKI, C. G. 2008. Transient nutlin-3a treatment promotes endoreduplication and the generation of therapy-resistant tetraploid cells. *Cancer Res,* 68**,** 8260-8.

SHEN, H., PEREZ, R. E., DAVAADELGER, B. & MAKI, C. G. 2013. Two 4N cell-cycle arrests contribute to cisplatin-resistance. *PLoS One,* 8**,** e59848.

SHERR, C. J. & ROBERTS, J. M. 1999. CDK inhibitors: positive and negative regulators of G1-phase progression. *Genes Dev,* 13**,** 1501-12.

SHI, Q. & KING, R. W. 2005. Chromosome nondisjunction yields tetraploid rather than aneuploid cells in human cell lines. *Nature,* 437**,** 1038-1042.

SIEBER, O. M., HEINIMANN, K., GORMAN, P., LAMLUM, H., CRABTREE, M., SIMPSON, C. A., DAVIES, D., NEALE, K., HODGSON, S. V., ROYLANCE, R. R., PHILLIPS, R. K., BODMER, W. F. & TOMLINSON, I. P. 2002. Analysis of chromosomal instability in human colorectal adenomas with two mutational hits at APC. *Proc Natl Acad Sci U S A,* 99**,** 16910-5.

SILKWORTH, W. T., NARDI, I. K., PAUL, R., MOGILNER, A. & CIMINI, D. 2012. Timing of centrosome separation is important for accurate chromosome segregation. *Mol Biol Cell,* 23**,** 401-11.

SILKWORTH, W. T., NARDI, I. K., SCHOLL, L. M. & CIMINI, D. 2009. Multipolar spindle pole coalescence is a major source of kinetochore mis-attachment and chromosome mis-segregation in cancer cells. *PLoS One,* 4**,** e6564.

SOLOMON, D. A., KIM, T., DIAZ-MARTINEZ, L. A., FAIR, J., ELKAHLOUN, A. G., HARRIS, B. T., TORETSKY, J. A., ROSENBERG, S. A., SHUKLA, N., LADANYI, M., SAMUELS, Y., JAMES, C. D., YU, H., KIM, J. S. & WALDMAN, T. 2011. Mutational inactivation of STAG2 causes aneuploidy in human cancer. *Science,* 333**,** 1039-43.

SOTILLO, R., HERNANDO, E., DÍAZ-RODRÍGUEZ, E., TERUYA-FELDSTEIN, J., CORDÓN-CARDO, C., LOWE, S. W. & BENEZRA, R. 2007. Mad2 Overexpression Promotes Aneuploidy and Tumorigenesis in Mice. *Cancer Cell,* 11**,** 9-23.

STEIGEMANN, P., WURZENBERGER, C., SCHMITZ, M. H., HELD, M., GUIZETTI, J., MAAR, S. & GERLICH, D. W. 2009. Aurora B-mediated abscission checkpoint protects against tetraploidization. *Cell,* 136**,** 473-84.

STEPANOVA, T., SLEMMER, J., HOOGENRAAD, C. C., LANSBERGEN, G., DORTLAND, B., DE ZEEUW, C. I., GROSVELD, F., VAN CAPPELLEN, G., AKHMANOVA, A. & GALJART, N. 2003. Visualization of microtubule growth in

cultured neurons via the use of EB3-GFP (end-binding protein 3-green fluorescent protein). *J Neurosci,* 23**,** 2655-64.
STEPHENSON, M. & KUTTEH, W. 2007. Evaluation and management of recurrent early pregnancy loss. *Clin Obstet Gynecol,* 50**,** 132-45.
STINGELE, S., STOEHR, G., PEPLOWSKA, K., COX, J., MANN, M. & STORCHOVA, Z. 2012. Global analysis of genome, transcriptome and proteome reveals the response to aneuploidy in human cells. *Mol Syst Biol,* 8**,** 608.
STOLZ, A., ERTYCH, N., KIENITZ, A., VOGEL, C., SCHNEIDER, V., FRITZ, B., JACOB, R., DITTMAR, G., WEICHERT, W., PETERSEN, I. & BASTIANS, H. 2010. The CHK2-BRCA1 tumour suppressor pathway ensures chromosomal stability in human somatic cells. *Nat Cell Biol,* 12**,** 492-9.
STORCHOVA, Z., BRENEMAN, A., CANDE, J., DUNN, J., BURBANK, K., O'TOOLE, E. & PELLMAN, D. 2006. Genome-wide genetic analysis of polyploidy in yeast. *Nature,* 443**,** 541-7.
STORCHOVA, Z. & KUFFER, C. 2008. The consequences of tetraploidy and aneuploidy. *J Cell Sci,* 121**,** 3859-66.
STRACKER, T. H., USUI, T. & PETRINI, J. H. 2009. Taking the time to make important decisions: the checkpoint effector kinases Chk1 and Chk2 and the DNA damage response. *DNA Repair (Amst),* 8**,** 1047-54.
STUMP, G. L., WALLACE, A. A., REGAN, C. P. & LYNCH, J. J., JR. 2005. In vivo antiarrhythmic and cardiac electrophysiologic effects of a novel diphenylphosphine oxide IKur blocker (2-isopropyl-5-methylcyclohexyl) diphenylphosphine oxide. *J Pharmacol Exp Ther,* 315**,** 1362-7.
SUBRAMANIAN, A., TAMAYO, P., MOOTHA, V. K., MUKHERJEE, S., EBERT, B. L., GILLETTE, M. A., PAULOVICH, A., POMEROY, S. L., GOLUB, T. R., LANDER, E. S. & MESIROV, J. P. 2005. Gene set enrichment analysis: a knowledge-based approach for interpreting genome-wide expression profiles. *Proc Natl Acad Sci U S A,* 102**,** 15545-50.
SUDAKIN, V., CHAN, G. K. & YEN, T. J. 2001. Checkpoint inhibition of the APC/C in HeLa cells is mediated by a complex of BUBR1, BUB3, CDC20, and MAD2. *J Cell Biol,* 154**,** 925-36.
SVARTMAN, M., STONE, G. & STANYON, R. 2005. Molecular cytogenetics discards polyploidy in mammals. *Genomics,* 85**,** 425-30.
TANAKA, T. U., RACHIDI, N., JANKE, C., PEREIRA, G., GALOVA, M., SCHIEBEL, E., STARK, M. J. & NASMYTH, K. 2002. Evidence that the Ipl1-Sli15 (Aurora kinase-INCENP) complex promotes chromosome bi-orientation by altering kinetochore-spindle pole connections. *Cell,* 108**,** 317-29.
TANG, Y. C., WILLIAMS, B. R., SIEGEL, J. J. & AMON, A. 2011. Identification of aneuploidy-selective antiproliferation compounds. *Cell,* 144**,** 499-512.
TAYLOR, C. F., PLATT, F. M., HURST, C. D., THYGESEN, H. H. & KNOWLES, M. A. 2014. Frequent inactivating mutations of STAG2 in bladder cancer are associated with low tumour grade and stage and inversely related to chromosomal copy number changes. *Hum Mol Genet,* 23**,** 1964-74.
TEIXEIRA, J. H., SILVA, P., FARIA, J., FERREIRA, I., DUARTE, P., DELGADO, M. L., QUEIROS, O., MOREIRA, R., BARBOSA, J., LOPES, C. A., DO AMARAL, J. B., MONTEIRO, L. S. & BOUSBAA, H. 2015. Clinicopathologic significance of BubR1 and Mad2 overexpression in oral cancer. *Oral Dis*.
THOMPSON, D. A., DESAI, M. M. & MURRAY, A. W. 2006. Ploidy controls the success of mutators and nature of mutations during budding yeast evolution. *Curr Biol,* 16**,** 1581-90.
THOMPSON, S. L. & COMPTON, D. A. 2008. Examining the link between chromosomal instability and aneuploidy in human cells. *J Cell Biol,* 180**,** 665-72.

THOMPSON, S. L. & COMPTON, D. A. 2010. Proliferation of aneuploid human cells is limited by a p53-dependent mechanism. *J Cell Biol,* 188**,** 369-81.

THOMPSON, S. L. & COMPTON, D. A. 2011a. Chromosome missegregation in human cells arises through specific types of kinetochore-microtubule attachment errors. *Proc Natl Acad Sci U S A,* 108**,** 17974-8.

THOMPSON, S. L. & COMPTON, D. A. 2011b. Chromosomes and cancer cells. *Chromosome Res,* 19**,** 433-44.

THORESEN, S. B., CAMPSTEIJN, C., VIETRI, M., SCHINK, K. O., LIESTOL, K., ANDERSEN, J. S., RAIBORG, C. & STENMARK, H. 2014. ANCHR mediates Aurora-B-dependent abscission checkpoint control through retention of VPS4. *Nat Cell Biol,* 16**,** 550-60.

THOTA, S., VINY, A. D., MAKISHIMA, H., SPITZER, B., RADIVOYEVITCH, T., PRZYCHODZEN, B., SEKERES, M. A., LEVINE, R. L. & MACIEJEWSKI, J. P. 2014. Genetic alterations of the cohesin complex genes in myeloid malignancies. *Blood,* 124**,** 1790-8.

TOJI, S., YABUTA, N., HOSOMI, T., NISHIHARA, S., KOBAYASHI, T., SUZUKI, S., TAMAI, K. & NOJIMA, H. 2004. The centrosomal protein Lats2 is a phosphorylation target of Aurora-A kinase. *Genes Cells,* 9**,** 383-97.

TOMASINI, R., MAK, T. W. & MELINO, G. 2008. The impact of p53 and p73 on aneuploidy and cancer. *Trends Cell Biol,* 18**,** 244-52.

TORRES, E. M., SOKOLSKY, T., TUCKER, C. M., CHAN, L. Y., BOSELLI, M., DUNHAM, M. J. & AMON, A. 2007. Effects of aneuploidy on cellular physiology and cell division in haploid yeast. *Science,* 317**,** 916-24.

TOSO, A., WINTER, J. R., GARROD, A. J., AMARO, A. C., MERALDI, P. & MCAINSH, A. D. 2009. Kinetochore-generated pushing forces separate centrosomes during bipolar spindle assembly. *J Cell Biol,* 184**,** 365-72.

TOYODA, H., BREGERIE, O., VALLET, A., NALPAS, B., PIVERT, G., BRECHOT, C. & DESDOUETS, C. 2005. Changes to hepatocyte ploidy and binuclearity profiles during human chronic viral hepatitis. *Gut,* 54**,** 297-302.

UETAKE, Y. & SLUDER, G. 2004. Cell cycle progression after cleavage failure: mammalian somatic cells do not possess a "tetraploidy checkpoint". *J Cell Biol,* 165**,** 609-15.

ULLAH, Z., KOHN, M. J., YAGI, R., VASSILEV, L. T. & DEPAMPHILIS, M. L. 2008. Differentiation of trophoblast stem cells into giant cells is triggered by p57/Kip2 inhibition of CDK1 activity. *Genes Dev,* 22**,** 3024-36.

UMAR, A., BOLAND, C. R., TERDIMAN, J. P., SYNGAL, S., DE LA CHAPELLE, A., RUSCHOFF, J., FISHEL, R., LINDOR, N. M., BURGART, L. J., HAMELIN, R., HAMILTON, S. R., HIATT, R. A., JASS, J., LINDBLOM, A., LYNCH, H. T., PELTOMAKI, P., RAMSEY, S. D., RODRIGUEZ-BIGAS, M. A., VASEN, H. F., HAWK, E. T., BARRETT, J. C., FREEDMAN, A. N. & SRIVASTAVA, S. 2004. Revised Bethesda Guidelines for hereditary nonpolyposis colorectal cancer (Lynch syndrome) and microsatellite instability. *J Natl Cancer Inst,* 96**,** 261-8.

UZBEKOV, R., KIREYEV, I. & PRIGENT, C. 2002. Centrosome separation: respective role of microtubules and actin filaments. *Biol Cell,* 94**,** 275-88.

VAN HARN, T., FOIJER, F., VAN VUGT, M., BANERJEE, R., YANG, F., OOSTRA, A., JOENJE, H. & TE RIELE, H. 2010. Loss of Rb proteins causes genomic instability in the absence of mitogenic signaling. *Genes Dev,* 24**,** 1377-88.

VEIGL, M. L., KASTURI, L., OLECHNOWICZ, J., MA, A. H., LUTTERBAUGH, J. D., PERIYASAMY, S., LI, G. M., DRUMMOND, J., MODRICH, P. L., SEDWICK, W. D. & MARKOWITZ, S. D. 1998. Biallelic inactivation of hMLH1 by epigenetic gene silencing, a novel mechanism causing human MSI cancers. *Proc Natl Acad Sci U S A,* 95**,** 8698-702.

VENKITARAMAN, A. R. 2007. Chromosomal instability in cancer: causality and interdependence. *Cell Cycle,* 6**,** 2341-3.

VITALE, I., GALLUZZI, L., VIVET, S., NANTY, L., DESSEN, P., SENOVILLA, L., OLAUSSEN, K. A., LAZAR, V., PRUDHOMME, M., GOLSTEYN, R. M., CASTEDO, M. & KROEMER, G. 2007. Inhibition of Chk1 kills tetraploid tumor cells through a p53-dependent pathway. *PLoS One,* 2**,** e1337.

VITALE, I., JEMAA, M., SENOVILLA, L., GALLUZZI, L., RELLO-VARONA, S., METIVIER, D., RIPOCHE, H., LAZAR, V., DESSEN, P., CASTEDO, M. & KROEMER, G. 2010a. Involvement of p38alpha in the mitotic progression of p53(-/-) tetraploid cells. *Cell Cycle,* 9**,** 2823-9.

VITALE, I., SENOVILLA, L., JEMAA, M., MICHAUD, M., GALLUZZI, L., KEPP, O., NANTY, L., CRIOLLO, A., RELLO-VARONA, S., MANIC, G., METIVIER, D., VIVET, S., TAJEDDINE, N., JOZA, N., VALENT, A., CASTEDO, M. & KROEMER, G. 2010b. Multipolar mitosis of tetraploid cells: inhibition by p53 and dependency on Mos. *EMBO J,* 29**,** 1272-84.

WAINBERG, M. A. & HOWE, C. 1973. Factors affecting cell fusion induced by Sendai virus. *J Virol,* 12**,** 937-9.

WALTHER, A., HOULSTON, R. & TOMLINSON, I. 2008. Association between chromosomal instability and prognosis in colorectal cancer: a meta-analysis. *Gut,* 57**,** 941-50.

WANG, K., LI, M. & HAKONARSON, H. 2010. ANNOVAR: functional annotation of genetic variants from high-throughput sequencing data. *Nucleic Acids Res,* 38**,** e164.

WANG, Q., LIU, T., FANG, Y., XIE, S., HUANG, X., MAHMOOD, R., RAMASWAMY, G., SAKAMOTO, K. M., DARZYNKIEWICZ, Z., XU, M. & DAI, W. 2004a. BUBR1 deficiency results in abnormal megakaryopoiesis. *Blood,* 103**,** 1278-85.

WANG, X., ZOU, L., ZHENG, H., WEI, Q., ELLEDGE, S. J. & LI, L. 2003. Genomic instability and endoreduplication triggered by RAD17 deletion. *Genes Dev,* 17**,** 965-70.

WANG, Z., CUMMINS, J. M., SHEN, D., CAHILL, D. P., JALLEPALLI, P. V., WANG, T. L., PARSONS, D. W., TRAVERSO, G., AWAD, M., SILLIMAN, N., PTAK, J., SZABO, S., WILLSON, J. K., MARKOWITZ, S. D., GOLDBERG, M. L., KARESS, R., KINZLER, K. W., VOGELSTEIN, B., VELCULESCU, V. E. & LENGAUER, C. 2004b. Three classes of genes mutated in colorectal cancers with chromosomal instability. *Cancer Res,* 64**,** 2998-3001.

WATSON, J. V., CHAMBERS, S. H. & SMITH, P. J. 1987. A pragmatic approach to the analysis of DNA histograms with a definable G1 peak. *Cytometry,* 8**,** 1-8.

WELBURN, J. P., VLEUGEL, M., LIU, D., YATES, J. R., 3RD, LAMPSON, M. A., FUKAGAWA, T. & CHEESEMAN, I. M. 2010. Aurora B phosphorylates spatially distinct targets to differentially regulate the kinetochore-microtubule interface. *Mol Cell,* 38**,** 383-92.

WILLIAMS, B. R., PRABHU, V. R., HUNTER, K. E., GLAZIER, C. M., WHITTAKER, C. A., HOUSMAN, D. E. & AMON, A. 2008. Aneuploidy affects proliferation and spontaneous immortalization in mammalian cells. *Science,* 322**,** 703-9.

WILLIAMS, G. H. & STOEBER, K. 2012. The cell cycle and cancer. *J Pathol,* 226**,** 352-64.

WONG, C. & STEARNS, T. 2005. Mammalian cells lack checkpoints for tetraploidy, aberrant centrosome number, and cytokinesis failure. *BMC Cell Biol,* 6**,** 6.

WU, C. C., YANG, T. Y., YU, C. T., PHAN, L., IVAN, C., SOOD, A. K., HSU, S. L. & LEE, M. H. 2012a. p53 negatively regulates Aurora A via both transcriptional and posttranslational regulation. *Cell Cycle,* 11**,** 3433-42.

WU, P., VAN OVERBEEK, M., ROONEY, S. & DE LANGE, T. 2010. Apollo contributes to G overhang maintenance and protects leading-end telomeres. *Mol Cell,* 39**,** 606-17.

WU, Z. Q., BRABLETZ, T., FEARON, E., WILLIS, A. L., HU, C. Y., LI, X. Y. & WEISS, S. J. 2012b. Canonical Wnt suppressor, Axin2, promotes colon carcinoma oncogenic activity. *Proc Natl Acad Sci U S A,* 109**,** 11312-7.

YANG, X., YU, K., HAO, Y., LI, D. M., STEWART, R., INSOGNA, K. L. & XU, T. 2004. LATS1 tumour suppressor affects cytokinesis by inhibiting LIMK1. *Nat Cell Biol,* 6**,** 609-17.

YANG, Z., LONCAREK, J., KHODJAKOV, A. & RIEDER, C. L. 2008. Extra centrosomes and/or chromosomes prolong mitosis in human cells. *Nat Cell Biol,* 10**,** 748-51.

YAU, C., MOURADOV, D., JORISSEN, R. N., COLELLA, S., MIRZA, G., STEERS, G., HARRIS, A., RAGOUSSIS, J., SIEBER, O. & HOLMES, C. C. 2010. A statistical approach for detecting genomic aberrations in heterogeneous tumor samples from single nucleotide polymorphism genotyping data. *Genome Biol,* 11**,** R92.

YE, J., COULOURIS, G., ZARETSKAYA, I., CUTCUTACHE, I., ROZEN, S. & MADDEN, T. L. 2012. Primer-BLAST: a tool to design target-specific primers for polymerase chain reaction. *BMC Bioinformatics,* 13**,** 134.

YOSHIHARA, T., ISHIDA, M., KINOMURA, A., KATSURA, M., TSURUGA, T., TASHIRO, S., ASAHARA, T. & MIYAGAWA, K. 2004. XRCC3 deficiency results in a defect in recombination and increased endoreduplication in human cells. *EMBO J,* 23**,** 670-80.

YU, F. X., ZHAO, B., PANUPINTHU, N., JEWELL, J. L., LIAN, I., WANG, L. H., ZHAO, J., YUAN, H., TUMANENG, K., LI, H., FU, X. D., MILLS, G. B. & GUAN, K. L. 2012. Regulation of the Hippo-YAP pathway by G-protein-coupled receptor signaling. *Cell,* 150**,** 780-91.

YVON, A. M., WADSWORTH, P. & JORDAN, M. A. 1999. Taxol suppresses dynamics of individual microtubules in living human tumor cells. *Mol Biol Cell,* 10**,** 947-59.

ZACK, T. I., SCHUMACHER, S. E., CARTER, S. L., CHERNIACK, A. D., SAKSENA, G., TABAK, B., LAWRENCE, M. S., ZHANG, C. Z., WALA, J., MERMEL, C. H., SOUGNEZ, C., GABRIEL, S. B., HERNANDEZ, B., SHEN, H., LAIRD, P. W., GETZ, G., MEYERSON, M. & BEROUKHIM, R. 2013. Pan-cancer patterns of somatic copy number alteration. *Nat Genet,* 45**,** 1134-1140.

ZHANG, C. Z., SPEKTOR, A., CORNILS, H., FRANCIS, J. M., JACKSON, E. K., LIU, S., MEYERSON, M. & PELLMAN, D. 2015. Chromothripsis from DNA damage in micronuclei. *Nature,* 522**,** 179-84.

ZHANG, Y., FOREMAN, O., WIGLE, D. A., KOSARI, F., VASMATZIS, G., SALISBURY, J. L., VAN DEURSEN, J. & GALARDY, P. J. 2012. USP44 regulates centrosome positioning to prevent aneuploidy and suppress tumorigenesis. *J Clin Invest,* 122**,** 4362-74.

ZHAO, B., LI, L., WANG, L., WANG, C. Y., YU, J. & GUAN, K. L. 2012. Cell detachment activates the Hippo pathway via cytoskeleton reorganization to induce anoikis. *Genes Dev,* 26**,** 54-68.

ZHENG, L., DAI, H., HEGDE, M. L., ZHOU, M., GUO, Z., WU, X., WU, J., SU, L., ZHONG, X., MITRA, S., HUANG, Q., KERNSTINE, K. H., PFEIFER, G. P. & SHEN, B. 2011. Fen1 mutations that specifically disrupt its interaction with PCNA cause aneuploidy-associated cancer. *Cell Res,* 21**,** 1052-67.

ZHENG, L., DAI, H., ZHOU, M., LI, X., LIU, C., GUO, Z., WU, X., WU, J., WANG, C., ZHONG, J., HUANG, Q., GARCIA-AGUILAR, J., PFEIFER, G. P. & SHEN, B. 2012. Polyploid cells rewire DNA damage response networks to overcome replication stress-induced barriers for tumour progression. *Nat Commun,* 3**,** 815.

ZHOU, X. & PLATT, J. L. 2011. Molecular and cellular mechanisms of mammalian cell fusion. *Adv Exp Med Biol,* 713**,** 33-64.

ZHU, J., PAVELKA, N., BRADFORD, W. D., RANCATI, G. & LI, R. 2012. Karyotypic determinants of chromosome instability in aneuploid budding yeast. *PLoS Genet,* 8**,** e1002719.

ZOU, L. & ELLEDGE, S. J. 2003. Sensing DNA damage through ATRIP recognition of RPA-ssDNA complexes. *Science,* 300**,** 1542-8.

ZYBINA, E. V. & ZYBINA, T. G. 1996. Polytene chromosomes in mammalian cells. *Int Rev Cytol,* 165**,** 53-119.